BEST AVAILABLE IMAGES

Defective images within this document are accurate representation of The original documents submitted by the applicant.

Defects in the images may include (but are not limited to):

- BLACK BORDERS
- TEXT CUT OFF AT TOP, BOTTOM OR SIDES
- FADED TEXT
- ILLEGIBLE TEXT
- SKEWED/SLANTED IMAGES
- COLORED PHOTOS
- BLACK OR VERY BLACK AND WHITE DARK PHOTOS
- GRAY SCALE DOCUMENTS

IMAGES ARE BEST AVAILABLE COPY.

As rescanning documents *will not* correct images, please do not report the images to the Image Problem Mailbox.

C14

EFFECT OF IRRADIATION ON CHEMICALLY CROSSLINKED ULTRAHIGH MOLECULAR WEIGHT POLYETHYLENE

by

Fu-wen Shen

A Dissertation Presented to the

FACULTY OF THE GRADUATE SCHOOL

UNIVERSITY OF SOUTHERN CALIFORNIA

In Partial Fulfillment of the

Requirements for the Degree

DOCTOR OF PHILOSOPHY

(Materials Science)

December 1994

UNIVERSITY OF SOUTHERN CALIFORNIA
THE GRADUATE SCHOOL
UNIVERSITY PARK
LOS ANGELES, CALIFORNIA 90007

This dissertation, written by

Fu-Wen Shen

under the direction of his *Dissertation Committee, and approved by all its members, has been presented to and accepted by* The *Graduate School, in partial fulfillment of requirements for the degree of*

DOCTOR OF PHILOSOPHY

Dean of Graduate Studies

Date October 27, 1994

DISSERTATION COMMITTEE

Chairperson

Acknowledgements

I would like to thank Dr. Ronald Salovey for his guidance, advice and encouragement throughout the course of this work. He is gentle and scholarly. It is my honor to work with him and learn from him. I would also like to thank Dr. Harry McKellop for his advice and assistance for this work. He is an expert in the biomechanics area, and guides me in my studies. He always shares his experience regarding joint replacement with us. Thanks are also due to Dr. Eric Amis and Dr. Murray Gershenzon who served as the guidance committee and dissertation committee. Thanks to my friends, Dr. S. Park, Ms. P. Campell, Mr. B. Lu and B. Yeom, who were always there when needed. Finally, I would like to extend my cordial thanks to my family for their support and encouragement.

Contents

List of Tables

List of Figures

ABSTRACT

Chemically crosslinked ultrahigh molecular weight polyethylene (UHMWPE) networks were synthesized by compression molding of polyethylene in the presence of peroxide at 170 °C for 2 h. To examine the effect of high energy irradiation, crosslinked specimens were irradiated with gamma-rays up to 34 kGy (3.4 Mrad). The effect of irradiation on thermal properties, swelling properties, crystal perfection, surface morphology, and mechanical properties of peroxide crosslinked UHMWPE was extensively studied.

Peroxide crosslinking leads to a decrease in the degree of crystallinity, peak melting temperature, and recrystallization temperature. This is because peroxide crosslinking suppresses recrystallization on cooling a crosslinked melt, leading to crystal imperfections and decreased crystallite size. The degree of swelling decreases with increasing peroxide concentration. Wide-angle x-ray scattering shows that crystal perfection and size decrease with increasing peroxide concentration. Examination of the morphology of fracture surfaces by scanning electron microscopy (SEM) shows that peroxide crosslinked UHMWPE exhibits ductile fracture. Morphological examination after permanganic etching indicates that peroxide crosslinked UHMWPE suffers more oxidation than the uncrosslinked polymer and the number of spherulites decreases. Tensile tests show that yield stress, elongation at break, tensile strength at break, and Young's modulus decrease with increasing peroxide concentration because of decreased crystallinity and increasingly crosslinked amorphous regions.

Irradiation of peroxide crosslinked UHMWPE produces further crosslinking in amorphous regions plus extensive chain scission of taut tie molecules and leads to increased crystallinity and crystal perfection, reduces gel content, and increases degree of swelling of

the crosslinked network. However, peroxide crosslinking reduces the effect of irradiation on the crosslinked network. We suggest that peroxide crosslinking stabilizes chain fragments resulting from scission and suppresses recrystallization of broken chains from amorphous regions. Wide-angle x-ray scattering shows that crystal perfection increases after irradiation. After irradiation, yield stress, elongation at break, and tensile strength at break increase because of increased crystallinity, whereas, elongation at the yield point decreases. For peroxide-free samples, Young's modulus increases after irradiation because of increased crystallinity, whereas, for peroxide crosslinked samples, changes in Young's modulus are less noticeable.

CHAPTER 1

INTRODUCTION

1.1 Radiation Chemistry of Polymers

The study of radiation effects on polymers is technologically important because of the commercial development of radiation processes for modifying the properties of polymeric materials. The development of radiation-induced modification (crosslinking, degradation, grafting) of polymeric materials applied to manufacturing areas includes tires, wire and cable insulation, heat-shrinkable film and tubing, controlled polymer modification (molecular weight reduction for ease of molding or chemical grafting of monomers onto polymer surfaces for ease of bonding, and dye acceptance), curing of coatings, and microlithographic process for electronic applications [1]. In addition, high energy radiation is used to sterilize medical devices. In the microlithographic process, polymer materials which undergo radiation-induced changes in solubility are used to define the individual elements of integrated circuits. This aspect of the microlithographic process is illustrated in Figure 1.1 [2]. The desired semiconductor substrate is first coated with a thin layer (~0.5-2.0 μm thick) of a resist which is then exposed to some form of radiation. The radiation sources used in the microlithographic process include conventional (> 300 nm) and deep-UV (< 300 nm) light, electron beam, ion beam, and x-ray sources [2-3]. Radiation-sensitive moieties of the resist undergo reaction to generate the desired circuit pattern in the polymeric material. This pattern may then be developed into a relief image through

treatment with an appropriate solvent. If exposure to radiation results in reduced solubility or crosslinking, the material is classified as a negative resist. On the other hand, a positive

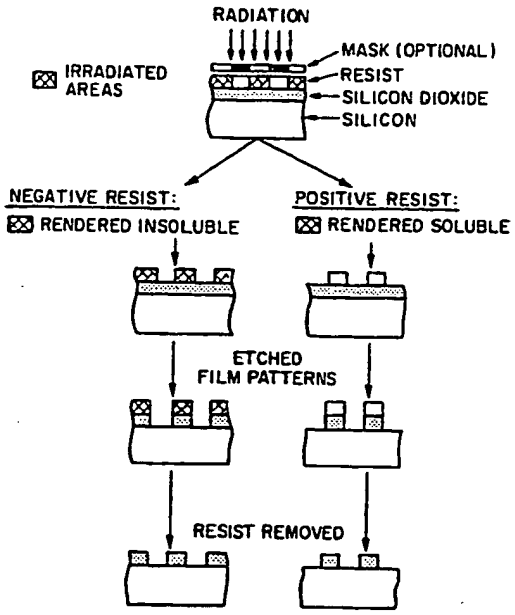

Figure 1.1. The schematic illustration of microlithographic process [2].

resist undergoes radiation-induced reactions that lead to enhanced solubility in the exposed regions. After definition of the circuit pattern into the resist layer, the features are transferred into the substrate by either a wet-, or dry-etching technique. The resist is then stripped from the substrate. Subsequent dielectric, insulator or conducting materials are then deposited onto the surface of the device substrate and patterned in a similar manner. The most popular polymer used as positive electron beam resist is poly (methyl

methacrylate), whereas polymers used as negative resists are polystyrene, halogenated polystyrene, and copolymers of dimethylsiloxane, methylphenylsiloxane or methylvinylsiloxane [2-3].

We are concerned with the chemical effects of high energy radiation on materials. High energy radiation generally includes beams of fast electrons or β-particles; heavier particles of high energy such as fast protons, fast neutrons, α-particles and charged particles of higher mass; and electromagnetic radiation such as γ-rays or x-rays [5]. In the irradiation of polymers, attention is mainly focused on fast electrons and on γ-radiation. Electron irradiation is normally obtained from electron accelerators which give rise to beams with energies in the MeV range. The gamma-rays emitted by radioactive isotopes (e.g., cobalt-60) cover a very broad spectrum of energies and penetrate uniformly through material. For instance, 1 MeV γ-rays may penetrate through about a meter of solid or liquid, whereas electron beams penetrate no more than a few mm in solid or liquid [6].

For high energy radiation, the most convenient unit of energy is the electron volt (eV), defined as the energy obtained by a single electron (charge 1.602×10^{-19} coulombs) falling through a potential difference of 1 V [5]. This small unit of energy amounting to 1.602×10^{-12} ergs or 1.602×10^{-19} joules is most frequently used in relation to a single atom, molecule or chemical bond. The energy equivalents for one mole of molecules or chemical bonds of a specific type which consist of 6.02×10^{23} molecules or bonds are [5]

1 eV per molecule or bond = 6.02×10^{23} eV/mole

= $1.602 \times 10^{-19} \times 6.02 \times 10^{23}$ or 9.6×10^{4} joules/mole

= 23.05×10^{3} cal/mole = 23.05 Kcal/mole

The amount of absorbed energy and the nature of the material being irradiated determine the number of molecules which are ionized or excited. For a particular material, the number of

these events is proportional to the energy absorbed, and does not seem to depend very much on the nature or energy of the radiation used, at least for energies greater than 20 KeV [6]. The absorbed dose (i.e. the energy absorbed) is usually expressed in terms of a unit called the rad, corresponding to 100 ergs of energy absorbed per gram of material irradiated. The SI unit is the gray (Gy), which is 1 joule per kg. Thus, 1 Gy = 100 rad = 1 joule/kg and 1 Mrad = 10 kGy. The amount of chemical change (chemical yield) due to radiation can be related to the absorbed energy by using the G value. The G value represents the average number of chemical changes of a specific type per 100 eV of absorbed energy. Typical G values used are G(x) and G(s), representing the crosslink and scission events, respectively. For molecules of molecular weight M, there are A (Avogadro's number)/M molecules per gram. With G(x) changes of nature x per 100 eV, a dose of 1 kGy (0.624×10^{19} eV) will produce 0.624×10^{17}G changes x per gram, where x refers to the effect of irradiation such as scission, crosslinking. Therefore, the total changes of nature x per molecule will be $0.624 \times 10^{17}GM/A = 1.04 \times 10^{-7}GM$ [7]. With a dose of τ kGy, for an average of one change per molecule, $\tau GM \equiv 9.6 \times 10^{6}$ is needed. For the same G values, we can see the advantage of high molecular weight materials, which need only low radiation dose to get same chemical changes (per molecule).

The effects of radiation on polymeric materials has been extensively studied [5-13]. Absorption of high-energy radiation in a polymer produces excitation and ionization, and these excited and ionized species are the initial chemical reactants [5-10]. An ionization process in which an orbital electron is removed from its parent nucleus gives rise to a free electron and a positively charged atom or molecule. In an excitation process, an electron is raised to a higher energy level but remains bound to its parent nucleus, producing a neutral atom or molecule. The ejected electron must lose energy until it reaches thermal energy. Geminate recombination with the parent cation radical may then occur and is more likely in substrates of low dielectric constant. The resultant excited molecule may undergo homolytic

bond scission to give two free radicals or heterolytic bond scission to give an ion pair. On the other hand, the parent cation radical may undergo spontaneous decomposition to give a more stable ion and a free radical, or ion-molecule reactions. The initially ejected electron may be stabilized by interaction with polar groups, as a solvated species or as an anion radical . These primary processes can be summarized in the following schemes [14]:

(a) ionization

$$\text{Polymer (P)} \xrightarrow{\gamma} P^{+\cdot} + e^{-} \qquad (1)$$

(b) excitation

$$\text{Polymer (P)} \xrightarrow{\gamma} P^{*} \qquad (2)$$

(c) ejected e^- loses energy

$$e^{-} \longrightarrow e^{-}_{th} \qquad (3)$$

(d) germinate recombination

$$P^{+\cdot} + e^{-}_{th} \longrightarrow P \qquad (4)$$

(e) homolytic scission

$$P^{*} \longrightarrow R_1^{\cdot} + R_2^{\cdot} \qquad (5)$$

(f) heterolytic scission

$$P^{*} \longrightarrow A^{+} + B^{-} \qquad (6)$$

(g) dissociation

$$P^{+\cdot} \longrightarrow C^{+} + D^{\cdot} \qquad (7)$$

(h) ion-molecule reaction

$$P^{+\cdot} + P \longrightarrow PD^{+} + E^{\cdot} \qquad (8)$$

(i) e^- stabilization

$$e^{-} + S \longrightarrow e^{-}_{solv} , S^{-\cdot} \qquad (9)$$

Therefore, the radiation chemistry of polymers is the chemistry of neutral, cation and anion radicals, cations and anions, and excited species.

Although the absorption of radiation energy is spatially and molecularly random, the subsequent chemical changes are not random. Some chemical bonds and groups are particularly sensitive to radiation-induced reaction. They include COOH, C-X where X= halogen, $-SO_2-$, NH_2, and C=C. Spatial selectivity of chemical reactions may result from intramolecular or intermolecular migration of energy or reactive species such as free radicals or ions [13]. Typical free radicals in irradiated polyethylene include the alkyl radical, $-CH_2\dot{C}HCH_2-$, the allyl, $-\dot{C}HCH{=}CH-$, and the polyenyl free radicals, $-\dot{C}H-(CH{=}CH)_n-$, although the latter are produced in significant yields only at high doses [9]. The reactions of free radicals can be classified as (i) abstraction of hydrogen atoms, with preference for tertiary H, or halogen atoms; (ii) addition to double bonds, which are very efficient scavengers for radicals; (iii) decomposition to give both small molecule products, such as H_2, CO, CO_2, CH_4 and chain scission, resulting in a decrease in molecular weight and substantial changes in polymer material properties; (iv) chain crosslinking or combination, resulting in an increase in molecular weight and formation of a network; and (v) disproportionation, producing unsaturates. When main-chain bond scission occurs in polymer molecules in the solid state to form two free radicals, the limited mobility of the resultant chain fragments mitigates against permanent scission. This is the cage effect and leads to increased yields of scission in amorphous compared with crystalline polymers [6]. Polymers subjected to radiation in the absence of oxygen can be grouped into two categories, in terms of the predominance of scission vs crosslinking [5]: polymers with a high concentration of quaternary carbon atoms along the chain (e.g., polyisobutylene, poly(methyl methacrylate), poly(α-methylstyrene)) undergo primarily scission; polymers lacking this structural feature (e.g., polyethylene, polypropylene, polystyrene, natural rubber) undergo primarily crosslinking. This was attributed to the steric inhibition of radical-radical recombination following chain break, resulting in an increased yields of scission.

In the presence of oxygen, some of the free radicals combine with oxygen dissolved and/ or diffused in the polymers to initiate chain reactions and form thermally unstable products. These oxidative processes can be summarized in the following scheme[15]:

$$\text{Polyolefin (PH)} \xrightarrow{\gamma} \text{R}\cdot \xrightarrow{O_2} \text{RO}_2\cdot \qquad (10)$$

$$\text{RO}_2\cdot + \text{PH} \longrightarrow \text{ROOH} + \text{P}\cdot \qquad (11)$$

$$\text{P}\cdot + \text{O}_2 \longrightarrow \text{PO}_2\cdot \qquad (12a)$$

$$\text{PO}_2\cdot + \text{PH} \longrightarrow \text{POOH} + \text{P}\cdot \xrightarrow{O_2} \text{PO}_2\cdot \qquad (12b)$$

$$\text{RO}_2\cdot\ ,\ \text{PO}_2\cdot \longrightarrow \text{some chain scission products} \qquad (13)$$

$$\text{ROOH}\ ,\ \text{POOH} \xrightarrow{\text{R.T.}} \text{free radicals, ROH, POH} \qquad (14)$$

The oxidative process involves peroxyl radicals derived directly from radiation reactions (reaction 10) and also from the attack of these initial peroxyl radicals on polymer (reactions 11 and 12). The latter resulted in the formation of hydroperoxides (ROOH and POOH). Post-irradiation effects may be attributed to (i) trapped (i.e. long lived) free radicals produced by irradiation, which react slowly with the polymer molecules and with oxygen which diffuses into the polymer ; (ii) peroxides formed by irradiation in the presence of oxygen or oxygen trapped within polymers irradiated in vacuum or in an inert atmosphere, which slowly decompose to form reactive radicals, usually leading to scission; (iii) trapped gases in amorphous and crystalline polymers; and (iv) oxidation of double bonds and / or tertiary carbons [14]. For hard plastics with low gas permeation constants, radiation-

induced gaseous products result in subsequent crazing and cracking as gaseous products cannot escape the polymer matrix and begin to aggregate into bubbles. Radical lifetime strongly depends on temperature and can be hours or even weeks at room temperature. Less stable radicals can be observed to convert to more stable radicals with time. For instance, as secondary radicals, $-CH_2-\dot{C}H-CH_2-$, encounter double bonds in low concentration and abstract an allylic hydrogen atom, secondary radicals decay whereas allylic radicals, $-CH_2-\dot{C}H-CH=CH-$, appear. Usually, the decay time for radical intermediates is on the order of one day for alkyl radicals and several months for allyl radicals at 77 K. The polyene radicals are very stable even at room temperature [1]. In addition, free radicals formed in crystalline regions where oxygen solubility is very low have much lower mobility and longer lifetimes. Such radicals can migrate slowly to the amorphous region where oxygen dissolves, and subsequently react [4] . Post-irradiation reactions of free radicals can be observed by electron spin resonance (ESR) spectroscopy if the polymer is irradiated below T_g or T_m. Both types of hydroperoxide (ROOH and POOH) are believed to decompose slowly but steadily at room temperature to generate free radicals [16-17]. Post-irradiation effects depend on the reactivity of the radicals, the mobility of the matrix, and the diffusion of oxygen into the polymer. It was shown that diffusion-limited oxidation depended on material geometry coupled with the oxygen consumption rate in a material and the oxygen permeability coefficient [18]. This effect leads to a heterogeneity in oxidation across the material, with equilibrium oxidation (e.g., corresponding to air-saturated conditions) occurring at the sample surfaces and reduced or non-existent oxidation in the interior. Post-irradiation effects in polymer materials result in progressive reduction in strength, as well as, cracking and embrittlement. Reduction in these effects may be achieved by the annealing of trapped radicals, addition of appropriate scavengers, release of trapped gases, and control of the polymer morphology.

1.2 Radiation-Induced Changes in Polyethylene

Because of chemical simplicity and wide commercial application, the effects of high-energy irradiation on polyethylene have been extensively studied. The major effects of irradiation on polyethylene include crosslinking, main chain scission, double bond formation, and evolution of hydrogen [5-10]. The extent of chemical changes upon irradiation depends on molecular structure and the environment in which irradiation takes place. From the point of view of physical property changes, crosslinking and chain scission are the most important. Crosslinking occurs mainly by the recombination of two free radicals and increases the molecular weight of polyethylene, leading to network formation, a decrease in solubility, and improvement in physical properties such as memory effects (i.e., shape preservation as a crosslinked network is heated above its melting point and deformed and subsequently cooled to room temperature), creep and thermal resistance. Chain scission breaks up molecules and decreases molecular weight, resulting in mechanical property changes. If there is no simultaneous chain scission, 100% gel fraction can be obtained with high doses.

For polyethylene, crosslinking is the predominant result of high-energy irradiation. However, the distribution of crosslinks depends on morphology and cannot be random. There are two different crosslink models. One model developed by Keller et al. [19-26] suggests that radiation-induced crosslinking occurs preferentially at the fold surfaces of folded-chain lamellae or in the amorphous phase of bulk materials. The absence of crosslinks inside the crystal lattice at relatively low radiation doses had been ascribed to the fact that carbon atoms on adjacent chains are too far apart (4.1 Å) to allow a primary bond between adjacent chains, and the lattice is too rigid at room temperature to form typical interchain C-C bonds (1.54 Å) [23-24]. Based on a far-infrared study of PE before and after irradiation, Frank [27] observed that absorption due to a lattice vibration in the

crystalline regions did not change its intensity after irradiation, whereas, the background absorption increased, and suggested that no crosslinks were produced in the crystalline regions by the irradiation. The other model by Hosemann et al. [28-31] suggests that crosslinks are located primarily at defects within crystal cores, a suggestion based on the observation of an orthorhombic to hexagonal transition on irradiation of single crystals. The effect of a high dose of radiation on polyethylene crystals was found by Ungar and Keller [26] to produce an orthorhombic $\rightarrow$ hexagonal (o $\rightarrow$ h) phase transition on subsequent heating of the sample. The transition temperature $T_{o\rightarrow h}$ increased with crystal thickness and decreased with increasing radiation dose. Eventually , crystal destruction occurred as $T_{o\rightarrow h}$ approached the irradiation temperature, because of the higher radiation sensitivity of the hexagonal phase [26]. They also suggested that a change in preferred crosslinking location occurred, from at-the-fold at low dose to inside-the-crystal at doses beginning at about 500 to 800 Mrad [26,32].

The crosslinking efficiency of radiation in polyethylene, as assessed by network properties, depends on crystallization history [19-21,33-39]. Salovey and Keller [19] found that the gelation behavior of polyethylene single crystals strongly depends on interlamellar contact; the better the contact the more gel is produced for a given irradiation dose. In melt-crystallized bulk polyethylene, it was found that quenched material gave more gel [34], whereas, samples having a higher degree of crystallinity and/or higher long spacings gave less gel [35-37]. It was concluded that for bulk polyethylene, higher crystallization temperature and associated higher degree of crystallinity may result in better defined lamellae, thus more regular fold surfaces with less intermeshing between consecutive lamellae, consequently less chance for interlamellar links. This will affect the gel content. Figure 1.2 illustrates a crosslinking model in a chain folded polyethylene crystal layer [40]. If the layer is not in close contact with others, the crosslinks will occur within the same layer surface, thus a significant portion of them will be intramolecular and

ineffective for network formation (Fig. 1.2a). On the other hand, if consecutive layers are close enough, there will be a possibility of crosslinking between layers and these links will be intermolecular (Fig. 1.2b). Only intermolecular crosslinks are effective in gel formation.

The environment where irradiation takes place also affects the crosslinking efficiency. Mitsui et al. [41-43] studied the chemical aspects of polyethylene radiation-induced crosslinking in the presence of acetylene, and found that crosslinking was accelerated by acetylene. Ward et al. [44-45] investigated radiation-induced crosslinking of polyethylene in the presence of acetylene with fast electron irradiation. They found that the gel content of PE fiber irradiated in acetylene was much higher than for an equivalent dose in

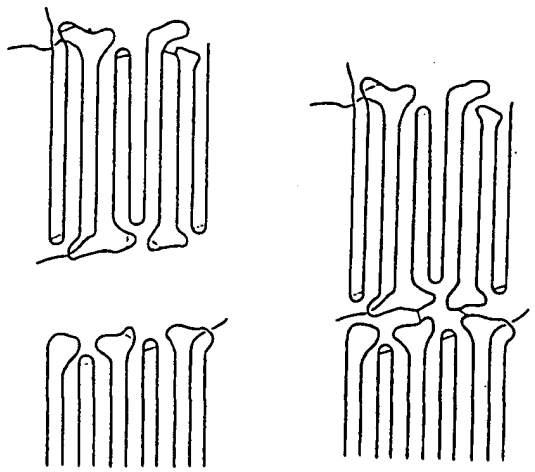

Figure 1.2. Diagrammatic illustration of a crosslinking model in a chain folded polyethylene crystal layer [40].

vacuum, and the creep rate at high stress for an acetylene treated sample was less than that of a sample irradiated to a similar gel content in vacuum. It was concluded that acetylene

radicals produced by irradiation diffuse into amorphous regions, and enhance crosslinking and reduce the significance of chain scission in the crystal [44]. The mechanism can be illustrated as follows [44]:

$$HC \equiv CH \xrightarrow{e^- \text{ beam}} H\dot{C}=\dot{C}H \qquad (15)$$

$$2 \sim\!CH_2\!\sim + H\dot{C}=\dot{C}H \longrightarrow \begin{matrix} \} \\ \dot{C}H\text{-}CH_2\text{-}CH_2\text{-}\dot{C}H \\ \} \end{matrix} \qquad (16)$$

Ultra-high molecular weight polyethylene (UHMWPE) exhibits excellent toughness and impact resistance [46-47], and wear and abrasion resistance [48-50], making it a good candidate for producing high tenacity fibers and a substitute for the thigh and the knee bone [51]. As a result of its extremely high molecular weight, the crystallinity of UHMWPE is much lower than that of conventional linear polyethylene. In addition to lower crystallinity, large concentrations of taut tie molecules must exist in UHMWPE. Taut tie molecules are parts of polyethylene chains that connect two crystals and result from the separate crystallization of parts of long polyethylene chains. A radiation-induced increase in crystallinity of UHMWPE was first reported by Roe et al. [52] in studies of UHMWPE used for medical prostheses. Subject to high-energy irradiation with gamma rays or electron beams, UHMWPE exhibits an increase in crystallinity [53-59]. It was suggested that irradiation-induced scission of taut tie molecules permitted recrystallization of broken chains from noncrystalline regions, and resulted in an increase in the degree of crystallinity and an increased perfection of existing folded-chain crystallites [53-59]. This effect is rather small in conventional HDPE, but quite pronounced in UHMWPE. It is attributed to the higher concentration of tie molecules in UHMWPE, which are more susceptible to the influence of high-energy irradiation [54,57,60]. In addition to radiation-induced chain scission, irradiation also produces a crosslinking effect which occurs preferentially in the

amorphous phase. Both scission and crosslinking are sensitive to the irradiation environment. If irradiated samples are melted and recrystallized, crosslinking inhibits crystal growth, resulting in a decreased crystallinity. Shinde and Salovey [56] found that if irradiated specimens were melted and recrystallized, radiation-induced scission in oxygen enhanced subsequent recrystallization, whereas radiation-induced crosslinking, which was dominant in a nitrogen atmosphere, suppressed recrystallization. Dijkstra et al. [61] found that degassed UHMWPE crosslinked in the melt at 200 °C, in a nitrogen atmosphere, by means of electron beam irradiation, revealed a gel fraction up to 100%, indicating that effectively no chain scission occurred in the absence of oxygen, suggesting that the radicals formed by chain scission recombined in a cage reaction.

Following irradiation, the aging of irradiated UHMWPE yields effects reported by Bhateja and coworkers [62-65]. Aging results in an increase in the heat of fusion with time at ambient temperature, but the peak melting temperature (T_m) decreases relative to initial post-irradiation values. It was suggested that the subsequent rise in crystallinity was caused by the slow growth of thin lamellae at ambient temperature, which was supported by the gradual development of a low-melting peak in the DSC thermogram [63-65]. The drop in T_m results from the reestablishment of a tie molecule population during the growth of new lamellae, which results in a T_m depression in the existing thick lamellae by the same strain-energy mechanism as existed before irradiation [63-65].

1.3 Peroxide-Initiated Crosslinking in Polyethylene

Since radiation-induced crosslinks are formed essentially in the amorphous regions in UHMWPE, irradiation crosslinking in the solid state produces a highly inhomogeneous network. It has been suggested that, in order to obtain a homogeneous network, crosslinking of UHMWPE should be performed in the melt state at temperatures above 150

°C, to avoid irregularities due to the presence of remnants of the initial solid state of polyethylene [66-67].

In contrast to energetic irradiation in air, chemical crosslinking does not involve molecular chain scission [66]. Chemical crosslinking of polyethylene can be achieved by peroxide crosslinking and by silane-grafted moisture crosslinking. Peroxide crosslinking reactions are accompanied by the decomposition of peroxide and abstraction of hydrogen atoms, and the resulting combination of alkyl radicals to produce carbon-carbon crosslinks [68-74]. The efficiency of peroxide crosslinking is determined by the ability to produce gel at a given peroxide concentration in polyethylene. Generally, the degree of crosslinking and gel content increase with increased peroxide concentration, whereas the crystallinity and peak melting temperature decrease when the peroxide concentration increases. Crosslinks suppress recrystallization from a cooled crosslinked melt. From the analysis of gel content, the gel content increases rapidly at an initial stage of irradiation and then slows down. This results because redundant crosslinks are formed between two molecules which are already crosslinked and the net increase in gel content will be lower [69]. Kunert et al. [75] studied the structure of chemically crosslinked low density polyethylene and found that different peroxides produced a slightly different topology of polyethylene networks. They concluded that crosslinking introduced only slight changes in the dimension of the crystals.

A wide variety of peroxides are available for reaction with polyolefins and investigations of their relative efficiencies have been reported [76-78]. Differences in decomposition rates are perhaps the main factor in selecting a particular peroxide for an intended application. Bremner et al. [78] compared three dialkyl peroxides on the basis of their ability to increase the gel content, crosslinking efficiency, and storage modulus of virgin polyethylene through a crosslinking mechanism and found that they decreased in the order α,α-bis(tertiary butylperoxy)-p-diisopropyl benzene > dicumyl peroxide > 2,5-dimethyl-2,5-di-(tertiary butylproxy)-hexyne-3 at the same active peroxide radical

concentrations and temperature. They concluded that low reaction temperatures favor chain-coupling reactions (i.e., crosslinking), whereas, increasing reaction temperatures tend to favor a beta-scission process involving alkoxy radical fragments and nongrowth disproportionation reactions [78].

Peroxide crosslinking of ultra-high molecular weight polyethylene has been reported [67,79-81]. Boer et al. crosslinked UHMWPE in the melt at 180 °C by means of 2,5-dimethyl-2,5-di-(tert-butylperoxy)-hexyne-3 and found that crosslinks and entanglements, whether trapped or not, contributed to the same degree to the decrease in crystallinity of UHMWPE upon crosslinking [79]. It was concluded that an almost completely crosslinked (or gelled)material with high crystallinity and good mechanical properties could be obtained by using as little as 0.2-0.3 wt% of peroxide. The scheme for the thermal decomposition of 2,5-dimethyl-2,5-di-(tert- butylperoxy)-hexyne-3 can be summarized as follows [82]:

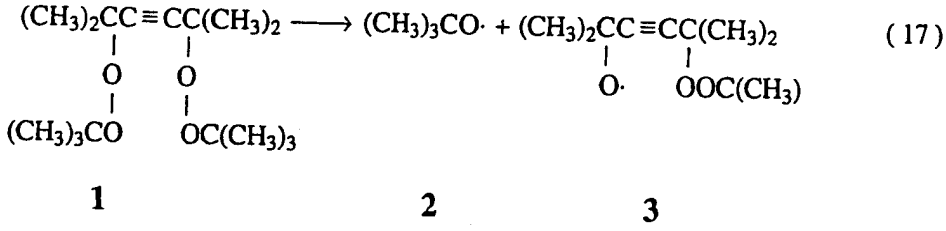

(17)

1 2 3

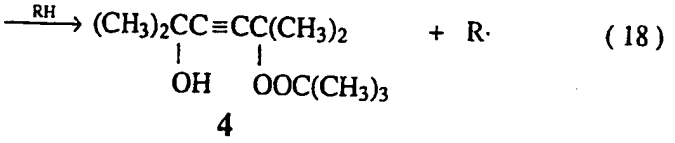

(18)

4

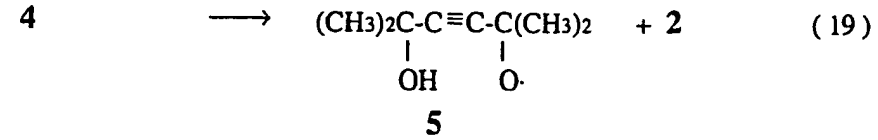

(19)

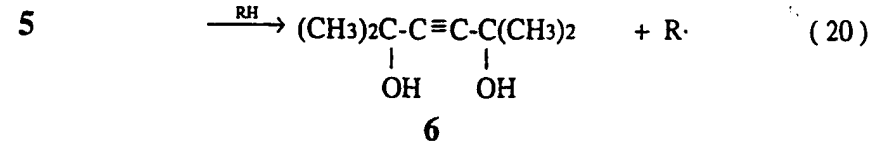

(20)

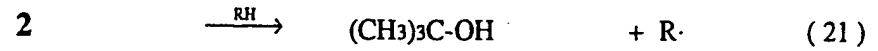

(21)

(22)

(23)

(24)

Narkis et al. [81] compared the effects of irradiation and peroxide crosslinking on three grades of polyethylene and concluded that (i) irradiation causes both crosslinking and chain scission, resulting in a gel content less than 100% even at relatively high irradiation doses, whereas, peroxide crosslinking leads to 100% gelation; (ii) crystal perfection and crystallinity are enhanced by irradiation due to scission of strained tie molecules in the amorphous phase, leading to additional crystallinity and crystal reorganization, whereas, peroxide crosslinking in the molten state followed by cooling to a semicrystalline solid results in a decreased crystallinity and depression of melting temperature; and (iii) peroxide crosslinking results in a more homogeneous network than that obtained by irradiation.

1.4 Silane-Grafted Moisture-Crosslinking in Polyethylene

In contrast to both peroxide and irradiation crosslinking methods, which produce carbon-carbon crosslinks, grafting of vinyl triethoxy silane onto the polyethylene backbone, followed by hydrolysis in an aqueous environment, gives rise to -C-Si-O-Si-C- crosslinks [83-84]. Both irradiation and siloxane crosslinking take place in the solid state while peroxide crosslinking is achieved above the polymer melting temperature, resulting in a homogeneous network and density reduction due to hindered crystallization of a crosslinked melt.

The grafting and crosslinking procedures are as follows [85]. Silane-grafting of polyethylene is carried out in the melt in a continuous compounding machine or in a batch operation using Banbury type internal mixers. The materials required for the grafting reaction include polyethylene, vinyl trialkoxysilane, and peroxide. The sole purpose of the peroxide is to initiate the grafting reaction. Compounding of such a mixture in the melt at high temperature causes thermal decomposition of the peroxide and grafting of alkoxysilyl groups to the polyethylene chains. When the shaped articles are exposed to hot water, steam or humid air, crosslinking occurs through condensation of the reactive Si-OR groups on adjacent polyethylene chains with the formation of a stable Si-O-Si crosslink. Since the crosslinking reaction occurs in the solid state at a temperature well below the melting temperature of polyethylene, the density of the crosslinked polyethylene is virtually the same as that of the parent polyethylene [84]. The schemes for grafting and crosslinking are summarized in the following [86]:

$$-CH_2-CH_2- \xrightarrow{\text{Peroxide, } \Delta} -CH_2-\dot{C}H- + H\cdot \qquad (25)$$

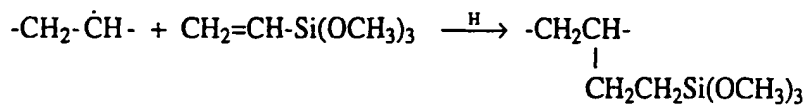

(26)

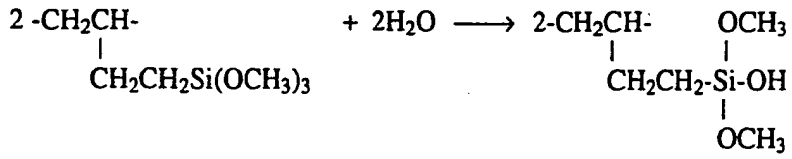

(27)

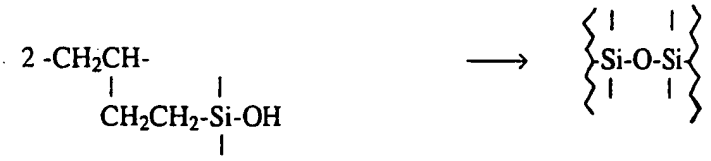

(28)

Although the grafted silane has three alkoxy groups present at each silicon atom, it is not probable that all of them react. Based on kinetic and thermodynamic considerations, the most probable hypothesis seems to be that, on average, only two of the three alkoxy groups react [86]. Therefore, four polyethylene chains are bound in each crosslinking point of the network by Si-O-Si bonds.

Salyer et al. [87] compared retention of the heats of fusion of polyethylenes crosslinked by various methods (i.e., irradiation, peroxide, and siloxane) and found that the siloxane crosslinking produced the highest percent retention of heat of fusion. This was attributed to the fact that the major portion of the hydrolysis crosslinking takes place at the surface, and only to a lesser extent in the interior of the specimen. It is important to note that silane-grafting moisture-crosslinking provides a very stable network due to the high bonding energy of the -Si-O-Si- crosslinks and the formation of a polyfunctional network, leading

[16] D. J. Carlsson, C. J. B. Dobbin, J. P. T. Jensen, and D. M. Wiles, *ACS Symposium Series* **280**, 359, 1985.

[17] D. J. Carlsson, C. J. B. Dobbin, and D. M. Wiles, *Macromolecules*, **18**, 2092 (1985).

[18] K. T. Gillen and R. L. Clough, "Quantitative Confirmation of Simple Theoretical Models for Diffusion-Limited Oxidation", *Radiation Effects on Polymers*, R. L. Clough and S. W. Shalaby, Eds., ACS Symposium Series **475**, Washington, D.C. , 1991.

[19] R. Salovey and A. Keller, *J. Bell System Tech.*, **40**, 1397, 1409 (1961).

[20] R. Salovey and D. C. Bassett, *J. Appl. Phys.*, **35**, 3216 (1964).

[21] T. Kawai, A. Keller, A. Charlesby, and M. G. Ormerod, *Phil. Mag.*, **12**, 657 (1965).

[22] T. Kawai and A. Keller, *Phil. Mag.*, **12**, 673 (1965).

[23] G. N. Patel and A. Keller, *J. Polym. Sci., Polym. Phys. Ed.*, **13**, 303 (1975).

[24] G. N. Patel and A. Keller, *J. Polym. Sci., Polym. Phys. Ed.*, **13**,323,333 (1975).

[25] H. Jenkins and A. Keller, *J. Macromol. Sci., Phys.* **B11**, 301 (1975).

[26] G. Ungar and A. Keller, *Polymer*, **21**, 1273 (1980).

[27] W. Frank, *J. Polym. Sci., Polym. Lett. Ed.*, **15**, 679 (1977).

[28] R. Hosemann, J. Loboda-Cackovic, and H. Cackovic, *J. Mater. Sci.*, **7**, 963 (1972).

[29] J. Loboda-Cackovic, H. Cackovic, and R. Hosemann, *Kolloid and Polym. Sci.*, **252**, 738 (1974).

[30] J. Loboda-Cackovic and H. Cackovic, *Kolloid Z Z Polym.*, **250**, 511 (1972).

[31] T. Nagasawa and K. Kobayashi, *J. Appl. Phy.*, **41**, 4276 (1970).

[32] G. Ungar, *J. Mater. Sci.*, **16**, 2635 (1981).

[33] R. Salovey, *J. Polym. Sci.*, **61**, 463 (1962).

[34] R. Salovey, *J. Polym. Sci. B*, **2**, 833 (1964).

[35] T. Kawai and A. Keller, *Phil. Mag.*, **14**, 1123 (1966).

[36] T. Kawai, A. Keller, A. Charlesby, and M. G. Ormerod, *Phil. Mag.*, **10**, 779 (1964).

[37] H. Jenkins and A. Keller, *J. Macromol. Sci. B*, **11**, 301 (1975).

[38] R. Salovey, "Single Crystals", *The Radiation Chemistry of Macromolecules*, **Vol. 2**, M. Dole, Ed., Academic Press, New York, 1973.

[39] M. Dole, *Polym. Plast. Technol. Eng.*, **13**, 41 (1979).

[40] A. Keller and G. Ungar, *Radiat. Phys. Chem.*, **22**, 155 (1983).

[41] H. Mitsui, F. Hosoi, and T. Kagiya, *Polym. J.*, **6**, 20 (1974).

[42] H. Mitsui and F. Hosoi, *Polym. J.*, **3**, 108 (1972).

[43] H. Mitsui and F. Hosoi, *Polym. J.*, **4**, 79 (1973).

[44] P. G. Klein, D. W. Woods, and I. M. Ward, *J. Polym. Sci., Polym. Phys. Ed.*, **25**, 1359 (1987).

[45] R. A. Jones, G. A. Salmon, and I. M. Ward, *J. Polym. Sci., Polym. Phys. Ed.*, **31**, 807 (1993).

[46] S. K. Bhateja, J. K. Rieke, and E. H. Andrews, *J. Mater. Sci.*, **14**, 2103 (1979).

[47] S. K. Bhateja, J. K. Rieke, and E. H. Andrews, *Ind. Eng. Chem. Prod. Res. Dev.*, **19**, 607 (1980).

[48] J. H. Dumbleton and C. Shen, *Wear*, **37**, 279 (1976).

[49] J. R. Atkinson, K. J. Brown, and D. Dowson, *J. Lub. Technol.*, **100**, 208 (1978).

[50] S. K. Bhateja, *Polymer*, **22**, 23 (1981).

[51] A. M. Grugnola, E. L. Radin, R. M. Rose, J. L. Paul, S. R. Simon, and M. B. Berry, *J. Appl. Polym. Sci.*, **20**, 809 (1976).

[52] R. J. Roe, E. S. Grood, R. Shastri, C. A. Gosselin, and F. R. Noyes, *J. Biomed. Mater. Res.*, **15**, 209 (1981).

[53] S. K. Bhateja, *J. Macromol. Sci. Phys.*, **B 22**, 159 (1983).

[54] S. K. Bhateja, E. H. Andrews, and R. J. Young , *J. Polym. Sci., Polym. Phys. Ed.*, **21**, 523 (1983).

[55] I. Kamel and L. Finegold, *J. Polym. Sci., Polym. Phys. Ed.*, **23**, 2407 (1985).

[56] A. Shinde and R. Salovey, *J. Polym. Sci., Polym. Phys. Ed.*, **23**,1681 (1985).

[57] S. K. Bhateja and E. H. Andrews, *J. Mater. Sci.*, **20**, 2839 (1985).

[58] S. Sawatari, H. Nishikido, and M. Matsuo, *Colloid Polym. Sci.*, **266**, 316 (1988).

to excellent mechanical and aging properties of cured polymers [88]. Atkinson et al. [89-90] investigated the creep and wear behavior of silane crosslinked high density polyethylene and compared these properties with those of UHMWPE. The conclusions were as follows.

(i) In dry, reciprocating wear tests against steel counterfaces, there is no significant difference in the wear rates for silane crosslinked HDPE and for UHMWPE. For UHMWPE, the wear rate is independent of applied load up to a load of 100 N but increases significantly when the applied load is 140 N. For the silane crosslinked HDPE, the wear rates are independent of applied load over the load range studied and markedly lower than the non-crosslinked UHMWPE at the highest load (140 N).

(ii) Microscopy shows that silane crosslinked HDPE wears in a somewhat similar fashion than UHMWPE. However, wear surfaces of silane crosslinked HDPE are cleaner and less deformed, with no evidence of fatigue cracks.

(iii) Creep results show that silane crosslinked HDPE is more resistant to creep deformation than UHMWPE and particularly so at higher temperatures. Creep studies also show that the higher the degree of crosslinking, the lower the creep strain and the lower the final, steady, creep rate.

(iv) There is no reason to think that the silane crosslinking agent will impart any degree of toxicity to the final product.

1.5 References

[1] V. D. McGinniss, "Crosslinking with Radiation", *Encyclopedia of Polym. Sci. & Eng.*, **Vol. 4**, 418 (1985).

[2] E. Reichmanis, *"Radiation Chemistry of Polymers for Electronic Applications"*, The Effects of Radiation on High-Technology Polymers", E. Reichmanis and J. H. O'Donnell, Eds., ACS Symposium Series **381**, Washington, D. C., 1989.

[3] R. A. Pethrick, *"Microlithography"*, *Irradiation Effects on Polymers*, D. W. Clegg and A. A. Collyer, Eds., Elsevier Applied Science, New York, 1991.

[4] R. L. Clough, K. T. Gillen, J. L. Campan, G. Gaussens, H. Schonbacher, T. Seguchi, H. Wilski, and S. Machi, *Nucl. Safety*, **25**, 146 (1984).

[5] A. Charlesby, *"Atomic Radiation of Polymers"*, Pergamon, London, 1960.

[6] O'Donnell and Sangster,*"Principles of Radiation Chemistry"*, Edward Arnold, London, 1970.

[7] A. Charlesby, in *"Irradiation Effects on Polymers"*, D. W. Clegg and A. A. Collyer, Eds. , Elsevier Applied Science, New York, 1991.

[8] A. Chapiro, *"Radiation Chemistry of Polymeric Systems"*, High Polymers, **Vol. 15**, Interscience, New York, 1962.

[9] M. Dole, Ed., *"The Radiation Chemistry of Macromolecules"*, **Vol. 1**, Academic Press, New York, 1972.

[10] M. Dole, Ed., *"The Radiation Chemistry of Macromolecules"*, **Vol. 2**, Academic Press, New York, 1973.

[11] E. Reichmanis and J. H. O'Donnell, Eds., *"The Effects of Radiation on High-Technology Polymers"*, ACS Symposium Series **381**, Washington, D. C., 1989.

[12] R. L. Clough and S. W. Shalaby, Eds., *"Radiation Effects on Polymers"*, ACS Symposium Series **475**, Washington, D. C., 1991.

[13] E. Reichmanis, C. W. Frank, and J. H. O'Donnell, Eds., *"Irradiation of Polymeric Materials"*, ACS Symposium Series **527**, Washington, D. C., 1993.

[14] J. H. O'Donnell, "Radiation Chemistry of Polymers", *The Effects of Radiation on High-Technology Polymers*, E. Reichmanis and J. H. O'Donnell, Eds., ACS Symposium Series **381**, Washington, D. C., 1989.

[15] D. J. Carlsson, S. Chmela, and J. Lacoste, "Stabilization of Polyolefins to Gamma Irradiation", *Radiation Effects on Polymers*, R. L. Clough and S. W. Shalaby, Eds., ACS Symposium Series **475**, Washington, D. C., 1991.

[59] Y. Zhao, Y. Luo, and B. Jiang, *J. Appl. Polym. Sci.*, **50**, 1797 (1993).

[60] L. Minkova, *Colloid Polym. Sci.*, **266**, 6 (1988).

[61] D. J. Dijkstra, W. Hoogsteen, and A. J. Pennings, *Polymer*, **30**, 866 (1989).

[62] S. K. Bhateja, *Polymer*, **23**, 654 (1982).

[63] S. K. Bhateja, *J. Appl. Polym. Sci.*, **28**, 861 (1983).

[64] S. K. Bhateja, E. H. Andrews, and S. M. Yarbrough, *Polym. J.*, **21**,739 (1989).

[65] S. K. Bhateja, S. M. Yarbrough, and E. H. Andrews, *J. Macromol. Sci. Phys.* **B 29**, 1 (1990).

[66] A. Posthuma de Boer and A. J. Pennings, *J. Polym. Sci., Polym. Phys. Ed.*, **14**, 187 (1976).

[67] J. de Boer and A. J. Pennings, *Makromol. Chem. Rapid Commun.*, **2**, 749 (1981).

[68] M. Narkis and J. Miltz, *J. Appl. Polym. Sci.*, **13**, 713 (1969).

[69] T. R. Manley and M. M. Qayyum, *Polymer*, **12**, 176 (1971).

[70] G. E. Hulse, R. J. Kersting, and D. R. Warfel, *J. Polym. Sci., Polym. Chem. Ed.*, **19**, 655 (1981).

[71] Y. H. Kao and P. J. Phillips, *Polymer*, **27**, 1669 (1986).

[72] A. J. Peacock, *Polym. Commun.*, **28**, 259 (1987).

[73] A. K. Mukherjee, P. K. Tyagi, and B. D. Gupta, *Angew. Makromol. Chemie*, **173**, 205 (1989).

[74] T. Bremner, A. Rudin, and S. Haridoss, *Polym. Eng. Sci.*, **32**, 939 (1992).

[75] K. A. Kunert, H. Soszynska, and N. Pislewski, *Polymer*, **22**, 1355 (1981).

[76] K. W. Lem and C. D. Han, *J. Appl. Polym. Sci.*, **27**, 1367 (1982).

[77] E. M. Kampouris and A. G. Andreopoulos, *J. Appl. Polym. Sci.*, **34**, 1209 (1987).

[78] T. Bremner and A. Rudin, *J. Appl. Polym. Sci.*, **49**, 785 (1993).

[79] J. de Boer and A. J. Pennings, *Polymer*, **23**,1944 (1982).

[80] J. de Boer, H. J. van den Berg, and A. J. Pennings, *Polymer*, **25**, 513 (1984).

[81] M. Narkis, I. Raiter, S. Shkolnik, A. Siegmann, and P. Eyerer, *J. Macromol. Sci. Phys.*, **B 26**, 37 (1987).

[82] F. Tang and E. S. Huyser, *J. Org. Chem.*, **42**, 2160 (1977).

[83] H. G. Scott, *U. S. Pat.* **3,646,155** (1972).

[84] H. G. Scott and J. F. Humphries, *Modern Plastics*, **50**, 82, Mar. (1973).

[85] M. Narkis, A. Tzur, A. Vaxman, and H. G. Fritz, *Polym. Eng. Sci.*, **25**, 857 (1985).

[86] D. Munteanu, "Moisture-Crosslinkable Silane-Grafted Polyolefins", in *Metal-Containing Polymeric Systems*, J. E. Sheats, C. E. Carraher, and C. U. Pittman, Eds., Plenum Press, New York, 1985.

[87] I. O. Salyer and J. E. Davison, *J. Appl. Polym. Sci.*, **28**, 2903 (1983).

[88] S. Cartasegna, *Rubber Chem. Technol.*, **59**, 722 (1986).

[89] J. R. Atkinson and R. Z. Cicek, *Biomaterials*, **4**, 267 (1983).

[90] J. R. Atkinson and R. Z. Cicek, *Biomaterials*, **5**, 326 (1984).

CHAPTER 2

EFFECT OF IRRADIATION ON ULTRA-HIGH MOLECULAR WEIGHT POLYETHYLENE CROSSLINKED WITH 2,5-DIMETHYL-2,5-BIS(TERT-BUTYLPEROXY)-3-HEXYNE: PRELIMINARY CHARACTERIZATION- DSC, SWELLING, AND FTIR MEASUREMENTS

The aim of this study is to investigate the effects of irradiation on chemically crosslinked ultra-high molecular weight polyethylene (UHMWPE). It deals with the synthesis and characterization of networks, by means of differential scanning calorimetry (DSC), sol-gel analysis, equilibrium swelling, and FTIR measurements. Wide angle x-ray scattering (WAXS), surface morphology, permanganic etching, and mechanical characterization will be reported in subsequent sections.

2.1 Experimental Details

2.1.1 Sample Preparation

Commercial-grade UHMWPE is GUR 415 (from Hoechst), with a weight average molecular weight of 6×10^6, which is used as received. The peroxide is 2,5-dimethyl-2,5-bis(tert-butylperoxy)-3-hexyne(Lupersol 130, Atochem Inc.). The reason for choosing

Lupersol 130 is because of its long half-life at elevated temperature. The peroxide will decompose slowly and the resulted free radicals can diffuse in specimen to form a homogeneous network at elevated temperatures. Half-lives of the peroxide in dodecane at different temperatures are summarized in Table 2.1 [1]. Mixing of the UHMWPE and the peroxide was accomplished by dispersing polyethylene powder in an acetone solution of the peroxide and subsequently evaporating the solvent [2-3]. Networks were synthesized by compression molding the mixed powder into 1 mm thick circular disks in a Dake press. Specimens were compressed in 1 mm thick circular mold between two stainless-steel plates at 170 °C and ram pressure 7.5 x 10^3 kPa for 2 h. The half-life time of peroxide at 170 °C in dodecane is about 9 min [1]. After 2 h, pressure was increased to 15 x 10^3 kPa to avoid cavities inside the polymer and specimens were slowly cooled in the press to room temperature. Quench-crystallized specimens were prepared by dropping the molten specimens into liquid nitrogen.

The specimens were irradiated with γ-rays at room temperature in air by SteriGenics International (Tustin, CA). Cobalt-60 was used as a source of gamma irradiation. The radiation doses were delivered at a dose rate of 5 kGy/hr. Specimens received doses up to 34 kGy (3.4 Mrad).

Table 2.1. Half-lives of the peroxide (Lupersol 130) in dodecane

Temp. (°C)	150	160	170	180	190	200	210
Half-life (min)	72.4	25.4	9.4	3.6	1.4	0.6	0.3

2.1.2 Differential Scanning Calorimetry

Samples (7-10 mg) were melted at a heating rate of 10 °C/min in a differential scanning calorimeter (Perkin-Elmer DSC-4). After being heated to 170 °C, samples were recrystallized in DSC by cooling at 10 °C/min to 50 °C and then remelted by reheating at 10 °C/min to 170 °C. Indium was used for calibration of temperature and heat of fusion. The heat of fusion was determined by comparing the area under the melting endotherm with the area of fusion of an Indium sample having a known heat of fusion of 6.8 cal/g [4]. The degree of crystallinity C was calculated as [5]

$$C = \frac{h_f}{h_f^{'}} \qquad (1)$$

where $h_f^{'} = 292$ J/g is the heat of fusion of the ideal polyethylene crystal [6].

2.1.3 Swelling Measurements

Sol-gel measurements and equilibrium swelling were conducted using a method reported by de Boer and Pennings [2-3]. Extraction of the sol-fraction was performed in stirred, boiling p-xylene for 72 h. 0.5 wt% of anti-oxidant (2,6-di-t-butyl-4-methyl phenol) was added to prevent oxidation. After extraction, the gel was transferred to fresh p-xylene and allowed to equilibrate at 120 °C for 2 h. The swollen gel was then picked up and quickly transferred to a weighing bottle, covered and weighed. The data were obtained as the average of five measurements. Samples were then deswollen in acetone and dried at 60 °C in a vacuum oven to constant weight. The gel fraction was determined from the ratio of the weight of the dried extracted to the initial dry non-extracted network. The degree of swelling (q) can be calculated according to the expression:

$$q = \frac{\text{wt. of swollen gel}}{\text{wt. of dried extracted gel}} \qquad (2)$$

The equilibrium degree of swelling, q, was used to calculate the network chain density, υ^*, using the theory of Flory and Rehner [7]:

$$\upsilon^* = -\frac{\ln(1-q^{-1}) + q^{-1} + \chi q^{-2}}{V_1(q^{-1/3} - 0.5q^{-1})} \qquad (3)$$

where q is the equilibrium degree of swelling; V_1 is the partial molar volume of the swelling solvent; and χ is the Flory-Huggins interaction parameter between solvent and polymer. For p-xylene at 120 °C, V_1 = 136 ml/mol and with polyethylene χ = 0.37 according to the literature [2]. The number-average molecular weight between crosslinks, $\overline{M_c}$, was calculated according to

$$\frac{1}{\overline{M_c}} = \upsilon^* \cdot V \qquad (4)$$

where V is the specific volume of crosslinked polyethylene. The crosslink density, XLD, is defined as the mole fraction of crosslinked units [7]:

$$\text{XLD} = \frac{M_o}{\overline{M_c}} \qquad (5)$$

where M_o is the molecular weight of the polymer repeat unit. For polyethylene M_o = 14.

2.1.4 Fourier Transform Infrared Spectroscopy (FTIR)

200 μm thick specimens were used for FTIR analysis. Specimens were prepared by compression molding UHMWPE powder in 200 μm thick rectangular mold in a Dake press. Specimens were compressed between two stainless-steel plates at 170 °C and ram pressure 7.5×10^3 kPa for 2 h, and subsequently slowly cooled to room temperature. For chemically crosslinked specimens, 1 and 2 wt% peroxide were used. The specimens were irradiated with γ-rays at room temperature in air, up to 34 kGy. Examination of carbonyl group (1713 cm^{-1}) concentrations was performed using Mattson polaris FTIR (model IR 10410) with a Spectra-Tech IR plan microscope. Spectra were measured by transmission mode with a microscope at a resolution of 16 cm^{-1}.

2.2 Results and Discussion

On heating in DSC at 10 °C/min, nascent UHMWPE powder (GUR 415) showed a single sharp melting endotherm. The peak melting temperature and crystallinity were 141 °C and 63%, respectively. Heating up to 170 °C and then recrystallizing on cooling at 10 °C/min back to 50 °C, a crystallization exotherm at 116 °C was observed. Subsequently, a second melting at a heating rate of 10 °C yielded a single broad melting endotherm. The peak melting temperature and crystallinity dropped to 130.9 °C and 47.7%, respectively. From the high melting point and crystallinity, it was suggested that nascent UHMWPE was in an extended chain crystal form [8-14]. On cooling and reheating in DSC, the melting point and crystallinity decreased, suggesting that a folded-chain crystal was obtained and the crystal size was significantly reduced. It was reported that nascent UHMWPE exhibited the phenomenon of superheating above the equilibrium melting point of the polymer [9-10]. The superheating of the transition at 145 °C suggested that the crystalline structure

should be in the extended-chain form because, generally, the chain-fold morphology did not show appreciable superheating [9-10]. By optical microscopy, Zachariades et al. [9] also observed that the melt of UHMWPE was highly anisotropic above its equilibrium melting point and concluded that the melt had not been randomized completely.

Since crystallization on cooling the melt takes place when the polymer is a viscous liquid, and in this state the chains are highly entangled, sufficient time must be allowed for the chains to diffuse into the three-dimensional order required for crystallite formation. This suggests that the crystallinity and crystalline perfection of the sample are dependent on the thermal history [15]. For a compression molded, slowly cooled sample, first melting in DSC showed a peak melting temperature at 132.6 °C and a crystallinity of 49.2%. The depression of melting point and crystallinity, compared with those of nascent UHMWPE, was attributed to the formation of folded chain crystals. On cooling in DSC, the sample recrystallized at 115.5 °C. A subsequent second melting showed a peak melting temperature at 131 °C and a crystallinity of 47%. The decrease in peak melting temperature and crystallinity for a subsequent second melting is due to thermal history. The cooling rate in the press was about 2 °C/min, whereas, in DSC, it was 10 °C/min. The higher the crystallization temperature (low supercoolings), the higher the crystal perfection (higher melting temperature) and crystallinity. For quench crystallized UHMWPE, the peak melting temperature and crystallinity on first melting were 129.3 °C and 44.2%, respectively. On cooling in DSC, the sample recrystallized at 115.2 °C. Following reheating at 10 °C/min, the peak melting temperature and crystallinity were increased to 131.2 °C and 49.1%, respectively. The depression of first melting point and crystallinity of quench crystallized sample, compared with those of slowly cooled sample, suggested that rapid cooling from the melt resulted in further crystal imperfection and prevented the development of significant crystallinity. Annealing (i.e., first melting in DSC) resulted in an improvement of crystal perfection and an increase in the size of crystallites. Therefore, the second

melting point and crystallinity in the quench crystallized sample were higher than those in the first melting. It was suggested that cooling rate, heating rate, and annealing affected crystal perfection and crystallinity. In addition, from the melting behavior of slowly cooled and quench crystallized samples after two heating cycles, we note that crystallization during the DSC scan at 10 °C/min is faster than slow-cooling but slower than quenching.

Effect of Peroxide Crosslinking on Thermal Properties

The degree of crystallinity and peak melting temperatures of the first and second melting, and recrystallization temperatures of chemically crosslinked UHMWPE with varied peroxide concentrations, which had been cooled slowly from 170 °C to room temperature, are tabulated in Table 2.2. The effects of quenching on crystallinity, peak melting temperatures, and recrystallization are listed in Table 2.3. As shown in Table 2.2, the degree of crystallinity at the first melting decreased systematically with increasing peroxide concentrations. For example, the degree of crystallinity at 0.2 wt% peroxide was 44%, and dropped to 36.5% at 2 wt% peroxide. The peak melting temperatures of first and second melting, and recrystallization temperatures also decreased with increasing peroxide concentrations. As shown in Table 2.3, for quench crystallized samples, the degree of crystallinity at the first melting, peak melting temperatures of first and second melting, and recrystallization temperatures decreased with increasing peroxide concentrations. The decrease of recrystallization temperature with increasing peroxide concentrations in both slowly cooled and quench crystallized samples can be attributed to the inhibition of crystal growth by peroxide induced crosslinks. It was observed that in slow-cooled samples, the peak melting temperature of first melting was slightly higher than that of second melting because cooling in DSC was faster than slow cooling in the press. For quench crystallized samples, the first melting temperature was slightly lower than or equal to the second one (at

Table 2.2. Thermal properties of **slowly cooled** samples with varied peroxide concentration. **Before irradiation**

Wt% Peroxide	Peak Melting Temp. (°C) (1st melting)	Peak Melting Temp. (°C) (2nd melting)	Recrystalliz-ation Temp. (°C)	Crystallinity (%) (1st melting)	Crystallinity (%) (2nd melting)
original powder (GUR 415)	140.8	130.9	115.9	63.0	47.7
0	132.6	131.0	115.5	49.2	47.0
0.2	129.6	128.1	114.7	44.0	43.4
0.4	126.1	125.1	113.2	41.6	43.0
0.6	125.5	124.1	112.1	41.3	41.8
0.8	123.8	122.6	111.3	40.0	41.5
1.0	122.3	121.2	110.1	39.8	42.0
1.5	116.4	115.5	104.5	36.8	37.7
2.0	114.7	113.7	102.0	36.5	37.5

Table 2.3. Thermal properties of **quench crystallized** samples with varied peroxide concentration. **Before irradiation**

Wt% Peroxide	Peak Melting Temp. (°C) (1st melting)	Peak Melting Temp. (°C) (2nd melting)	Recrystalliz-ation Temp (°C)	Crystallinity (%) (1st melting)	Crystallinity (%) (2nd melting)
0	129.3	131.2	115.2	44.2	49.1
0.2	127.6	128.5	114.8	42.8	45.5
0.4	125.2	126.0	113.6	42.1	45.3
0.6	124.6	125.1	113.0	40.9	43.2
0.8	124.2	124.6	112.0	40.1	42.6
1.0	121.3	121.3	110.5	40.0	42.9
1.5	116.2	116.2	104.7	36.1	38.2
2.0	114.9	114.9	102.6	35.9	38.6

peroxide > 1 wt%). This is because a melting cycle in DSC results in an improvement of crystal perfection and an increase in the size of crystallites for quenched samples with low crosslinking. Here, cooling in DSC was slower than quench cooling. Comparing Table 2.2 with Table 2.3, it was shown that the effect of quenching on the crystallinity (first melting) of the crosslinked network was not significant, especially at high peroxide concentrations.

Peroxide crosslinking reactions are accompanied by the decomposition of peroxide and abstraction of hydrogen atoms, and the resulting combination of alkyl radicals to produce carbon-carbon crosslinks. Generally, this reaction was performed above the melting temperature of the polymer. Thus the crosslinking step preceded the crystallization step. It was suggested that crystallization from a crosslinked melt produced an imperfect crystal, and crosslinks suppressed crystal growth, resulting in the depression of melting temperature and a decreased crystallinity [16-29]. Flory [30-31] suggested that the melting point depression of a crosslinked polymer was due to a reduction in concentration of segments of a length suitable for crystallization. The relationship between the melting point depression and average molecular weight between crosslinks will be discussed later.

In slow-cooled samples, the first melting temperature was slightly higher than that of second melting. This can be explained as a result of the difference in thermal history. In the slow-cooling process, the cooling rate was about 2 °C/min, whereas the cooling rate in DSC was 10 °C/min. Lower supercooling will lead to a higher crystal perfection and the formation of larger crystallites. In quench crystallized samples, that the second melting temperature was slightly higher than the first one can be explained as a result of heating in DSC. Therefore, it was observed that the crystallinity of second melting was slightly higher than that of first melting. As peroxide concentration increased, however, the difference in melting temperatures between first and second melting became smaller, and eventually they were equal (e.g., above 1 wt% peroxide). We suggest that the reason for this behavior is that quenching produced smaller crystals and resulted in a more homogeneous network at

high peroxide concentration. In addition, it is known that small lamellae will thicken on heating to the melting temperature and give a higher melting temperature. However, for highly crosslinked network, recrystallization will be hindered and crystal thickness is suppressed by the crosslinks [32-33]. Since the melting temperature in DSC is a measure of size and perfection of the crystal, annealing (i.e., first melting in DSC) does not improve crystal perfection of quench crystallized samples with higher peroxide concentrations (above 1 wt% peroxide). Figure 2.1 illustrates the crystallinity of first melting in slowly cooled and quench crystallized samples with varied peroxide concentrations. Above 0.6 wt% peroxide, we found that the degree of crystallinity for these two kinds of samples were almost the same. This is because peroxide crosslinking inhibits molecular chain motions so that the effect of quenching will be reduced when sufficient crosslinks are introduced. Comparison of first melting temperatures between slowly cooled and quench crystallized samples with varied peroxide concentrations was shown in Figure 2.2. It was observed that after crosslinking, the difference in melting temperature became smaller. Indeed, at high peroxide concentrations, they were equal. It was suggested that at higher peroxide concentrations, quenching had no significant effect on crystallinity and on the melting temperature of a crosslinked network. Again, this is because peroxide crosslinking inhibits molecular chain motions so that the effect of quenching will be reduced when sufficient crosslinks are introduced. On the other hand, at low peroxide concentrations, the peak melting temperatures of first melting for quench crystallized samples were systematically lower than those of slowly cooled samples. This indicates that quenching produces smaller and more imperfect crystals, compared to slow-cooling process.

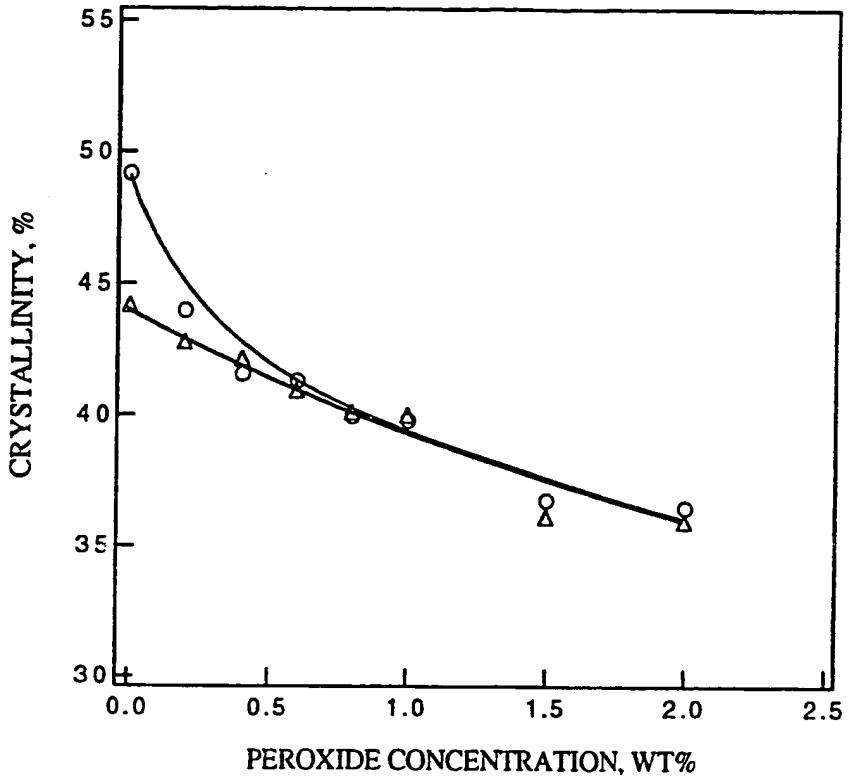

Figure 2.1. Comparison of crystallinity of first melting between slowly cooled (o) and quench crystallized (Δ) samples with varied peroxide concentration. **Before irradiation.**

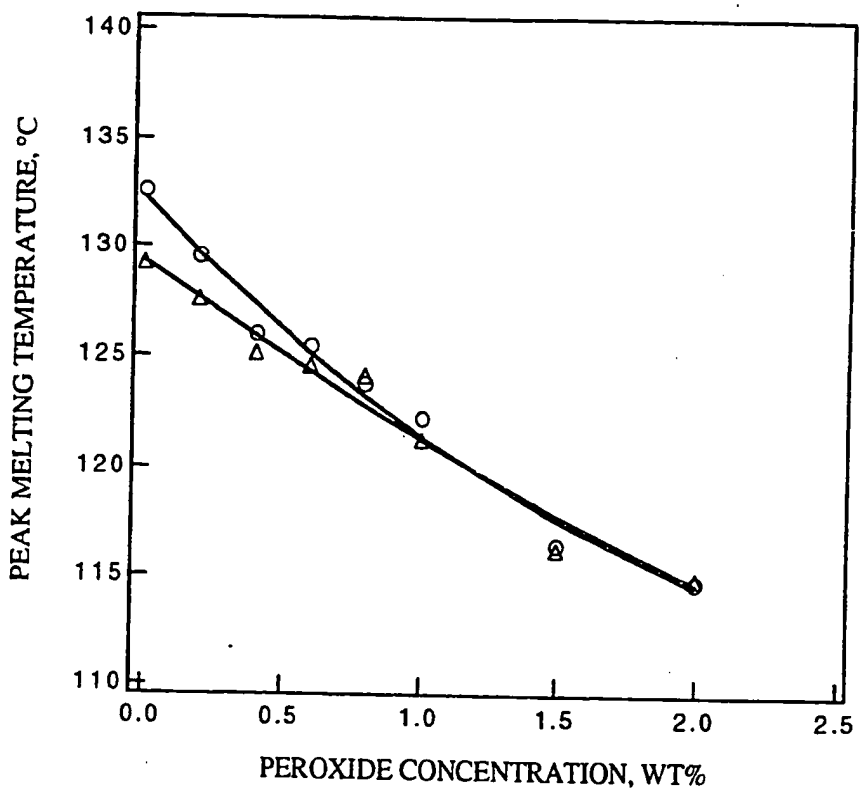

Figure 2.2. Comparison of first melting temperature between slowly cooled (○) and quench crystallized (Δ) samples with varied peroxide concentration. **Before irradiation.**

Effect of Irradiation on the Thermal Properties of a Crosslinked Network

The degree of crystallinity and peak melting temperatures of first and second melting, and recrystallization temperatures after irradiation, for slowly cooled and quench crystallized samples, are shown in Table 2.4 and Table 2.5, respectively. After exposure to high energy irradiation (3.4 Mrad), both slowly cooled and quench crystallized samples (before peroxide crosslinking) exhibit an increase in degree of crystallinity and peak melting temperature of first melting, in agreement with literature [28,34-43]. It was suggested that irradiation-induced scission of taut tie molecules permits recrystallization of broken chains from the noncrystalline regions, and results in an increase in the degree of crystallinity and an increased perfection of existing folded chain crystallites [28,35-43]. It was found that this effect was rather small in conventional HDPE, but quite pronounced in UHMWPE [28,36,39-40]. This was attributed to the higher concentration of tie molecules in UHMWPE, which are more susceptible to the influence of high-energy irradiation. In addition to radiation-induced chain scission, irradiation also produces crosslinking. It was shown that in the slowly cooled sample (before peroxide crosslinking), the degree of crystallinity and peak melting temperature of the second melting decreased compared to those of first melting. It was suggested that if irradiated samples were melted and recrystallized, crosslinks inhibited crystal growth, resulting in a decreased crystallinity and depression of melting temperature [28,38]. This effect was not observed in the quench crystallized sample (before peroxide crosslinking).

Comparison of recrystallization temperatures before and after irradiation for both slowly cooled and quench crystallized samples (before peroxide crosslinking) showed that after irradiation, recrystallization temperature decreased in both cases. Comparison of peak melting temperatures of second melting before and after irradiation for both slowly cooled

and quench crystallized samples (before peroxide crosslinking) showed the same trend as recrystallization temperature. For slowly cooled sample (before peroxide crosslinking), recrystallization temperature dropped from 115.5 (before irradiation) to 114.6 °C (after irradiation), whereas, second melting temperature dropped from 131 (before irradiation) to 130.6 °C (after irradiation). For quench crystallized samples (before peroxide crosslinking) recrystallization temperature dropped from 115.2 (before irradiation) to 114 °C (after irradiation), whereas, second melting temperature dropped from 131.2 (before irradiation) to 130.6 °C (after irradiation). This is because irradiation-induced crosslinking inhibits crystal growth from the melt, resulting in crystal imperfection and lower recrystallization temperature. The decrease in recrystallization temperature after irradiation also corresponds to the decrease in second melting temperature after irradiation for both samples (before peroxide crosslinking) because melting temperature in DSC is a measure of size and perfection of crystals, implying that crystallization from a crosslinked melt produces smaller and imperfect crystals.

Radiation-induced crosslinking had been suggested to occur preferentially at the fold surfaces of folded-chain lamellae or in the amorphous phase of bulk materials [32,44-52]. The absence of crosslinks inside the crystal lattice at relatively low radiation doses was ascribed to the fact that carbon atoms on adjacent chains are too far apart (4.1 Å) to allow a primary bond between adjacent chains, and the lattice is too rigid at room temperature to form typical interchain C-C bonds (1.54 Å) [47-48]. Since radiation-induced crosslinks are formed essentially in the amorphous regions in UHMWPE, irradiation crosslinking in the solid state produces a highly inhomogeneous network. In contrast to irradiation crosslinking, peroxide crosslinking occurs in the molten state. It was suggested that, in order to obtain a homogeneous network, crosslinking of UHMWPE should be performed at temperatures above 150 °C or higher, to avoid irregularities due to the presence of remnants of the initial solid state of polyethylene [2-3].

Table 2.4. Thermal properties of **slowly cooled** samples with varied peroxide concentration. **After irradiation**

Wt% Peroxide	Peak Melting Temp. (°C) (1st melting)	Peak Melting Temp. (°C) (2nd melting)	Recrystalliz-ation Temp (°C)	Crystallinity (%) (1st melting)	Crystallinity (%) (2nd melting)
0	135.0	130.6	114.6	55.8	50.8
0.2	133.1	129.2	114.3	50.0	49.0
0.4	129.2	126.9	114.0	46.8	44.2
0.6	128.7	126.4	114.0	46.2	45.4
0.8	126.6	124.1	111.9	45.0	43.8
1.0	125.1	122.7	110.9	42.0	42.6
1.5	119.1	117.3	105.3	36.8	38.2
2.0	116.8	115.3	103.6	36.7	38.0

Table 2.5. Thermal properties of **quench crystallized** samples with varied peroxide concentration. **After irradiation**

Wt% Peroxide	Peak Melting Temp. (°C) (1st melting)	Peak Melting Temp. (°C) (2nd melting)	Recrystalliz-ation Temp (°C)	Crystallinity (%) (1st melting)	Crystallinity (%) (2nd melting)
0	130.0	130.6	114.0	49.8	53.4
0.2	129.7	129.9	113.4	47.3	50.0
0.4	127.0	127.5	113.2	46.1	48.2
0.6	126.8	126.6	113.0	45.4	47.2
0.8	125.5	125.2	113.3	44.8	48.2
1.0	123.3	123.0	110.2	43.2	48.4
1.5	117.0	116.7	104.7	36.6	39.5
2.0	116.5	116.0	104.0	37.3	39.7

Comparison of melting temperatures (first melting) before and after irradiation as a function of peroxide concentration, for slowly cooled and quench crystallized samples, is shown in Fig. 2.3 and Fig. 2.4, respectively. It was shown that after irradiation the first melting temperature of the network increased in both cases. This effect was explained as a result of an improvement in crystal perfection because of chain scission. It is believed that irradiation-induced scission of taut tie molecules will release constraints on the crystalline region (particularly on the lamellar or fold surfaces) and hence crystal perfection is improved. However, slow-cooled samples showed a slightly higher increase than quench crystallized samples. This could be due to the retention of highly entangled chains in the quench process. It was reported that UHMWPE contained a high concentration of entanglements even after melting [41,53]. A quenching process will prevent the chains from disentangling. Comparison of crystallinity (first melting) before and after irradiation as a function of peroxide concentration, for slowly cooled and quench crystallized samples, are shown in Fig. 2.5 and Fig. 2.6, respectively. It was shown that after irradiation the crystallinity of the network increased in both cases. The reason for the crystallinity increase is that irradiation-induced scission of taut tie molecules permits recrystallization of broken chains from the noncrystalline regions. However, as the peroxide concentration was increased, the effect of irradiation on the crystallinity of the network became less significant. Approximately above 1 wt% peroxide, in both cases, the degree of crystallinity, before and after irradiation, was almost the same. We suggest that peroxide crosslinking reduces the effect of irradiation on the crosslinked network because crosslinks introduced by peroxide crosslinking stabilize chain fragments resulting from the scission of taut tie molecules and suppress recrystallization of broken chains.

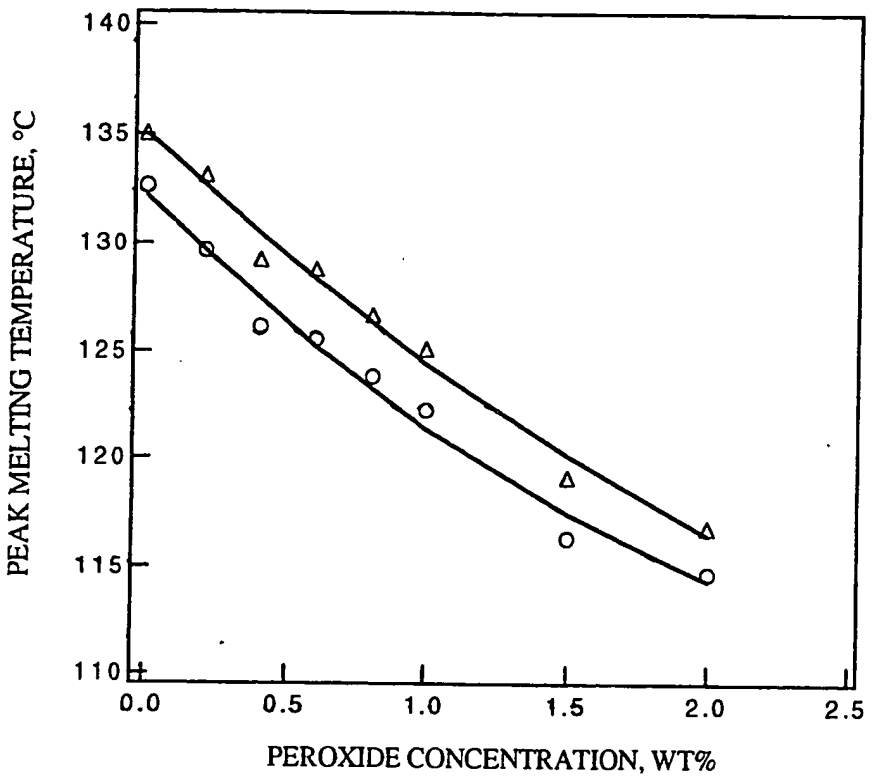

Figure 2.3. Comparison of first melting temperature before (o) and after (Δ) irradiation as a function of peroxide concentration. **Slowly cooled.**

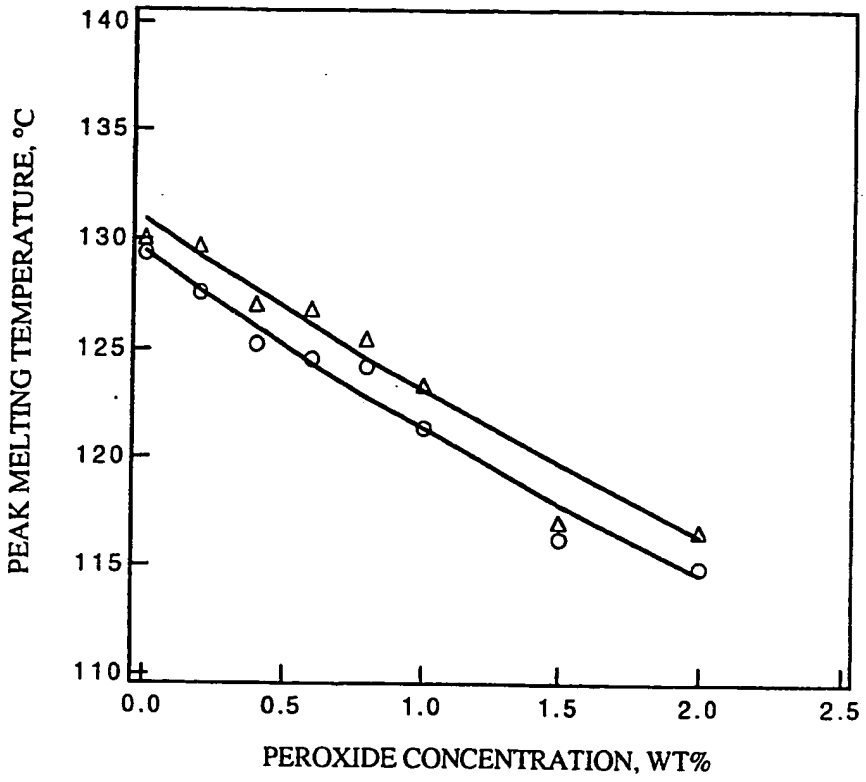

Figure 2.4. Comparison of first melting temperature before (○) and after (Δ) irradiation as a function of peroxide concentration. **Quench crystallized.**

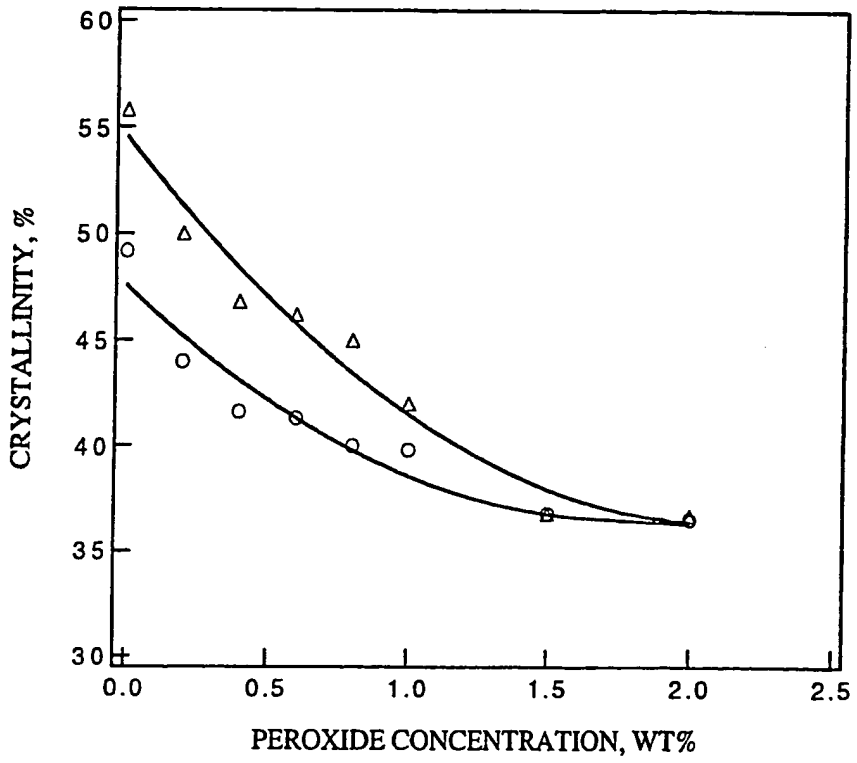

Figure 2.5. Comparison of crystallinity of first melting before (○) and after (Δ) irradiation as a function of peroxide concentration. **Slowly cooled.**

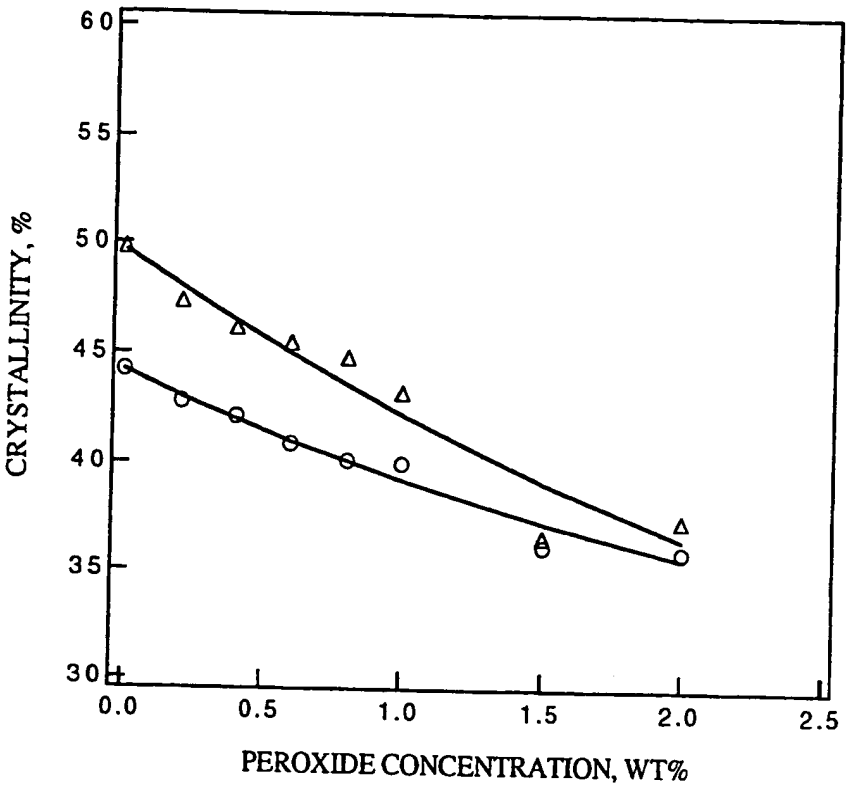

Figure 2.6. Comparison of crystallinity of first melting before (o) and after (Δ) irradiation as a function of peroxide concentration. **Quench crystallized.**

Swelling Properties of the Network

The gel content, degree of swelling, network chain density, average molecular weight between crosslinks, and crosslink density of the slowly cooled network as a function of peroxide concentration, before irradiation, are shown in Table 2.6. Swelling properties of the quenched network are shown in Table 2.7. It was shown that the degree of swelling and average molecular weight between crosslinks decreased as the peroxide concentration increased, in agreement with literature [2-3,26-28]. In addition, crosslink density increased systematically with increasing peroxide. Because of the extremely long polymer chains in UHMWPE, only a few crosslinks were needed for gelation [26,41]. Above the point of gel formation, the change of gel content with peroxide concentration can be calculated according to methods originally proposed by Charlesby and Pinner [54] and later modified by Barton [55]:

$$S + S^{0.5} = \frac{p_o}{q_o} + \frac{1}{2m \times E \times \overline{X_n} \times [i]} \qquad (6)$$

where S is the sol fraction; p_o and q_o are the probabilities of degradation and crosslinking per monomer unit per unit initiator (peroxide); m is the molecular weight of monomer; E is the crosslinking efficiency or the number of crosslinks per decomposed peroxide molecule; $\overline{X_n}$ is the number average degree of polymerization; [i] is the peroxide concentration in moles per gram of polymer. A plot of $S + S^{0.5}$ as a function of the reciprocal peroxide concentration is shown in Fig. 2.7. By extrapolating to high peroxide concentration, the intercept at $S + S^{0.5}$ is equal to p_o/q_o. From Fig. 2.7, a value of $p_o/q_o \cong 0$ was obtained, which meant that no chain scission occurred by peroxide crosslinking. Thus 100% gel can be obtained by peroxide crosslinking. Extrapolating to a value of $S + S^{0.5} = 2$ (not shown

in Fig. 2.7), i.e., inception of gelation, a very small value of peroxide concentration was obtained. It meant that only a few crosslinks were needed for gelation because of the extremely long polymer chains of UHMWPE [26,41,56].

Comparison of degree of swelling (q) for slowly cooled and quench crystallized samples as a function of peroxide concentration is illustrated in Figure 2.8. It was shown that at low peroxide concentration (below 0.4 wt% peroxide), the slowly cooled sample exhibited higher degree of swelling. This implies that quenching preserves the physical crosslinks (entanglements), leading to a lower degree of swelling. At higher peroxide concentration, the effect of quenching on the degree of swelling becomes less significant because sufficient crosslinks introduced by peroxide crosslinking inhibit molecular chain motions. A plot of $\overline{M_c}^{-1}$ vs peroxide concentration for both slowly cooled and quench crystallized samples is illustrated in Figure 2.9. Extrapolating the lower part of curve to 0% peroxide gives a measure of molecular weight between entanglements. The molecular weight between entanglements for slowly cooled and quench crystallized samples is 6000 and 5000, respectively. Apparently, quenching preserves the physical crosslinks (entanglements) and leads to a lower molecular weight between entanglements.

Based on Flory's theory [30-31], Akana and Stein [57] obtained an expression for the melting point depression of a crosslinked polymer as follows:

$$\frac{T_m^\circ - T_m}{T_m^\circ T_m} = \frac{R}{H_f} K M_\circ \frac{1}{\overline{M_c}} \qquad (7)$$

where T_m° and T_m are the equilibrium melting temperatures of the uncrosslinked and crosslinked polymer, respectively; R is the gas constant; H_f is the heat of fusion per monomer unit; K is the number of monomer units excluded from the crystal per network chain; $M_\circ$ is the molecular weight of the monomer unit; and $\overline{M_c}$ is the molecular weight

Table 2.6. Network properties of **slowly cooled** samples with varied peroxide concentration. **Before irradiation**

Wt% Peroxide	Gel content (%)	Degree of swelling (q)	Network chain density $\upsilon^* \times 10^4$ (mol cm^{-3})	$\overline{M_c} \times 10^{-3}$ (g mol^{-1})	Crosslink density (mol %)
0	———	———	———	———	———
0.2	99.5	3.69	2.572	3.539	0.40
0.4	99.7	2.98	4.413	2.055	0.68
0.6	99.7	2.78	5.301	1.710	0.82
0.8	99.8	2.75	5.443	1.662	0.84
1.0	99.6	2.53	6.842	1.322	1.05
1.5	99.7	2.40	7.927	1.135	1.23
2.0	99.6	2.37	8.215	1.095	1.28

Table 2.7. Network properties of **quench crystallized** samples with varied peroxide concentration. **Before irradiation**

Wt% Peroxide	Gel content (%)	Degree of swelling(q)	Network chain density $\upsilon^{*} \times 10^{4}$ (mol cm^{-3})	$\overline{M_c} \times 10^{-3}$ (g mol^{-1})	Crosslink density (mol %)
0	———	———	———	———	———
0.2	99.5	3.46	3.016	3.012	0.46
0.4	99.7	2.90	4.728	1.920	0.73
0.6	99.7	2.75	5.443	1.664	0.84
0.8	99.7	2.68	5.843	1.548	0.90
1.0	99.7	2.55	6.696	1.350	1.03
1.5	99.8	2.49	7.151	1.257	1.11
2.0	99.6	2.45	7.489	1.200	1.16

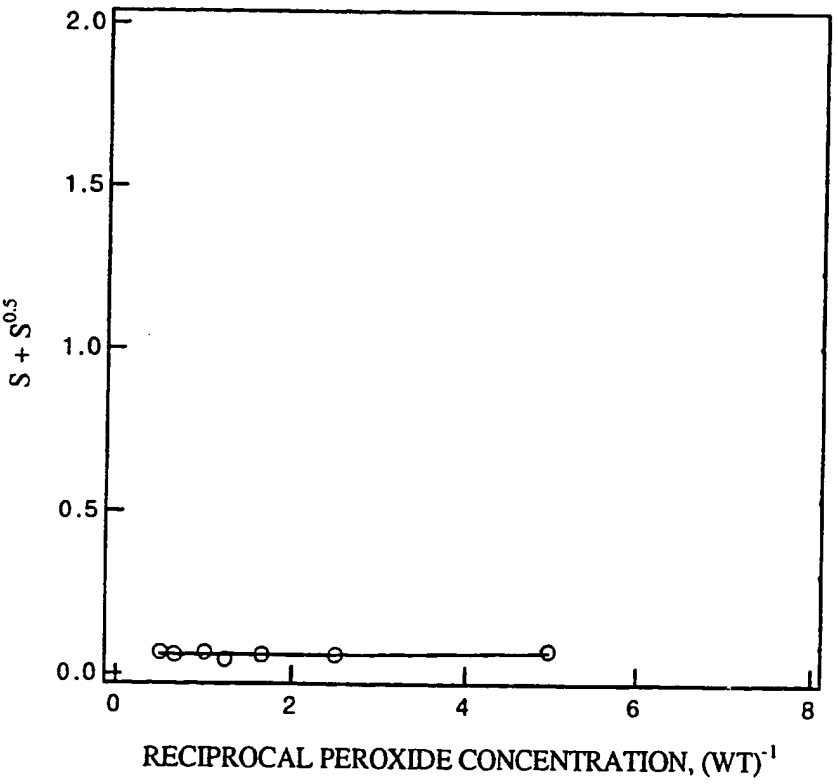

Figure 2.7. A plot of $S + S^{0.5}$ as a function of the reciprocal peroxide concentration. **Slowly cooled. Before irradiation.**

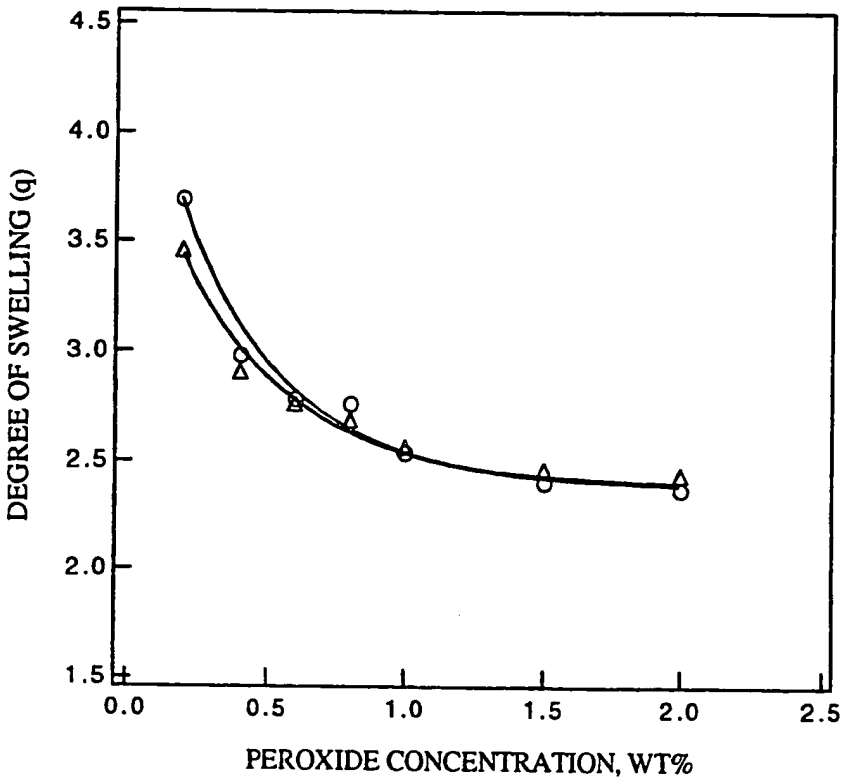

Figure 2.8. Degree of swelling (q) of slowly cooled (o) and quench crystallized (Δ) samples as a function of peroxide concentration. **Before irradiation.**

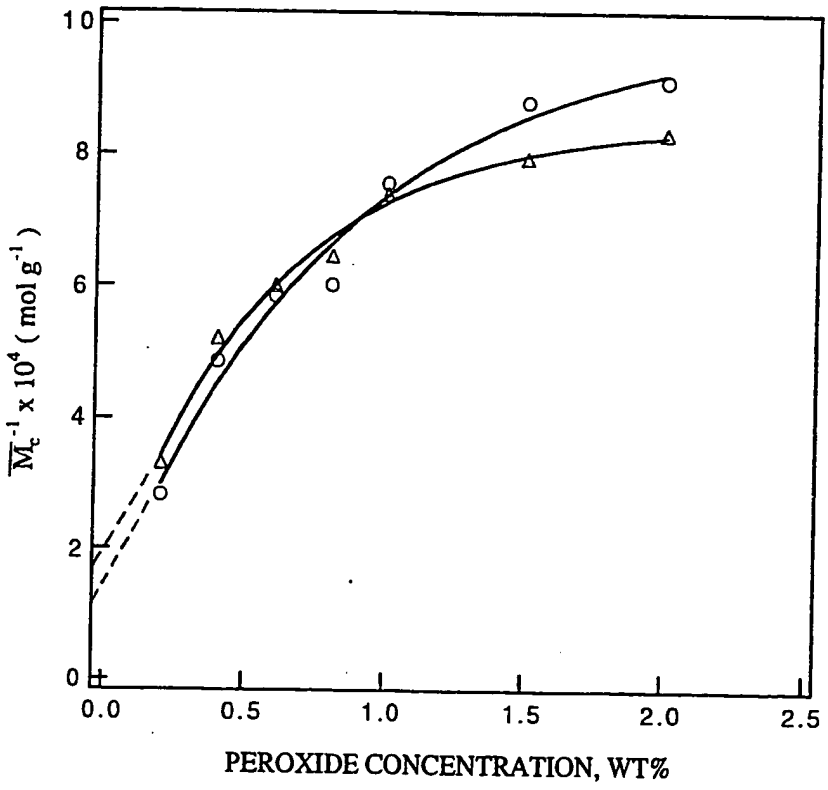

Figure 2.9. A plot of $\overline{M_c}^{-1}$ vs peroxide concentration for slowly cooled (o) and quench crystallized (Δ) samples. **Before irradiation.**

between crosslinks. According to equation (7), a plot of $(T_m^\circ - T_m)/T_m^\circ T_m$ vs $\overline{M_c}^{-1}$ should give a straight line. Tables 2.8 and 2.9 showed the values of end melting point (first melting) and $(T_m^\circ - T_m)/T_m^\circ T_m$ at varied peroxide concentration for slowly cooled and quench crystallized samples, respectively. A plot of $(T_m^\circ - T_m)/T_m^\circ T_m$ as a function of $\overline{M_c}^{-1}$ for slow-cooling samples is given in Fig. 2.10. For quench crystallized samples, such a plot is illustrated in Fig. 2.11. As we can see, a rather good straight line was obtained in both cases at high peroxide concentrations, i.e. at high values of $\overline{M_c}^{-1}$, in agreement with literature [26]. At low peroxide concentrations (low values of $\overline{M_c}^{-1}$), the melting point depression was negligible. By extrapolating this straight line to $(T_m^\circ - T_m)/T_m^\circ T_m$ =0, where melting point depression was first observed, a critical $\overline{M_c}^{-1}$ value of 3.22×10^{-4} or $\overline{M_c}$ = 3100 was obtained for slow-cooling samples. This $\overline{M_c}$ value was explained as the molecular weight between entanglements. For quench crystallized samples, $\overline{M_c}$ is equal to 2100 . A corresponding critical $\overline{M_c}$ value of 7600 was reported by de Boer and Pennings [26] when they studied peroxide crosslinking of UHMWPE (Hifax 1900, $\overline{M_w}$ ~ 4×10^6) at 180 °C for 3 h.

Effect of Irradiation on Swelling Properties of the Crosslinked Network

After irradiation, the gel content, degree of swelling, network chain density, average molecular weight between crosslinks, and crosslink density of the gel network as a function of peroxide concentration, for slowly cooled and quench crystallized samples, are shown in Tables 2.10 and 2.11, respectively. After irradiation, for both slowly cooled and quenched samples of peroxide crosslinked UHMWPE, the gel content, network chain density, and crosslink density decreased. Similarly, the degree of swelling and average molecular weight between crosslinks increased after irradiation for both cases. Apparently,

Table 2.8. End melting temperature, $(T_m^\circ - T_m)/T_m^\circ T_m$, and $\overline{M_c}^{-1}$ for **slowly cooled** samples at varied peroxide concentration. **Before irradiation**

Wt% Peroxide	End Melting Temp. (°K) (1st melting)	$\frac{(T_m^\circ - T_m)}{T_m^\circ T_m} \times 10^5$	$\overline{M_c}^{-1} \times 10^4$
0	408.1	0	0
0.2	405.2	1.75	2.825
0.4	402.5	3.41	4.864
0.6	401.6	3.96	5.845
0.8	400.5	4.65	6.015
1.0	398.6	5.84	7.564
1.5	393.0	9.41	8.805
2.0	391.5	10.39	9.129

Table 2.9. End melting temperature, $(T_m^\circ - T_m)/T_m^\circ T_m$, and $\overline{M_c}^{-1}$ for **quench crystallized** samples at varied peroxide concentration. **Before irradiation**

Wt% peroxide	End Melting Temp. (°K) (1st melting)	$\frac{(T_m^\circ - T_m)}{T_m^\circ T_m} \times 10^5$	$\overline{M_c}^{-1} \times 10^4$
0	405.3	0	0
0.2	403.0	1.41	3.319
0.4	401.1	2.58	5.208
0.6	401.3	2.46	6.006
0.8	400.4	3.02	6.457
1.0	399.4	3.64	7.402
1.5	392.6	7.98	7.952
2.0	391.0	9.02	8.330

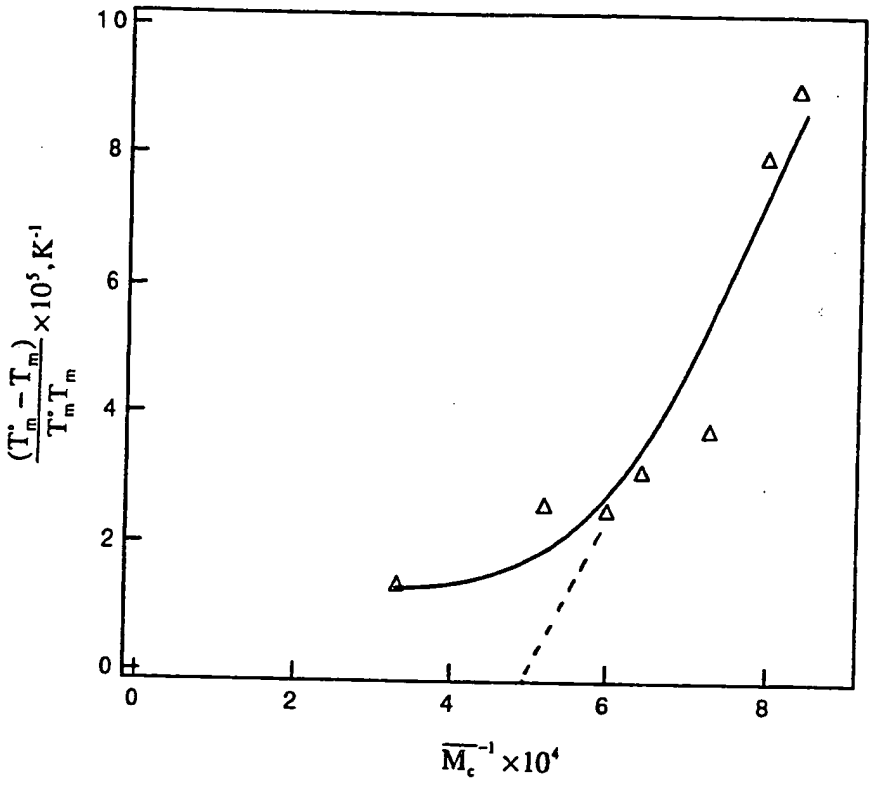

Figure 2.10. A plot of $(T_m^\circ - T_m)/T_m^\circ T_m$ vs $\overline{M_c}^{-1}$ for slowly cooled samples. Before irradiation.

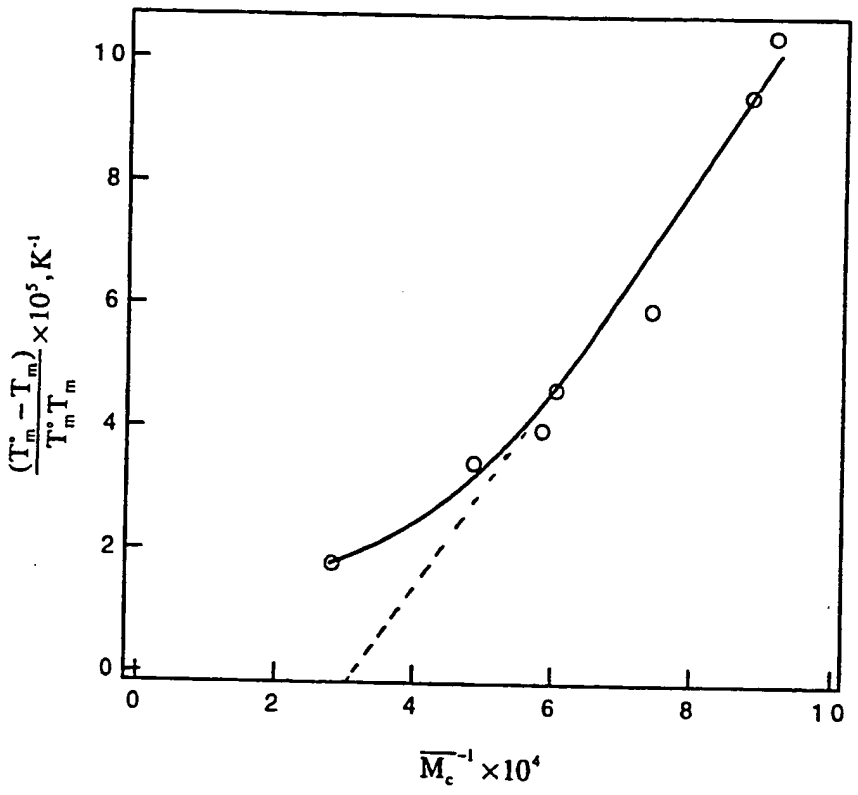

Figure 2.11. A plot of $(T_m^\circ - T_m)/T_m^\circ T_m$ vs $\overline{M_c}^{-1}$ for quench crystallized samples. Before irradiation.

irradiation-induced chain scission resulted in a decreased gel content. Compared to peroxide crosslinking, which can produce 100% gel, irradiation crosslinking in air gives a gel content below 100% because of simultaneous irradiation-induced chain scission. It was reported that degassed UHMWPE crosslinked in the melt state at 200 °C, in a nitrogen atmosphere, by means of electron beam irradiation, revealed a gel fraction up to 100%, indicating that effectively no chain scission occurred in the absence of oxygen implying that any radicals formed by chain fragmentation recombined in a cage reaction [41].

For the peroxide-free, quench crystallized sample, irradiation crosslinking produced a higher gel content (76.7%) compared to 70.8% gel in the peroxide-free, slow-cooled sample. This is in agreement with literature [58-61]. It was suggested that for bulk polyethylene, higher crystallization temperature for the slow-cooled sample results in better defined lamellae and a higher degree of crystallinity. Thus, more regular crystal surfaces with less intermeshing between consecutive lamellae allowed less chance for interlamellar links as well as producing a reduced amorphous fraction. Radiation induced crosslinking occurs primarily in amorphous areas or between lamellae at the fold surfaces [37-46]. Therefore, irradiation produced less gel fraction for the peroxide-free, slowly cooled sample. Comparison of gel content before and after irradiation for slowly cooled samples as a function of peroxide concentration is illustrated in Figure 2.12. Such a comparison for quench crystallized samples is shown in Figure 2.13. In both cases, the gel content decreases after irradiation. However, at high peroxide concentration, the difference in gel content before and after irradiation became smaller. Comparison of the degree of swelling (q) before and after irradiation for slowly cooled and quench crystallized samples is illustrated in Figures 2.14 and 2.15, respectively. After irradiation, the degree of swelling increased because of chain scission for both slowly cooled and quenched samples. With increasing peroxide concentration, the difference in the degree of swelling gradually became smaller for both slowly cooled and quenched samples. In Figures 2.16 and 2.17,

we compare $\overline{M_c}$ before and after irradiation as a function of peroxide concentration, for slowly cooled and quench crystallized samples, respectively. From Figures 2.16 and 2.17, we can see that $\overline{M_c}$ increases after irradiation. At higher peroxide concentrations, the difference in $\overline{M_c}$ before and after irradiation became smaller. Comparison of crosslink density before and after irradiation as a function of peroxide concentration for slowly cooled and quench crystallized samples is illustrated in Figures 2.18 and 2.19, respectively. The same trend as mentioned above was observed in both cases (because the data are correlated).

From a consideration of irradiation effects on network properties, we conclude that irradiation resulted in an increase in the degree of swelling and average molecular weight between crosslinks, and a decrease in gel content, network chain density, and crosslink density. These effects were ascribed to radiation-induced chain scission. At high peroxide concentration, the effect of irradiation on network properties was mitigated. As a result of peroxide crosslinking, radiation induced chain scission becomes less important in determining gel content. We suggest that irradiation effects on a peroxide crosslinked network are suppressed because crosslinks introduced by peroxide crosslinking can stabilize chain fragments resulting from the scission of taut tie molecules. For the most crosslinked network, the effect of irradiation on network properties was reduced to the highest extent. In addition, from an analysis of network properties, we believe that the predominant result of sterilization by irradiation (3.4 Mard in our case) of UHMWPE is chain scission of tie molecules.

Table 2.10. Network properties of **slowly cooled** samples with varied peroxide concentration. **After irradiation**

Wt% peroxide	Gel content (%)	Degree of swelling (q)	Network chain density $\upsilon^{*} \times 10^{4}$ (mol cm^{-3})	$\overline{M_c} \times 10^{-3}$ (g mol^{-1})	Crosslink density (mol %)
0	70.8	8.44	0.426	21.753	0.06
0.2	79.0	5.95	0.872	10.542	0.13
0.4	94.0	4.75	1.412	6.478	0.21
0.6	96.0	4.31	1.767	5.169	0.27
0.8	97.4	3.45	3.030	3.010	0.46
1.0	97.5	3.35	3.262	2.782	0.50
1.5	98.8	2.70	5.732	1.570	0.89
2.0	99.0	2.59	6.410	1.404	1.0

Table 2.11. Network properties of **quench crystallized** samples with varied peroxide concentration. **After irradiation**

Wt% peroxide	Gel content (%)	Degree of swelling (q)	Network chain density $\upsilon^{\bullet} \times 10^{4}$ (mol cm^{-3})	$\overline{M_c} \times 10^{-3}$ (g mol^{-1})	Crosslink density (mol%)
0	76.7	6.03	0.839	10.952	0.13
0.2	84.1	4.90	1.328	6.893	0.20
0.4	95.6	4.39	1.717	5.321	0.26
0.6	96.2	3.96	2.167	4.211	0.33
0.8	96.2	3.95	2.192	4.159	0.34
1.0	97.5	3.36	3.235	2.811	0.50
1.5	99.0	2.64	6.086	1.478	0.95
2.0	99.1	2.58	6.471	1.392	1.0

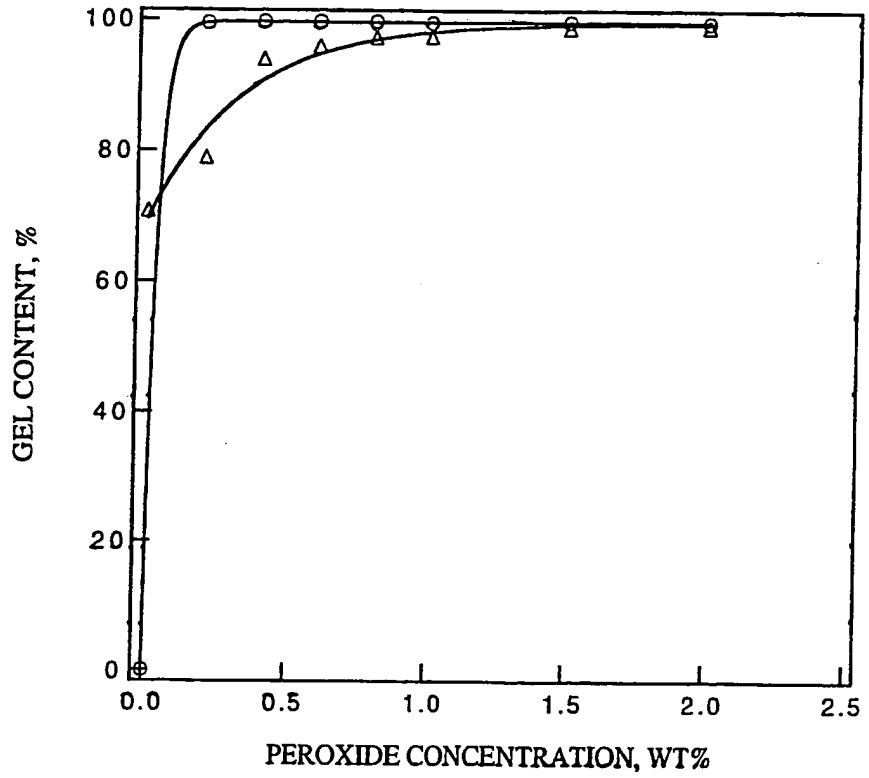

Figure 2.12. Comparison of gel content before (○) and after (Δ) irradiation as a function of peroxide concentration. **Slowly cooled.**

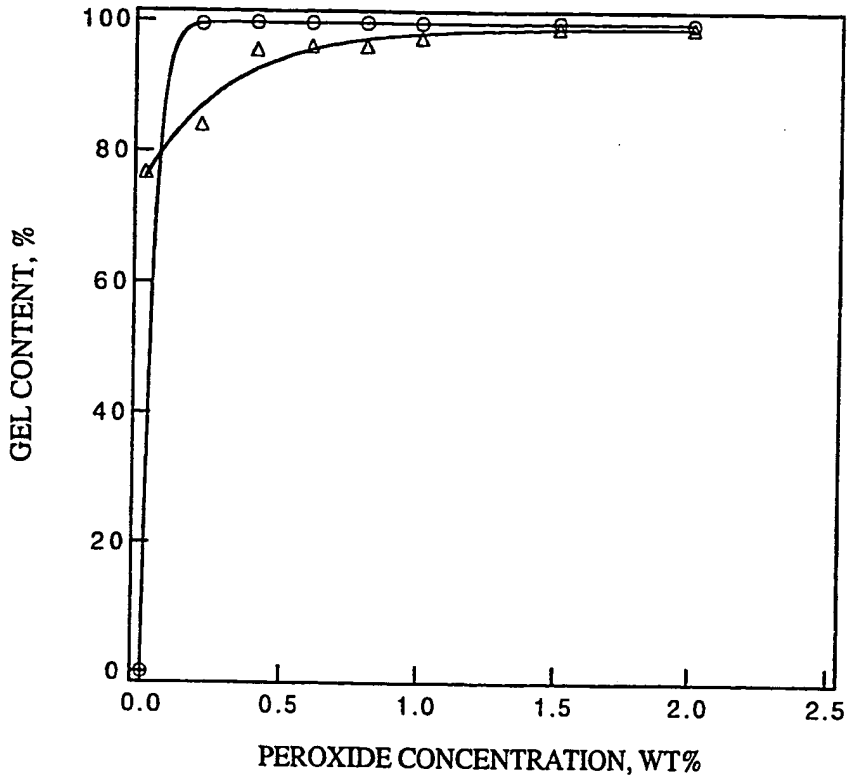

Figure 2.13. Comparison of gel content before (o) and after (Δ) irradiation as a function of peroxide concentration. **Quench crystallized.**

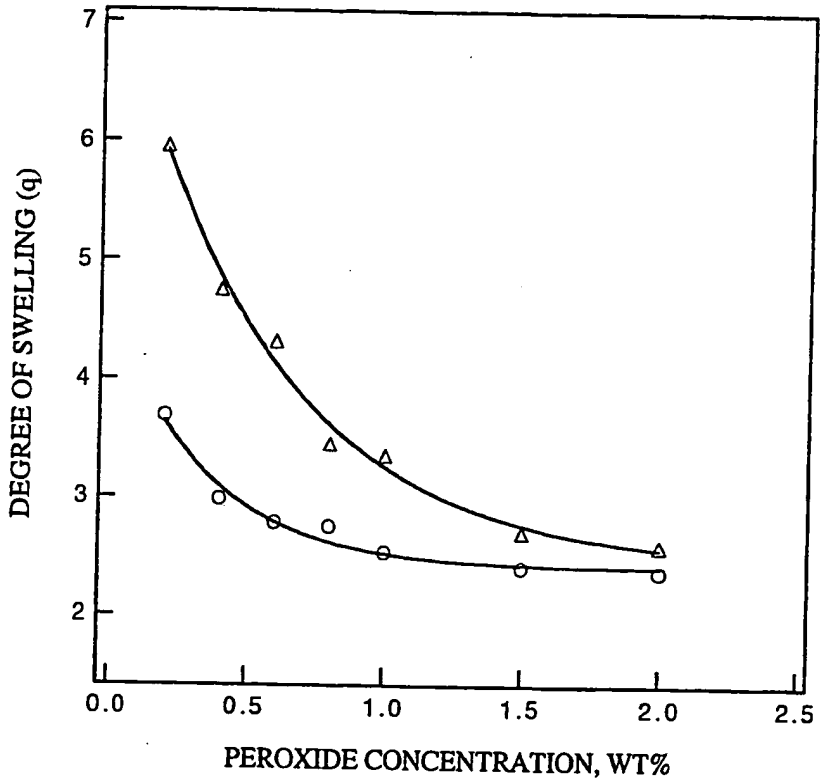

Figure 2.14. Comparison of degree of swelling (q) before (○) and after (Δ) irradiation as a function of peroxide concentration. **Slowly cooled.**

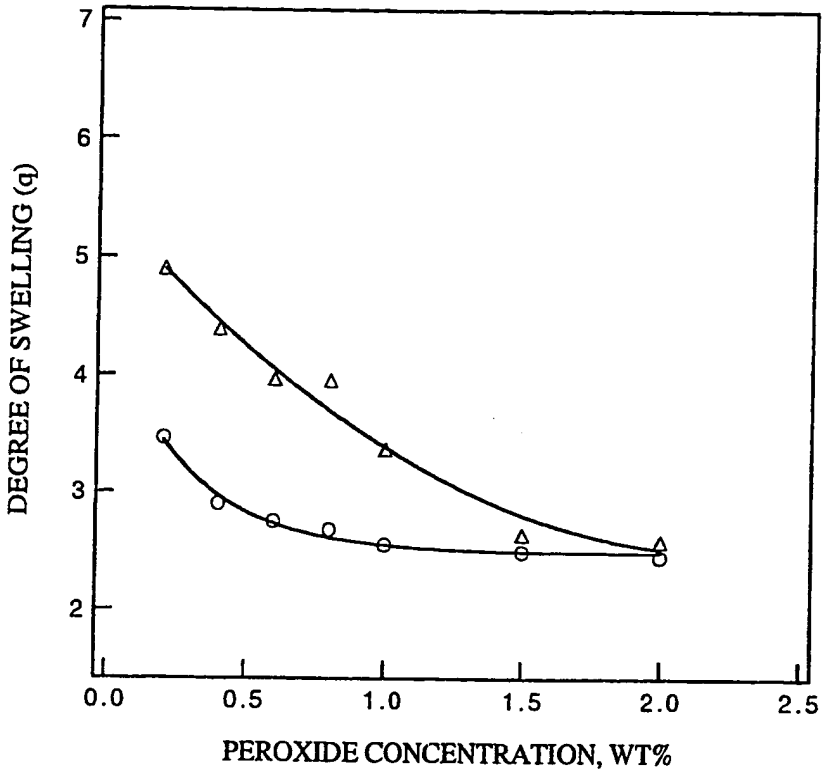

Figure 2.15. Comparison of degree of swelling (q) before (○) and after (Δ) irradiation as a function of peroxide concentration. **Quench crystallized.**

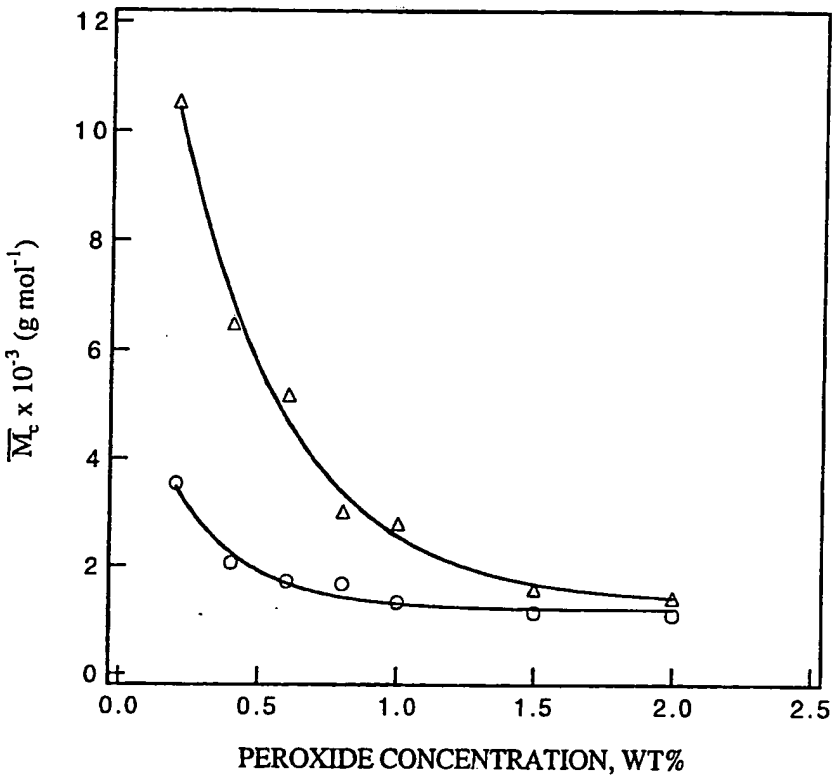

Figure 2.16. Comparison of $\overline{M_c}$ before (○) and after (Δ) irradiation as a function of peroxide concentration. **Slowly cooled.**

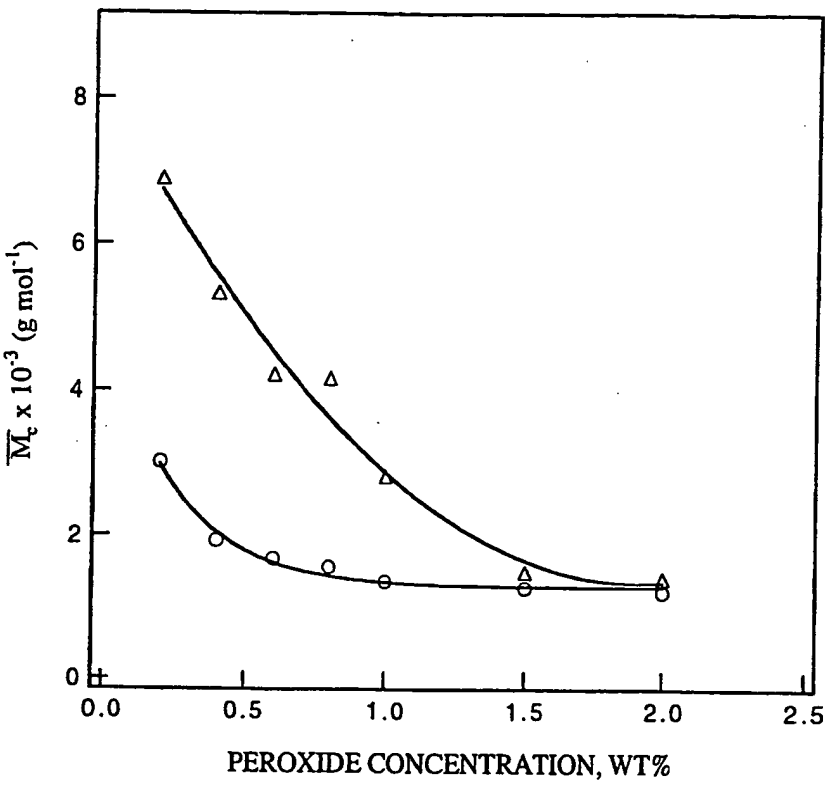

Figure 2.17. Comparison of $\overline{M_c}$ before (o) and after (Δ) irradiation as a function of peroxide concentration. **Quench crystallized.**

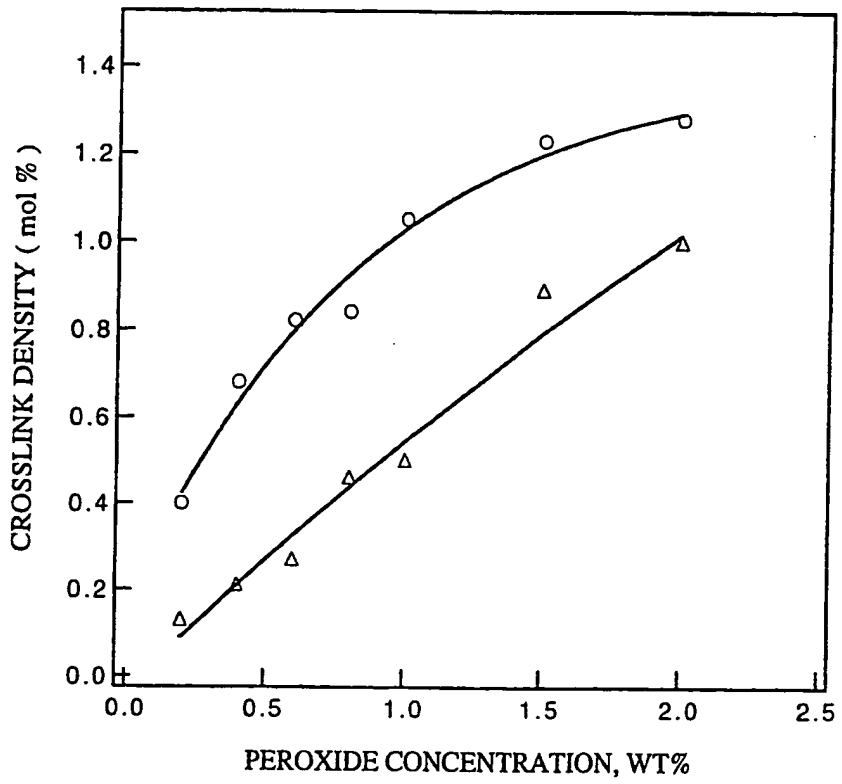

Figure 2.18. Comparison of crosslink density before (○) and after (Δ) irradiation as a function of peroxide concentration. **Slowly cooled.**

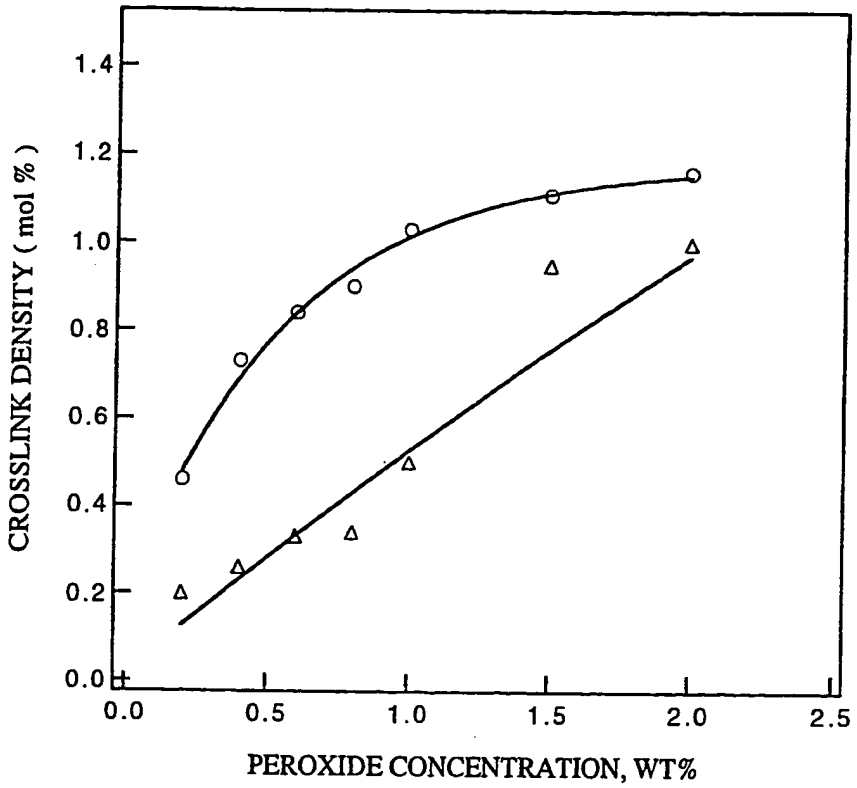

Figure 2.19. Comparison of crosslink density before (○) and after (Δ) irradiation as a function of peroxide concentration. **Quench crystallized.**

FTIR Measurements

FTIR spectra of compression molded UHMWPE crosslinked with 0, 1, and 2 wt% peroxide are shown in Figure 2.20. After irradiation, FTIR spectra of irradiated samples are shown in Figure 2.21. As shown in Figure 2.20, slight increase in carbonyl concentration after peroxide crosslinking was observed. Here, the carbonyl group concentration can be calculated by the ratio of peak heights of the carbonyl absorption band at 1713 cm^{-1} to the reference band at 2022 cm^{-1} ($-CH_2-$ vibration). This absorption band at 2022 cm^{-1} results from $-CH_2-$ vibration in both crystalline and amorphous polyethylenes and can be used as a reference band, independent of the degree of crystallinity and oxidation [62]. The ratios for 0, 1, and 2 wt% peroxide samples are 0.25, 0.26, and 0.62, respectively. Compared to Figure 2.21 (after irradiation), a significant increase in carbonyl concentration was observed for all three irradiated samples. The ratios for 0, 1, and 2 wt% peroxide samples (after irradiation) are 0.82, 1.0, and 1.1, respectively. This is because the free radicals produced by irradiation react with oxygen dissolved and/or diffused in the polymer. In addition, we observe that carbonyl concentration in irradiated peroxide-crosslinked samples is higher , compared to the peroxide free sample (after irradiation). Because peroxide crosslinking produces tertiary carbons, the concentration of tertiary carbons increases with increasing peroxide concentration. We believe that tertiary carbons are more susceptible to oxidation during irradiation. Therefore, carbonyl concentration in the irradiated peroxide-crosslinked samples increases with increasing peroxide concentration.

Exposure to high energy irradiation, Typical free radicals in irradiated polyethylene include the alkyl radical, $-CH_2\dot{C}HCH_2-$, the allyl, $-\dot{C}HCH{=}CH-$, and the polyenyl free radicals, $-\dot{C}H-(CH{=}CH)_n-$, although the latter are produced in significant yields only at high doses [63]. Radical lifetime strongly depends on temperature and can be hours or even

weeks at room temperature. Less stable radicals can be observed to convert to more stable radicals with time. For instance, as secondary radicals, $-CH_2-\dot{C}H-CH_2-$, encounter double bonds in low concentration and abstract an allylic hydrogen atom, secondary radicals decay whereas allylic radicals, $-CH_2-\dot{C}H-CH=CH-$, appear. Usually, the decay time for radical intermediates is on the order of one day for alkyl radicals and several months for allyl radicals at 77 K, whereas, the polyene radicals are very stable even at room temperature [64]. It is known that irradiation produces free radicals randomly within samples irrespective of their crystal morphology [65]. Free radicals formed in the crystalline regions have much lower mobility and longer lifetimes, and can migrate slowly along crystalline chains to the fold regions where reaction occurs to form crosslinks or peroxy radicals in the presence of oxygen [65]. Therefore, the higher the degree of crystallinity, the higher the lifetime of free radicals [65]. Peroxy radicals may rearrange or react with polymer to form hydroperoxide [65-67]. Eventually, peroxy radicals and hydroperoxides can decompose to form carbonyl groups. It was reported that at same irradiation doses, the longer lifetimes of free radicals in slowly cooled and isothermally crystallized samples with higher crystallinity made them more susceptible to oxidation (higher carbonyl concentration) after irradiation in vacuum and subsequent exposure to air for 1 year, compared to quenched samples with lowest crystallinity [68]. Hydroperoxides are believed to decompose slowly but steadily at room temperature to form carboxyl groups or to generate free radicals to continuously resume the oxidation [69]. The breakdown of metastable peroxy or hydroperoxy species introduced during irradiation in the presence of oxygen was considered as the cause of the post-irradiation aging [70-73].

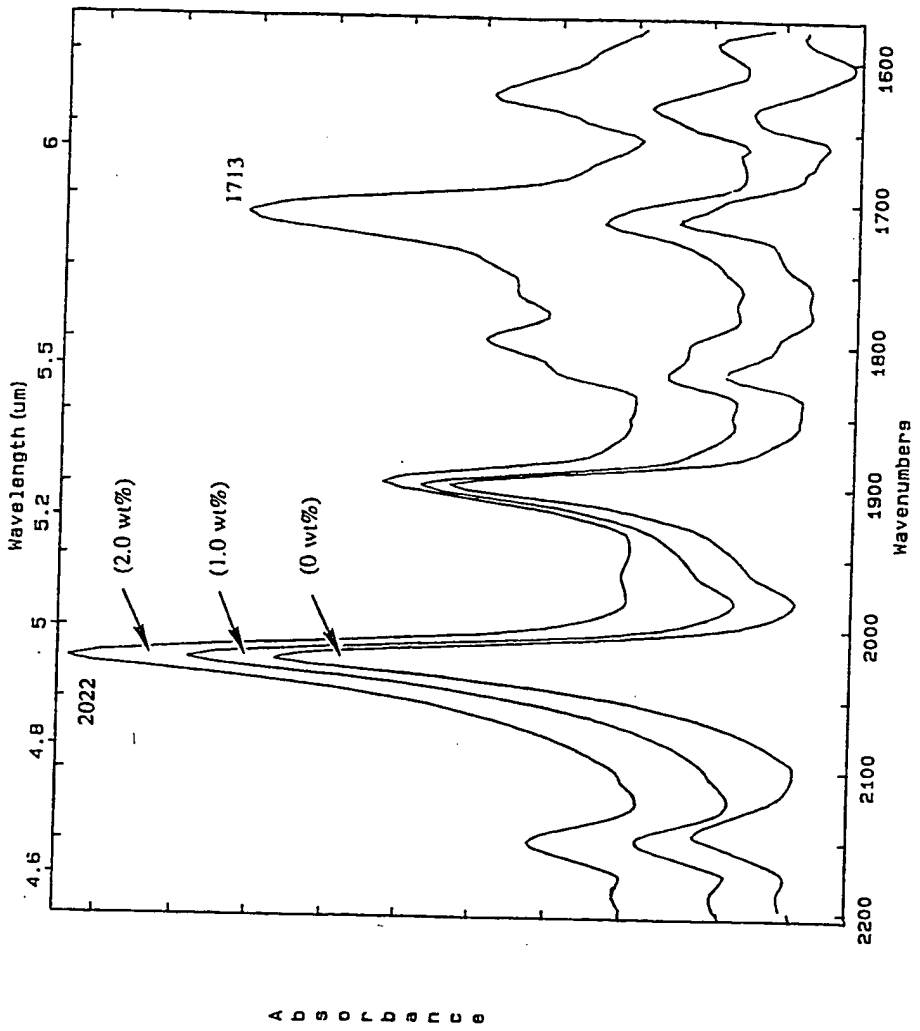

Figure 2.20. FTIR spectra of compression molded UHMWPE crosslinked with 0, 1 and 2 wt% peroxide. **Before irradiation.**

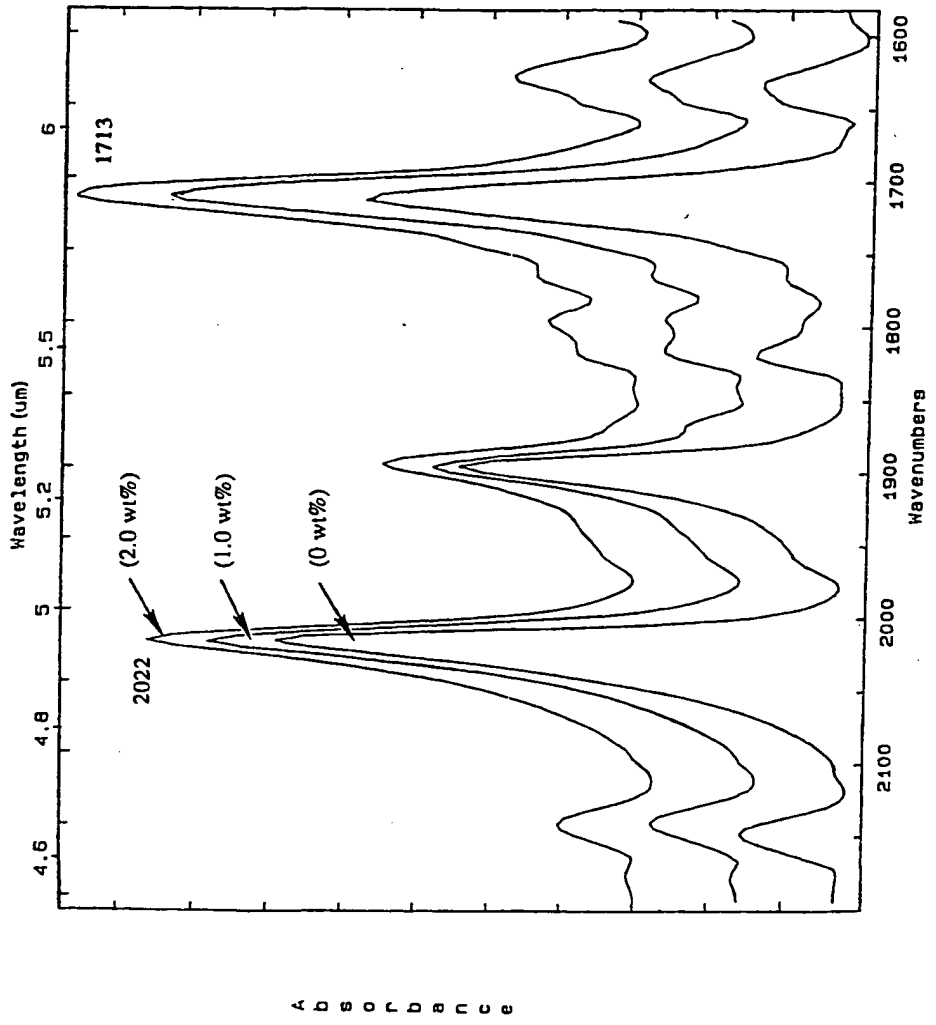

Figure 2.21. FTIR spectra of compression molded UHMWPE crosslinked with 0, 1 and 2 wt% peroxide. **After irradiation.**

2.3 Conclusions

Based on the present studies, the following conclusions are drawn.

Before Peroxide Crosslinking and Irradiation

(1) From DSC measurements, we know that repeated heating and cooling cycles, cooling rate and heating rate, and annealing affect crystal perfection and crystallinity.

(2) Quenching reduces size, perfection, and amount of crystals, resulting in a decrease in crystallinity and melting temperature.

(3) The rate of cooling (and resulting crystallization) during a repeated DSC scan at 10 °C/min from 170 °C is faster than slow-cooling but slower than quenching.

(4) Melting temperature in DSC measures size and perfection of crystal, whereas, heat of fusion in DSC measures the fraction of polymer chains contained in crystals.

After Irradiation without Peroxide Crosslinking

(1) Irradiation-induced scission of tie molecules leads to an increase in crystallinity and melting temperature (i.e., an improvement in crystal size and perfection) for both slowly cooled and quench crystallized samples.

(2) For slowly cooled samples, irradiation-induced crosslinking leads to a decrease in crystallinity and melting temperature in the second melting, compared to those of the first melting.

(3) The gel content of slowly cooled and quench crystallized samples is increased from 0% to 70.8% and 76.7%, respectively. Since the crystallinity decreases from 49.2 to 44.2% by quenching, crosslinking and gel formation are enhanced by amorphous content.

After Peroxide Crosslinking without Irradiation

(1) Peroxide crosslinking leads to a decrease in the degree of crystallinity, peak melting temperatures, and recrystallization temperatures for both slowly cooled and quench crystallized samples. This is because peroxide crosslinking inhibits the growth of crystals from a crosslinked melt, leading to crystal imperfections and a decreased crystallite size.

(2) For a peroxide crosslinked network, the effect of quenching on the crystallinity and melting temperature is less important. This is because peroxide crosslinking inhibits molecular chain motions so that the effect of quenching will be reduced when sufficient crosslinks are introduced.

(3) Quenching produces a more homogeneous network at high peroxide concentration. This is because peroxide crosslinking and quenching produce smaller crystal domains.

After Peroxide Crosslinking and Irradiation

(1) Peroxide crosslinking suppresses crystallization and limits recrystallization during DSC, leading to a decrease in degree of crystallinity and melting temperature.

(2) Irradiation produces crosslinking in amorphous regions plus extensive scission of taut tie molecules and leads to increased crystallinity and crystal perfection, reduces gel content, and increases degree of swelling of a crosslinked network.

(3) Peroxide crosslinking reduces the effect of irradiation on the crosslinked network. This is because crosslinks introduced by peroxide crosslinking can stabilize the chain fragments resulting from the scission of taut tie molecules and suppress recrystallization of broken chains.

(4) FTIR measurements showed that a significant increase in carbonyl concentration was observed for all three irradiated samples (peroxide free, 1, and 2 wt% peroxide samples).

This is because the free radicals produced by irradiation react with oxygen dissolved and/or diffused in the polymer. In addition, carbonyl concentration in the irradiated peroxide-crosslinked samples is higher, compared to the peroxide free sample (after irradiation). This is because peroxide crosslinking produces tertiary carbons which are more susceptible to oxidation during irradiation so that the carbonyl concentration in the irradiated peroxide-crosslinked samples increases with increasing peroxide concentration.

2.4 References

[1] Atochem Inc., Technical Report, 1992.

[2] A. Posthuma de Boer and A. J. Pennings, *J. Polym. Sci., Polym. Phys. Ed.*, **14**, 187(1976).

[3] J. de Boer and A. J. Pennings, *Makromol. Chem., Rapid Commun.*, **2**, 749(1981).

[4] B. Wunderlich and C. M. Cormier, *J. Polym. Sci.* **A-2**, **5**, 987(1967).

[5] S. Kavesh and J. M. Schultz, *Polym. Eng. Sci.*, **9**, 452(1969).

[6] B. Wunderlich and G. Czorny, *Macromolecules*, **10**, 906(1977)

[7] P. J. Flory, *Principles of Polymer Chemistry*, Cornell University Press, Ithaca, New York, 1953.

[8] R. W. Truss, K. S. Han, J. F. Wallace, and P. H. Geil, *Polym. Eng. Sci.*, **20**, 747 (1980).

[9] A. E. Zachariades and J. A. Logan, *J. Polym. Sci., Polym. Phys. Ed.*, **21**, 821 (1983).

[10] X. Y. Wang and R. Salovey, *J. Appl. Polym. Sci.*, **34**, 593(1987).

[11] H. D. Chanzy, E. Bonjour, and R. H. Marchessault, *Colloid Polym. Sci.*, **252**, 8 (1974).

[12] J. F. Revol, W. Luk, and R. H. Marchessault, *J. Cryst. Growth*, **48**, 240(1980).

[13] G. Broza, U. Rick, A. Kawaguchi, and J. Petermann, *J. Polym. Sci., Polym. Phys. Ed.*, **23**, 2623(1985).

[14] D. Hofmann, E. Schulz, D. Fanter, H. Fuhrmann, and D. Bilda, *J. Appl. Polym. Sci.*, **42**, 863(1991).

[15] J. M. G. Cowie, *"Polymers: Chemistry & Physics of Modern Materials"*, 2nd Ed., Chapman & Hall, New York, 1991.

[16] M. Narkis and J. Miltz, *J. Appl. Polym. Sci.*, **13**, 713(1969).

[17] T. R. Manley and M. M. Qayyum, *Polymer*, **12**, 176(1971).

[18] G. E. Hulse, R. J. Kersting, and D. R. Warfel, *J. Polym. Sci., Polym. Chem. Ed.*, **19**, 655(1981).

[19] Y. H. Kao and P. J. Phillips, *Polymer*, **27**, 1669(1986).

[20] A. J. Peacock, *Polym. Commun.*, **28**, 259(1987).

[21] A. K. Mukherjee, P. K. Tyagi, and B. D. Gupta, *Angew. Makromol. Chemie*, **173**, 205(1989).

[22] T. Bremner, A. Rudin, and S. Haridoss, *Polym. Eng. Sci.*, **32**,939(1992).

[23] K. W. Lem and C. D. Han, *J. Appl. Polym. Sci.*, **27**, 1367(1982).

[24] E. M. Kampouris and A. G. Andreopoulos, *J. Appl. Polym. Sci.*, **34**, 1209(1987).

[25] T. Bremner and A. Rudin, *J. Appl. Polym. Sci.*, **49**, 785(1993).

[26] J. de Boer and A. J. Pennings, *Polymer*, **23**, 1944(1982).

[27] J. de Boer, H. J. van den Berg, and A. J. Pennings, *Polymer*, **25**, 513(1984).

[28] M. Narkis, I. Raiter, S. Shkolnik, A. Siegmann, and P. Eyerer, *J. Macromol. Sci. Phys.*, **B26**, 37(1987).

[29] P. J. Hendra, A. J. Peacock, and H. A. Willis, *Polymer*, **28**, 705(1987).

[30] P. J. Flory, *Trans. Faraday Soc.*, **51**, 848(1955).

[31] P. J. Flory, *J. Am. Chem. Soc.*, **78**, 5222(1956).

[32] R. Salovey and D. C. Bassett, *J. Appl. Phys.*, **35**, 3216(1964).

[33] H. E. Bair and R. Salovey, *J. Polym. Sci., Polym. Lett. Ed.*, **5**, 429(1967).

[34] R. J. Roe, E. S. Grood, R. Shastri, C. A. Gosselin, and F. R. Noyes, *J. Biomed. Mater. Res.*, **15**, 209(1981).

[35] S. K. Bhateja, *J. Macromol. Sci. Phys.*, **B22**, 159(1983).

[36] S. K. Bhateja, E. H. Andrews, and R. J. Young, *J. Polym. Sci., Polym. Phys. Ed.*, **21**, 523(1983).

[37] I. Kamel and L. Finegold, *J. Polym. Sci., Polym. Phys. Ed.*, **23**, 2407(1985).

[38] A. Shinde and R. Salovey, *J. Polym. Sci., Polym. Phys. Ed.*, **23**, 1681(1985).

[39] S. K. Bhateja and E. H. Andrews, *J. Mater. Sci.*, **20**, 2839(1985).

[40] L. Minkova, *Colloid Polym. Sci.*, **266**, 6(1988).

[41] D. J. Dijkstra, W. Hoogsteen, and A. J. Pennings, *Polymer*, **30**, 866(1989).

[42] L. Minkova and M. Mihailov, *Colloid Polym. Sci.*, **268**, 1018(1990).

[43] Y. Zhao, Y. Luo, and B. Jiang, *J. Appl. Polym. Sci.*, **50**, 1797(1993).

[44] R. Salovey and A. Keller, *J. Bell System Tech.*, **40**, 1397,1409(1961).

[45] T. Kawai, A. Keller, A. Charlesby, and M. G. Ormerod, *Phil. Mag.*, **12**, 657 (1965).

[46] T. Kawai and A. Keller, *Phil. Mag.*, **12**, 673(1965).

[47] G. N. Patel and A. Keller, *J. Polym. Sci., Polym. Phys. Ed.*, **13**, 303(1975).

[48] G. N. Patel and A. Keller, *J. Polym. Sci., Polym. Phys. Ed.*, **13**, 323, 333(1975).

[49] G. Ungar and A. Keller, *Polymer*, **21**, 1273(1980).

[50] G. Ungar, *J. Mater. Sci.*, **16**, 2635(1981).

[51] A. Keller and G. Ungar, *Radiat. Phys. Chem.*, **22**, 155(1983).

[52] M. Dole, *Polym. Plast. Technol. Eng.*, **13**, 41(1979).

[53] M. Kresteva, E. Nedkov, and A. Radilova, *Colloid Polym. Sci.*, **263**, 273(1985).

[54] A. Charlesby and S. H. Pinner, *Proc. Roy. Soc.*, **A249**, 367(1959).

[55] J. Barton, *J. Polym. Sci.* A-1, **6**, 1315(1968).

[56] W. H. Stockmayer, *J. Chem. Phys.*, **12**, 125(1944).

[57] Y. Akana and R. S. Stein, *J. Polym. Sci., Polym. Phys. Ed.*, **13**, 2195(1975).

[58] R. Salovey, *J. Polym. Sci.* B, **2**, 833(1964).

[59] T. Kawai and A. Keller, *Phil. Mag.*, **14**, 1123(1966).

[60] T. Kawai, A. Keller, A. Charlesby, and M. G. Ormerod, *Phil. Mag.*, **10**, 779 (1964).

[61] H. Jenkins and A. Keller, *J. Macromol. Sci.* **B**, **11**, 301(1975).

[62] M. A. McRae and W. F. Maddams, *Makromol. Chem.*, **177**, 473(1976).

[63] M. Dole, Ed., *"The Radiation Chemistry of Macromolecules"*, **Vol. 1**, Academic Press, New York, 1972.

[64] V. D. McGinniss, "Crosslinking with Radiation", *Encyclopedia of Polym. Sci. and Eng.*, **Vol. 4**, 418(1985).

[65] A. Keller, in *"Developments in Crystalline Polymers"*, Part I, D. C. Bassett, Ed., p 37, Appl. Sci. Publ., 1982.

[66] M. Iring, F. Tüdös, Z. Fodor, and T. Kelen, *Polym. Degrad. Stab.*, **2**, 143(1980).

[67] D. J. Carlsson, C. J. B. Dobbin, and D. M. Wiles, *Macromolecules*, **18**, 2092 (1985).

[68] R. Hikmet and A. Keller, *Radiat. Phys. Chem.*, **29**, 15(1987).

[69] D. J. Carlsson, C. J. B. Dobbin, J. P. T. Jensen, and D. M. Wiles, *ACS Symposium Series* **280**, 359, 1985.

[70] C. Birkinshaw, M. Buggy, S. Daly, and M. O'Neill, *Polym. Degrad. Stab.*, **22**, 285(1988).

[71] D. J. Carlsson, G. Colin, S. Chmela, and D. M. Wiles, *Textile Res. J.*, **58**, 520 (1988).

[72] C. M. Rimnac, R. W. Klein, N. Khanna, and J. T. Weintraub, *The 19th Annual Meeting of the Society for Biomaterials*, Birmingham, AL, 1993.

[73] C. M. Rimnac, R. W. Klein, F. Betts, and T. M. Wright, *J. Bone and Joint Surgery*, 76-A, 1052(1994).

CHAPTER 3

X-RAY SCATTERING FROM ULTRA-HIGH MOLECULAR WEIGHT POLYETHYLENE

3.1 Introduction

In chapter 2, we reported that peroxide crosslinking during compression molding at elevated temperature (170 °C) followed by crystallization on cooling reduced the degree of crystallinity and the melting temperature of ultra-high molecular weight polyethylene (UHMWPE) because crosslinks inhibit crystallization from the molten state. After exposure to high energy irradiation (gamma-rays) in the solid state at room temperature, UHMWPE exhibits an increase in degree of crystallinity and peak melting temperature because of the scission of taut tie molecules. Taut tie molecules are parts of polyethylene chains that connect two crystals and result from the separate crystallization of parts of long polyethylene chains. Irradiation-induced scission of taut tie molecules permits recrystallization of broken chains from noncrystalline regions, and results in an increase in the degree of crystallinity and an increased crystal perfection. However, for highly crosslinked UHMWPE (i.e., above 1 wt% peroxide), the effect of irradiation is reduced because peroxide crosslinking limits the length of scissioned chains and suppresses further crystallization. In this chapter, we describe a wide angle x-ray scattering (WAXS) technique to investigate the structure of peroxide crosslinked UHMWPE before and after irradiation.

The special usefulness of x-ray diffraction in the study of solid substances lies in its ability to distinguish ordered from disordered states [1]. For amorphous materials such as liquids and glasses, x-ray diffraction patterns consist of one or more diffuse halos, whereas, well-crystallized substances produce diffraction patterns consisting of sharp circles or spots [1]. When x-rays interact with matter, there are three scattering modes [2]:

(1) By atoms arranged randomly in space, as in a monatomic gas. This scattering occurs in all directions and is weak. Intensities of scattered rays are additive for different atoms.

(2) By atoms arranged periodically in space, as in a perfect crystal:

(a) In a very few directions, those satisfying Bragg's law, the scattering is strong and is called diffraction. Amplitudes of scattered rays add.

(b)In most directions, those not satisfying Bragg's law, there is no scattering because the scattered rays cancel one another.

Diffraction is essentially a scattering phenomenon in which a large number of atoms cooperate [2]. A diffracted beam can be defined as a beam composed of a large number of scattered rays mutually reinforcing one another [2]. Thus, the diffracted beam from a crystal is built up of rays scattered by all the atoms of the crystal which lie in the path of the incident beam. Because the atoms are arranged periodically on a lattice, the rays scattered by them have definite phase relations between them. These phase relations are such that destructive interference occurs in most directions of scattering, but in a few directions, constructive interference occurs and diffracted beams are formed. Therefore, the diffraction of x-rays occurs only at those particular angles of incidence which satisfy the Bragg law [2].

Diffraction of x-rays by a crystal is illustrated in Figure 3.1 [2]. In the crystal, atoms are arranged on a set of parallel planes A, B, C, D, ..., and spaced a distance d apart. Assume that a beam of perfectly parallel, perfectly monochromatic x-rays of wavelength λ

is incident on this crystal at an angle θ, called the Bragg angle, where θ is measured between the incident beam and the particular crystal plane under consideration.

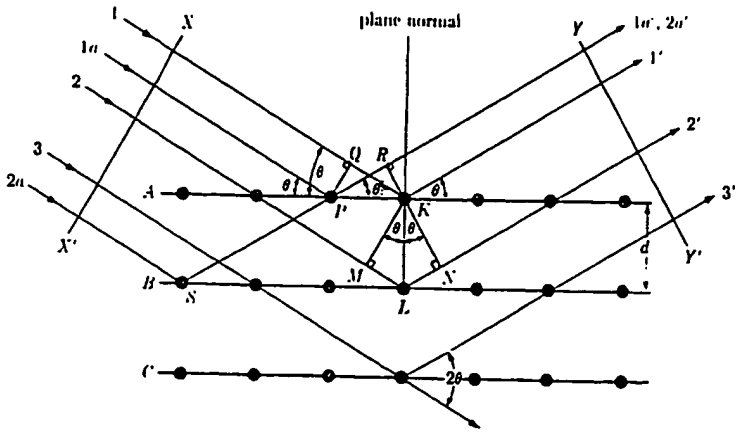

Figure 3.1. Diffraction of x-rays by a crystal [2].

First, consider rays 1 and 1a in the incident beam. They strike atoms K and P in the first plane of atoms and are scattered in all directions. Only in the directions 1' and 1a', however, are these scattered beams completely in phase and so capable of reinforcing one another; they do so because the difference in their length of path between the wave fronts XX' and YY' is equal to

$$QK - PR = PK\cos\theta - PK\cos\theta = 0. \qquad (1)$$

Similarly, the rays scattered by all the atoms in the first plane in a direction parallel to 1' are in phase and add their contributions to the diffracted beam. This will be true of all the

planes separately, and it remains to find the condition for reinforcement of rays scattered by atoms in different planes. For example, Rays 1 and 2 are scattered by atoms K and L, and the path difference for rays 1K1' and 2L2' is

$$ML + LN = d\sin\theta + d\sin\theta. \qquad (2)$$

This is also the path difference for the overlapping rays scattered by S and P in the direction shown, because in this direction there is no path difference between rays scattered by S and L or P and K. Scattered rays 1' and 2' will be completely in phase if this path difference is equal to a whole number n of wavelengths, or if

$$n\lambda = 2d\sin\theta. \qquad (3)$$

This relation is known as Bragg's law. When Bragg's law is satisfied, the diffracted beams are in phase and interfere constructively. n is called the order of reflection; it may take on any integral value consistent with sin θ not exceeding unity and is equal to the number of wavelengths in the path difference between rays scattered by adjacent planes. Therefore, for fixed values of λ and d, there may be several angles of incidence $\theta_1, \theta_2, \theta_3$..... at which diffraction may occur, corresponding to n = 1, 2, 3,..... In a first-order reflection (n =1), the scattered rays 1' and 2' would differ in length of path (and in phase) by one wavelength, ray 1' and 3' by two wavelengths, rays 1' and 4' by three wavelengths, and so on throughout the crystal. The rays scattered by all the atoms in all the planes are therefore completely in phase and reinforce one another (constructive interference) to form a diffracted beam in the direction shown. In all other directions of space, the scattered beams are out of phase and annul one another (destructive interference).

For UHMWPE, a radiation-induced increase in the DSC degree of crystallinity had been reported [3-15]. It was suggested that irradiation-induced scission of taut tie molecules

permits recrystallization of broken chains from noncrystalline regions, and results in an increase in the degree of crystallinity and an increased perfection of existing folded chain crystallites. From wide angle x-ray scattering (WAXS), an increase in x-ray crystallinity due to irradiation was also reported [6]. However, Minkova [10] reported that the x-ray degree of crystallinity did not change with dose up to 6 Mrad. He suggested that irradiation did not affect polymer crystallinity, but influenced the thermodynamic heat of melting. Using Peterlin's formula [16], it was explained that irradiation-induced scission of tie molecules in the amorphous regions, which predominated over crosslinking up to a dose of 3 Mrad, leads to an increase in the conformational mobility of molecules and to an increase in enthalpy of the amorphous regions [10]. By small angle x-ray scattering (SAXS), it was reported that the long spacing significantly decreased over the initial 16 Mrad of irradiation and then remained constant [6]. However, small angle x-ray scattering measurements showed that the actual lamellar thickness remained constant regardless of irradiation dose. It was suggested that if the regions of crystalline imperfection were relatively gross, their repair due to irradiation could produce a reduction in long spacing [6]. In addition, the growth of new lamellae due to recrystallization of broken tie molecules in the amorphous regions would reduce the long spacing without greatly affecting the average lamellar thickness [6]. A similar decrease in long spacing by irradiation was also observed by other authors [12]. On the other hand, it was reported that the long spacing did not change significantly with dose, but the thickness of lamellae first increased slightly and subsequently decreased with increasing dose [14]. It was suggested that molecular chains in noncrystalline surfaces of lamellae underwent crystallization due to radiation-induced chain scission at low doses, and crosslinking occurred in the surfaces of crystals as the irradiation dose increased to higher values [14]. Long spacing is the mean distance between the centers of successive crystalline regions along the chain direction and has a large-scale periodic character [1]. Multiplication of long spacing by the degree of crystallinity gives a

measure of lamellar thickness. For melt-crystallized polyethylene, the lamellar thickness increases with increasing crystallization temperature. In addition, increasing pressure during crystallization (e.g., above 3 kbar) and annealing also increase the lamellar thickness [17].

Compared to UHMWPE, conventional linear polyethylene of normal molecular weight exhibited a less pronounced increase in crystallinity by irradiation to low doses because of its low concentration of tie molecules[6,9-11]. Thus, radiation-induced crosslinking is the predominant result of high-energy irradiation of conventional linear polyethylene. By x-ray diffraction, Slichter et al. [18] studied the structure of polyethylene irradiated by fast electrons to high doses and found that the amorphous x-ray pattern became more prominent with increasing dose, at the expense of the crystalline pattern. In addition, both the amorphous and crystalline spacings tend to greater values with increasing dose up to a certain point [18]. They postulated that the increase in spacing corresponded to the introduction of voids into the structure, perhaps produced by radiation-induced chain branching or crosslinking. Katq et al.[19] studied the structural changes of high-density polyethylene irradiated by gamma-rays up to 4000 Mrad and found that the lattice constants a and b increased with increasing dose, and a continuous change of crystalline structure from the orthorhombic to hexagonal form was observed at doses above 1000 Mrad. It was suggested that the interior of the crystallites or microcrystallites were strained elastically under the influence of crosslinking near the surfaces of crystallites and in the amorphous regions, which leads to lattice distortion and expansion [19]. Similar changes in the lattice constants of highly gamma-irradiated polyethylene crystals were reported by Yoda et al. [20]. It also was reported that polyethylene films irradiated in vacuum exhibited a greater change in unit cell dimension than those irradiated in air at the same irradiation dose [20]. It was suggested that irradiation in vacuum mainly produced crosslinks and double bonds in the absence of oxygen, which resulted in larger lattice distortion and expansion of the lattice

spacing, whereas, irradiation in air induced chain scission in addition to the above two reactions, which possibly reduced lattice distortion and changes in unit cell dimension [20]

Yoda et al. [21] studied the crystallite size distribution and lattice distortion in gamma-irradiated linear polyethylene at high doses and found that the lateral crystallite size was little affected by irradiation up to 1000 Mrad, whereas, in the chain direction , the crystallite size decreased almost linearly with increasing irradiation dose. The degree of lattice distortion increased in the lateral direction, whereas in the chain direction, it was not affected in the dose range up to 1000 Mrad. They suggested that radiation-induced crosslinking occurred predominantly in the amorphous region on the lamellar surface of folded chain crystals, which induced break-up of the crystalline order from the surface, and thereby the crystallite size in the chain direction was reduced [21]. It also was reported by Yoda et al. [22] in a study of the crystallite size and distribution in polyethylene gamma-irradiated up to 2000 Mrad, that degradation of the crystallites occurred at the lamellar surface by the formation of crosslinks, and the range amorphised by irradiation in the chain direction was equal for smaller and larger crystallites. Gielenz and Jungnickel [23] studied the structures of linear polyethylene irradiated with fast electrons up to 150 Mrad in both the molten and solid states, and reported that for solid state irradiated samples, the crystalline structure and morphology were not influenced significantly by irradiation-induced crosslinking. For the melt-irradiated samples, it was concluded from x-ray measurements that insertion of lattice distortions occurred on crystallization from the melt, and the crystallite size decreased markedly with increasing irradiation dose [23]. They also observed from wide angle x-ray scattering measurements that the intensity of reflections decreased, and the width became broader with increasing dose [23]. This is because radiation-induced crosslinking in the molten state inhibits the growth of crystals on subsequent cooling, leading to a decreased crystallite size. Yeh et al. [24] studied the effect of radiation-induced crosslinking on the structure of branched polyethylene irradiated with

gamma-rays at room temperature under vacuum and found that a decrease in crystallinity began at a radiation dose ~100 Mrad, whereas lattice expansion indicating onset of an orthorhombic-hexagonal transition began as low as 10 Mrad. They suggested that the decrease in crystallinity was attributed to additional lattice distortions primarily introduced by the crosslinks occurring at the lateral grain boundaries, while lattice expansion was associated with the same crosslinking mechanism which began at the defects both within the crystals as well as those outside the crystals at the lateral grain boundaries [24]. By small angle x-ray scattering, Yeh et al. [25] examined the effect of radiation-induced crosslinking on the crystalline and amorphous densities of polyethylene irradiated with gamma-rays and reported that the crystalline density remained essentially constant, whereas the amorphous density increased continuously with increasing radiation dose. On the other hand, Nikolova et al. [26] investigated the structure of low density polyethylene films irradiated with fast electrons and reported that the x-ray crystallinity, total intensity of wide angle x-ray scattering, and dimension of the mosaic blocks in the [110] and [200] directions remained almost independent of the irradiation dose.

Kunert et al. [27] studied the structure of chemically crosslinked low density polyethylene and found that different peroxides produced a slightly different topology of polyethylene networks. They concluded that peroxide crosslinking introduced only slight changes in the dimension of the crystals. Kao and Phillips [28] studied the structure of low density polyethylene crosslinked with dicumyl peroxide up to 6.8% peroxide and found that the FWHM (full width at half maximum) showed a large broadening as crosslink density increased, and unit cell parameters (a and b) remained approximately constant except for the highest dicumyl peroxide concentration. This is because peroxide crosslinking inhibits the growth of crystals on cooling the melt and produces smaller crystals, leading to a broadening in the FWHM.

3.2 Experimental Details

Sample preparation has been described in chapter 2. Both slowly cooled and quench crystallized UHMWPE crosslinked with varied peroxide concentration are used for wide angle x-ray scattering measurements. Comparison of results for non-irradiated and irradiated samples is made.

Wide angle x-ray scattering (WAXS) measurements are performed at room temperature in a Rigaku diffractometer (model RTP 300) equipped with an IBM personal computer. Ni-filtered Cu K_α radiation (λ=1.5418 Å) at 35 kV and 50 mA is used for the x-ray measurements. Diffraction patterns are recorded from 2θ=10° to 30° at a scan interval of 0.02 degree. The sample dimensions are 20 x 18 x 1 mm. The intensity is recorded with a proportional counter. The two principal crystalline reflection peaks of uncrosslinked UHMWPE are (110) and (200) at 2θ equal to about 21.4° and 23.74°, respectively. Intensities of crystalline reflections (110) and (200) are determined after subtracting the amorphous halo by fitting the scattering curve with an 8th order polynomial. The full width at half maximum (FWHM) of crystalline reflections (110) and (200) was measured. The degree of crystallinity is calculated according to the Hermans-Weidinger method [29]. In resolving crystalline peaks, amorphous peak and background, the following assumptions are made [30]:

(i) The total scattering from the sample is divided between crystalline peaks from crystallites and amorphous peaks from remaining amorphous regions (assuming a simple two phase model for the polymer).

(ii) The total scattering from the sample is included in resolved crystalline and amorphous regions.

(iii) The relative areas of crystalline peaks and amorphous peak are respectively proportional to the number of electrons (and thus mass) in the crystallite and the amorphous regions.

Therefore, the value of the crystalline fraction (i.e., crystallinity), X_c, is calculated according to the expression [29]:

$$X_c = \frac{A(\text{crystalline})}{A(\text{crystalline}) + KA(\text{amorphous})} \qquad (4)$$

where A(crystalline) and A(amorphous) are areas of crystalline reflections and amorphous halo, respectively; K is a constant and can be set to unity for comparative purposes. As shown in Figure 3.2, the degree of crystallinity is calculated from the ratio of the area remaining under the crystalline peaks to the area under the full scattering curve. Interplanar spacings (d_{110} and d_{200}) in the crystalline regions are calculated using the Bragg equation:

$$2d_{hkl} \sin \theta = \lambda \qquad (5)$$

Here, d_{hkl} is the interplanar spacing between parallel planes (h k l) in the crystallites, θ is the Bragg angle, and λ is the wavelength of radiation.

3.3 Results and Discussion

Effect of Peroxide Crosslinking on the Structure of UHMWPE

X-ray diffraction patterns of UHMWPE crosslinked with varied peroxide concentration are shown in Figures 3.3 and 3.4 for slowly cooled and quench crystallized samples, respectively. As shown in Figure 3.3, for slowly cooled samples, the total intensity

Figure 3.2. X-ray diffraction pattern of UHMWPE before peroxide crosslinking or irradiation and showing resolved peaks.

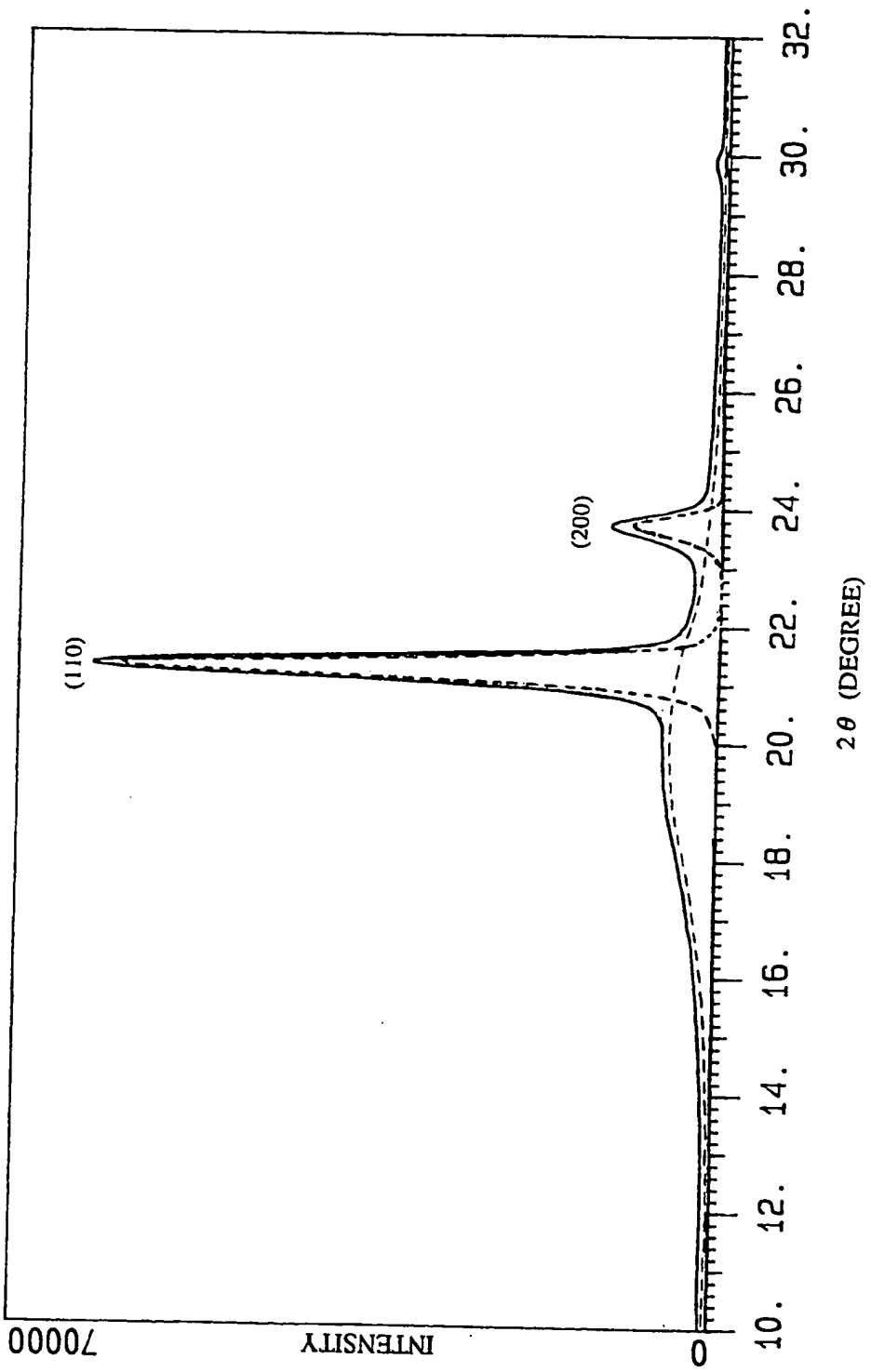
70000
INTENSITY
0
10.
12.
14.
16.
18.
20.
22.
24.
26.
28.
30.
32.
2θ (DEGREE)
(110)
(200)

Figure 3.3. X-ray diffraction patterns of UHMWPE crosslinked with varied peroxide concentrations before irradiation. (a) ; (b) curves superposed. **Slowly cooled.**

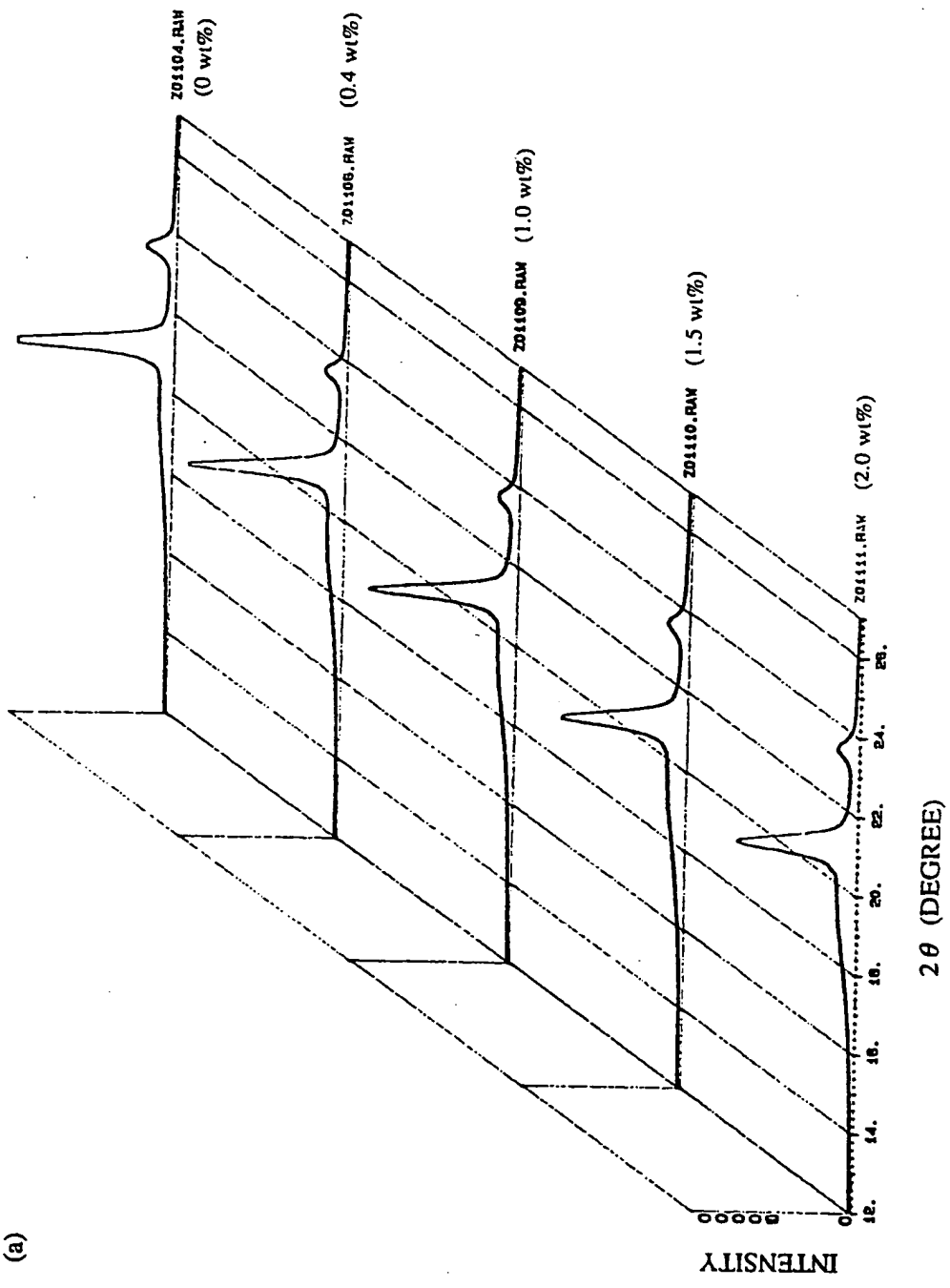
ZD1104.RAW (0 wt%)
ZD1105.RAW (0.4 wt%)
ZD1109.RAW (1.0 wt%)
ZD1110.RAW (1.5 wt%)
ZD1111.RAW (2.0 wt%)
INTENSITY
2θ (DEGREE)
(a)

(b)

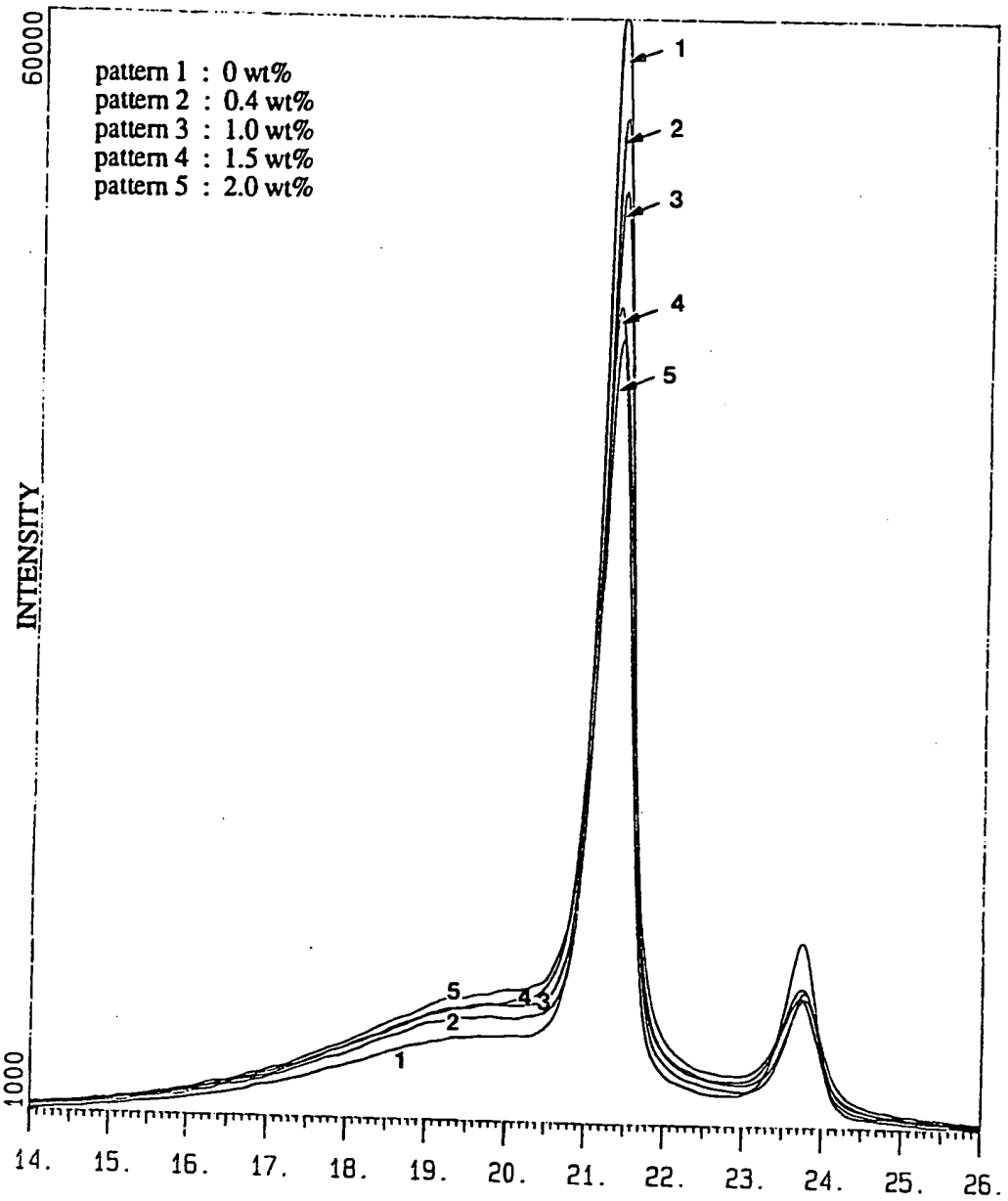
pattern 1 : 0 wt%
pattern 2 : 0.4 wt%
pattern 3 : 1.0 wt%
pattern 4 : 1.5 wt%
pattern 5 : 2.0 wt%
60000
1000
INTENSITY
1
2
3
4
5
14.
15.
16.
17.
18.
19.
20.
21.
22.
23.
24.
25.
26.
2θ (DEGREE)

Figure 3.4. X-ray diffraction patterns of UHMWPE crosslinked with varied peroxide concentrations before irradiation. (a) ; (b) curves superposed. **Quenched samples**

(a)

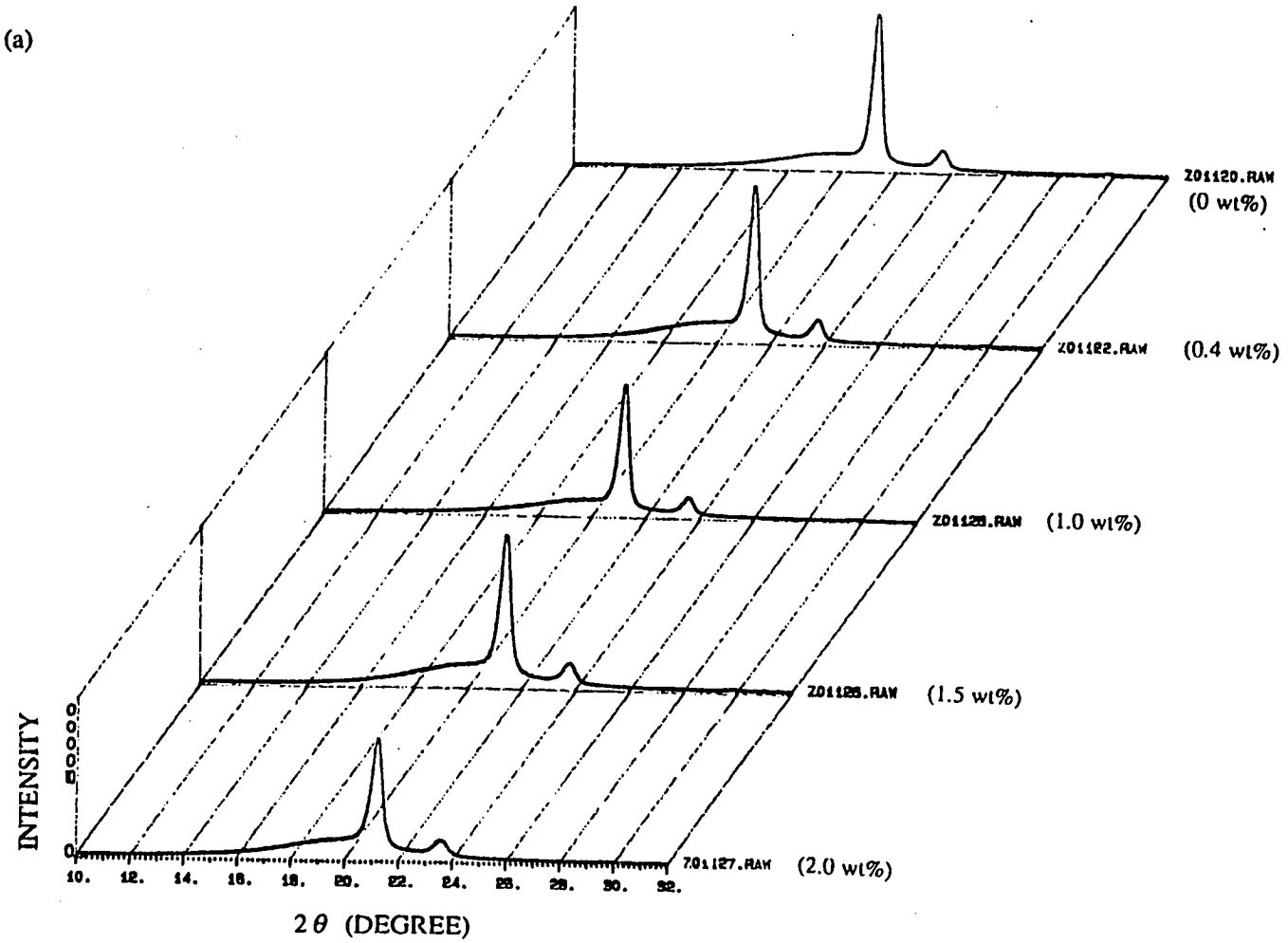
ZD1120.RAW
(0 wt%)
ZD1122.RAW
(0.4 wt%)
ZD1126.RAW
(1.0 wt%)
ZD1125.RAW
(1.5 wt%)
ZD1127.RAW
(2.0 wt%)
INTENSITY
50000
0
10. 12. 14. 16. 18. 20. 22. 24. 26. 28. 30. 32.
2θ (DEGREE)

(b)

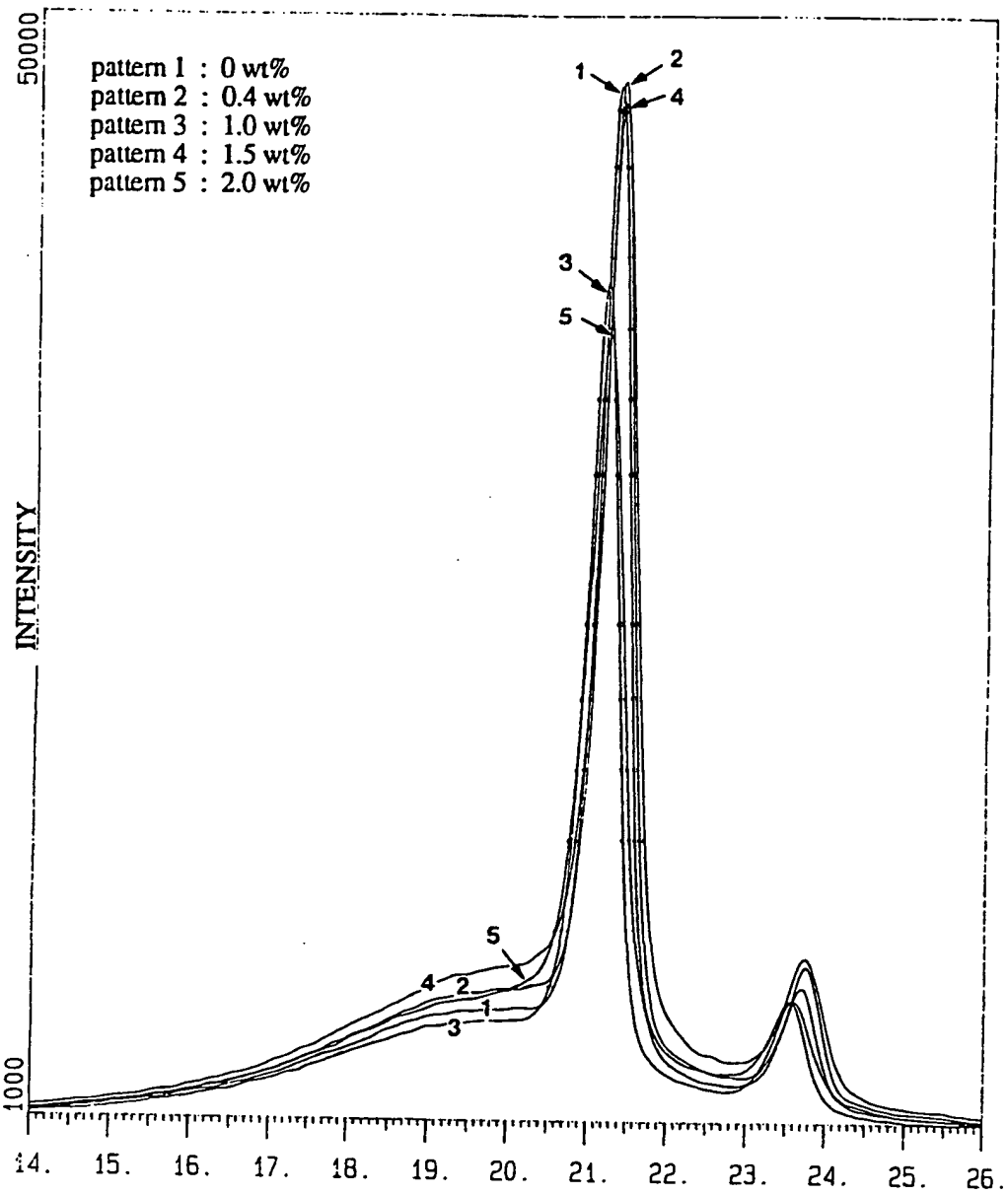
pattern 1 : 0 wt%
pattern 2 : 0.4 wt%
pattern 3 : 1.0 wt%
pattern 4 : 1.5 wt%
pattern 5 : 2.0 wt%
50000
1000
INTENSITY
14. 15. 16. 17. 18. 19. 20. 21. 22. 23. 24. 25. 26.
2θ (DEGREE)

systematically decreases with increasing peroxide concentration, while the intensity of the amorphous halo increases as the peroxide concentration increases. Similar trends are observed in quench crystallized samples except for the 1.5 wt% sample, which shows lower intensity of the amorphous halo. Comparison of the intensities of the crystalline peaks (110) and (200) between slowly cooled and quench crystallized samples as a function of peroxide concentration is shown in Figures 3.5 and 3.6, respectively. From Figure 3.5, it can be seen that the crystalline peak (110) intensity for slowly cooled samples is higher than that of quench crystallized ones and the intensities decrease with peroxide concentration. Similar trends are observed in Figure 3.6 for the peak (200) intensity. However, the difference in crystalline peak intensity for both slowly cooled and quenched samples becomes smaller as peroxide concentration increases. Gielenz et al. [23] reported a similar decrease in intensity with increasing radiation dose for melt-irradiated polyethylene. For melt-irradiated polyethylene, irradiation-induced crosslinking hinders the growth of crystals from the molten state and leads to the crystallinity decrease from 77 % for the non-irradiated sample to 30 % for the sample irradiated with 150 Mrad [23]. In addition, they reported that crystallite sizes decreased markedly and crystalline reflections became broader with increasing irradiation dose for the melt-irradiated sample. A comparison of x-ray crystallinity between slowly cooled and quench crystallized UHMWPE samples as a function of peroxide concentration is shown in Figure 3.7. It can be seen that both samples show a decreased crystallinity with increasing peroxide concentration, while the crystallinity of slowly cooled samples is higher than that of quench crystallized samples. Again, the difference in crystallinity for both samples becomes smaller as peroxide concentration increases. The results are consistent with DSC measurements which showed that above 0.6 wt% peroxide, the crystallinities of both slowly cooled and quench crystallized UHMWPE samples were equal (Chapter 2). Because of extremely long molecular chains and a high concentration of entanglements in UHMWPE (which produce

a high melt viscosity), quenching further limits crystallization from the melt. In addition, peroxide crosslinking inhibits molecular chain motion in the molten state. Therefore, with increasing peroxide concentration, the effect of quenching will be mitigated. Decreases in the intensities of crystalline reflections are ascribed to a decrease in the degree of crystallinity. Because peroxide crosslinking was performed above the melting temperature of the polymer, the crosslinking step preceded the crystallization step. Thus, crystallization from a crosslinked melt would lead to a decreased crystallinity because peroxide crosslinking inhibited the growth of crystals from the molten state.

Figures 3.8 and 3.9 show a comparison of FWHM of 2θ (110) and (200) between slowly cooled and quench crystallized samples as a function of peroxide concentration. It can be seen that FWHM increases with increasing peroxide concentration in both samples, in agreement with literature [28]. The FWHM is a measure of the size and perfection of crystals [17]. The higher the crystal perfection and / or the larger the crystal size, the lower the FWHM. Therefore, an increase in FWHM with increasing peroxide concentrations indicates that the size and perfection of crystals are reduced with increasing peroxide concentrations. In addition, slowly cooled samples have smaller values of FWHM than quench crystallized ones. This indicates that slowly cooled UHMWPE samples have larger crystal sizes and higher crystal perfection than quench crystallized ones. Interplanar spacings d_{110} and d_{200} for both slowly cooled and quench crystallized samples as a function of peroxide concentration are shown in Figures 3.10 and 3.11, respectively. As shown in Figure 3.10, interplanar spacings, d_{110} and d_{200}, for slowly cooled samples remain essentially constant, in agreement with literature [27]. From Figure 3.11 for quench crystallized UHMWPE, it can be seen that interplanar spacings, d_{110} and d_{200}, remain essentially constant at low peroxide concentration but may change slightly at higher peroxide concentration. It is possible that increased defects introduced by higher levels of peroxide crosslinking introduce changes in interplanar spacings in quenched samples.

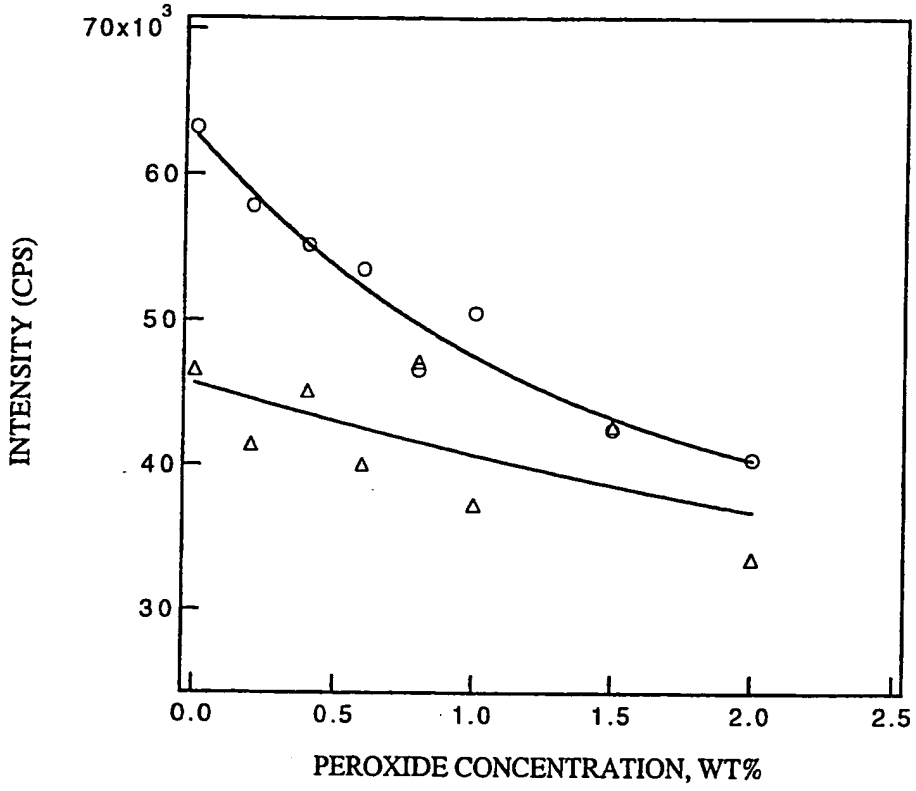

Figure 3.5. Comparison of peak (110) intensity between slowly cooled (○) and quench crystallized (Δ) samples as a function of peroxide concentration. **Before irradiation.**

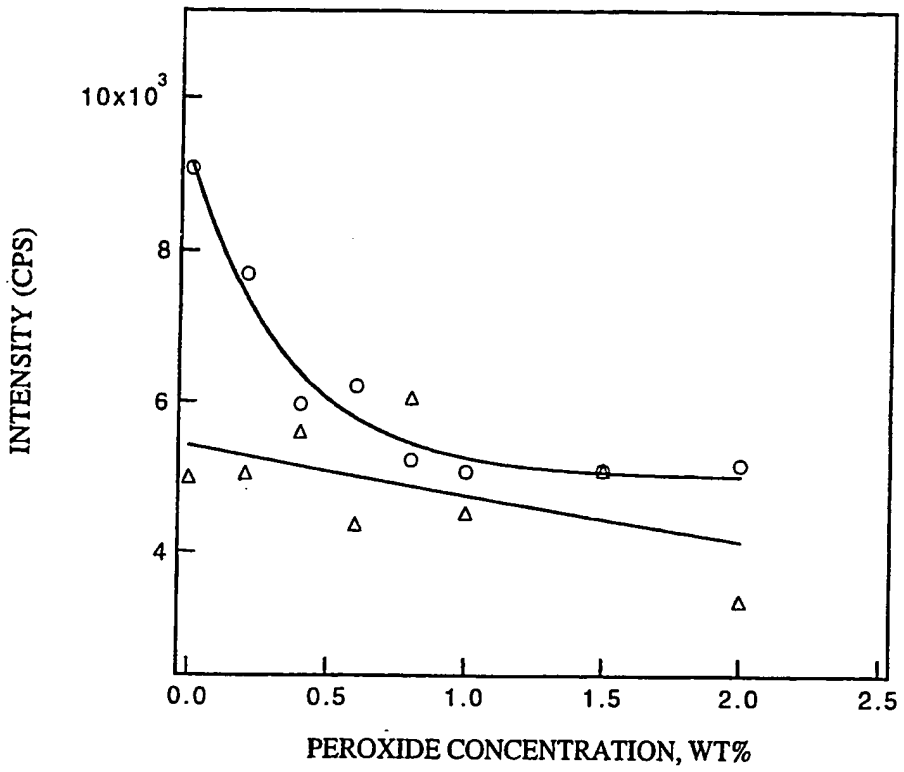

Figure 3.6. Comparison of peak (200) intensity between slowly cooled (○) and quench crystallized (Δ) samples as a function of peroxide concentration. **Before irradiation.**

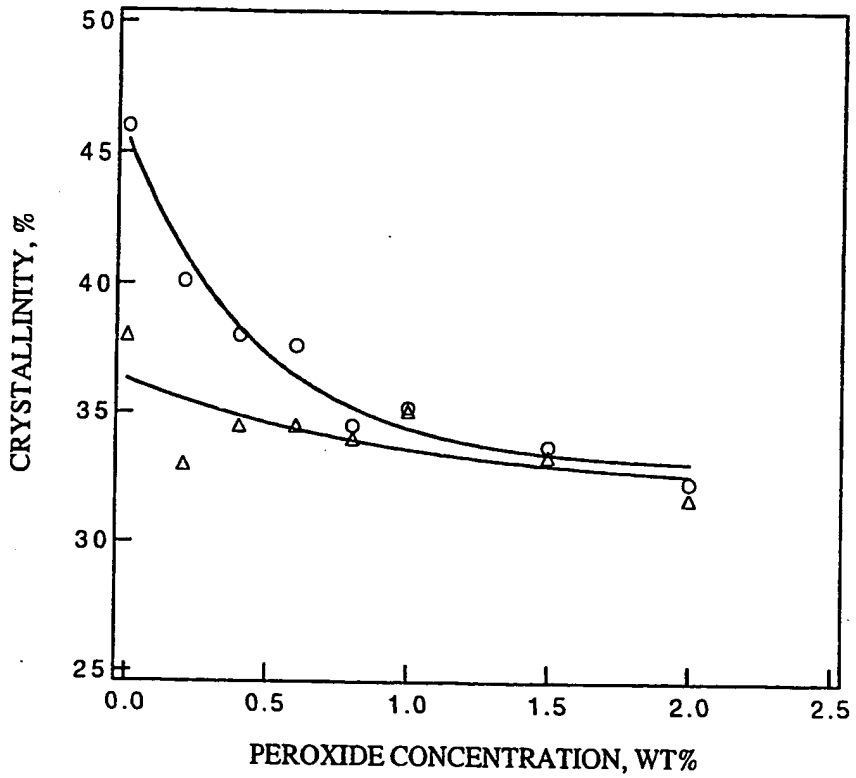

Figure 3.7. Comparison of x-ray crystallinity between slowly cooled (○) and quench crystallized (Δ) samples as a function of peroxide concentration. **Before irradiation.**

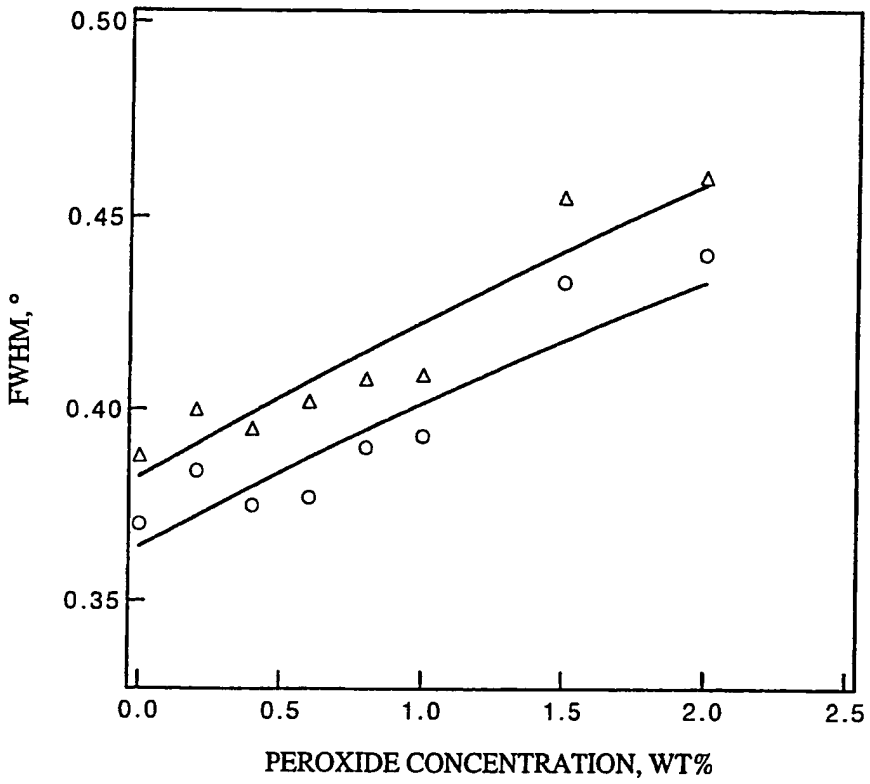

Figure 3.8. Comparison of FWHM of 2θ (110) between slowly cooled (○) and quench crystallized (Δ) samples as a function of peroxide concentration. **Before irradiation.**

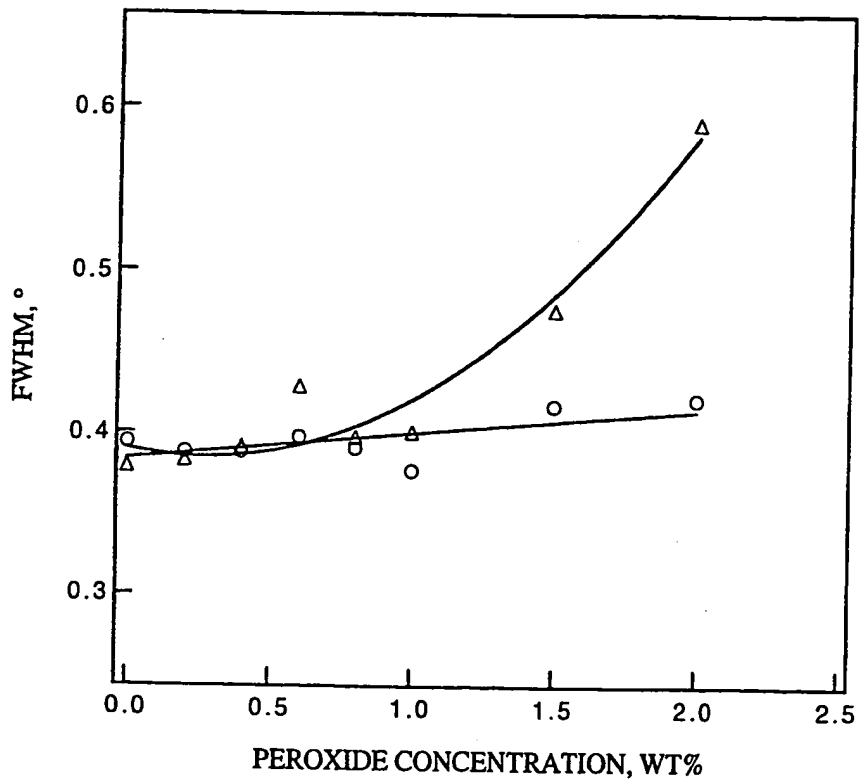

Figure 3.9. Comparison of FWHM of 2θ (200) between slowly cooled (o) and quench crystallized (Δ) samples as a function of peroxide concentration. **Before irradiation.**

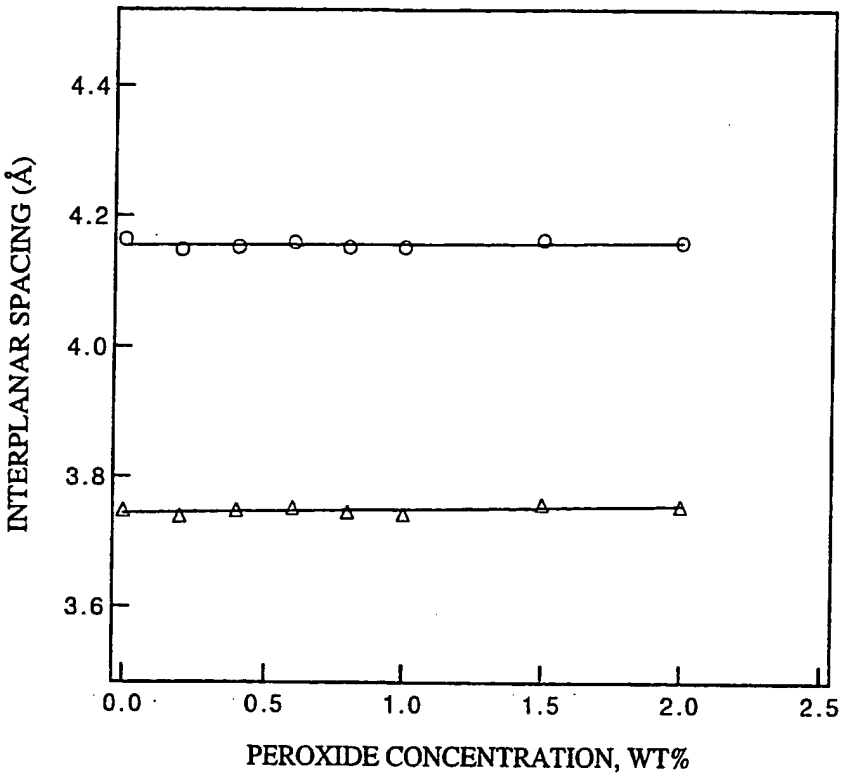

Figure 3.10. Interplanar spacings d_{110} (○) and d_{200} (Δ) of slowly cooled UHMWPE as a function of peroxide concentration. **Before irradiation.**

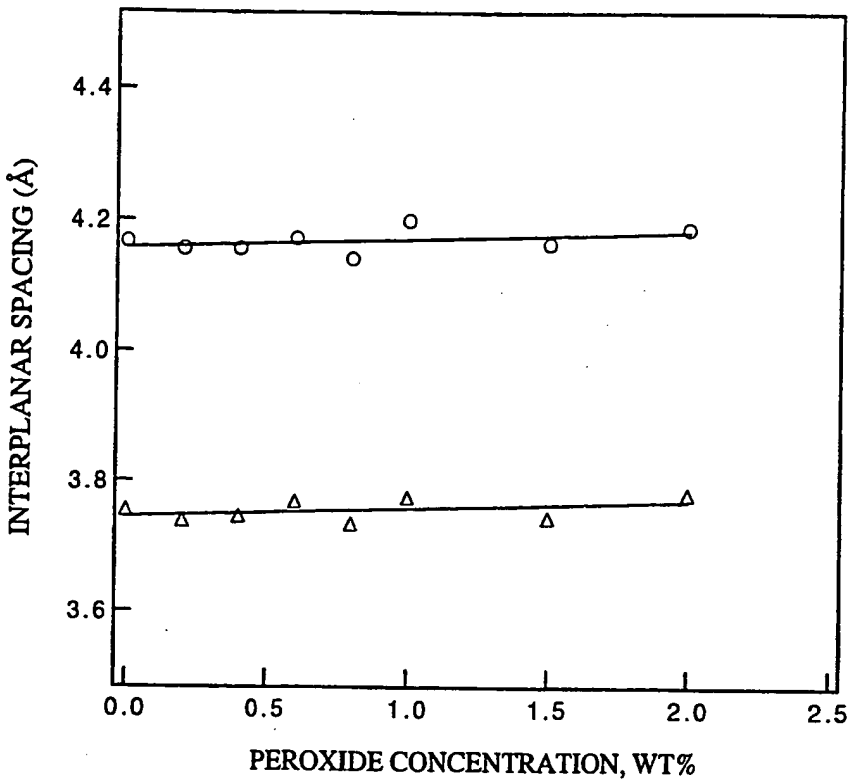

Figure 3.11. Interplanar spacings d_{110} (○) and d_{200} (Δ) of quench crystallized UHMWPE as a function of peroxide concentration. **Before irradiation.**

From x-ray diffraction theory, it is known that a well-defined and sharp crystalline diffraction pattern can be obtained for an ideal crystal of infinite size and long periodicity. Melt-crystallized polymers are only semi-crystalline. This is because there is a large number of chain entanglements in the melt and hence it is impossible to achieve the organization required to form a 100% crystalline polymer during crystallization [31]. Consequently, crystals formed from the melt have finite size and irregularities. The finite size and the presence of defects in a crystal will lead to a broadening of crystalline diffraction maxima. The types of defects include point defects such as vacancies or interstitial atoms, dislocations (e.g., screw and edge) due to the movement of line defects, the fold surface and chain folds, and the grain boundaries between crystals [31]. These defects result in a distortion of the crystal lattice and broaden the x-ray diffraction maxima. In general, distortions which occur in crystal lattices are classified as distortions of the first kind or as distortions of the second kind [30,32]. For distortions of the first kind, the long-range order of the crystal lattice is preserved, whereas for distortions of the second kind, the long-range order is destroyed [30]. Both types of distortion introduce local displacements of atoms, groups of atoms, or molecules from their positions in an ideal lattice [30]. When distortions of the first kind exist in crystal lattices, the Bragg reflections lose some of their intensity, which is incorporated into the background [32]. When distortions of the second kind exist, diffraction patterns consist of humps of different shapes, leading to an increase in reflection breadth and an decrease in intensity. The intensities of crystalline reflections give an indication of crystallinity [1]. The higher the intensity, the higher the crystallinity. Our experimental results on intensity and crystallinity are consistent with these interpretations.

In the peroxide crosslinking process, the degree of crystallinity decreases with increasing peroxide concentration because crosslinks hinder the growth of the crystal from a crosslinked melt. Therefore, the crystallite size of crosslinked UHMWPE must be smaller

than that of uncrosslinked UHMWPE and increasing the peroxide concentration will lead to a reduction in crystallite size. In addition, peroxide crosslinking will introduce crystal imperfections. Therefore, our experimental results show a decreased intensity and an increase in broadening of the crystalline reflections (i.e., an increased FWHM) with increasing peroxide concentration. Interplanar spacings d_{110} and d_{200} of slowly cooled UHMWPE remain essentially constant throughout the range of peroxide concentrations. That means that none or very few crystal distortions occur within slowly cooled samples. Thus, a reduction in crystallite size would be the main reason for broadening of the crystalline reflections.

Because of extremely long molecular chains, UHMWPE contains a high concentration of entanglements, even after melting [12,33]. Thus, in the melt state, chain entanglements lead to a significant increase in viscosity. Extensive crystal growth will be hindered by chain entanglements [34]. Since crystallization on cooling the melt takes place when the polymer is a very viscous liquid, and in this state the chains are highly entangled, sufficient time must be allowed for the chains to diffuse to form the three-dimensional order required for crystallite formation [35]. Thus, quenching (or rapid cooling) will provide less opportunity for crystal growth. In addition, the quenching process prevents the chains from disentangling, and due to the extremely long molecular chains and the presence of entanglements, one molecule can crystallize into several lamellae [12]. Consequently, the crystallinity, crystallize size, and crystalline perfection of quench crystallized samples will be reduced. Our experimental observations that quench crystallized UHMWPE has a lower intensity of crystalline reflections and decreased crystallinity, and higher values of FWHM compared to those of slowly cooled samples, are consistent with these arguments. Also, it is possible that increased defects introduced by higher levels of peroxide crosslinking introduce changes in interplanar spacings in quenched samples.

Effect of Irradiation on the Structure of Peroxide Crosslinked UHMWPE

The diffraction patterns of UHMWPE crosslinked with varied peroxide concentrations and gamma-irradiated to 3.4 Mrad are shown in Figures 3.12 and 3.13 for slowly cooled and quench crystallized samples, respectively. After irradiation, the total intensity of diffraction for slowly cooled UHMWPE systematically decreases with increasing peroxide concentration, while the intensity of the amorphous halo increases as the peroxide concentration increases. Comparing Figure 3.3a (before irradiation) to Figure 3.12a, it can be seen that the crystalline reflections become sharper, and that the intensity of the amorphous halo decreases after irradiation. Similar trends are observed in quench crystallized samples (Figures 3.4 and 3.13). A comparison of the intensities of crystalline reflections (110) and (200) before and after irradiation as a function of peroxide concentration for slowly cooled UHMWPE is shown in Figures 3.14 and 3.15, respectively. It can be seen that after irradiation the intensities of crystalline reflections (110) and (200) increase. However, the data are scattered, especially for reflection (200). This is because the intensity of reflection (200) is quite small, and after subtracting the intensity of the amorphous halo, more experimental variations occur. A similar comparison is made for quench crystallized UHMWPE samples and a similar trend is observed (not shown in Figure). For quench crystallized samples, the data are even much scattered. This is because the small crystals generated by quenching as well as irradiation-induced scission of tie molecules are insensitive to x-ray diffraction. Therefore, much more intensity variation exists for quench crystallized samples. A comparison of x-ray crystallinity before and after irradiation as a function of peroxide concentration for slowly cooled and quench crystallized samples is shown in Figures 3.16 and 3.17, respectively. After irradiation, the degree of crystallinity increases in both cases. In addition, it is observed that the difference

in crystallinity, before and after irradiation becomes smaller as peroxide concentration increases. It is suggested that radiation effects are mitigated at high peroxide concentration.

A comparison of FWHM of (110) peak before and after irradiation as a function of peroxide concentration for a slowly cooled UHMWPE is shown in Figures 3.18. A Similar comparison for quench crystallized UHMWPE is shown in Figures 3.19. The FWHM indicates the size and perfection of crystals. The higher the crystal perfection and / or the larger the crystal size, the lower the FWHM. It can be seen that after irradiation the FWHM of the (110) crystalline reflection decreases. A similar trend is observed for the (200) reflection (not shown in Figure) in both slowly cooled and quench crystallized samples, but the data are scattered. Again, this is because the (200) reflection is a small peak, and after subtracting the amorphous halo, more variations occur. It is suggested that crystal perfection is improved by radiation-induced scission of tie molecules in the amorphous regions. A comparison of interplanar spacings d_{110} and d_{200} before and after irradiation as a function of peroxide concentration for slowly cooled and quench crystallized samples is shown in Figures 3.20 and 3.21, respectively. It can be seen that after gamma-irradiation (3.4 Mrads), the unit cell dimensions are unaffected in both cases. It has been reported that irradiation to high doses would induce lattice distortions or orthorhombic $\rightarrow$ hexagonal phase transformation [18-24,36].

The effect of energetic irradiation on UHMWPE has been extensively studied [3-15]. Generally, irradiation to low doses leads to an increase in crystallinity and melting temperature. It was suggested that irradiation-induced scission of taut tie molecules permits recrystallization of broken chains from the amorphous regions, and results in an increase in the degree of crystallinity and an increased perfection of existing folded chain crystallites [3-15]. It is believed that radiation-induced scission of tie molecules will release constraints on the crystalline region (particularly on the lamellar or fold surfaces) and hence crystal perfection is improved. Our experimental results show that irradiated UHMWPE exhibits

Figure 3.12. X-ray diffraction patterns of slowly cooled UHMWPE crosslinked with varied peroxide concentrations. (a) ; (b) curves superposed. **After irradiation.**

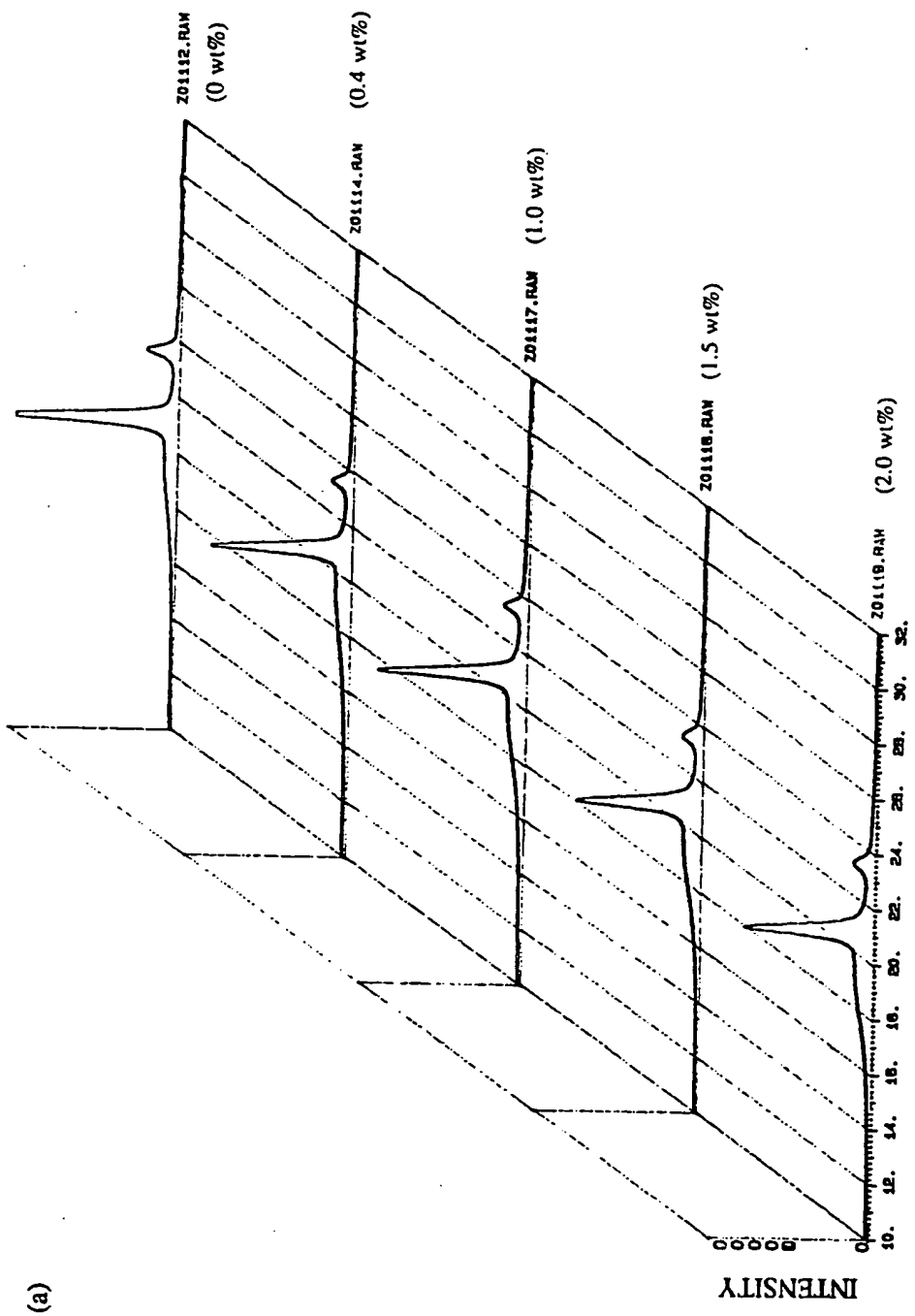
(a)
Z01112.RAW
(0 wt%)
Z01114.RAW
(0.4 wt%)
Z01117.RAW
(1.0 wt%)
Z01118.RAW
(1.5 wt%)
Z01119.RAW
(2.0 wt%)
INTENSITY
10.
12.
14.
16.
18.
20.
22.
24.
26.
28.
30.
32.
2θ (DEGREE)

(b)

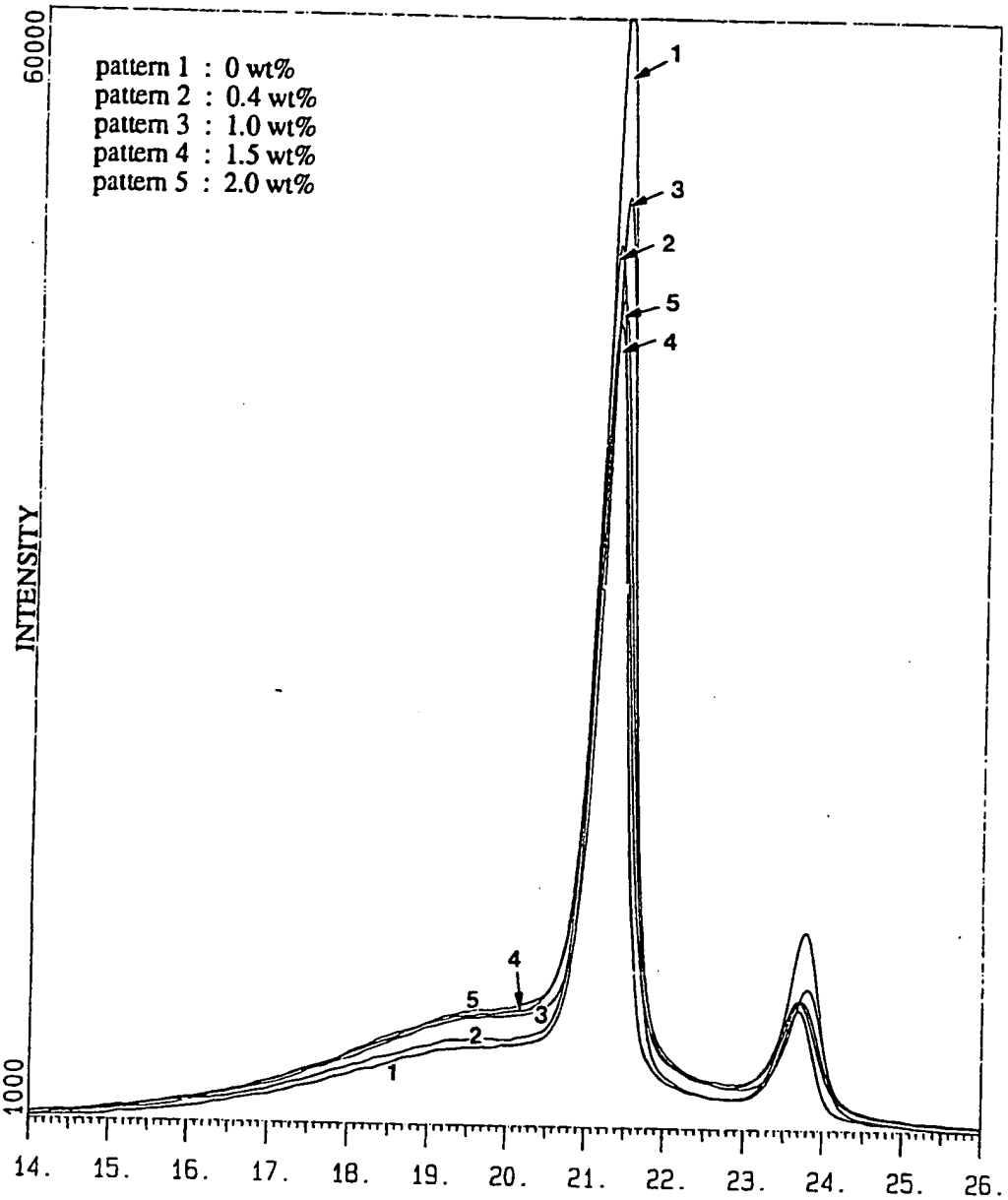
pattern 1 : 0 wt%
pattern 2 : 0.4 wt%
pattern 3 : 1.0 wt%
pattern 4 : 1.5 wt%
pattern 5 : 2.0 wt%
60000
1000
INTENSITY
1
2
3
4
5
14.
15.
16.
17.
18.
19.
20.
21.
22.
23.
24.
25.
26.
2θ (DEGREE)

Figure 3.13. X-ray diffraction patterns of quench crystallized UHMWPE crosslinked with varied peroxide concentrations. (a) ; (b) curves superposed. **After irradiation.**

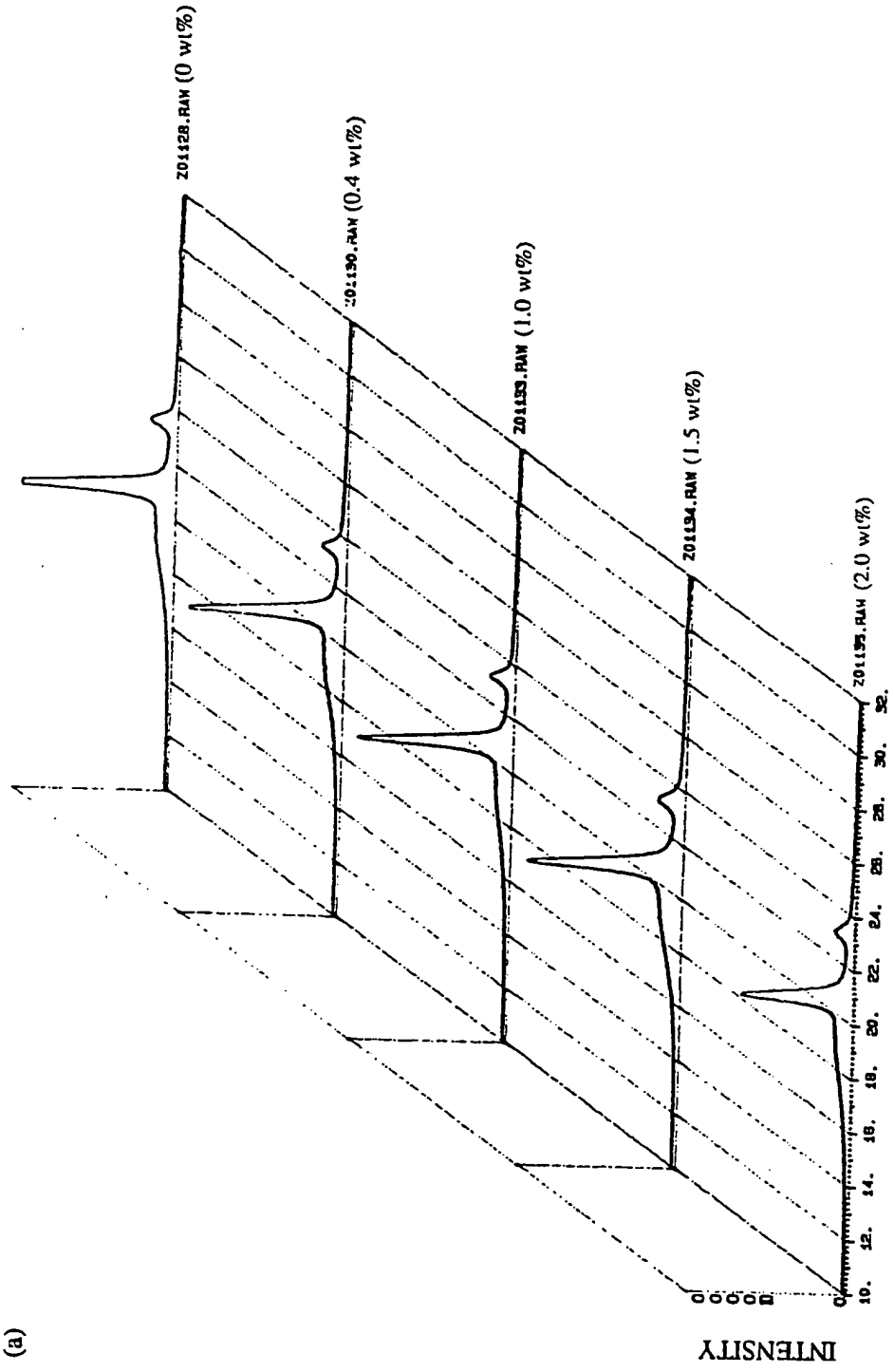
Z01128.RAW (0 wt%)
Z01130.RAW (0.4 wt%)
Z01133.RAW (1.0 wt%)
Z01134.RAW (1.5 wt%)
Z01135.RAW (2.0 wt%)
INTENSITY
2θ (DEGREE)

(a)

(b)

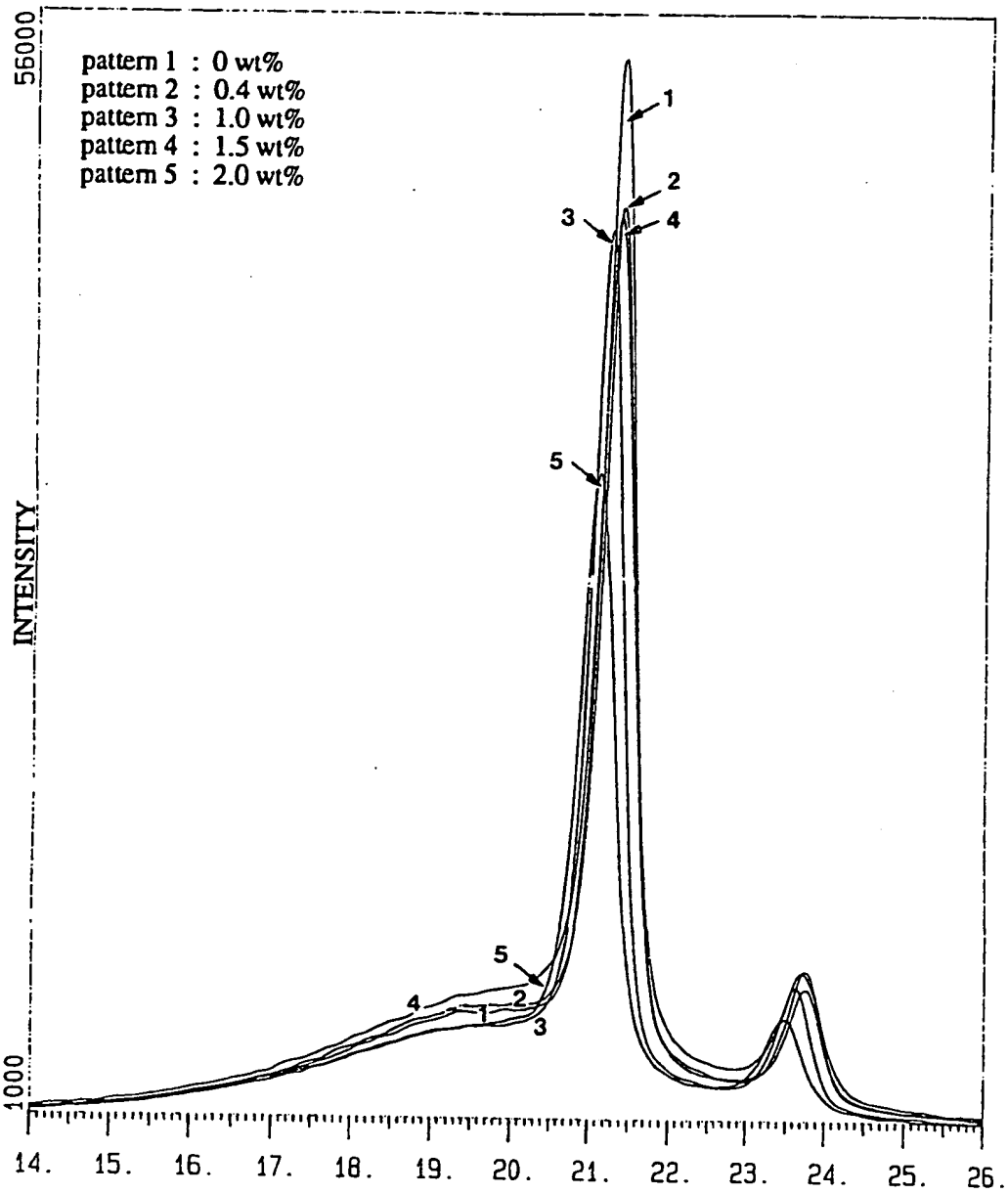
pattern 1 : 0 wt%
pattern 2 : 0.4 wt%
pattern 3 : 1.0 wt%
pattern 4 : 1.5 wt%
pattern 5 : 2.0 wt%
56000
1000
INTENSITY
14. 15. 16. 17. 18. 19. 20. 21. 22. 23. 24. 25. 26.
2θ (DEGREE)

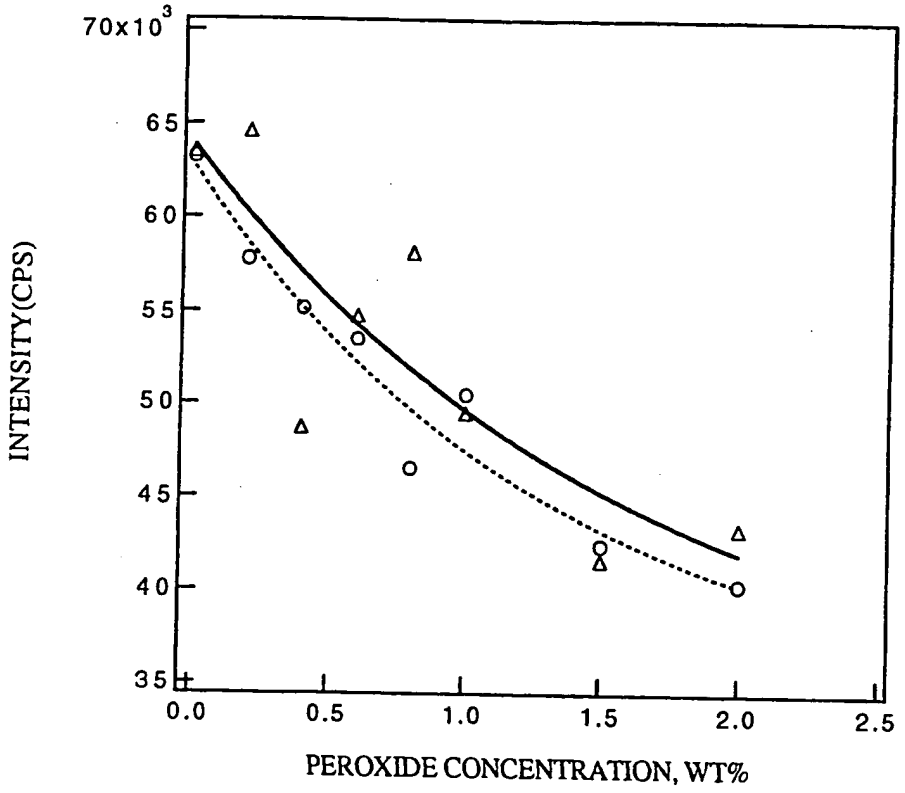

Figure 3.14. Comparison of peak (110) intensity before (o) and after (Δ) irradiation as a function of peroxide concentration. **Slowly cooled.**

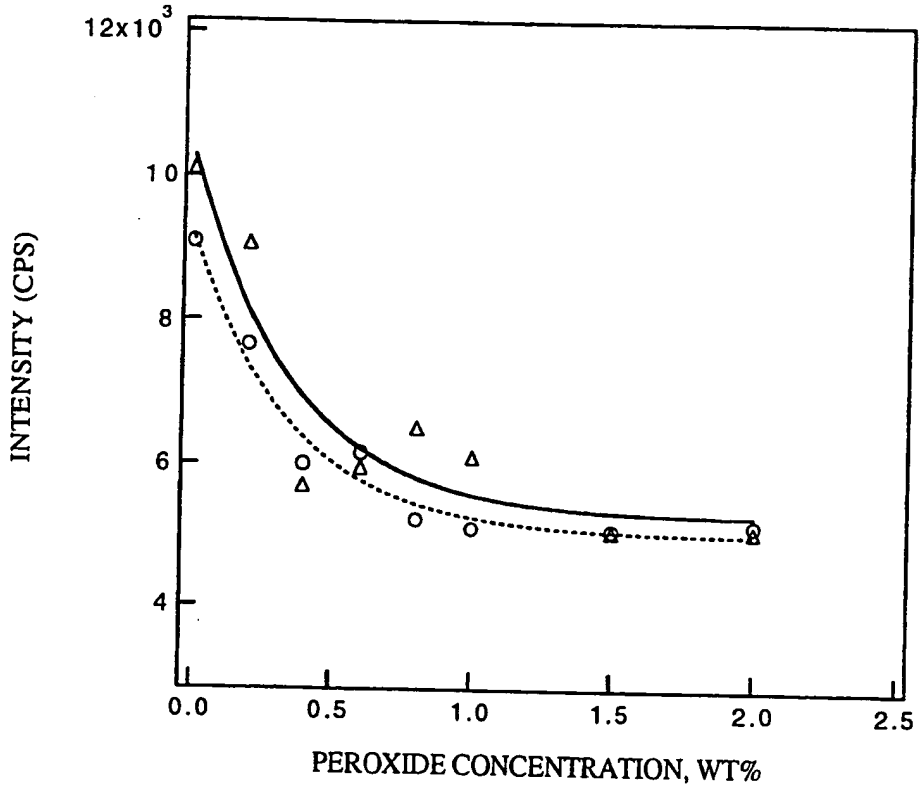

Figure 3.15. Comparison of peak (200) intensity before (○) and after (Δ) irradiation as a function of peroxide concentration. **Slowly cooled.**

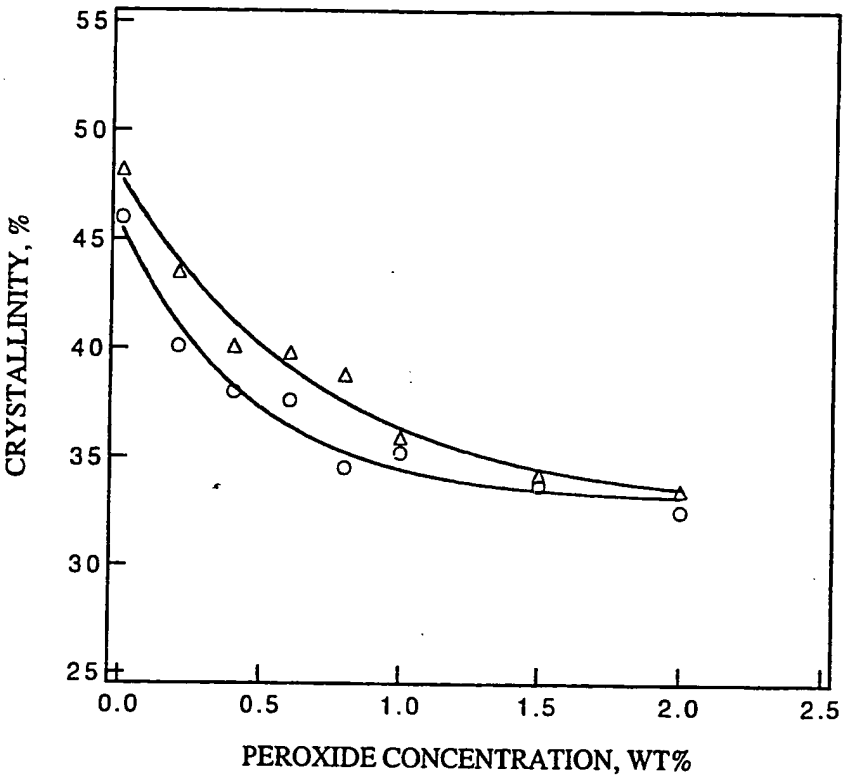

Figure 3.16. Comparison of x-ray crystallinity before (○) and after (Δ) irradiation as a function of peroxide concentration. **Slowly cooled.**

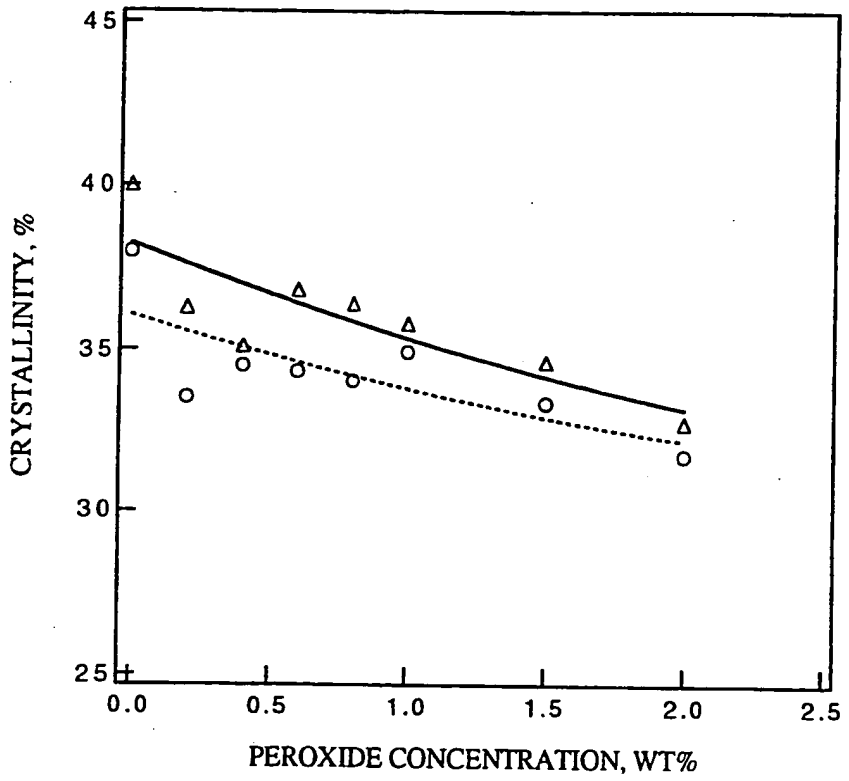

Figure 3.17. Comparison of x-ray crystallinity before (o) and after (Δ) irradiation as a function of peroxide concentration. **Quench crystallized.**

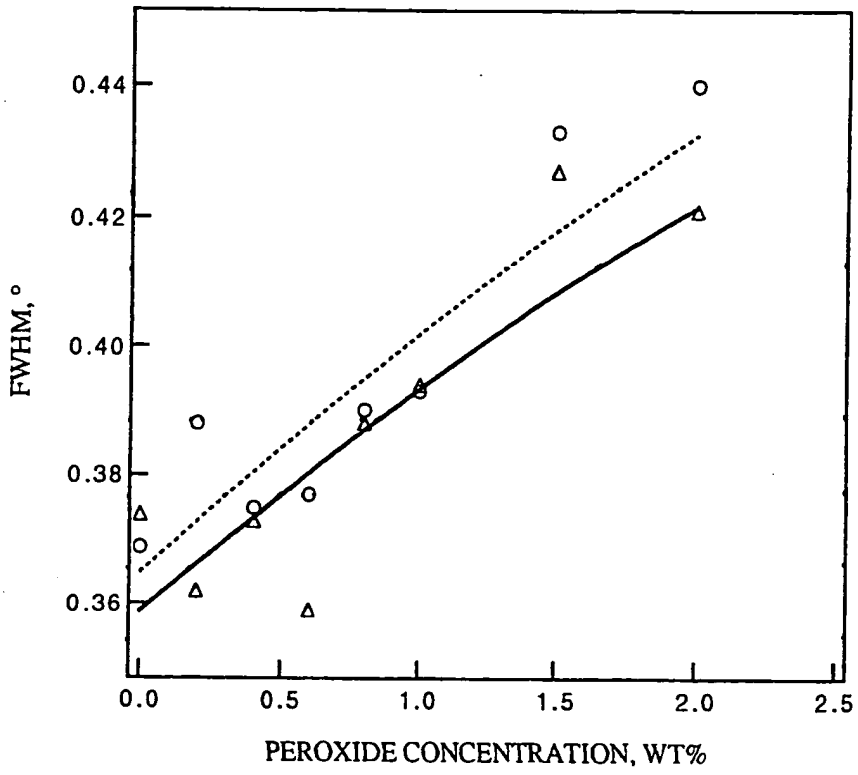

Figure 3.18. Comparison of FWHM of (110) peak (○) and after (Δ) irradiation as a function of peroxide concentration. **Slowly cooled.**

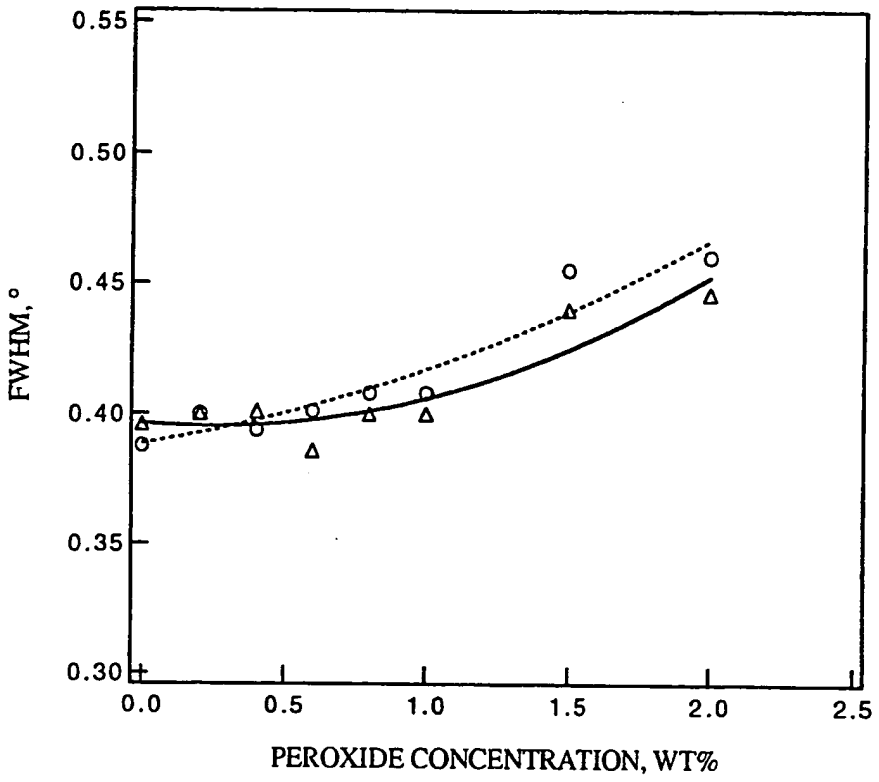

Figure 3.19. Comparison of FWHM of (110) peak before (o) and after (Δ) irradiation as a function of peroxide concentration. Quench crystallized.

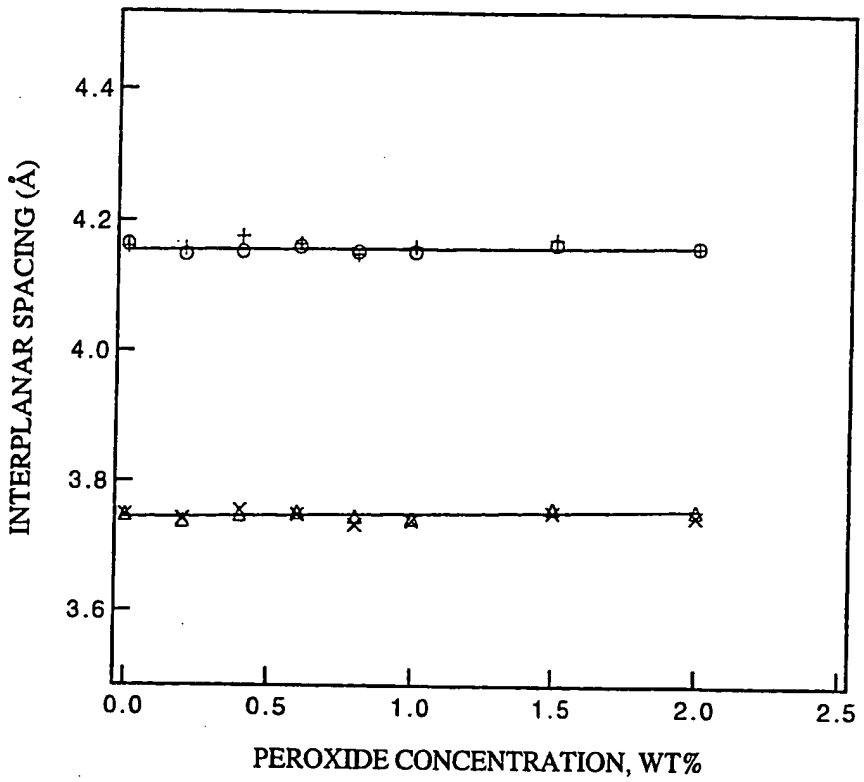

Figure 3.20. Comparison of interplanar spacings before (d_{110}, (○); d_{200}, (Δ)) and after (d_{110}, (+); d_{200} (×)) irradiation as a function of peroxide concentration. **Slowly cooled.**

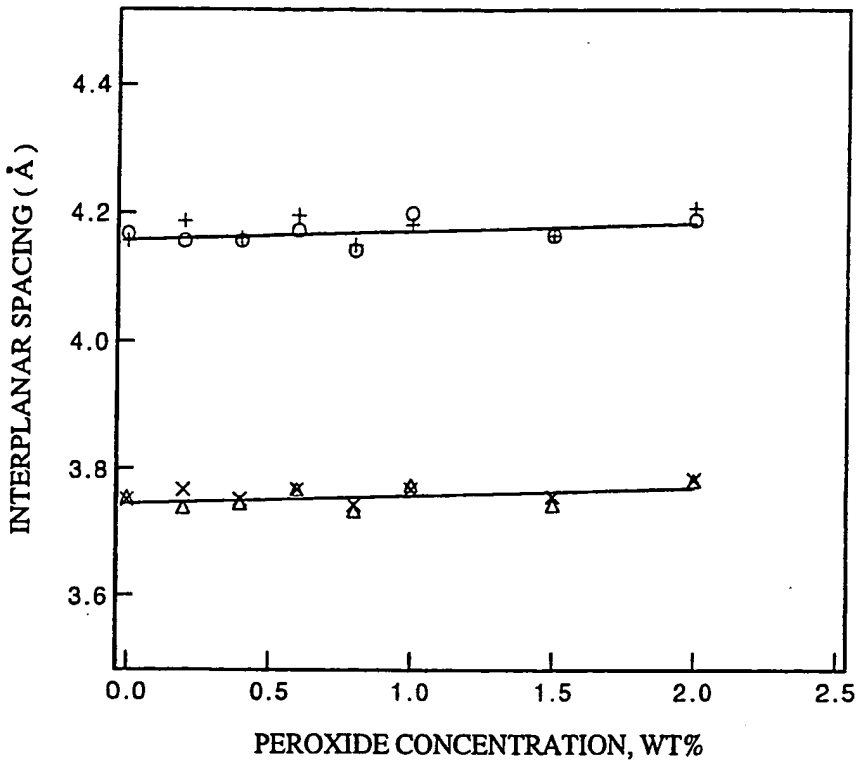

Figure 3.21. Comparison of interplanar spacings before (d_{110}, (○); d_{200}, (Δ)) and after (d_{110}, (+); d_{200}, (×)) irradiation as a function of peroxide concentration. **Quench crystallized.**

an increase in intensities of the crystalline reflections and crystallinity, and a reduction in FWHM.

A comparison between x-ray crystallinity and DSC crystallinity as a function of peroxide concentration for both slowly cooled and quench crystallized UHMWPE samples is shown in Table 3.1. After irradiation, a similar comparison is made in Table 3.2. We observe that the x-ray crystallinity is systematically lower than the DSC crystallinity. A similar observation was reported for melt-irradiated polyethylene [23], but no comment was made on this result. We believe that peroxide crosslinking in the molten state and quench cooling produce very small crystals on recrystallization. Recrystallization on cooling the melt takes place when the polymer is a very viscous liquid, and since in this state the chains are highly entangled, sufficient time above the melting point must be allowed for polymer chains to diffuse to form the three-dimensional order required for crystallite formation [35]. Therefore, quenching provides less opportunity for crystal growth. Moreover, peroxide crosslinking inhibits molecular chain motion, and hinders the growth of crystals from a crosslinked melt. Consequently, the crystal size will be reduced due to both effects. DSC can measure changes in the thermodynamic heat of fusion from small crystals. Therefore, DSC (i.e., ΔH_f) is sensitive to the formation of small crystals and can measure a wide range of crystal sizes, including smaller crystalline domains. On the other hand, x-ray diffraction may require a larger crystallite size and longer range order. Therefore, x-ray diffraction will be affected more by quenching and by peroxide crosslinking, which generate small crystals. A reduction in crystallite size, perfection and crystallinity was inferred from the preceding results on the intensities of crystalline reflections and FWHM for quench crystallized UHMWPE samples. In addition, decreased intensities of crystalline reflections and increased FWHM with increasing peroxide concentrations were obtained for slowly cooled UHMWPE samples. Even, lower intensities of crystalline reflections and higher FWHM were obtained for quench

Table 3.1. Comparison between x-ray crystallinity and DSC crystallinity as a function of peroxide concentration. **Before irradiation**

	Slowly Cooled		Quench Crystallized	
Wt% Peroxide	X-ray Crystallinity	DSC Crystallinity	X-ray Crystallinity	DSC Crystallinity
0	46.0	49.2	38.0	44.2
0.2	40.1	44.0	33.0	42.8
0.4	38.0	41.6	34.5	42.1
0.6	37.6	41.3	34.4	40.9
0.8	34.5	40.0	34.0	40.1
1.0	35.2	39.8	35.1	40.0
1.5	33.7	36.8	33.3	36.1
2.0	32.3	36.5	31.7	35.9

Table 3.2. Comparison between x-ray crystallinity and DSC crystallinity as a function of peroxide concentration. **After irradiation**

	Slowly Cooled		Quench Crystallized	
Wt% Peroxide	X-ray Crystallinity	DSC Crystallinity	X-ray Crystallinity	DSC Crystallinity
0	48.1	55.8	39.8	49.8
0.2	43.5	50.0	36.3	47.3
0.4	40.1	46.8	35.0	46.1
0.6	39.8	46.2	36.8	45.4
0.8	38.8	45.0	36.5	44.8
1.0	35.9	42.0	36.0	43.2
1.5	34.2	36.8	34.8	36.6
2.0	33.8	36.7	32.8	37.3

crystallized samples crosslinked with peroxide. The FWHM indicates the size and perfection of crystals, whereas, intensities of crystalline reflections are a measure of crystallinity. Consequently, the x-ray crystallinity is affected more than the DSC crystallinity by quenching and by peroxide crosslinking, and is systematically lower than the DSC crystallinity. In addition, radiation-induced scission of taut tie molecules permits recrystallization of broken chains from the amorphous regions, and leads to an increase in the degree of crystallinity [3-15]. On the other hand, the effects of irradiation on a peroxide crosslinked network are suppressed because crosslinks introduced by peroxide crosslinking can stabilize chain fragments resulting from scission. For the most crosslinked network, the effects of irradiation on network properties were reduced to the largest extent. Here, the number of scissioned chain lengths suitable for crystallization would be reduced. Therefore, irradiation-induced scission of taut tie molecules in a crosslinked network could generate small crystals which may be insensitive to x-ray diffraction, leading to a smaller increase in the x-ray crystallinity, compared to the increase in DSC crystallinity.

3.4 Conclusions

Based on the present studies, the following conclusions are drawn.

After Peroxide Crosslinking but Before Irradiation

(1) Peroxide crosslinking during compression molding suppresses crystallization from a cooled melt, and leads to a reduction in the intensities of crystalline reflections, a decrease in the relative area of the crystalline reflections, and to an increase in FWHM (full width at half maximum). This indicates that the crystal size and perfection and the crystallinity are reduced.

(2) Quenching further reduces crystal sizes, amount of crystals and perfection, leading to decreased intensities of crystalline reflections and x-ray crystallinity, and to increased FWHM, compared to those of slowly cooled samples.

(3) For slowly cooled samples, interplanar spacings d_{110} and d_{200} essentially remain constant with peroxide concentration, while for quench crystallized samples, the interplanar spacings remain constant at low peroxide concentration but may increase slightly at high peroxide concentration. It is possible that increased defects introduced by higher levels of peroxide crosslinking introduce changes in interplanar spacings in quenched samples. In addition, damage to the crystal lattice may be increased for smaller crystallites.

(4) Compared to x-ray scattering, measurements of the heat of fusion from DSC show a systematically higher value of crystallinity. This may be because DSC can measure changes in the thermodynamic heat of fusion from small crystals and is sensitive to the formation of small crystals after peroxide crosslinking and quenching, whereas, x-ray diffraction may require a larger crystallite size and longer range order and may not measure very small crystals.

After Peroxide Crosslinking and Irradiation

(1) Irradiation to 3.4 Mrad (34 kGy) with gamma-rays from cobalt-60 produces a small amount of crosslinking in amorphous regions but extensive scission of taut tie molecules and leads to increased intensities and relative area of crystalline reflections, and decreased FWHM, implying increased size and perfection of crystals and increased crystallinity.

(2) After irradiation (3.4 Mrad), the interplanar spacings d_{110} and d_{200} are not affected for both slowly cooled and quench crystallized samples.

(3) Peroxide crosslinking reduces the effect of irradiation on the crosslinked network because crosslinks introduced by peroxide crosslinking stabilize chain fragments resulting from the scission of taut tie molecules and suppress recrystallization of broken chains.

(4) Comparing to DSC crystallinity, x-ray crystallinity shows a smaller increase after irradiation. This is because irradiation-induced scission of taut tie molecules could generate small crystals which may be insensitive to x-ray diffraction.

3.5 References

[1] L. E. Alexander, *"X-ray Diffraction Methods in Polymer Science"*, John Wiley & Sons, New York, 1969.

[2] B. D. Cullity, *"Elements of X-Ray Diffraction"*, 2nd Ed., Addison-Wesley, 1978.

[3] S. K. Bhateja, Polymer, **23**, 654(1982).

[4] R. J. Roe, E. S. Grood, R. Shastri, C. A. Gosselin, and F. R. Noyes, *J. Biomed. Mater. Res.*, **15**, 209(1981).

[5] S. K. Bhateja, *J. Macromol. Sci. Phys.*, **B22**, 159(1983).

[6] S. K. Bhateja, E. H. Andrews, and R. J. Young, *J. Polym. Sci., Polym. Phys. Ed.*, **21**, 523(1983).

[7] I. Kamel and L. Finegold, *J. Polym. Sci., Polym. Phys. Ed.*, **23**, 2407(1985).

[8] A. Shinde and R. Salovey, *J. Polym. Sci., Polym. Phys. Ed.*, **23**, 1681(1985).

[9] S. K. Bhateja and E. H. Andrews, *J. Mater. Sci.*, **20**, 2839(1985).

[10] L. Minkova, *Colloid Polym. Sci.*, **266**, 6(1988).

[11] M. Narkis, I. Raiter, S. Shkolnik, A. Siegmann , and P. Eyerer, *J. Macromol. Sci. Phys.*, **B26**, 37(1987).

[12] D. J. Dijkstra, W. Hoogsteen, and A. J. Pennings, *Polymer*, **30**, 866(1989).

[13] L. Minkova and M. Mihailov, *Colloid Polym. Sci.*, **268**, 1018(1990).

[14] Y. Zhao, Y. Luo, and B. Jiang, *J. Appl. Polym. Sci.*, **50**, 1797(1993).

[15] R. S. Boggan, H. H. Trieu, K. C. Richelsoph, R. D. Paxson, and M. C. Carroll, *The 19th Annual Meeting of the Society for Biomaterials*, Birmingham, AL, 1993.

[16] G. Meinel and A. Peterlin, *J. Polym. Sci.*, **B5**, 613(1967).

[17] B. Wunderlich, *"Macromolecular Physics"*, **Vol. 1**, Academic Press, New York, 1973.

[18] W. P. Slichter and E. R. Mandell, *J. Phys. Chem.*, **62**, 334(1958).

[19] K. Katq, K. Ametani, M. Imai, and T. Seto, *Jpn. J. Appl. Phys.*, **20**, 691(1981).

[20] O. Yoda and I. Kuriyama, *Jpn. J. Appl. Phys.*, **16**, 1447(1977).

[21] O. Yoda and I. Kuriyama, *J. Mater. Sci.*, **14**, 1733(1979).

[22] O. Yoda and A. Odajima, *Jpn. J. Appl. Phys.*, **19**, 1241(1980).

[23] G. Gielenz and B. J. Jungnickel, *Colloid Polym. Sci.*, **260**, 742(1982).

[24] G. S. Y. Yeh, C. J. Chen, and D. C. Boose, *Colloid Polym. Sci.*, **263**, 109 (1985).

[25] C. J. Chen, D. C. Boose, and G. S. Y. Yeh, *Colloid Polym. Sci.*, **269**, 469 (1991).

[26] M. Nikolova, L. Minkova, and E. Nedkov, *J. Macromol. Sci. Phys.*, **B27**, 1 (1988).

[27] K. A. Kunert, H. Soszynska, and N. Pislewski, *Polymer*, **22**, 1355(1981).

[28] Y. H. Kao and P. J. Phillips, *Polymer*, **27**, 1669(1986).

[29] P. H. Hermans and A. Weidinger, *Makromol. Chem.*, **44-46**, 24(1961); **50**, 98 (1961).

[30] J. E. Spruiell and E. S. Clark, in *"Methods of Experimental Physics"* , L. Marton and C. Marton, Eds., **Vol. 16**, Part B, Academic Press, New York, 1980.

[31] R. J. Young and P. A. Lovell, *"Introduction to Polymers"*, 2nd Ed., Chapman & Hall, New York, 1991.

[32] F. J. Balta-Calleja and C. G. Vonk, *"X-ray Scattering of Synthetic Polymers"*, Elsevier Science Publishers, New York, 1989.

[33] M. Kresteva, E. Nedkov, and A. Radilova, *Colloid Polym. Sci.*, **263**, 273(1985).

[34] B. Wunderlich, *"Macromolecular Physics"*, **Vol. 2**, Academic Press, New York, 1976.

[35] J. M. G. Cowie, *"Polymers: Chemistry and Physics of Modern Materials"*, 2nd Ed., Chapman & Hall, New York, 1991.

[36] G. Ungar and A. Keller, *Polymer*, **21**, 1273(1980).

CHAPTER 4

SURFACE MORPHOLOGY OF ULTRA-HIGH MOLECULAR WEIGHT POLYETHYLENE

4.1 Introduction

Since the microstructure of a semicrystalline polymer affects the physical properties of bulk materials, elucidation of the internal microstructure is important in polymer science and engineering. Generally, examination of the internal microstructure (e.g., at the lamellar level) of a semicrystalline polymer is performed in the transmission electron microscope. For this technique, a sufficiently thin section is required. Microtomy of polymers is usually not easy and can only be achieved satisfactorily by sectioning at low temperature. On the other hand, the imaging electrons in transmission electron microscopy, in travelling through a polymer specimen, interact with the specimen and destroy its crystallinity and original texture[1]. Therefore, etching and surface replication are used to reveal details in internal or external surfaces of polymer specimens.

There are several etching techniques such as solvent, ozone, gas-discharge, strong oxidizing acid (fuming nitric acid) [2-3], and permanganic acid [1]. Solvent-etching techniques are based on the principle that amorphous polymer molecules are more soluble than crystalline ones. A solvent will remove molecules as a whole without breaking covalent bonds. It is useful if amorphous molecules are present on the surface which

dissolve and reveal structure on a larger scale (i.e., spherulitic structure) due to different dissolution rates. Ozone etching was proposed by Palmer and Cobbold [4]. Ozone is unstable and decomposes slowly to ordinary oxygen. Ozone slowly oxidizes saturated hydrocarbons, but reacts readily with unsaturated hydrocarbons by adding all three oxygen atoms at a double or triple bond. The reaction products are called ozonides, which decompose to form aldehydes, ketones, and dicarboxylic acid. Application of this gaseous oxidation reagent to polyethylene was studied by Priest [5]. Gas-discharge etching is used at pressure of 10^{-3} -10^{-4} mmHg.

Oxygen or other gaseous ions produced in a high-frequency discharge are used to impinge on polymers to remove consecutive layers of material [2]. Depending on crystal perfection, slightly different etching rates are established and some of the structure can be made visible by subsequent surface replication and electron microscopy. Nitric acid etching was widely used on polyethylene. Palmer and Cobbold [4] showed that oxidative attack with fuming nitric acid is selective enough to reveal the microstructure on a lamellar level. Oxidation changed the ends groups of cleaved polyethylene chains to -COOH and to a minor degree to -NO_2 [6]. Oxidation of polymers depends on acid concentration, reaction temperature, and time. Initial chain cleavage in disordered regions is a fast reaction. Oxidation is significantly inhibited at longer reaction times. Keller and Udagawa [6] showed that this slowing down was mainly because of a buildup of reaction products in front of crystal surfaces rather than a slower reaction at the crystal surface. After washing and drying, it was possible to restart the oxidation reaction. Polyethylene treated with nitric acid rapidly becomes brittle because interlamellar regions are etched away almost entirely [4]. Such materials are difficult to replicate and lose genuine microstructure to some extent. A less oxidizing acid, therefore, is required.

The permanganic acid etching technique developed by Bassett and coworkers [1,7-11] has proved to be superior in revealing genuine microstructure at a spherulitic or a lamellar

level. It has been applied successfully to a wide range of polymers, including polyethylene (linear and branched), isotactic polystyrene, isotactic polypropylene, isotactic poly(4-methyl-1-pentene), isotactic polybutene, poly(aryl ether ether ketone), poly(ethylene terephthalate), and certain liquid crystalline polymers [12]. The principle of this method is that an etchant will remove material selectively from the surface of polymer according to penetrability and chemical potential [1]. The composition of etchant can be adjusted for different materials to optimize detail. In general, permanganic acid does not penetrate into the interior of a sample and removes material only from surfaces and only to a limited extent. It removes defective crystalline and disordered material preferentially, and is sensitive to crystallographic (lamellar) orientation [1].

The basic permanganic etching technique is illustrated as follows [1]. Permanganic acid is prepared by adding crystals of potassium permanganate slowly to concentrated sulfuric acid in a conical flask with rapid agitation, in order to minimize formation of the unstable and explosive manganese heptoxide [13]. The flask is stoppered when all the permanganate crystals have been added, and stirred until the crystals dissolve to give a dark green solution. The active species in the solution is believed to be O_3MnOSO_3H [14]. A specimen (such as a polished, fractured, molded, or microtomed surface) is placed in 5 ml of etchant in a test tube and left for an appropriate time at a chosen temperature (room or elevated temperature). After treatment, the acid solution is decanted and the sample is washed for 2 min with a mixture of 2 parts by volume of concentrated sulfuric acid and 7 parts of water, which is precooled to near its freezing point with dry ice. This solution is decanted and the sample is washed successively with hydrogen peroxide (to remove manganese dioxide or permanganate present), several changes of distilled water, and finally acetone. 2 min is suitable for each washing. Etched samples are examined in the electron microscope using a standard two-stage replication process, making a first impression in

cellulose acetate and shadowing this first replica with gold-palladium, then depositing a carbon film. The resulting micrographs have the appearance of negative relief.

Etching conditions such as time, temperature and concentration can be adjusted to fit the needs of specific samples and morphologies. Prolonged etching and particular concentrations of etchant could produce artefacts [1,11,15]. It was shown that a cause of artefacts was precipitation of pinkish brown crystals from the etchant on the polyethylene surface as etching proceeded [11]. The presence of these crystals inhibits etching, but they are subsequently removed in the washing process, leaving the shapes of artefacts on the sample. Artefacts increase in size and number with increasing etching time, and probably are misinterpreted as genuine microstructure. An improved permanganic etchant by incorporating orthophosphoric acid was reported to avoid formation of artefacts on polyethylene [11].

For polymer blends, the permanganic etching technique can also reveal the lamellar organizations of different components because different polymers have different etching rates. For instance, a replica of an etched cut surface of a 50% polyethylene:50% isotactic propylene blend crystallized in bulk showed large banded areas of polyethylene and clear regions of polypropylene [1]. In addition,the polypropylene always was below the polyethylene because the polypropylene is etched more deeply [1]. Permanganic etching can also be used to study the morphology of a drawn or deformed crystallilne polymer [12]. In a drawn polymer, the decrease in penetrability within a sample will hinder differential attack. On the other hand, it was shown that in polyethylene crystallized at low supercooling, the pockets of thin lamellae were usually etched more deeply than the wider and thicker lamellae formed before them [8-10]. It was suggested that thinner lamellae possessed more surface regions for the etchant to penetrate. In quantitative permanganic etching studies, Freedman et al., [16] found that in sections cut at 20 °C, the lower melting population suffered substantially greater deformation and hence greater etching rate. For

cold-cut polyethylene sections, the etching rate decreased linearly with etching time. It was also found that if sections were annealed at a temperature between the two melting peaks, then there was little or no discrimination in etching rate between the two populations [16]. For linear low-density polyethylene (with branched molecules), it was shown that thinner lamellae were etched at a faster rate which was only slightly reduced after removing damage due to cutting (i.e., annealing)[17]. It was inferred that this was due to faster chain scission at fold surfaces which were more penetrable for linear low-density polyethylene than for linear polyethylene [17].

In the present study, first, we will examine the morphologies of fracture surfaces of several different specimens by scanning electron microscopy. Secondly, by using the permanganic etching technique, we will examine the morphologies of etched surfaces of molded and fractured specimens at a spherulitic level.

4.2 Experimental Details

Fracture Surfaces

Freeze fracture surfaces were prepared by cooling the specimens in liquid nitrogen and breaking with a hammer. Fracture surfaces were attached to an aluminum specimen mount and coated with gold and palladium under vacuum. The coated fracture surfaces were examined with a Zeiss, scanning electron microscope (model DSM 960), at a voltage of 5 kV. Specimens examined included: (1) GUR 412 , GUR 413, and GUR 415, which were compression molded at 170, 220, and 300 °C, respectively, for 2 h and then slowly cooled to room temperature; (2) slowly cooled samples (GUR 415), which were chemically crosslinked with peroxide; (3) quench crystallized samples (GUR 415), which also were chemically crosslinked with peroxide; and (4) specimens (2) and (3), after irradiation. The

reported average molecular weights ($\overline{M_w}$) of GUR 412, GUR 413, and GUR 415 are 2.5 ~ 3 × 10^6, 3 ~ 4 × 10^6, and 6 × 10^6, respectively. The measured crystallinities of the original powders from synthesis of GUR 412 and GUR 413 are comparable to that of GUR 415 (~ 63%).

Etched Surfaces

Permanganic acid etching experiments closely followed those developed by Olley et al. [1,11]. The concentration of permanganic acid is 1 % (w/v). This composition proved to be optimal for our morphological studies. The etchant was prepared by dissolving a given weight of potassium permanganate in a known volume of concentrated sulfuric acid. The potassium permanganate was added slowly to concentrated sulfuric acid in a conical flask and stirred with a magnetic stirrer. The flask was stoppered when all the permanganate crystals had been added and stirred until the crystals dissolved to give a dark green solution. Specimens (dimensions approximately 1×10×30 mm) were placed in 8 ml of etchant in a test tube and stored at room temperature. Occasionally, test tubes were shaken. In this study, etching times for 0 and 1 wt% peroxide specimens (molded surfaces) are 8 h and 5 h, respectively. The etching time for fracture surfaces is 5 h (for all specimens). After etching, the acid was decanted and the specimen was washed according to the following procedure [1,11]: (1) 2 min in 10 ml of an aqueous solution containing 2 parts by volume of concentrated sulfuric acid and 7 parts of water, which had been cooled to near its freezing point with dry ice; (2) 2 min in 10 ml of a 30% hydrogen peroxide solution; (3) 2 min in 10 ml of water; and (4) 2 min in 10 ml of acetone. Etched specimens were attached to an aluminum specimen mount and coated with gold and palladium under vacuum. The coated etched surface was examined with a Zeiss, scanning electron microscope (model

DSM 960), at a voltage of 5 kV. In order to examine the morphologies of etched surfaces, we studied fracture surfaces and compression molded samples.

For kinetic studies, specimens (dimensions $1 \times 18 \times 30$ mm) were immersed in 20 ml of etchant in a test tube and etched for a chosen time (1.5 h for each period) at room temperature. After etching, the specimens were washed and subsequently dried in a vacuum oven for 0.5 h, and then weighed. The specimens were reetched for another 1.5 h in a fresh etchant and subsequently washed, dried, and weighed. This procedure was repeated for 7 times. Cumulative weight loss was determined by adding up the weight loss at each stage. The result was presented by plotting the cumulative weight loss vs etching time. For comparison, peroxide-free, 1, and 2 wt% peroxide samples before and after irradiation were examined.

4.3 Results and Discussion

Powder Morphology

Scanning electron micrographs of three UHMWPE powders (GUR 412, GUR 413, and GUR 415) are shown in Figures 4.1- 4.3. The nascent (as-polymerized) UHMWPE powder or "flake" consists of fine particles of varying size. Surfaces of particles are highly convoluted and the shape is irregular. Some portions of particle surfaces are smooth, and others are highly porous. The particles appear to be composed of an aggregate of smooth, submicron size spheres. Close examination shows that voids in the porous regions are connected by an intricate three-dimensional network of fibrils [18-22]. The fibrils are evidence of a continuously operative strain effect throughout the growing polymer mass [18]. It was suggested that there was a continuous strain throughout the nascent polymer resulting from continuous insertion of polymer next to the catalyst surface [18]. Growth

occurs at the center of an already deposited polymer particle which consequently will inflate exterior concentric layers which are thus subjected to an equivalent biaxial stretch in directions perpendicular to the radius of particle [18]. This will result in the formation of cracks and fibrils, which are almost always tangential to the surfaces of polymer particles. The morphology of nascent powders affected compaction and processibility [19,23].

Crystals of linear polymers may be grown from polymer melts or solutions, as well as formed directly from the monomer by simultaneous polymerization and crystallization. Crystals obtained directly from monomer by simultaneous polymerization and crystallization are called nascent crystals [24]. The morphology of nascent PE depends on polymerization conditions such as polymerization temperature, catalyst system, polymerization medium and time, and can appear to be film [25], globular [26-27], cobweb [26-28], wormlike [26-27], fibrillar [26-29], and ribbonlike [30]. A study of the melting behavior of nascent polyethylene crystals indicated an extended chain micromorphology [23,27,31-38]. Characteristic of an extended chain crystal is a higher melting temperature (140 °C - 142 °C) observed during first melting in DSC, whereas, subsequent remelting after cooling from the melt in DSC occurs at a lower melting temperature (132 °C - 134 °C), comparable to that of a chain-folded crystal. The macroconformations of polymer chains in crystals are illustrated schematically in Figure 4.4 [2]. A represents an amorphous polymer which is glassy at a sufficiently low temperature. B represents a chain-folded crystalline polymer with a well-defined thickness. C represents a macroconformation of extended chain crystals. The term "extended chain crystal" is applied to any crystal of a linear high polymer of sufficiently high molecular weight to have a length of at least 2000 Å in the molecular axis direction [2] and which shows a reduced degree of folding. The area D represents an intermediate macroconformation, which is called a fringed micelle crystal.

(a)

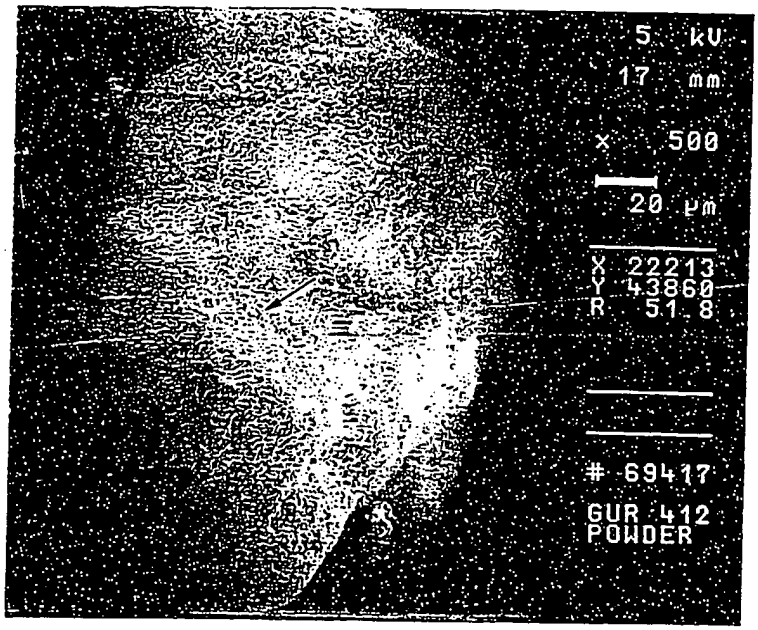

(b)

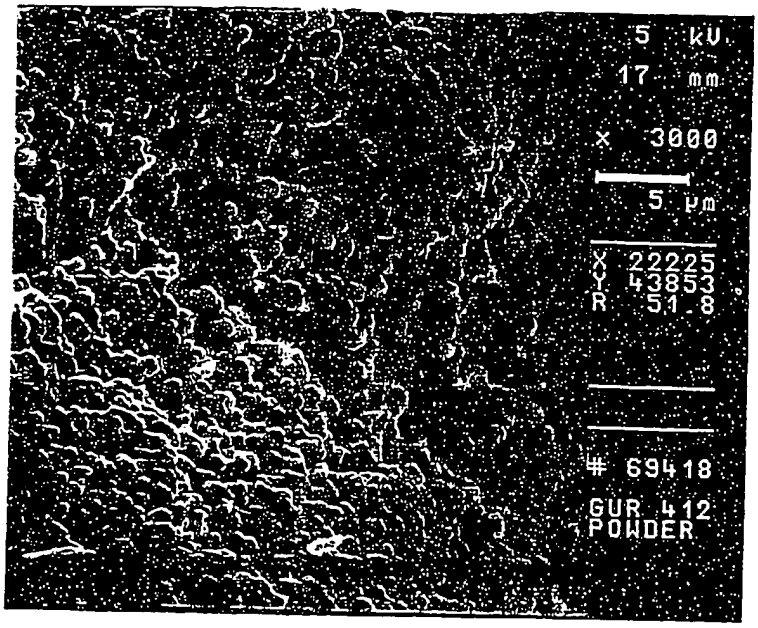

Figure 4.1. Scanning electron micrographs of nascent UHMWPE powder (GUR 412). (a) x 500 (b) x 3000.

(a)

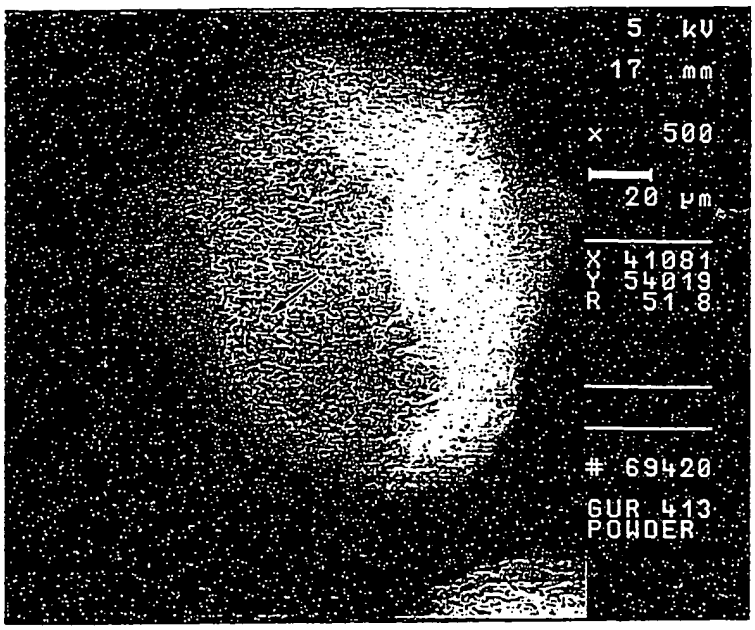

(b)

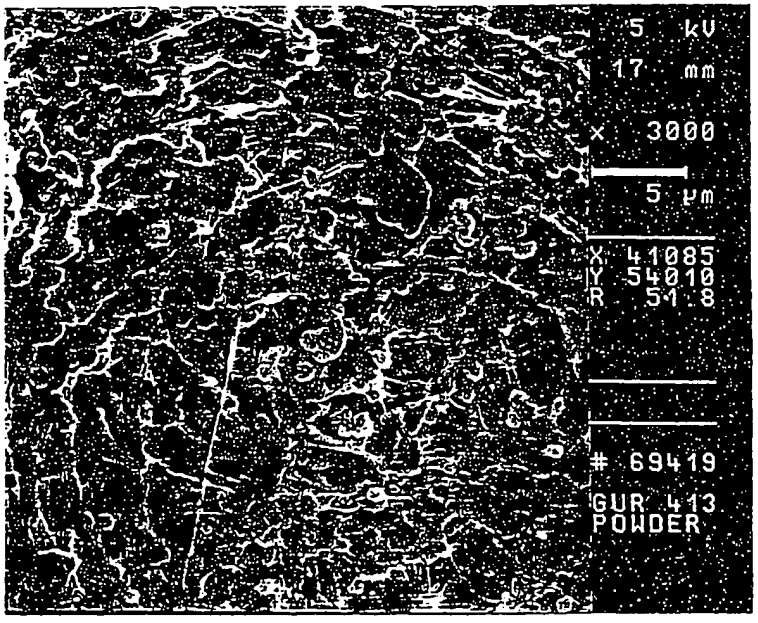

Figure 4.2. Scanning electron micrographs of nascent UHMWPE powder (GUR 413). (a) x 500 (b) x 3000.

(a)

(b)

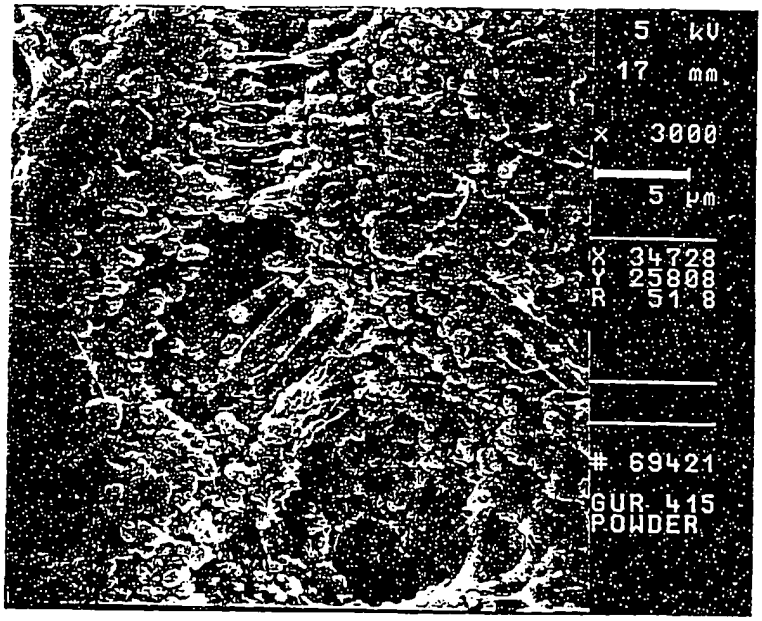

Figure 4.3. Scanning electron micrographs of nascent UHMWPE powder (GUR 415). (a) x 500 (b) x 3000.

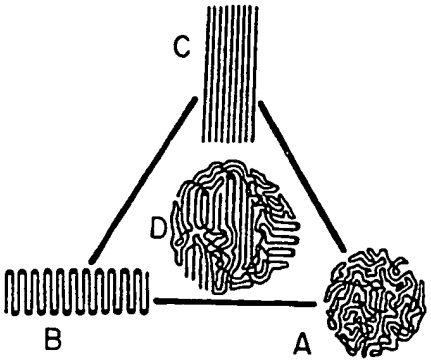

Figure 4.4. The macroconformations of polymer chains in crystals [2].

SEM Morphology of Fracture Surfaces

Scanning electron micrographs of fracture surfaces of GUR 412, GUR 413, and GUR 415, which had been compression molded at 170 °C for 2 h and subsequently slowly cooled to room temperature, are shown in Figures 4.5-4.7, respectively. As shown in these Figures, a brittle fracture boundary of size comparable to that of the original UHMWPE powder particles is observed. Close examination (x 5000 magnification) shows an oriented nodular structure, composed of many smooth, submicron spheres. These smooth, minute spheres are believed to exist originally in the raw UHMWPE powder and to form an aggregate. Scanning electron micrographs of fracture surfaces of GUR 412, GUR 413, and GUR 415, which had been compression molded at 220 °C for 2 h and subsequently slowly cooled to room temperature, are shown in Figures 4.8-4.10, respectively. It is noteworthy that fracture boundaries almost disappear in GUR 412 and instead a single fracture pattern appears. GUR 415 shows the same features as at 170 °C, while GUR 413

shows features intermediate between GUR 412 and GUR 415 at 220 °C. At high magnification, an oriented nodular structure still exists but now becomes slightly thinner and randomized. Scanning electron micrographs of fracture surfaces of GUR 412, GUR 413, and GUR 415, which were compression molded at 300 °C for 2 h and subsequently slowly cooled to room temperature, are shown in Figures 4.11-4.13, respectively. It can be seen that the oriented lines, which are observed in the previous two cases (i.e., 170 °C and 220 °C), completely disappear. In this case, a uniform "carpet-like" appearance is observed in these fracture surfaces. Close examination clearly shows a randomized nodular structure. Minute (submicron) spheres still exist and are embedded in a matrix. In addition, a few fibrils are observed on the fracture surfaces for all three materials, especially for GUR 415.

Consisting of extremely long molecular chains, UHMWPE contains a high concentration of entanglements, even after melting [39-40]. Thus in the melt state, chain entanglements lead to a significant increase in melt viscosity and inhibit molecular chain motion. The reported flow temperature for UHMWPE was 215-220 °C [33,41]. Complete fusion of the crystalline phase occurred only at a temperature above 220 °C, where sufficient disentanglement and chain translation might occur [33,42-43]. In the temperature range 145-210 °C, UHMWPE melt showed significant elasticity, which was manifested by the tendency of the powder particles to recoil upon removal of a compression load [33]. The recoiling phenomenon was explained by slow relaxation of an extremely viscous melt and hindrance of chain displacement due to a high degree of physical entanglements [33]. Therefore, following compression molding at 170 °C, these materials show particulate memory. However, at 220 °C, particulate memory almost disappears for GUR 412, which has the lowest molecular weight ($\overline{M_w} \cong 2.5-3\times10^6$). For GUR 415, which has the highest molecular weight ($\overline{M_w} \cong 6\times10^6$), particulate memory was the same as that at 170 °C. GUR 413 ($\overline{M_w} \cong 3-4\times10^6$) showed intermediate particulate memory between GUR

(a)

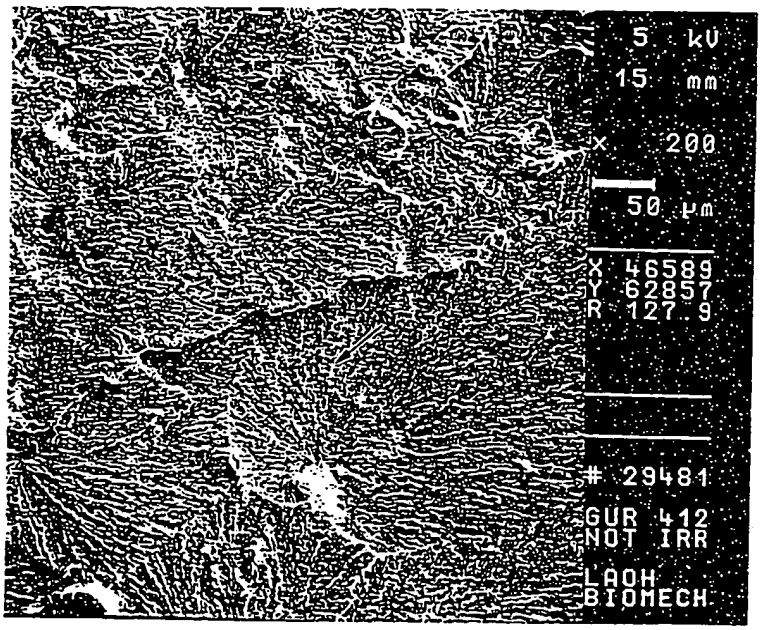

(b)

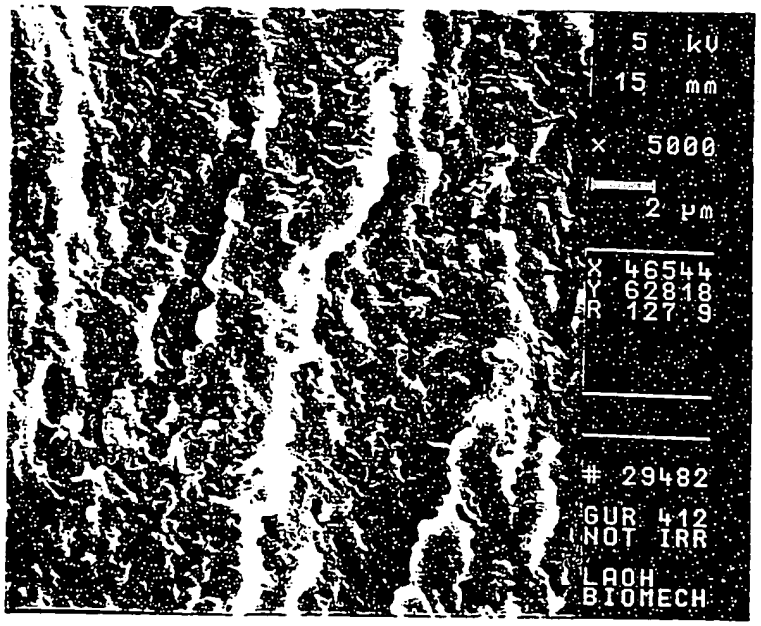

Figure 4.5. Scanning electron micrographs of fracture surfaces of compression molded UHMWPE (GUR 412). 170 °C. (a) x 200 (b) x 5000.

(a)

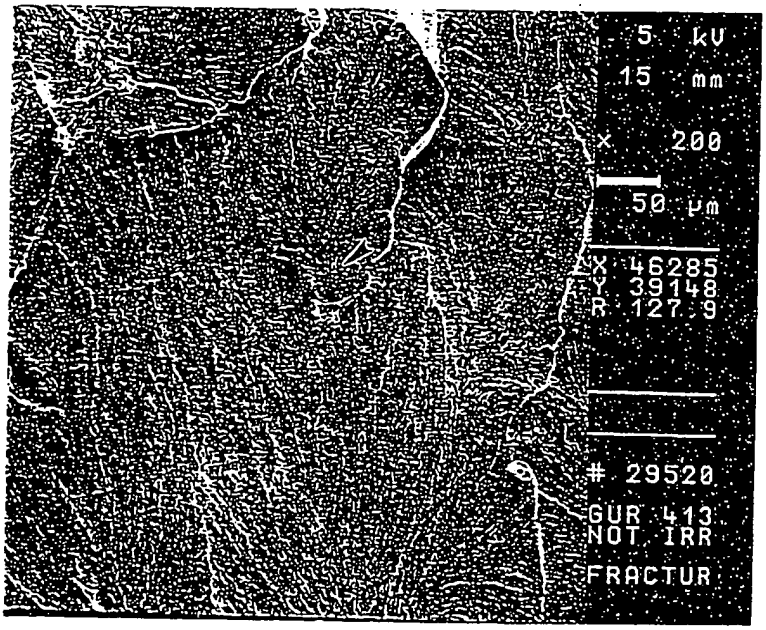

(b)

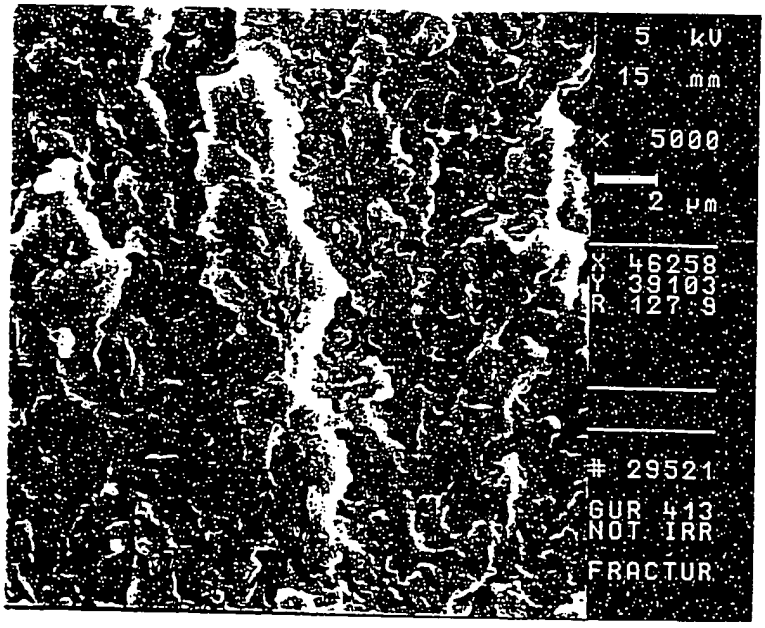

Figure 4.6. Scanning electron micrographs of fracture surfaces of compression molded UHMWPE (GUR 413). 170 °C. (a) x 200 (b) x 5000.

(a)

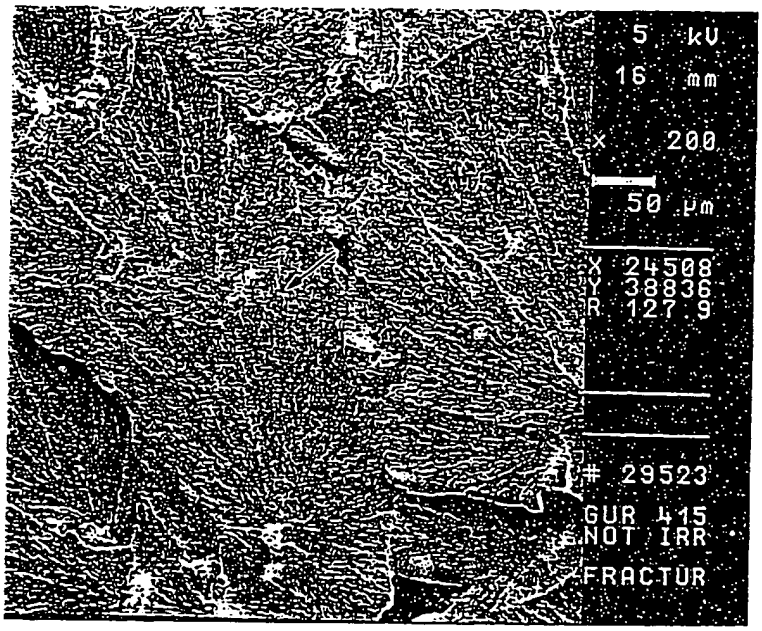

(b)

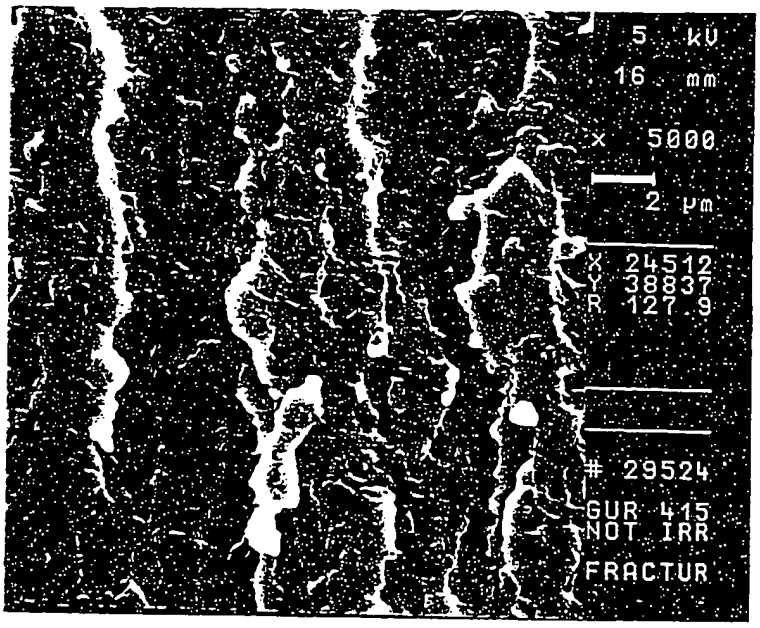

Figure 4.7. Scanning electron micrographs of fracture surfaces of compression molded UHMWPE (GUR 415). 170 °C. (a) x 200 (b) x 5000.

(a)

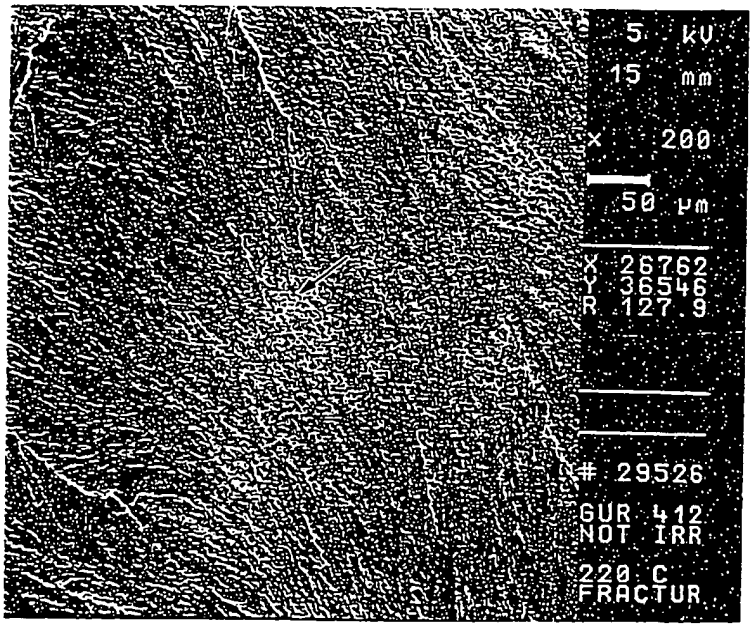

(b)

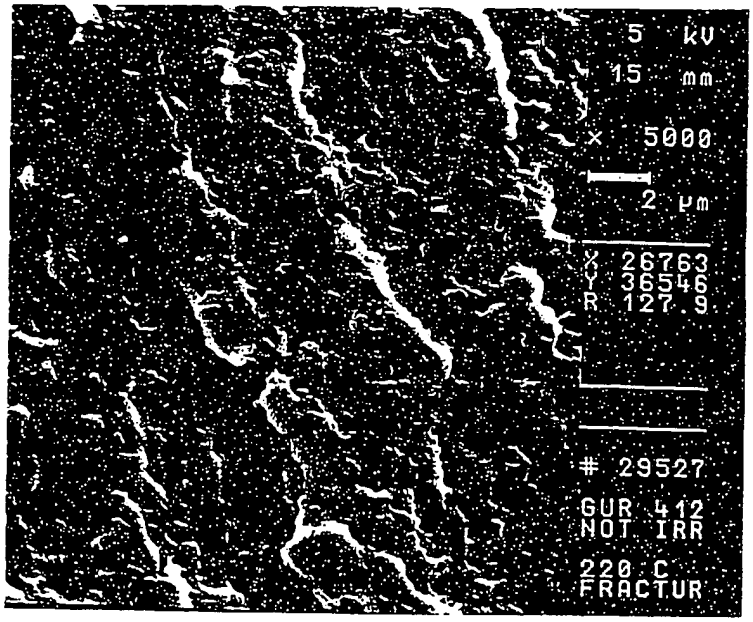

Figure 4.8. Scanning electron micrographs of fracture surfaces of compression molded UHMWPE (GUR 412). 220 °C. (a) x 200 (b) x 5000.

(a)

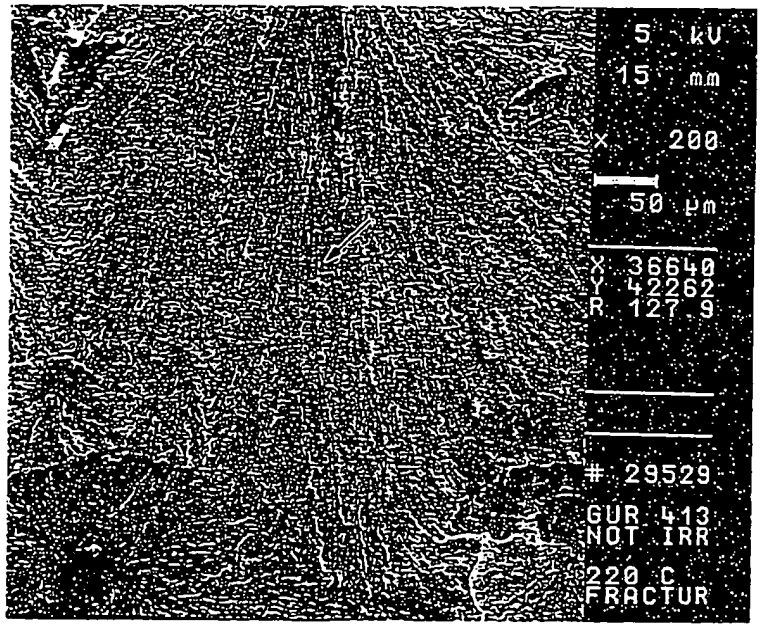

(b)

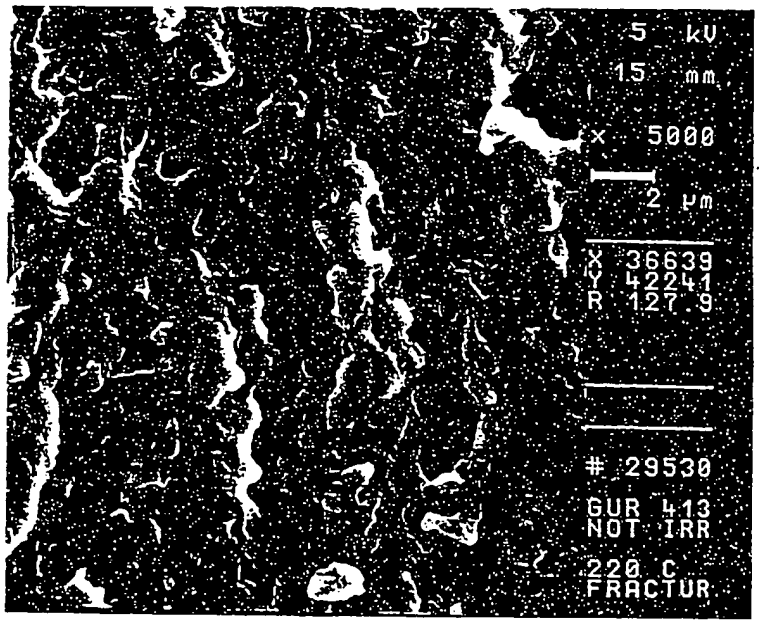

Figure 4.9. Scanning electron micrographs of fracture surfaces of compression molded UHMWPE (GUR 413). 220 °C. (a) x 200 (b) x 5000.

(a)

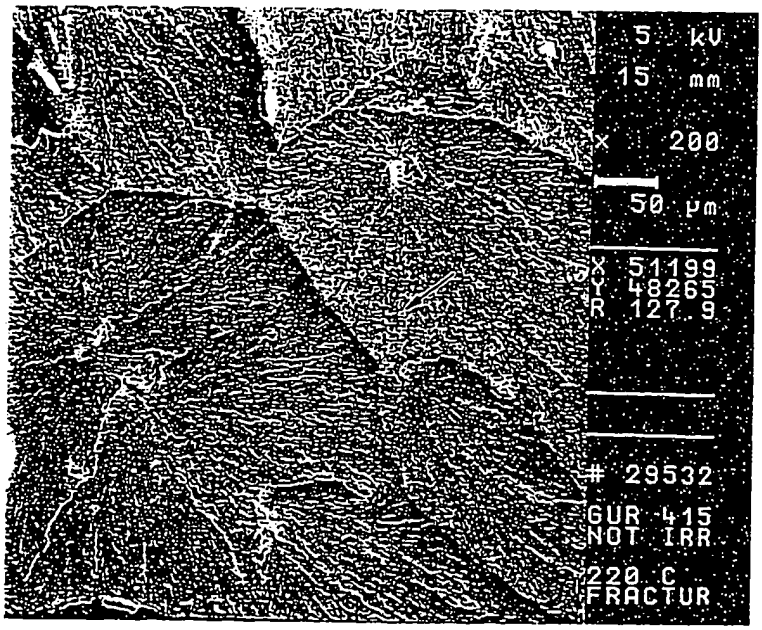

(b)

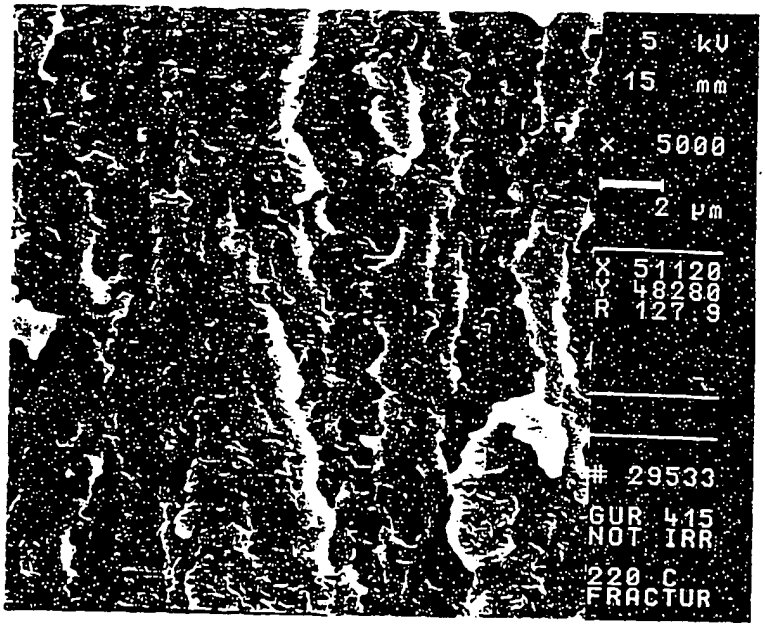

Figure 4.10. Scanning electron micrographs of fracture surfaces of compression molded UHMWPE (GUR 415). 220 °C. (a) x 200 (b) x 5000.

(a)

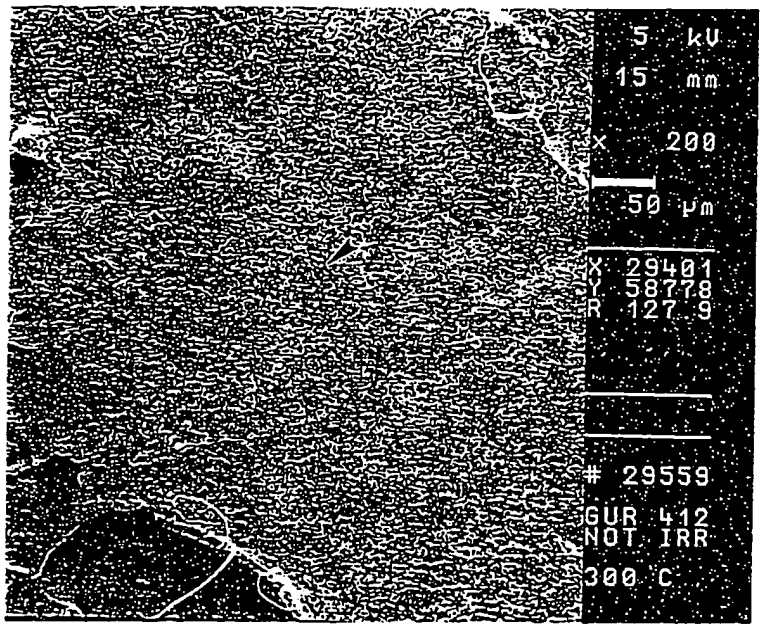

(b)

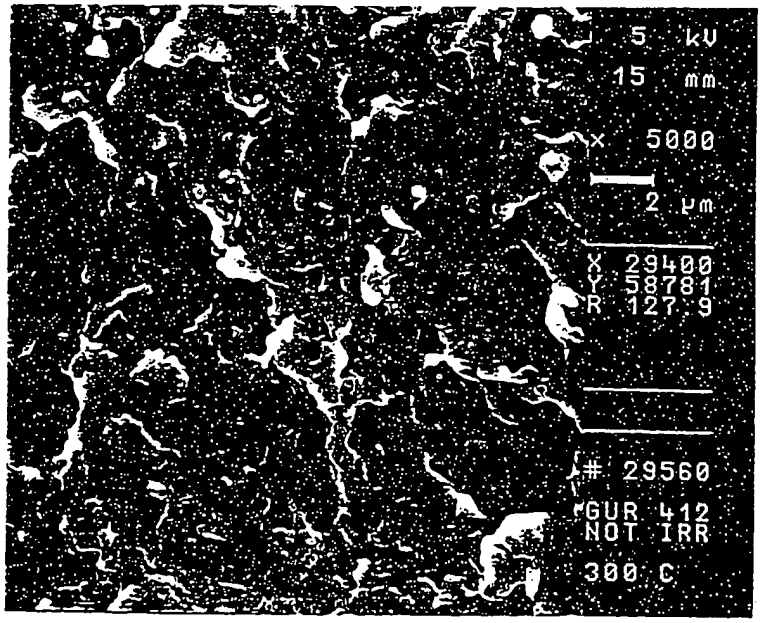

Figure 4.11. Scanning electron micrographs of fracture surfaces of compression molded UHMWPE (GUR 412). 300 °C. (a) x 200 (b) x 5000.

(a)

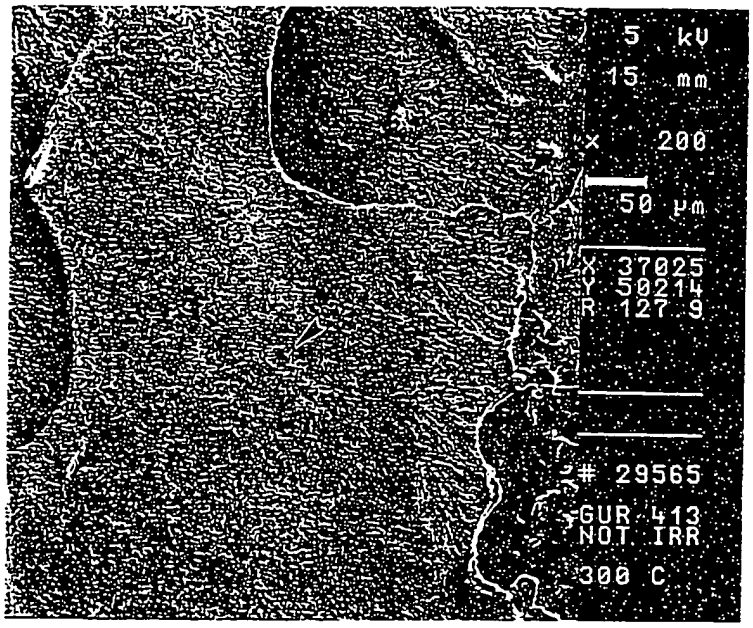

(b)

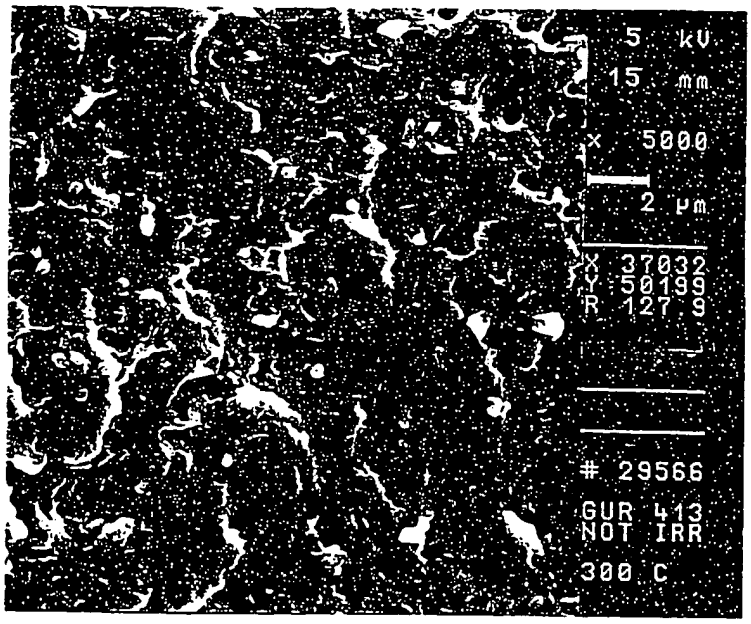

Figure 4.12. Scanning electron micrographs of fracture surfaces of compression molded UHMWPE (GUR 413). 300 °C. (a) x 200 (b) x 5000.

(a)

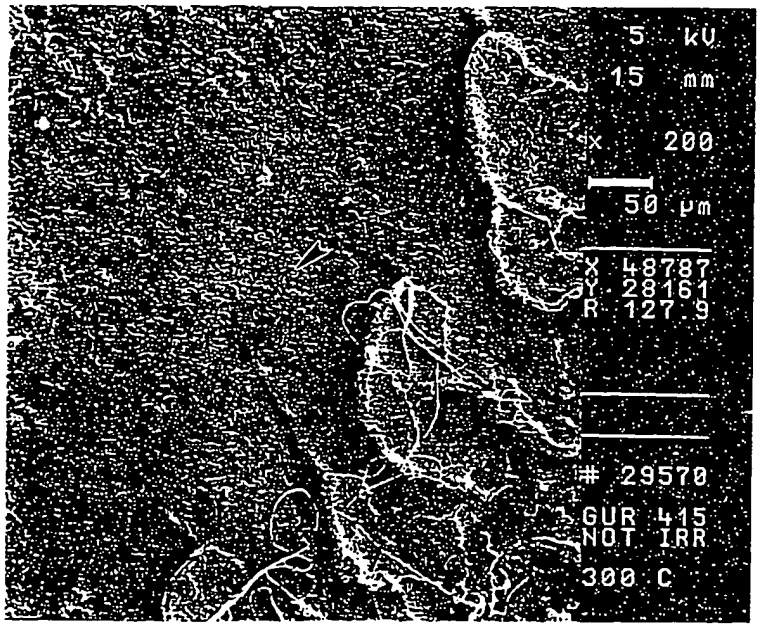

(b)

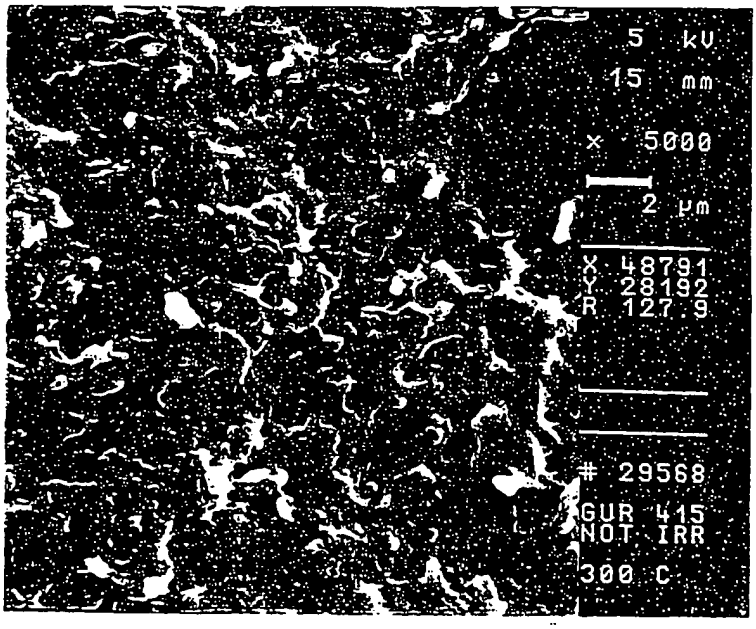

Figure 4.13. Scanning electron micrographs of fracture surfaces of compression molded UHMWPE (GUR 415). 300 °C. (a) x 200 (b) x 5000.

412 and GUR 415 and exhibited a larger fracture boundary than that at 170 °C. Apparently, GUR 412 exhibits a higher degree of melt flow at 220 °C.

Unlike conventional molecular weight polyethylene, UHMWPE exhibits anisotropic behavior in the melt because of extremely long molecular chains and a high concentration of chain entanglements [33,44]. It was shown that the anisotropic melt lost its elastic response reforming the globular particles on heating above 220 °C, but remained anisotropic even at temperatures above 300 °C, which was observed with polarizing optical microscope by pressing the powders between a microscope slide and cover slip [33]. Under these conditions, globular particles appear to interpenetrate. At a temperature of 300 °C, our experimental results show that complete fusion of the crystalline phase and hence, particulate interpenetration occurs for the three materials (refer to Figure 4.11-4.13). In addition, we believe that melt anisotropy disappears under our experimental conditions (300 °C and ram pressure 7.5 x 10^3 kPa for 2 h). This can be proved by a close examination (x 5000 magnification) of fracture surfaces, which show a randomized nodular structure. Consequently, we suggest that oriented nodular structures are due to melt anisotropy at temperatures below 220 °C. The individual fracture boundary, which corresponds to the dimension of raw polymer powder particles, is a result of incomplete fusion of the raw particles at temperatures below 220 °C, (and at 220 °C for GUR 415).

SEM Morphology of Fracture Surfaces of Chemically Crosslinked UHMWPE (Gur 415)

Before Irradiation

Scanning electron micrographs of fracture surfaces of chemically crosslinked UHMWPE with 1 and 2 wt% peroxide, compression molded at 170 °C for 2 h and

subsequently slowly cooled to room temperature, are shown in Figures 4.14-4.15, respectively. Peroxide crosslinked samples show a smooth fracture surface, compared to the rough fracture surface of peroxide-free samples (Figure 4.7). DSC crystallinities for peroxide-free, 1 and 2 wt% peroxide samples are 49.2, 39.8, and 36.5%, respectively (refer to chapter 2). The decrease in crystallinity for peroxide crosslinked samples results because peroxide crosslinking inhibits crystallization from a crosslinked melt. Consequently, the noncrosslinked sample shows a tendency to brittle fracture because of higher crystallinity, while the crosslinked samples show a ductile fracture behavior because of lower crystallinity [45]. Close examination shows that the 2 wt% peroxide crosslinked sample exhibits an even smoother fracture surface than that of the 1 wt% peroxide crosslinked sample. For 1 wt% peroxide crosslinked sample, there are two different features in fracture surfaces. One of them (Figure 4.14b) shows a smooth fracture surface where many individual minute (submicron) particles are embedded in the matrix. The other feature (Figure 4.14c) shows a thinner and smoother oriented nodular structure, which is quite different from that of peroxide-free samples (refer to Figure 4.7). Two different features in fracture surfaces of the 1 wt% peroxide crosslinked sample could be due to non-uniform distributions of peroxide crosslinking. In addition, as peroxide crosslinking prevents flow in the melt, more individual submicron spheres are observed in fracture surfaces of peroxide crosslinked samples.

Scanning electron micrographs of fracture surfaces of chemically crosslinked UHMWPEs with 1 and 2 wt% peroxide, compression molded at 170 °C for 2 h and subsequently quenched in liquid nitrogen, are shown in Figures 4.16-4.17, respectively. The crystallinities for 0, 1 and 2 wt% peroxide samples are 44.2, 40.0 and 35.9%, respectively. As shown in Figure 4.16, fracture surfaces for the quenched 1 wt% peroxide sample are similar to those of fracture surfaces for the slowly cooled 1 wt% peroxide sample (refer to Figure 4.14). However, (Figure 4.17), the quenched 2 wt% peroxide

(a)

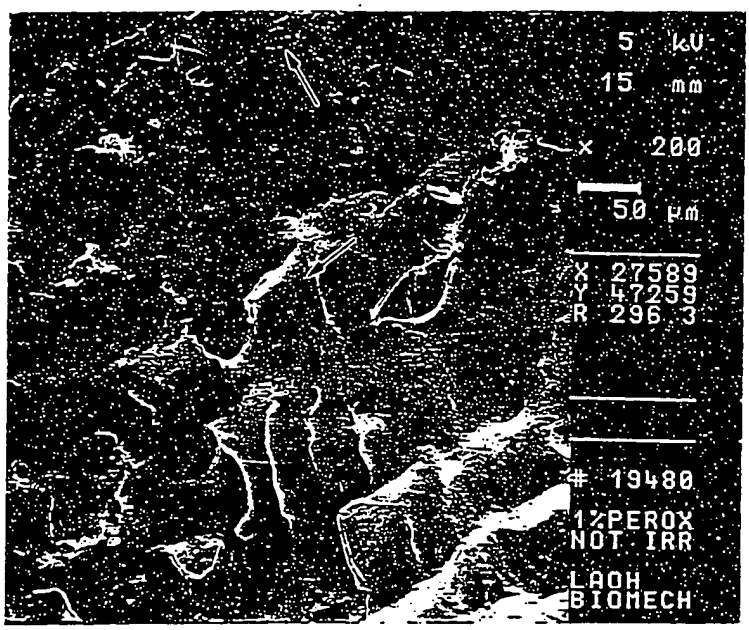

(b)

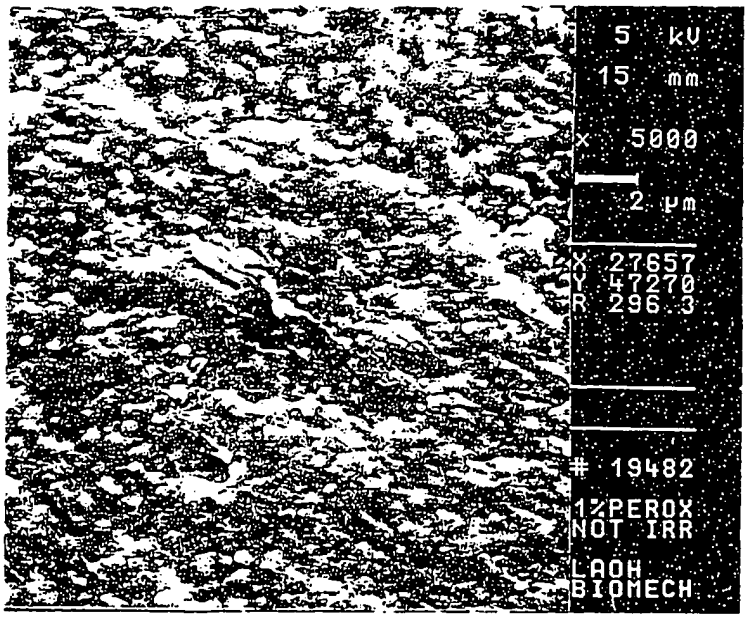

Figure 4.14. Scanning electron micrographs of fracture surfaces of UHMWPE (1 wt% peroxide). **Slowly cooled. Before irradiation.** (a) x 200 (b) x 5000 (center).

(c)

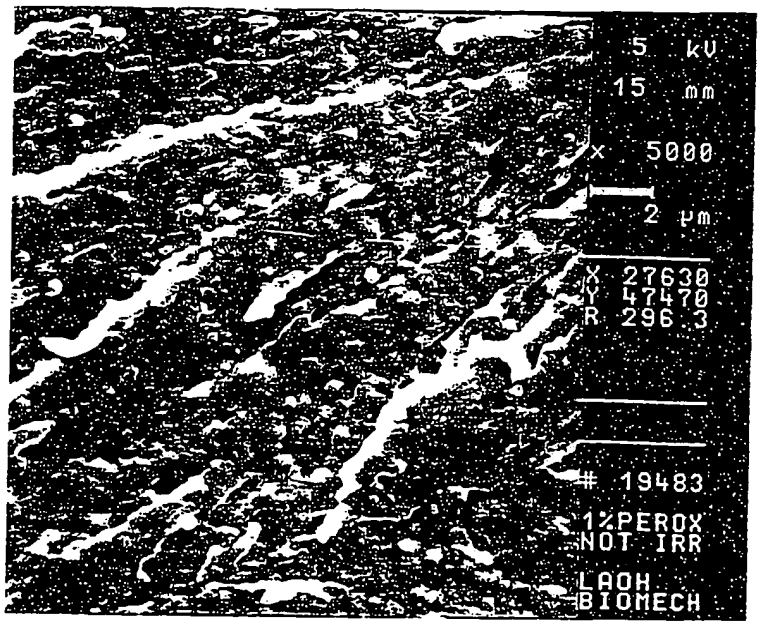

Figure 4.14. (continued) (c) x 5000 (top).

(a)

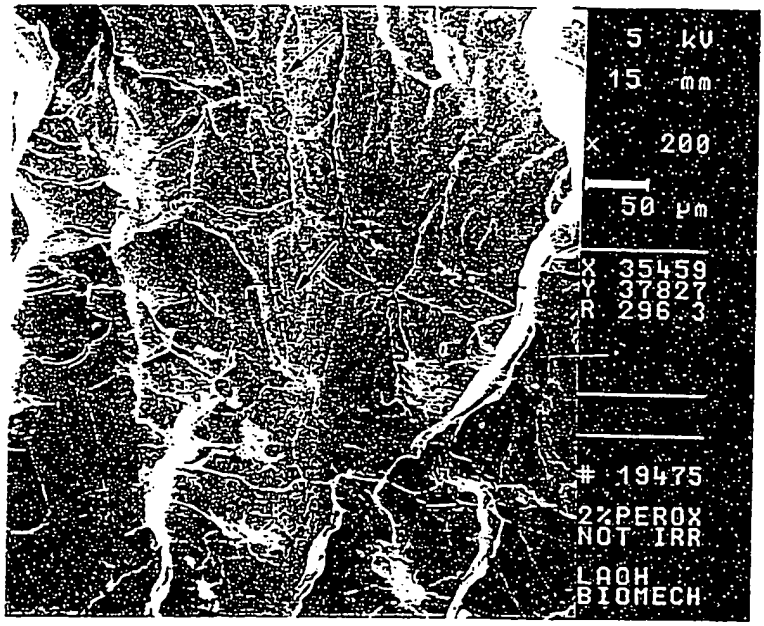

(b)

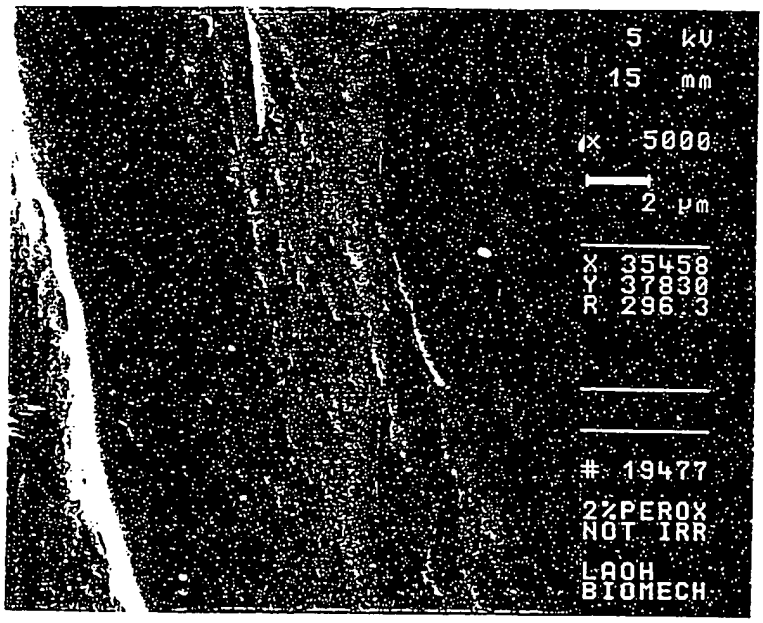

Figure 4.15. Scanning electron micrographs of fracture surfaces of UHMWPE (2 wt% peroxide). **Slowly cooled. Before irradiation.** (a) x 200 (b) x 5000 (center).

(c)

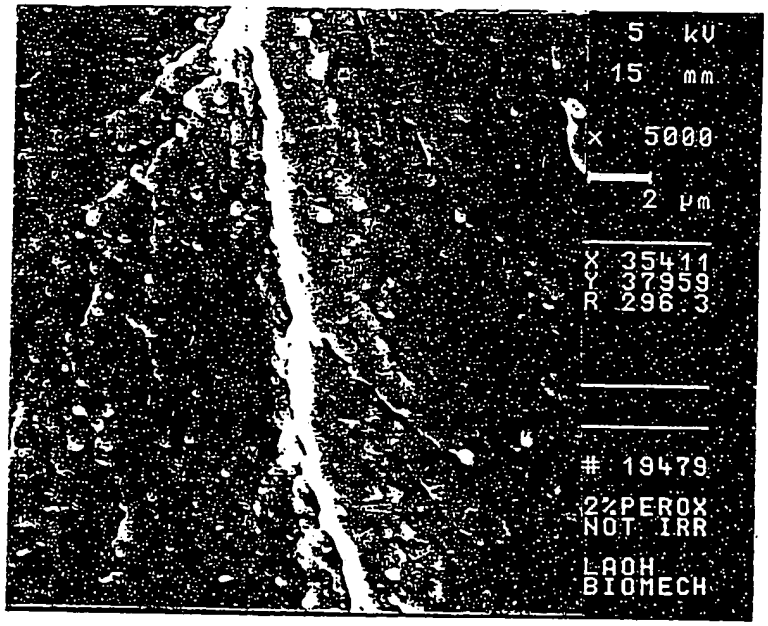

Figure 4.15. (continued) (c) x 5000 (top).

(a)

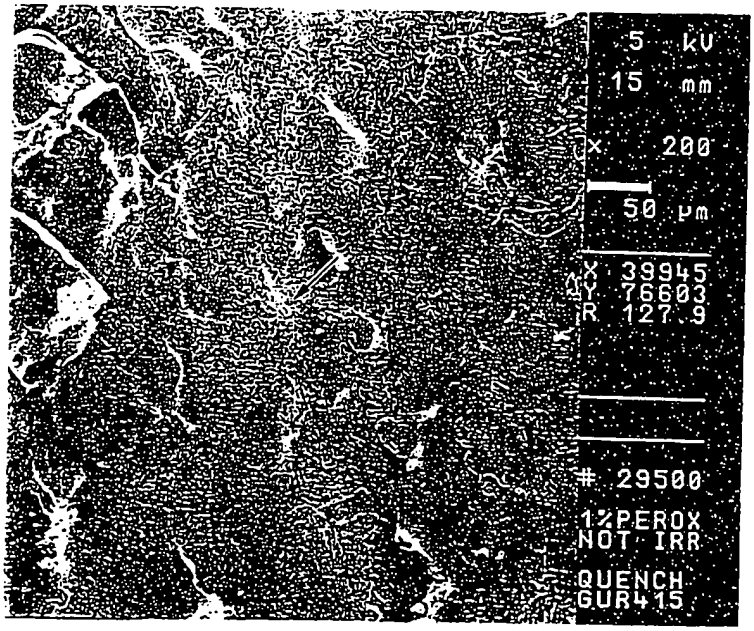

(b)

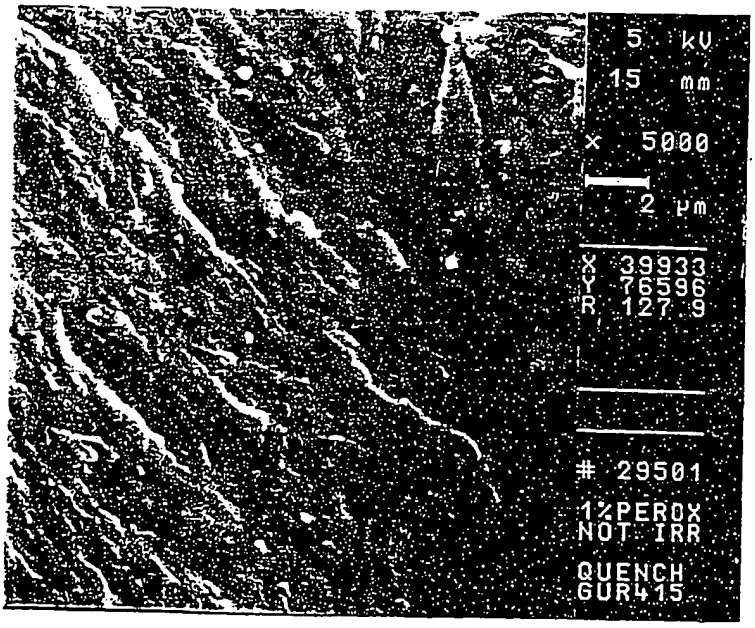

Figure 4.16. Scanning electron micrographs of fracture surfaces of UHMWPE (1 wt% peroxide). **Quench crystallized. Before irradiation.** (a) x 200 (b) x 5000.

(a)

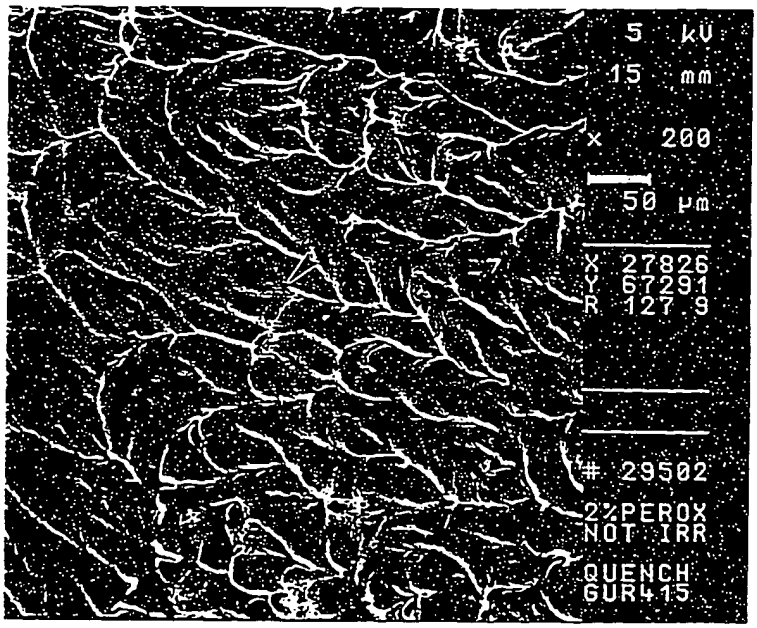

(b)

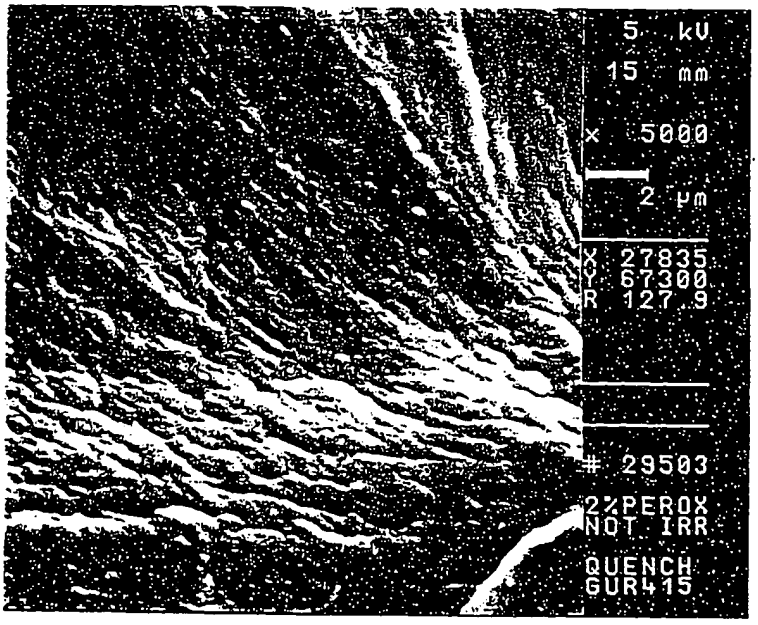

Figure 4.17. Scanning electron micrographs of fracture surfaces of UHMWPE (2 wt% peroxide). **Quench crystallized. Before irradiation.** (a) x 200 (b) x 5000.

sample shows a quite different morphology, compared to that of the slowly cooled 2 wt% peroxide sample (refer to Figure 4.15). A "ridge-like" network is observed in Figure 4.17. UHMWPE contains a high concentration of entanglements, even after melting [39-40]. A quenching process will "freeze" the entanglements and prevent chains from disentangling so that crystalline regions are very small. From thermal analyses of quenched crystallized samples (refer to chapter 2), we reported that the quenching process produced a more homogeneous network at high peroxide concentration because melting temperatures of first and second melting during the DSC scan were equal. Thus, the observed uniform "ridge-like" pattern of fracture surfaces could be due to a homogeneous network and very small crystalline domains produced during quenching.

Scanning electron micrograph of fracture surfaces of quenched peroxide-free sample, compression molded at 170 °C for 2 h and subsequently quenched in liquid nitrogen, is shown in Figure 4.18. The fracture surface indicates less brittle fracture compared to that of the slowly cooled peroxide-free sample (Figure 4.7), but more brittle fracture compared to that of the slowly cooled 1 wt% peroxide sample (Figure 4.14). Thus, crystallinity can be a dominant factor affecting the ductility of the fracture behavior.

After Irradiation (dose = 34 kGy)

Scanning electron micrographs of fracture surfaces of slowly cooled samples of GUR 415, compression molded at 170 °C and crosslinked with 0, 1, and 2 wt% peroxide and then irradiated with 34 kGy of gamma-rays, are shown in Figures 4.19-4.21, respectively. After irradiation, the DSC crystallinity for these three samples is 55.8, 42.0, and 36.7%, respectively (refer to chapter 2). For the peroxide-free sample, a neat and sharper fracture boundary indicating more brittle fracture is observed, compared to that of the similarly prepared peroxide-free sample without irradiation (Figure 4.7). This behavior results from

increased crystallinity produced by irradiation, because the radiation-induced scission of tie molecules permits the recrystallization of broken chains from noncrystalline regions. In addition, a "circle - like" feature is observed near notch areas. Close examination of this feature showed a radial fibrous structure within the circles. This could be induced by preferential crack initiation during the fracturing process because the area near the notch is more stress-sensitive. A 1 wt% peroxide crosslinked sample was similar to the same sample without irradiation (Figure 4.14). For the 2 wt% peroxide crosslinked sample, irradiation effect is even less important (compare with Figure 4.15).

Scanning electron micrographs of fracture surfaces of quench crystallized samples of GUR 415, compression molded at 170 °C and crosslinked with 0, 1, and 2 wt% peroxide and then quenched and irradiated, are shown in Figures 4.22-4.24, respectively. The crystallinity for these samples (i.e., 0, 1, and 2 wt% peroxide) is 49.8, 43.2, and 37.3%, respectively. The peroxide-free sample clearly shows more brittle fracture after irradiation than before irradiation (Figure 4.18). This is because of the crystallinity increase, as irradiation-induced scission of tie molecules permits recrystallization of broken chains from the noncrystalline regions and results in an increased crystallinity. For the 1 wt% peroxide sample, similar behavior is observed before and after irradiation (Figures 4.16 and 4.23). For the 2 wt% peroxide sample, it can be seen that the "ridge - like" pattern is destroyed slightly and a transverse fracture boundary appears (compare Figures 4.17 and 4.24).

Fracture can be defined as the creation of new surface within a material by the application of external forces [46]. It can be classified as either brittle or ductile, depending on polymer structure and the conditions of testing such as temperature and testing rate. Brittle and ductile behavior can be defined from the stress-strain curve. Brittle fracture occurs when the polymer fails at its maximum load, at relatively low strains without plastic deformation [47]. Ductile fracture exhibits a peak load in the stress-strain curve and then exhibits cold-drawing (i.e., plastic deformation). Semicrystalline polymers exhibit a drastic

(a)

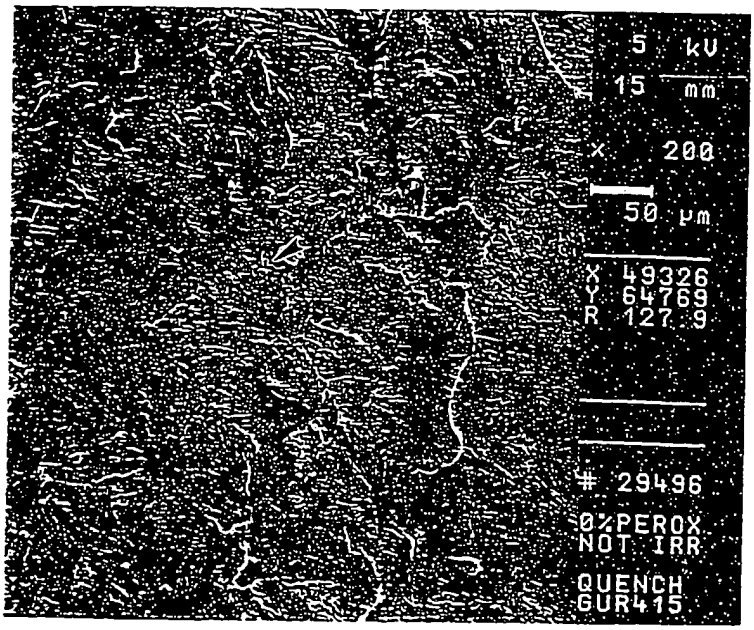

(b)

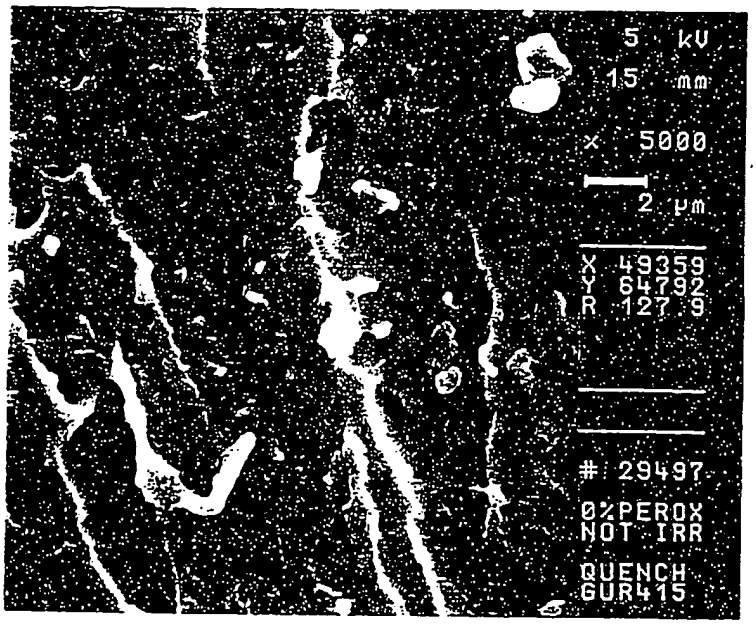

Figure 4.18. Scanning electron micrographs of fracture surfaces of quench crystallized UHMWPE (peroxide-free). **Before irradiation.** (a) x 200 (b) x 5000.

(a)

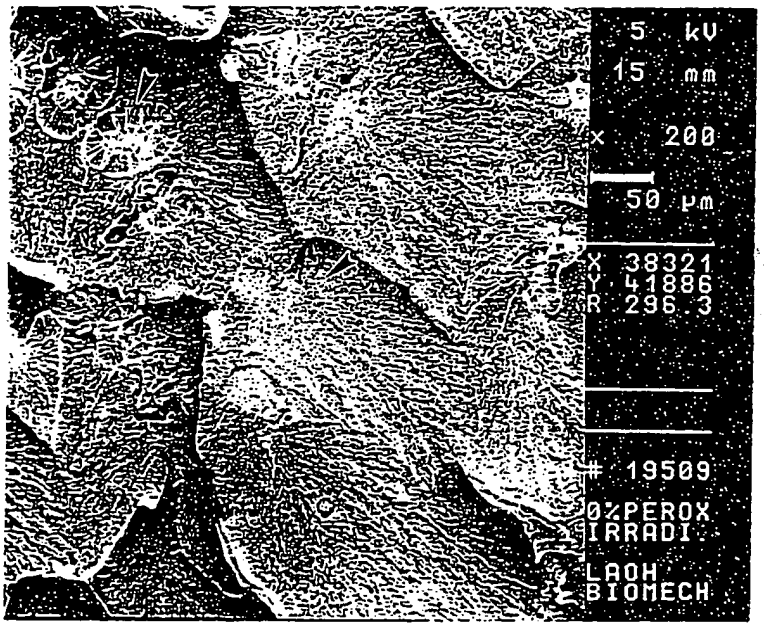

(b)

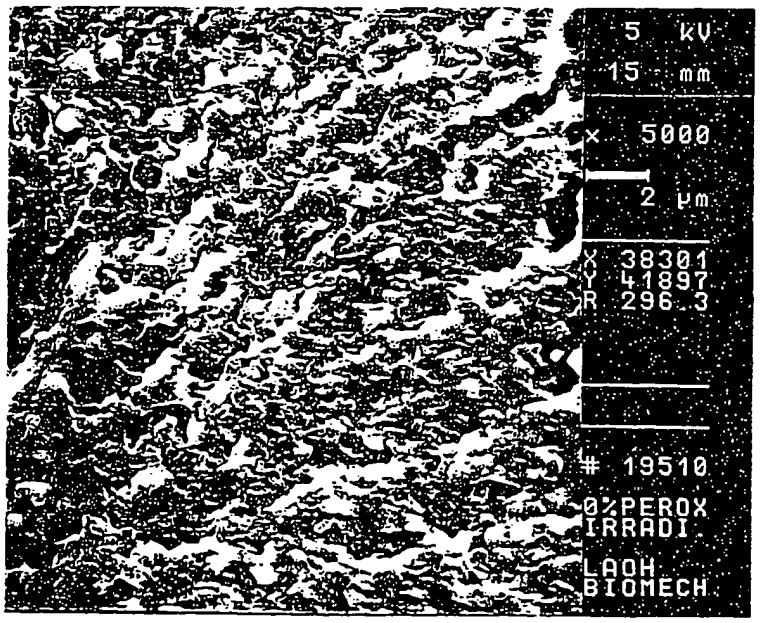

Figure 4.19. Scanning electron micrographs of fracture surfaces of UHMWPE (peroxide-free). **Slowly cooled. After irradiation.** (a) x 200 (b) x 5000.

(c)

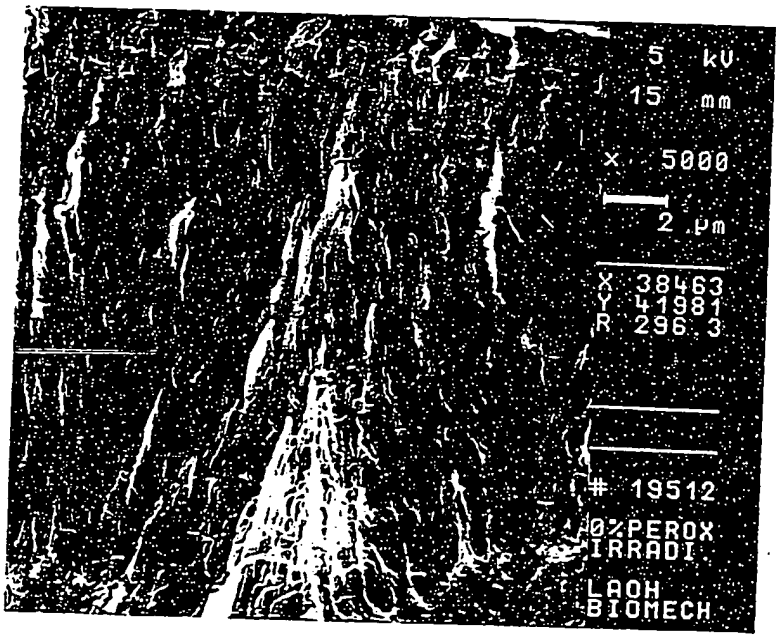

Figure 4.19. (continued) (c) x 5000.

(a)

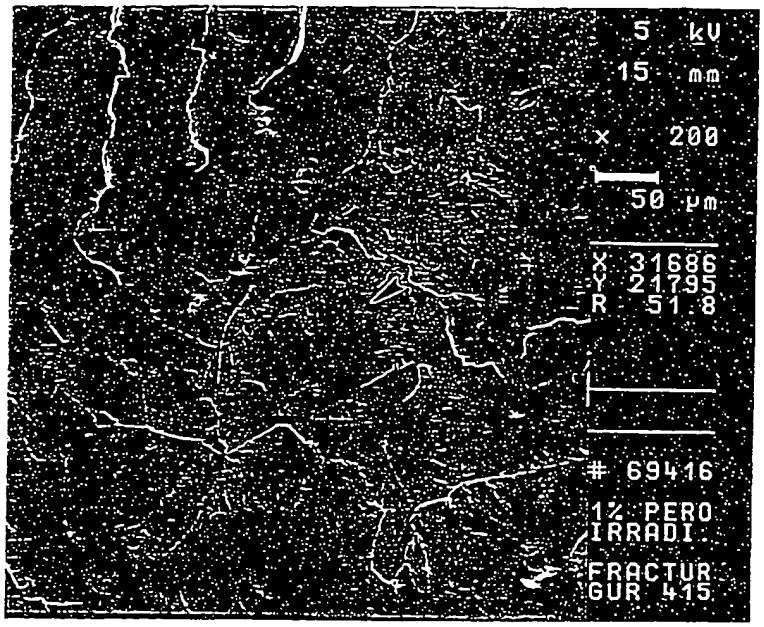

(b)

Figure 4.20. Scanning electron micrographs of fracture surfaces of UHMWPE (1 wt% peroxide). **Slowly cooled. After irradiation.** (a) x 200 (b) x 5000.

(a)

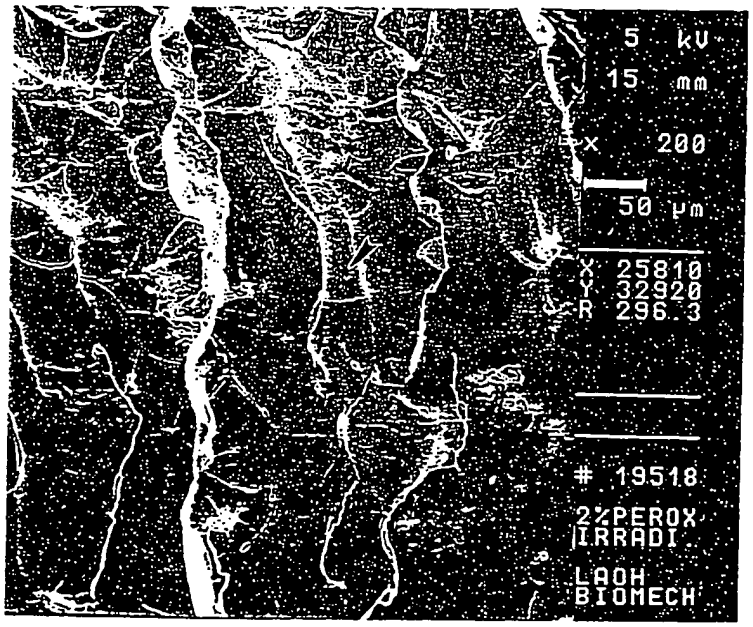

(b)

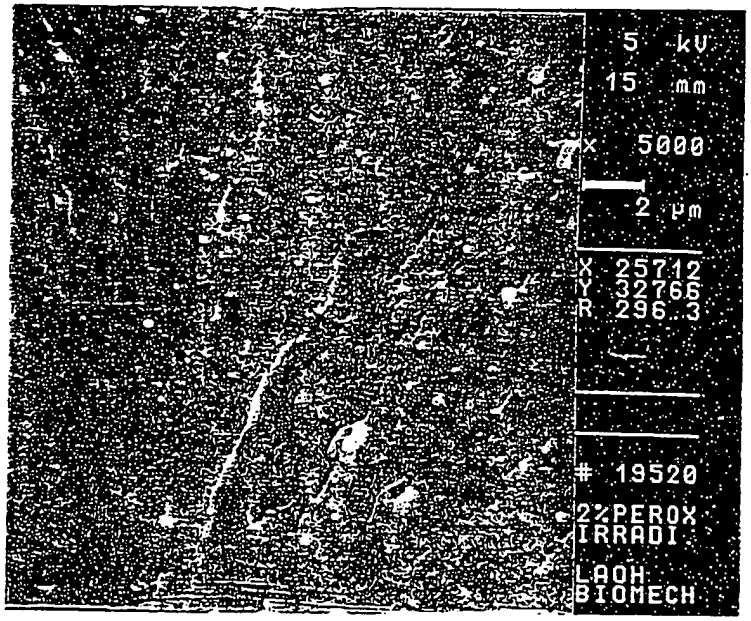

Figure 4.21. Scanning electron micrographs of fracture surfaces of UHMWPE (2 wt% peroxide). **Slowly cooled. After irradiation.** (a) x 200 (b) x 5000.

(a)

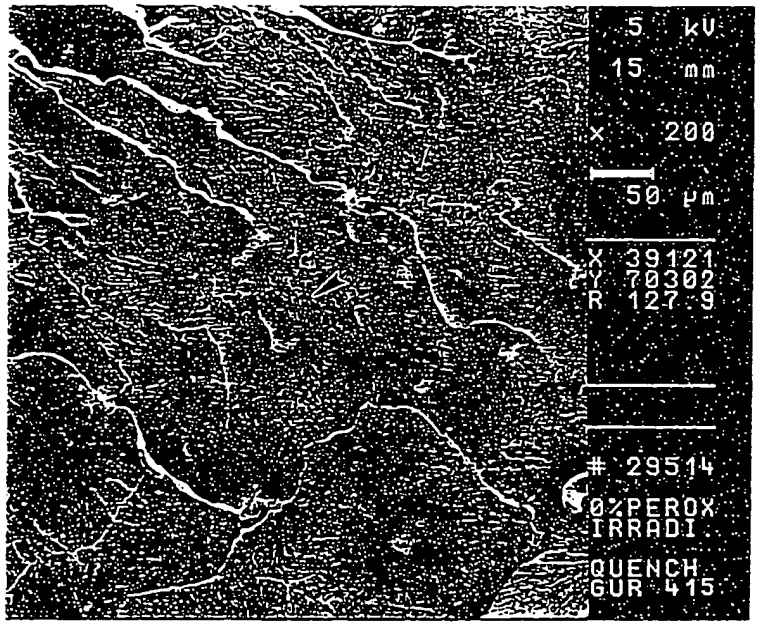

(b)

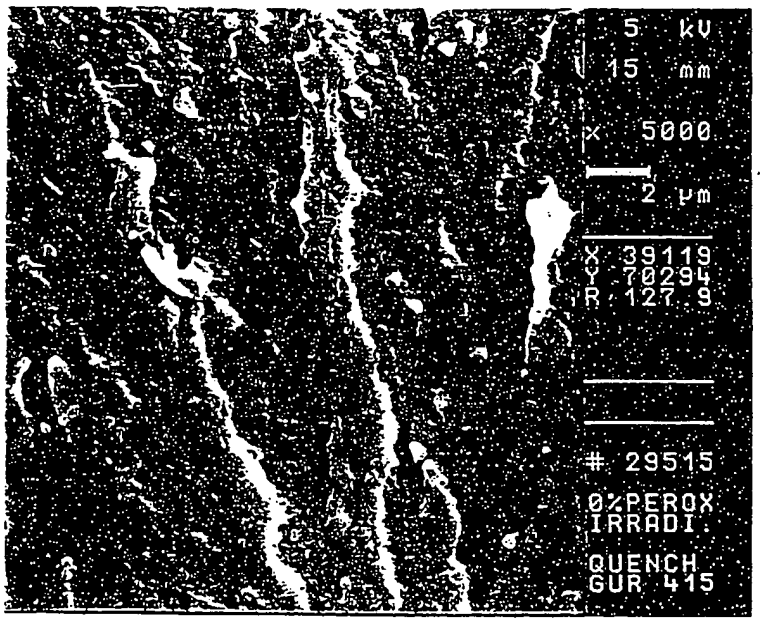

Figure 4.22. Scanning electron micrographs of fracture surfaces of quench crystallized UHMWPE (peroxide-free). After irradiation. (a) x 200 (b) x 5000.

(a)

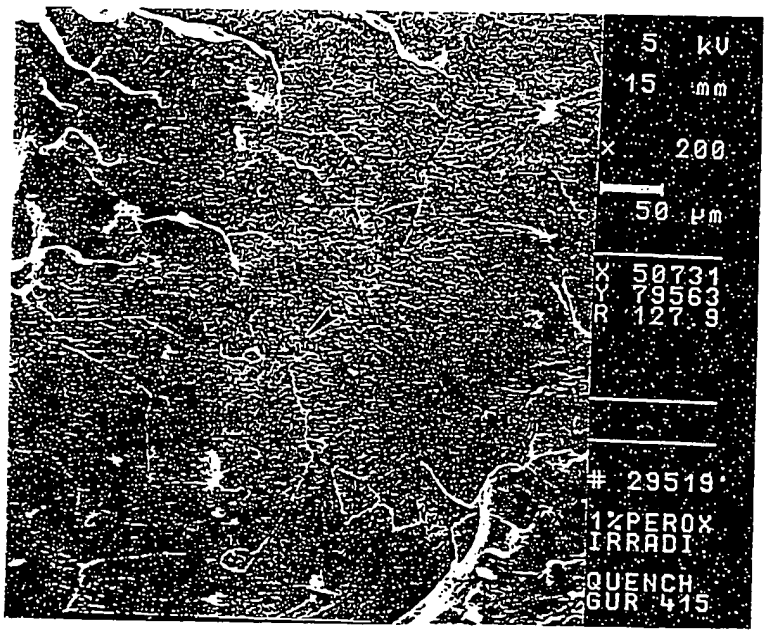

(b)

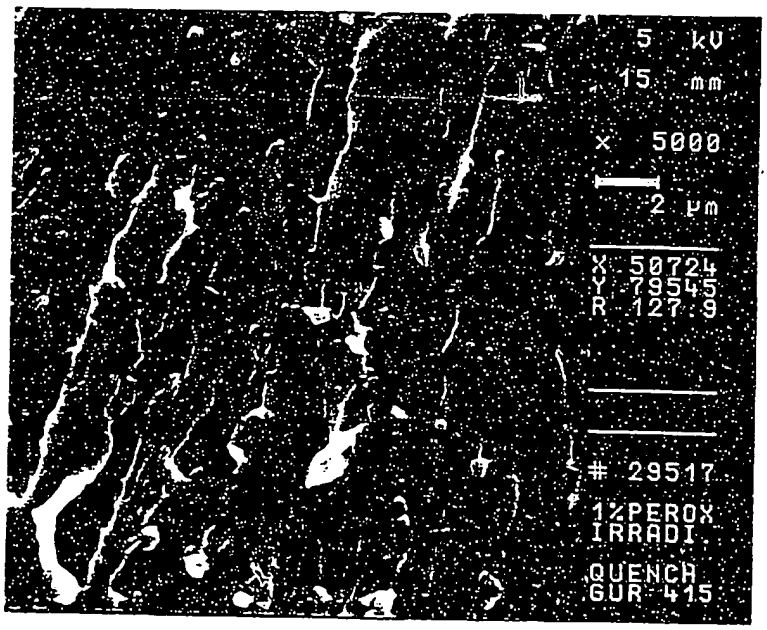

Figure 4.23. Scanning electron micrographs of fracture surfaces of UHMWPE (1 wt% peroxide). **Quench crystallized. After irradiation.** (a) x 200 (b) x 5000.

(a)

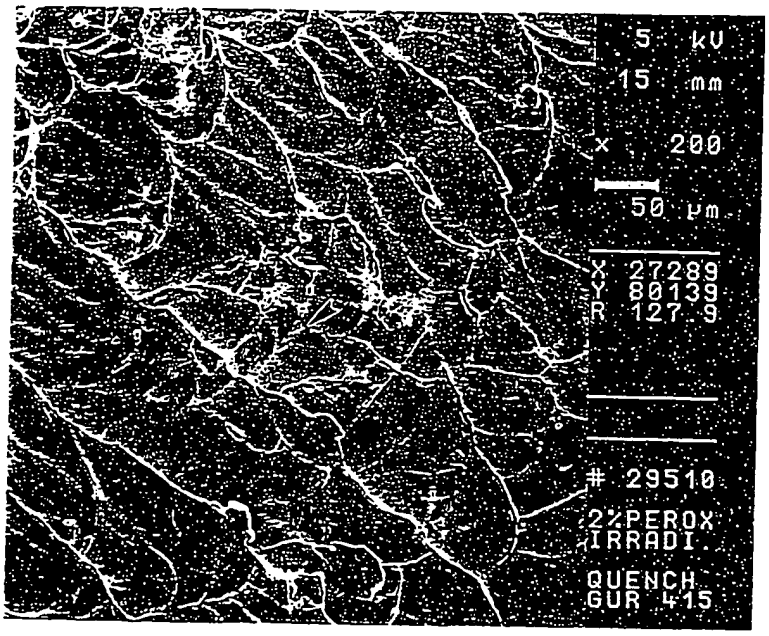

(b)

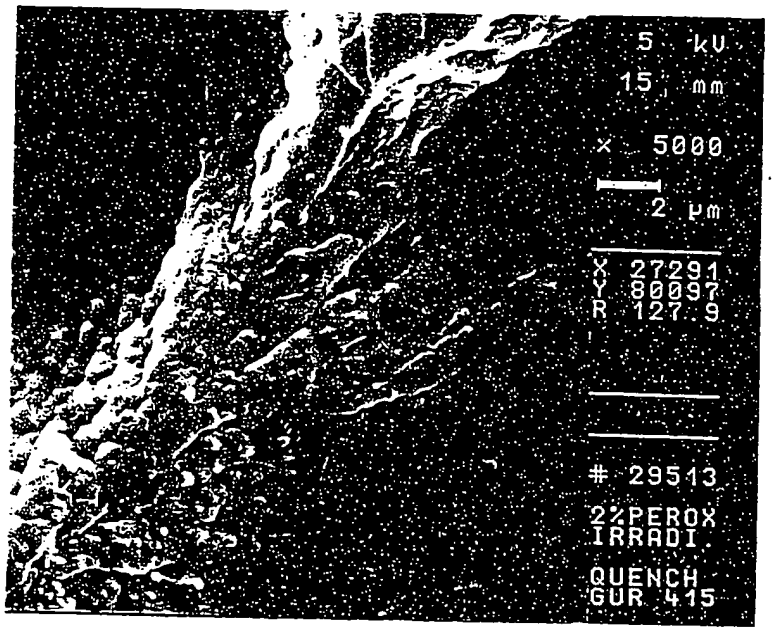

Figure 4.24. Scanning electron micrographs of fracture surfaces of UHMWPE (2 wt% peroxide). **Quench crystallized. After irradiation.** (a) x 200 (b) x 5000.

structural reorganization from spherulitic to fibrillar as the degree of plastic deformation increases [48]. The temperature at which a sample changes from brittle to ductile behavior is called the brittle-ductile transition temperature and is a function of testing rate. Generally, glassy polymers such as polystyrene and poly (methyl methacrylate) tend to be very brittle at room temperature, whereas, semicrystalline polymers, such as polyethylene, are normally more ductile, especially between T_g and T_m [46]. However, after cooling with liquid nitrogen, semicrystalline polymers exhibit brittle behavior. This is due to a reduction of molecular mobility and hence, the local motion of molecular chains is inhibited.

From cryogenically fractured surfaces, it is possible to examine the microstructure in bulk materials using electron microscopy. In our experimental results, it is interesting to compare the morphology of fracture surfaces of unirradiated peroxide free slowly cooled and irradiated quenched samples. The crystallinity of slowly cooled peroxide-free unirradiated and quenched peroxide-free irradiated samples is 49.2 and 49.8%, respectively. However, comparing Figure 4.7 with Figure 4.22, it is seen that the slowly cooled peroxide-free sample exhibits a more brittle fracture than the quenched peroxide-free one, even though their crystallinities are comparable. It was shown that in general, interspherulitic boundaries are more prone to brittle fracture [49]. Segregation occurs within interspherulitic boundaries, because short and noncrystallizable molecules are rejected at the crystal growth front and tend to locate between spherulites during the crystallization process [49]. This segregated material is intrinsically brittle. The extent of overall segregation is dependent on the crystallization conditions and is greatest for slow growth at low supercoolings. High supercooling (i.e., quenching) leads to an increase in nucleation rate and hence, a large number of small spherulites are formed. Interspherulitic boundaries are less important for this case. This is why quenched peroxide-free sample (after irradiation) shows less brittle fracture than the slowly cooled peroxide-free one (before irradiation).

SEM Morphology of Etched Fracture Surfaces

Before Irradiation

Scanning electron micrographs of etched fracture surfaces of GUR 415 compression molded (without peroxide) at 170 °C for 2 h and slowly cooled is shown in Figure 4.25. Scanning electron micrographs of etched fracture surfaces for samples crosslinked with 1 and 2 wt% peroxide are shown in Figures 4.26-4.27, respectively. Etching time is 5 h for all three samples. A spherulite structure can be seen in the etched fracture surfaces for all three materials. In Figure 4.25, the slowly cooled peroxide-free sample showed more damaged spherulite surfaces, compared to Figure 4.26 (1 wt% peroxide). Since the peroxide-free sample exhibits a more brittle fracture than peroxide crosslinked samples as shown in scanning electron micrographs of unetched fracture surfaces (Figures 4.7 and 4.14), it is believed that the peroxide-free sample suffers higher forces and less deformation during fracturing process, leading to smaller strains and more chain scission. The scissioned chains (chain ends) will be more susceptible to etchant attack (i.e., oxidation), leading to a coarser spherulite surface. On the other hand, comparing Figure 4.26 (1 wt% peroxide) to Figure 4.27 (2 wt% peroxide), it is found that spherulite surfaces for 2 wt% peroxide sample suffer more oxidation (lousy appearance). As peroxide crosslinking introduces tertiary carbons, which are susceptible to oxidation, the etching rate for 2 wt% peroxide sample is increased because of higher crosslink density. Corresponding to Figure 4.7 and 4.14-4.15 (before etching), it is shown that etched fracture surfaces consist of a large number of spherulites, and that the fracture boundary is composed of densely packed rows of spherulites. For comparison, we increased the etching time to 6 h. Resulting etched fracture surfaces for peroxide-free, 1 and 2 wt% peroxide samples are shown in Figures 4.28-4.30, respectively. We observe that spherulite

surfaces suffer further oxidation with increased etching time, and the spherulite size becomes larger. It is suggested that etching rate and spherulite size are time-dependent [15]. In addition, with these etching conditions (i.e., 1% (w/v) etchant, 5 h and 6 h at room temperature), no artefacts were observed.

Scanning electron micrograph of etched fracture surfaces of a peroxide-free sample, which was compression molded at 300 °C for 2 h and subsequently slowly cooled to room temperature, is shown Figure 4.31 (etching time 5 h). After an etching time of 6 h, scanning electron micrograph is shown in Figure 4. 32. Comparing Figure 4.31 to Figure 4.25, spherulite sizes for sample compression molded at 300 °C are increased. Comparing Figure 4.32 to Figure 4.28, a similar trend is observed. The reason for this behavior is that the higher crystallization temperature provides more opportunities for molecular chain motion to achieve the three-dimensional order required for crystallite formation. Therefore, crystallite size and hence, the spherulite size increase at higher crystallization temperature.

After Irradiation (34 kGy)

Scanning electron micrographs of etched fracture surfaces for GUR 415 crosslinked with 0, 1 and 2 wt% peroxide, which were compression molded at 170 C for 2 h and subsequently slowly cooled to room temperature, are shown in Figures 4.33-4.35. The etching time is 5 h for all samples. Comparing to Figures 4.25-4.27 (before irradiation), it is found that after irradiation, spherulite surfaces suffer more oxidation and some spherulites become larger. It is known that irradiation of UHMWPE leads to scission of tie molecules in addition to irradiation-induced crosslinking [50-60]. Thus, irradiation on UHMWPE will lead to an increase in the concentration of tertiary carbons and broken chains (i.e., chain ends) . These species are believed to be more susceptible to oxidation. An etching time of 6 h was examined in order to compare etching behavior. Etched fracture

(a)

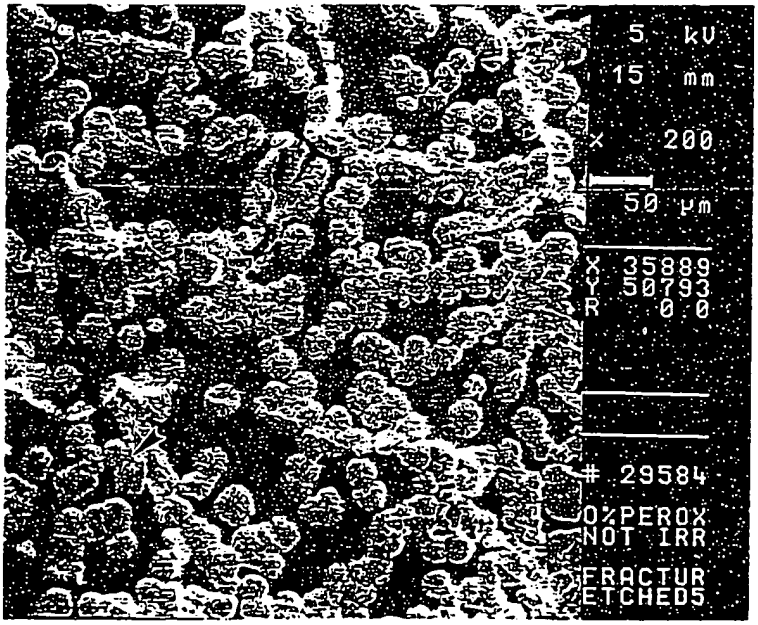

(b)

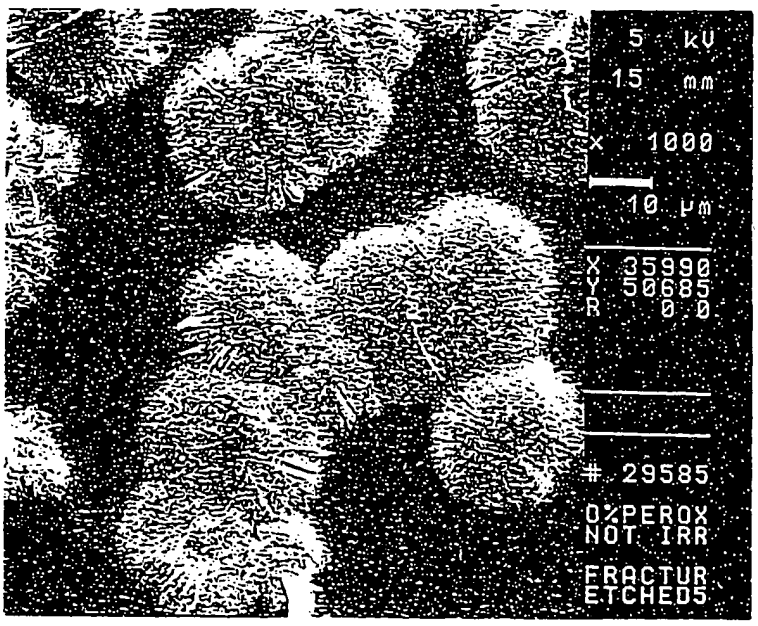

Figure 4.25. Scanning electron micrographs of etched (5 h) fracture surfaces of UHMWPE (peroxide-free). **Slowly cooled. Before irradiation.** (a) x 200 (b) x 1000.

(a)

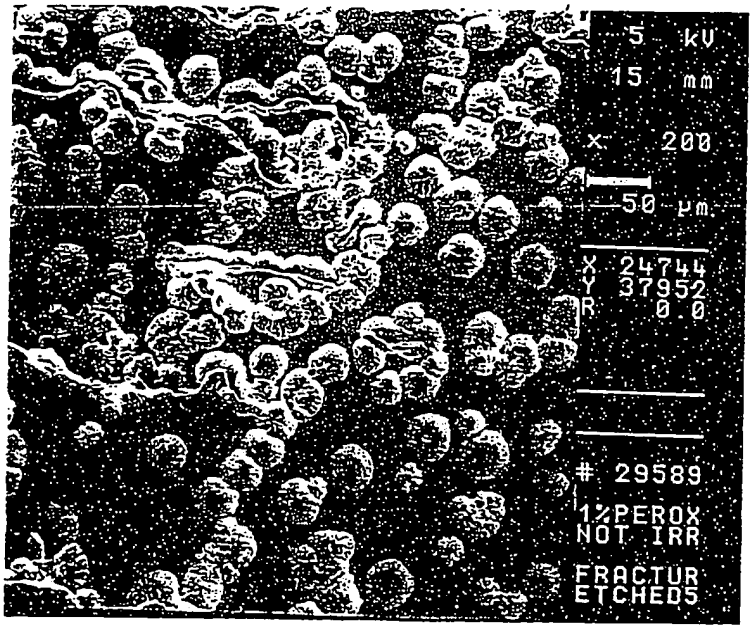

(b)

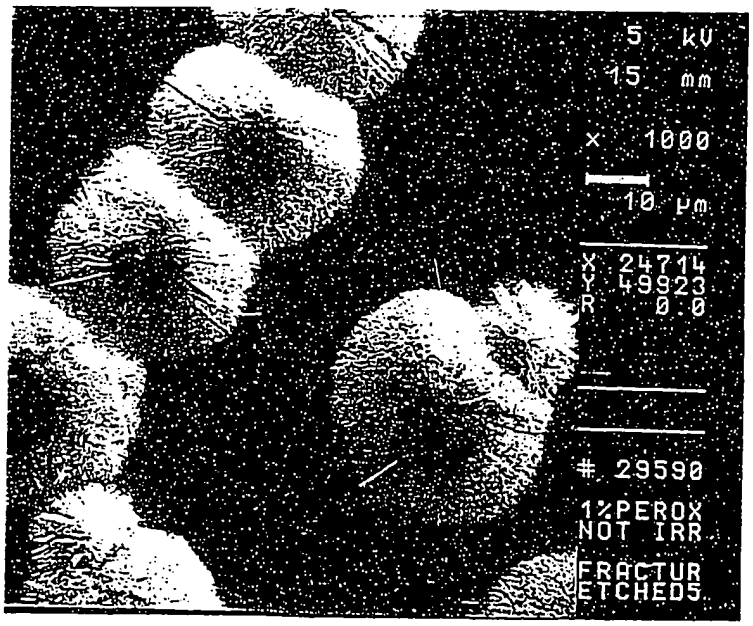

Figure 4.26. Scanning electron micrographs of etched (5 h) fracture surfaces of UHMWPE (1 wt% peroxide). **Slowly cooled. Before irradiation.** (a) x 200 (b) x 1000.

(a)

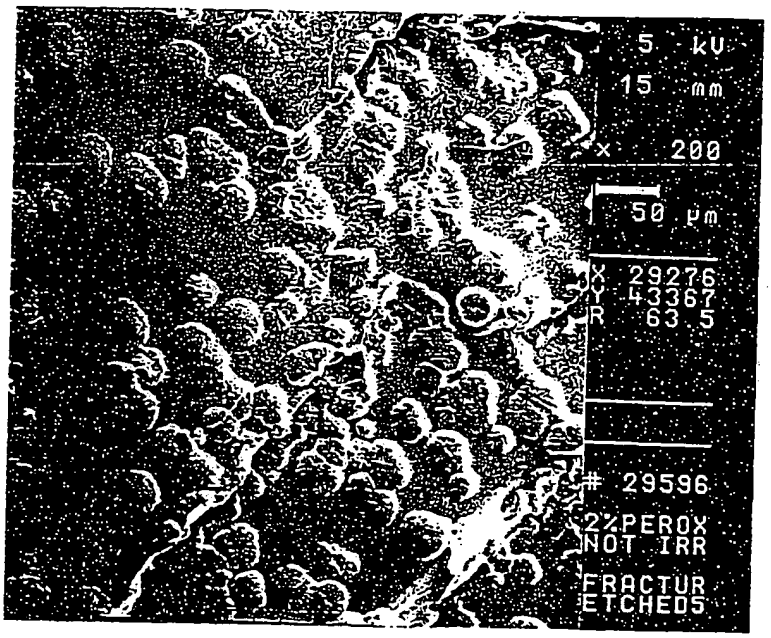

(b)

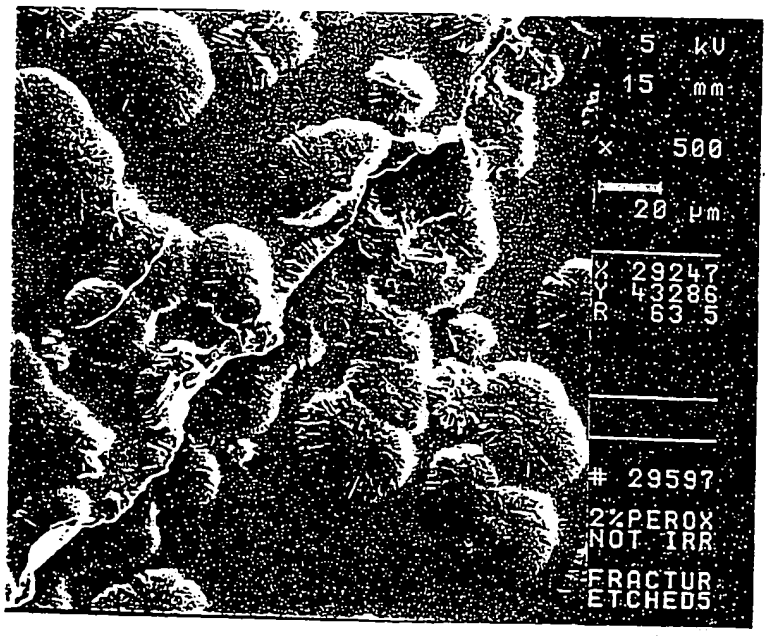

Figure 4.27. Scanning electron micrographs of etched (5 h) fracture surfaces of UHMWPE (2 wt% peroxide). **Slowly cooled. Before irradiation.** (a) x 200 (b) x 500.

(a)

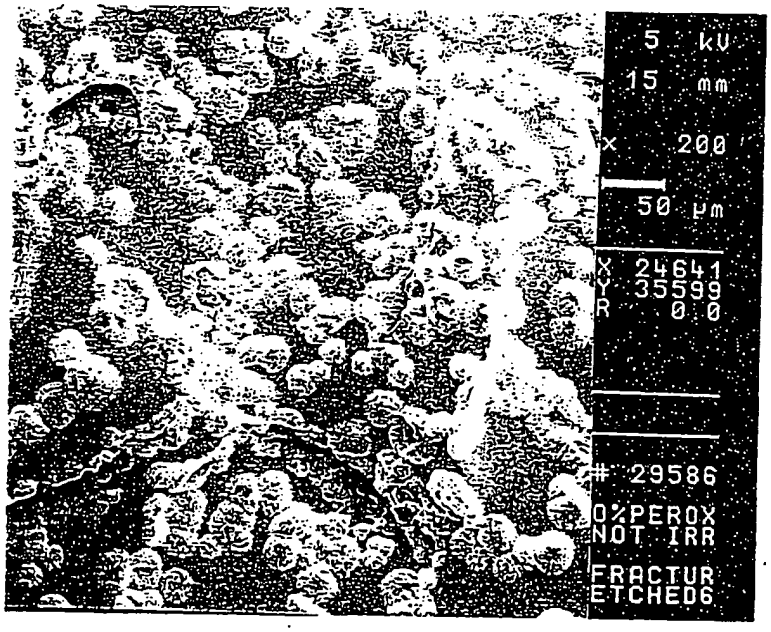

Figure 4.28. Scanning electron micrographs of etched (6 h) fracture surfaces of UHMWPE (peroxide-free). **Slowly cooled. Before irradiation.** (a) x 200.

(a)

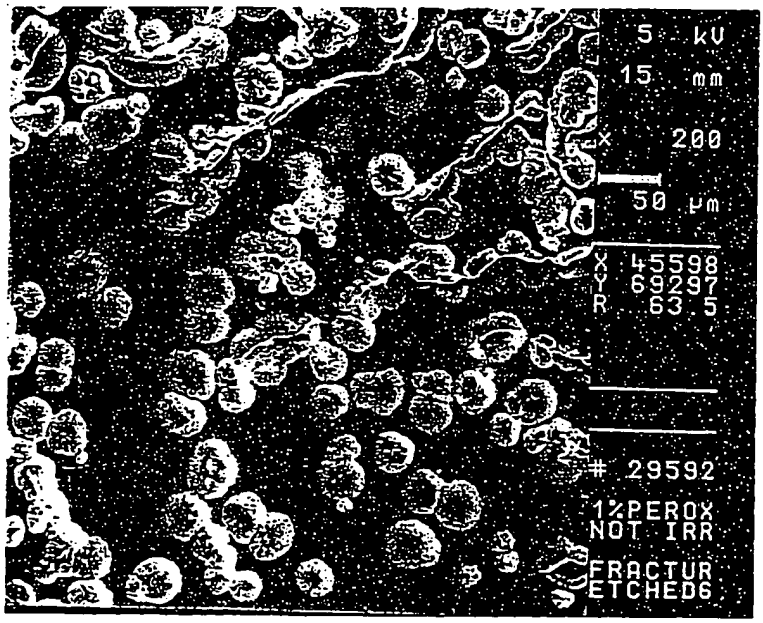

Figure 4.29. Scanning electron micrographs of etched (**6 h**) fracture surfaces of UHMWPE (1 wt% peroxide). **Slowly cooled. Before irradiation.** (a) x 200.

(a)

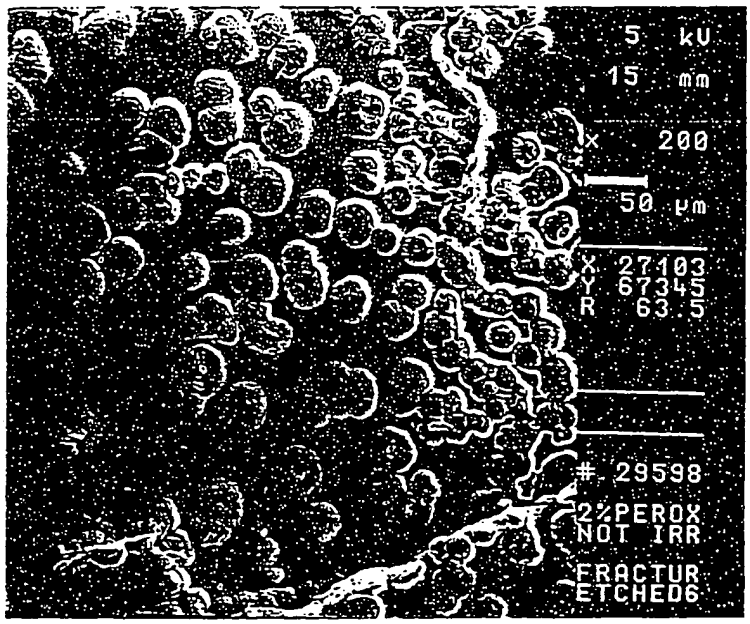

(b)

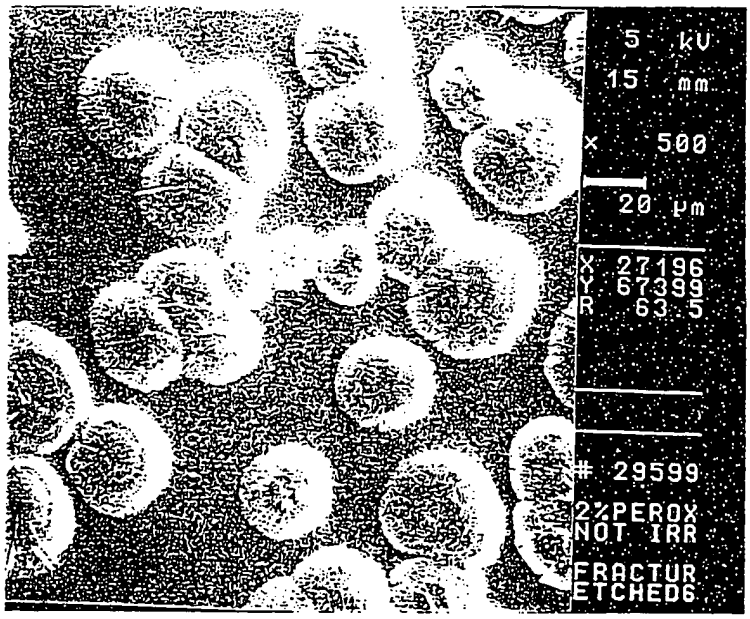

Figure 4.30. Scanning electron micrographs of etched (6 h) fracture surfaces of UHMWPE (2 wt% peroxide). **Slowly cooled. Before irradiation.** (a) x 200 (b) x 500.

(a)

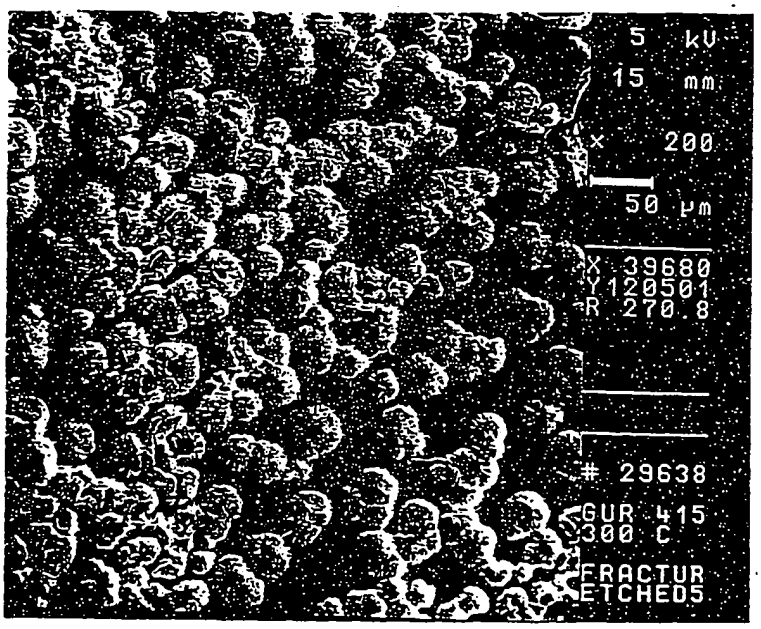

Figure 4.31. Scanning electron micrographs of etched (5 h) fracture surfaces of UHMWPE (peroxide-free). 300 °C. Slowly cooled. (a) x 200.

100

(a)

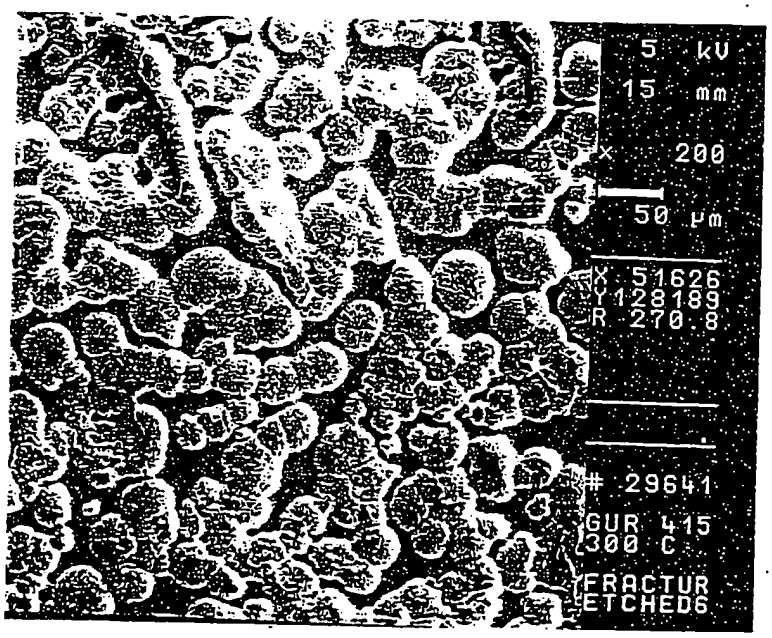

Figure 4.32. Scanning electron micrographs of etched (**6 h**) fracture surfaces of UHMWPE (peroxide-free). **300 °C. Slowly cooled.** (a) x 200.

(a)

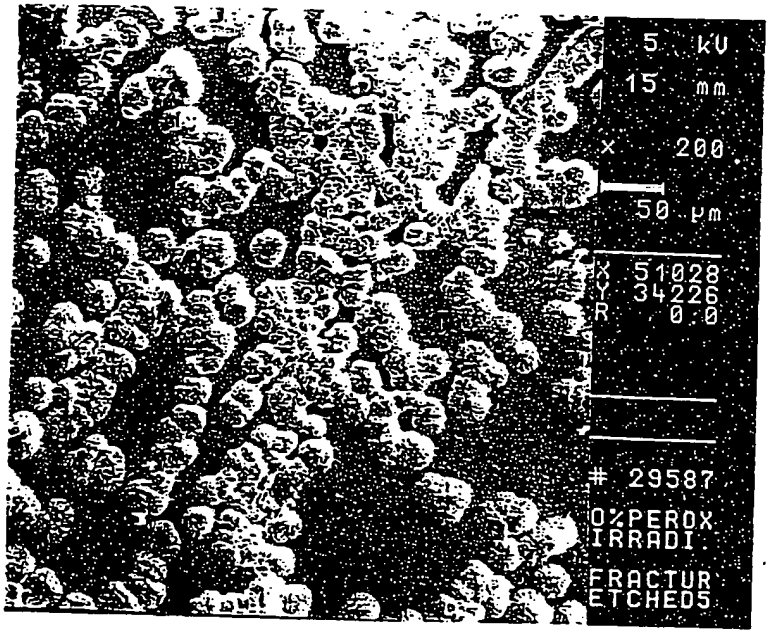

Figure 4.33. Scanning electron micrographs of etched (5 h) fracture surfaces of UHMWPE (peroxide-free). **Slowly cooled. After irradiation.** (a) x 200.

(a)

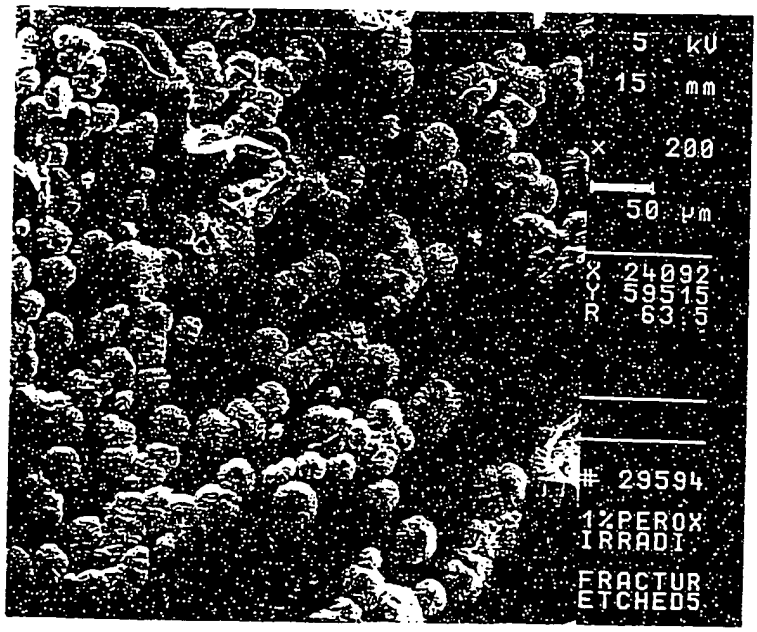

(b)

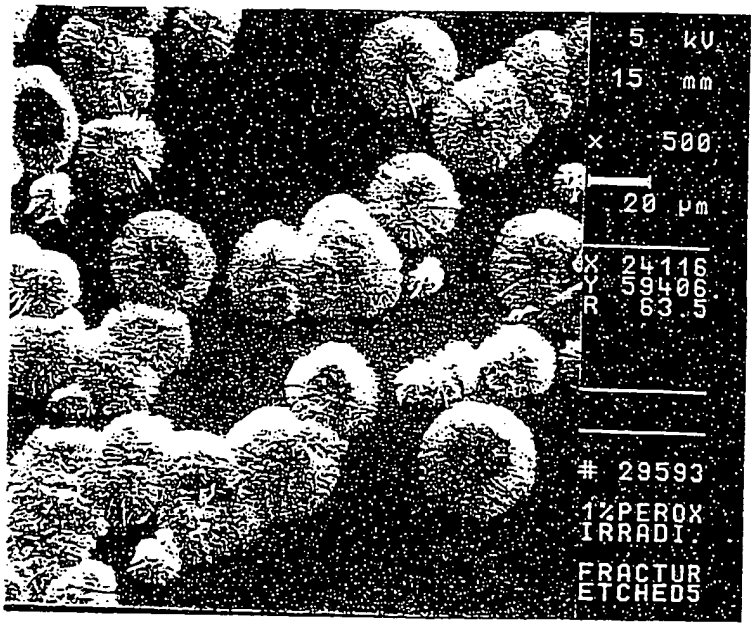

Figure 4.34. Scanning electron micrographs of etched (5 h) fracture surfaces of UHMWPE (1 wt% peroxide). **Slowly cooled. After irradiation.** (a) x 200 (b) x 500.

(a)

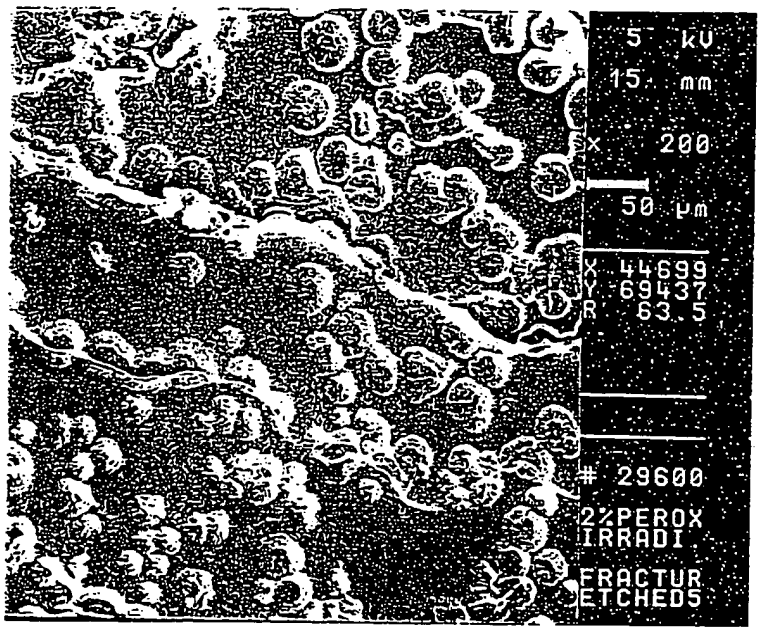

(b)

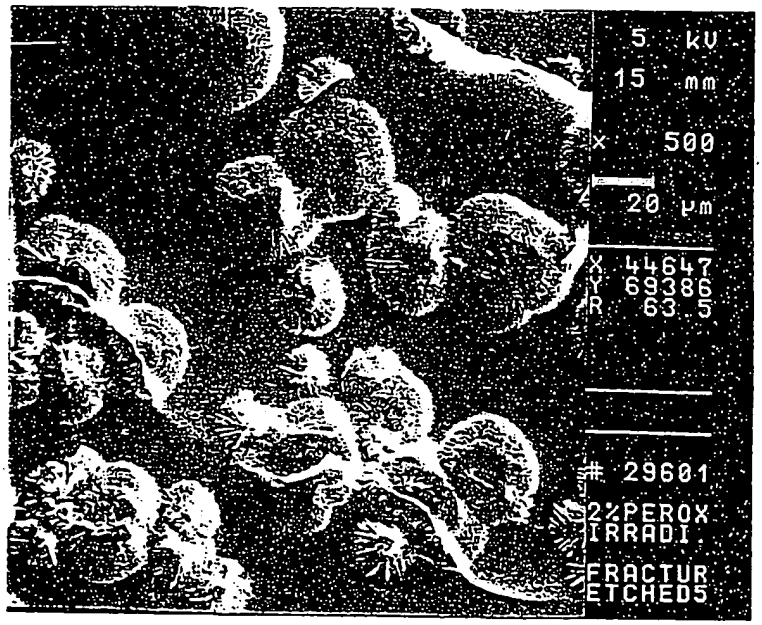

Figure 4.35. Scanning electron micrographs of etched (5 h) fracture surfaces of UHMWPE (2 wt% peroxide). Slowly cooled. After irradiation. (a) x 200 (b) x 500.

surfaces for peroxide-free, 1 and 2 wt% peroxide samples are shown in Figures 4.36-4.38, respectively. Compared to Figures 4.33-4.35 (etching time 5 h), further oxidation gives coarser appearance and worse contrast, as well as larger spherulites. This behavior again confirms that etching rate is time-dependent. In addition, compared to Figures 4.28-4.30 (before irradiation and also with an etching time of 6 h), it is found that after irradiation, the spherulites are further oxidized and some spherulite sizes increase. This is a result of irradiation-induced crosslinking and scission of tie molecules, which leads to structures more susceptible to etching. On the other hand, we believe that more amorphous materials are removed with increasing etching time, resulting in larger spherulites.

SEM Morphology of Etched Molded Surfaces

It must be pointed out that specimens prepared under different conditions (i.e., fractured or molded surfaces, crosslinked or non-crosslinked, irradiated or not irradiated) require different etching times. For example, peroxide crosslinking and irradiation lead to an increased etching rate. In addition, it was shown that the etching rate is time-dependent. The longer the time, the higher the etching rate. At present, we will show that fracture surfaces etch more rapidly than molded surfaces.

Before Irradiation

Scanning electron micrographs of etched molded surfaces of GUR 412, GUR 413, and GUR 415, which were compression molded at 170 °C for 2 h and subsequently slowly cooled to room temperature, are shown in Figures 4.39-4.41, respectively. Scanning electron micrographs of etched molded surfaces of GUR 412, GUR 413, and GUR 415, which were compression molded at 300 °C for 2 h and subsequently slowly cooled to room

temperature, are shown in Figures 4.42-4.44, respectively. The etching time for all these materials was 8 h. Comparing Figures 4.39-4.41 with Figures 4.42-4.44, respectively, larger spherulites were observed for materials which were compression molded at 300 °C for 2 h. Again, higher crystallization temperature provides more opportunities for molecular chain motion to develop the three -dimensional order required for crystallite formation, leading to an increase in spherulite size.

Scanning electron micrographs of etched molded surfaces of 1 and 2 wt% peroxide samples are shown in Figures 4.45-4.46, respectively. The optimal etching time is 5 h for this case. Comparing Figure 4.41 (peroxide free) to Figure 4 .45 (1 wt% peroxide), it is found that the number of spherulites in the peroxide-free sample (49.2% crystallinity) was clearly higher than that in the 1 wt% peroxide sample (39.8% crystallinity). Comparing Figure 4. 41 to Figure 4.46 (2 wt% peroxide, 36.5% crystallinity), a similar observation is obtained. To examine this observation, an etching time of 6 h was performed for the 1 wt% peroxide sample and the resulted scanning electron micrograph is shown in Figure 4. 47. It can be seen that further etching increases the sizes of spherulite, but the number of spherulites is still lower than that of peroxide-free samples (Figure 4.41). The increase in spherulite sizes is due to the removal of more amorphous materials. Comparing Figure 4.45 (1 wt% peroxide) to Figure 4.46 (2 wt% peroxide), it is found that more damage occurs on etched spherulite surfaces of the 2 wt% peroxide sample. Apparently, the concentration of tertiary carbons plays an important role in oxidative susceptibility. It is interesting to compare differences in etching behavior between fracture and molded surfaces. For molded surfaces of a peroxide-free sample, an etching time of 8 h was needed to clearly reveal the spherulitic structures, whereas, for fracture surfaces, only 5 h was needed and the resultant etched surfaces look damaged. This means that deformed or fracture surfaces are more susceptible to etchant attack.

(a)

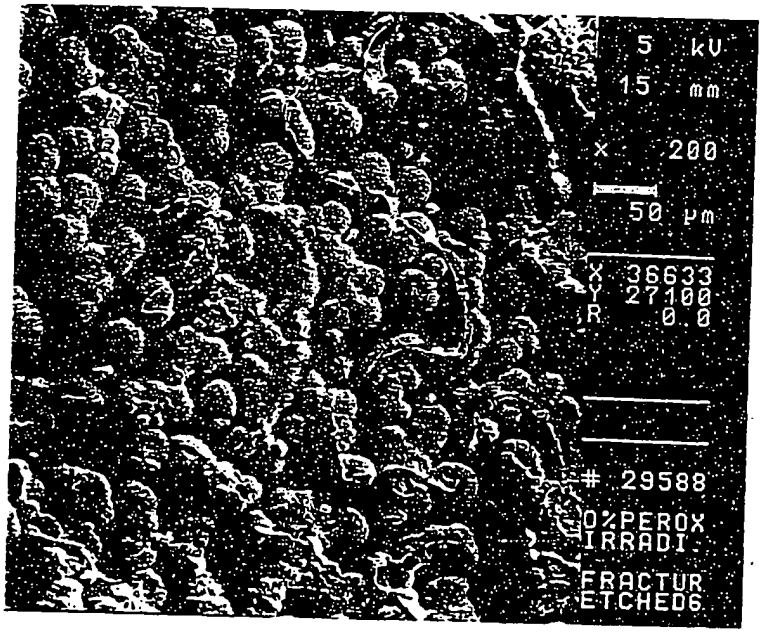

Figure 4.36. Scanning electron micrographs of etched (6 h) fracture surfaces of UHMWPE (peroxide-free). **Slowly cooled. After irradiation.** (a) x 200.

(a)

Figure 4.37. Scanning electron micrographs of etched (6 h) fracture surfaces of UHMWPE (1 wt% peroxide). Slowly cooled. After irradiation. (a) x 200.

(a)

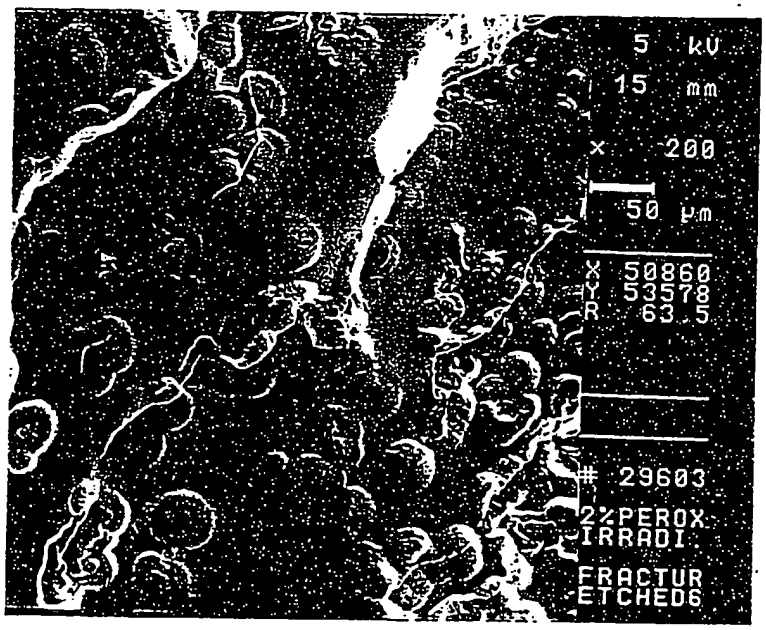

Figure 4.38. Scanning electron micrographs of etched (**6 h**) fracture surfaces of UHMWPE (2 wt% peroxide). **Slowly cooled. After irradiation.** (a) x 200.

(a)

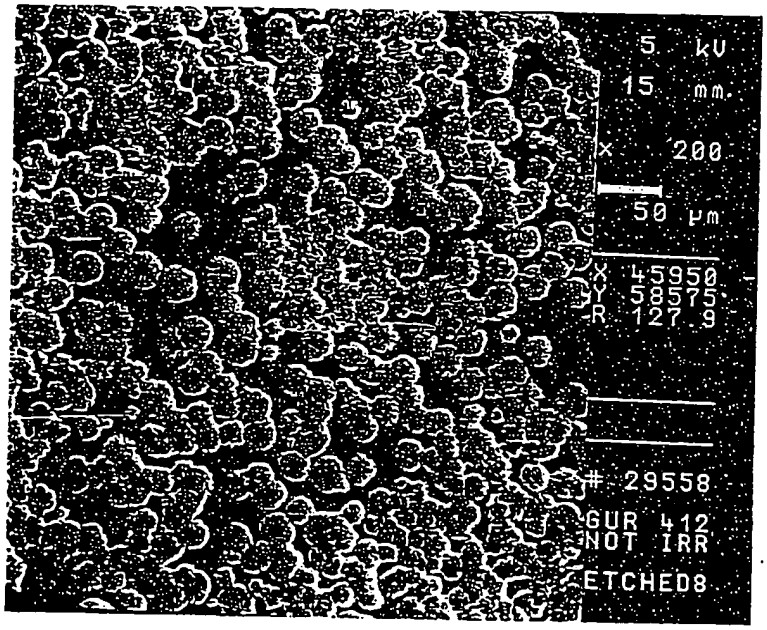

Figure 4.39. Scanning electron micrographs of etched (8 h) molded surfaces of GUR 412. 170 °C. (a) x 200.

(a)

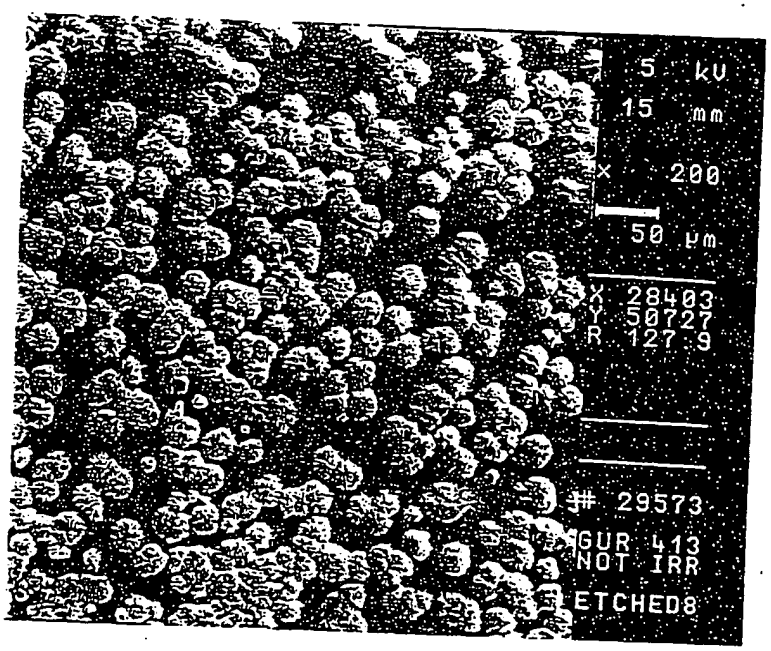

Figure 4.40. Scanning electron micrographs of etched (8 h) molded surfaces of GUR 413. 170 °C. (a) x 200.

(a)

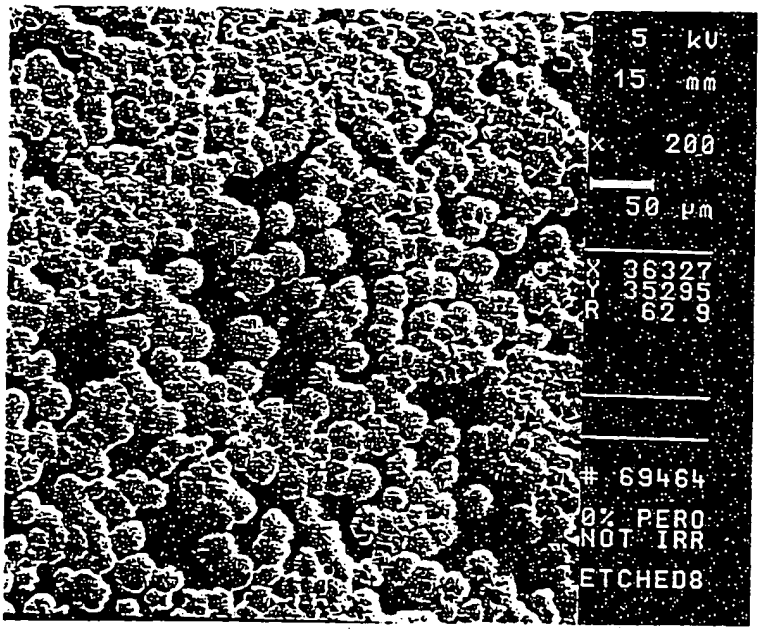

(b)

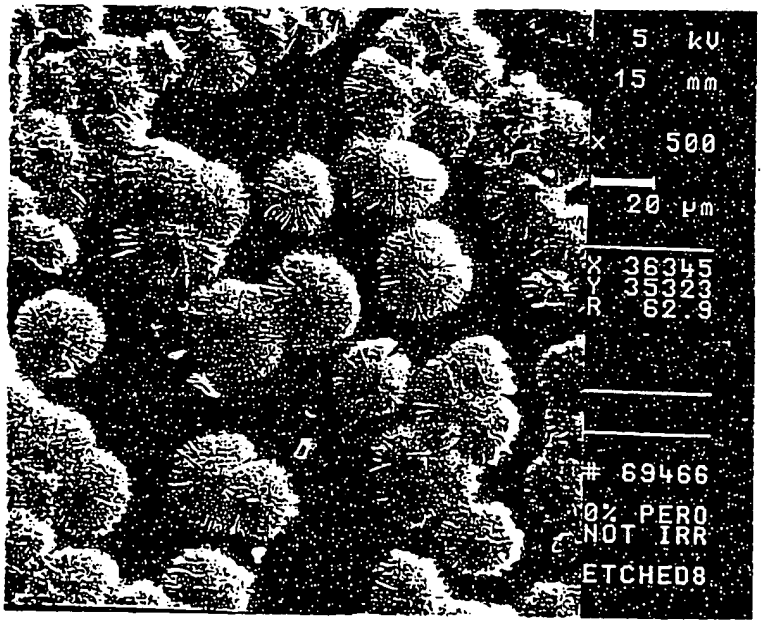

Figure 4.41. Scanning electron micrographs of etched (8 h) molded surfaces of GUR 415. 170 °C. (a) x 200 (b) x 500.

(a)

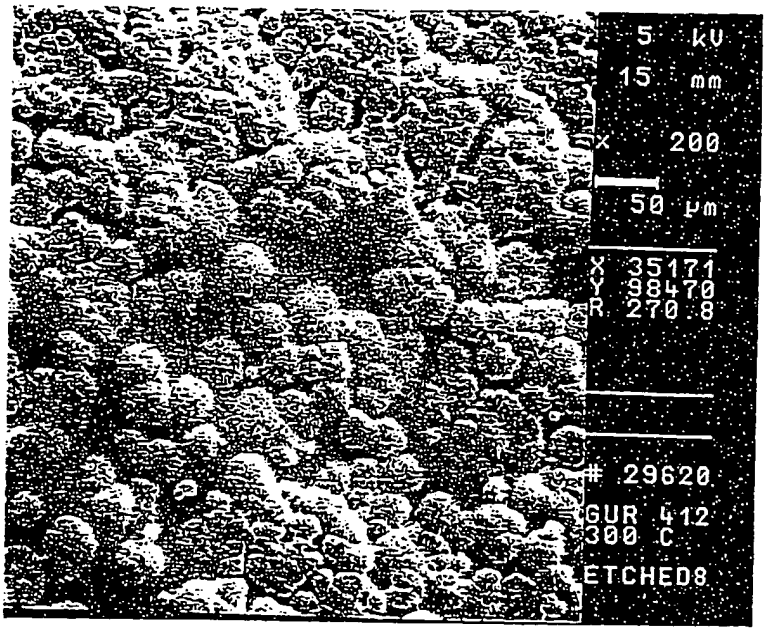

(b)

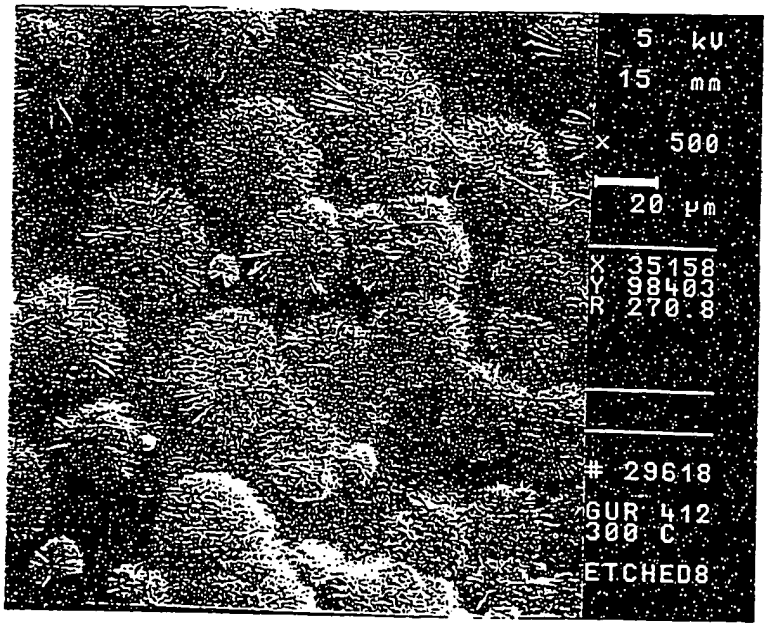

Figure 4.42. Scanning electron micrographs of etched (8 h) molded surfaces of GUR 412. 300 °C. (a) x 200 (b) x 500.

(a)

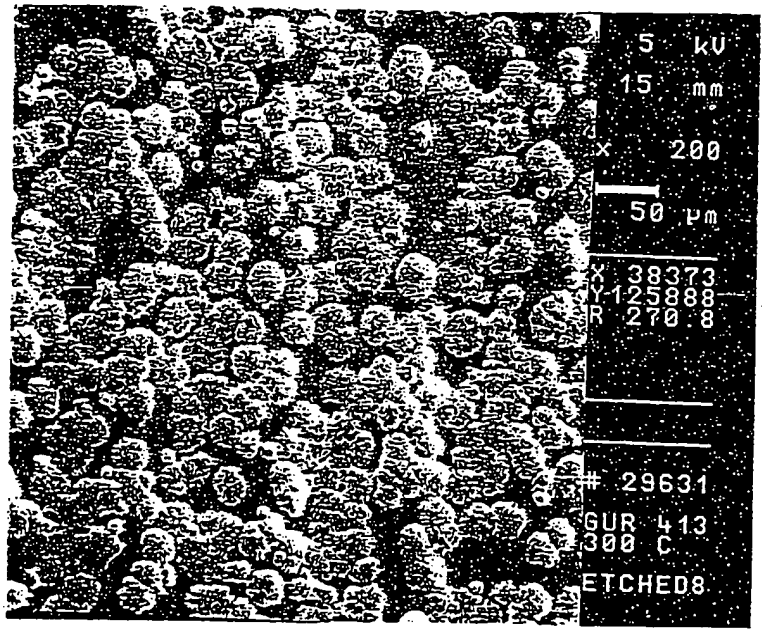

(b)

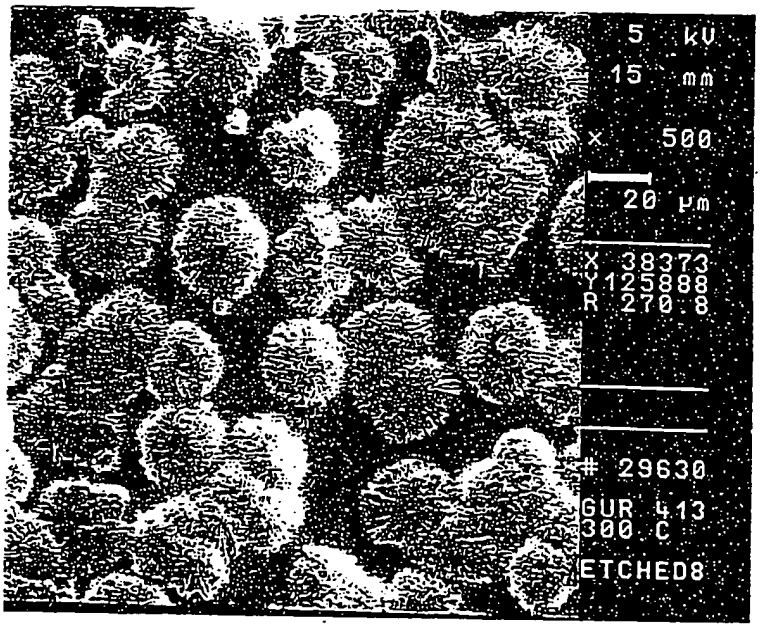

Figure 4.43. Scanning electron micrographs of etched (8 h) molded surfaces of GUR 413. 300 °C. (a) x 200 (b) x 500.

(a)

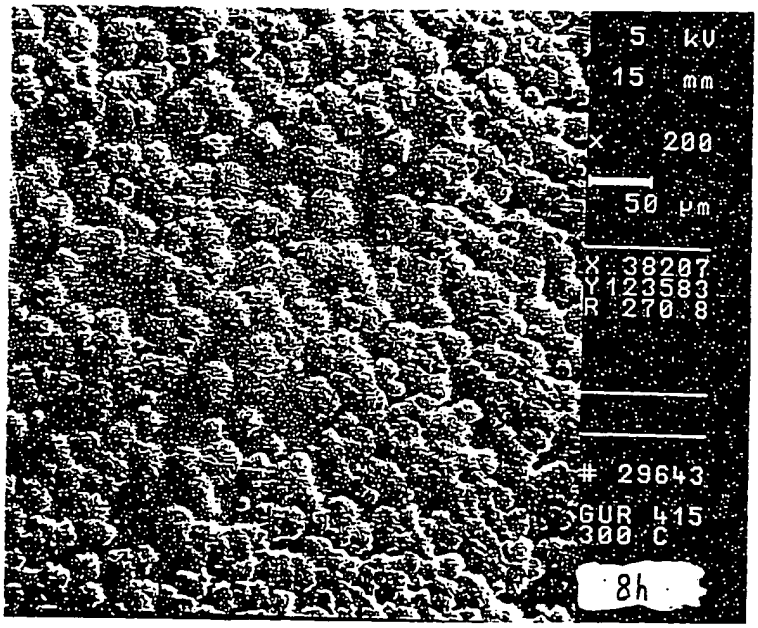

(b)

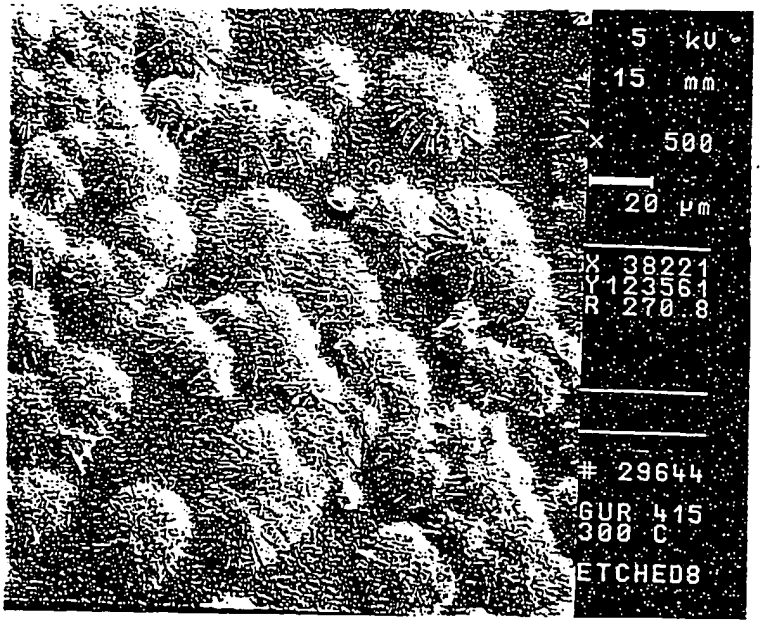

Figure 4.44. Scanning electron micrographs of etched (8 h) molded surfaces of GUR 415. 300 °C. (a) x 200 (b) x 500.

(a)

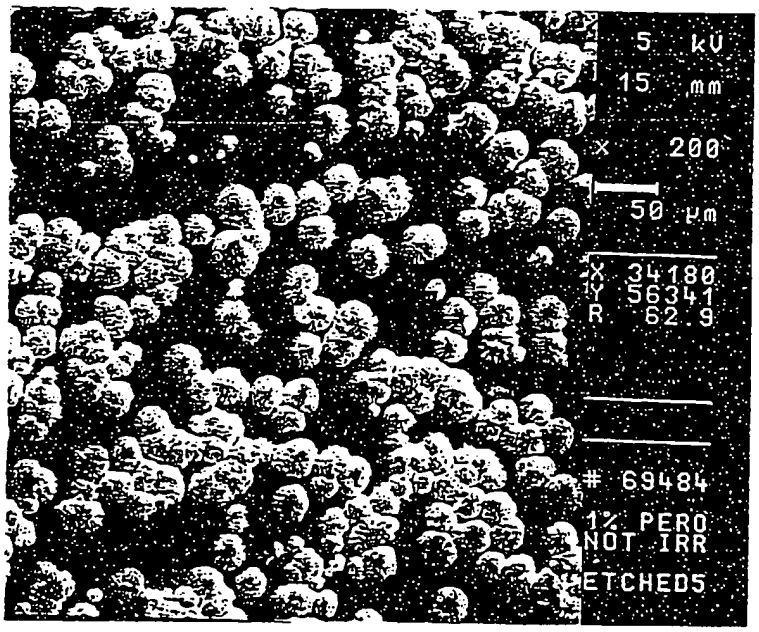

(b)

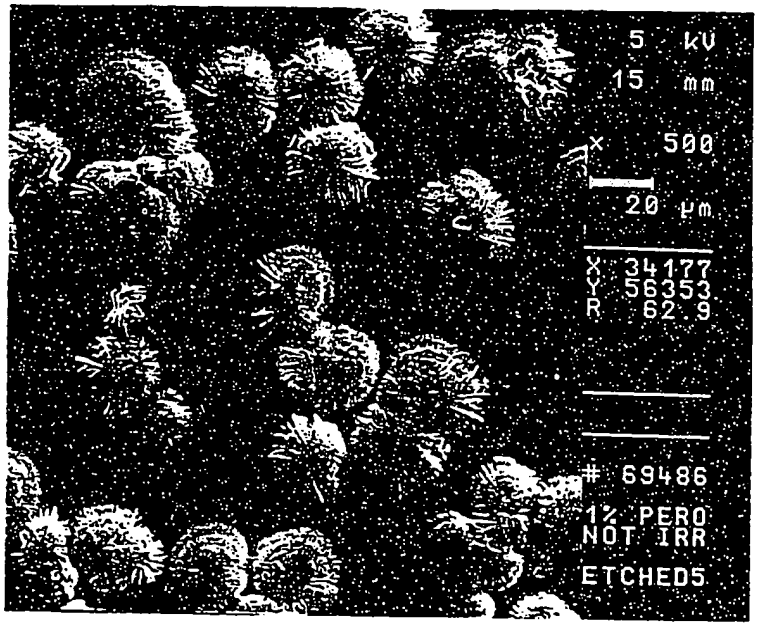

Figure 4.45. Scanning electron micrographs of etched (5 h) molded surfaces of GUR 415 (1 wt% peroxide). Before irradiation. (a) x 200 (b) x 500.

(a)

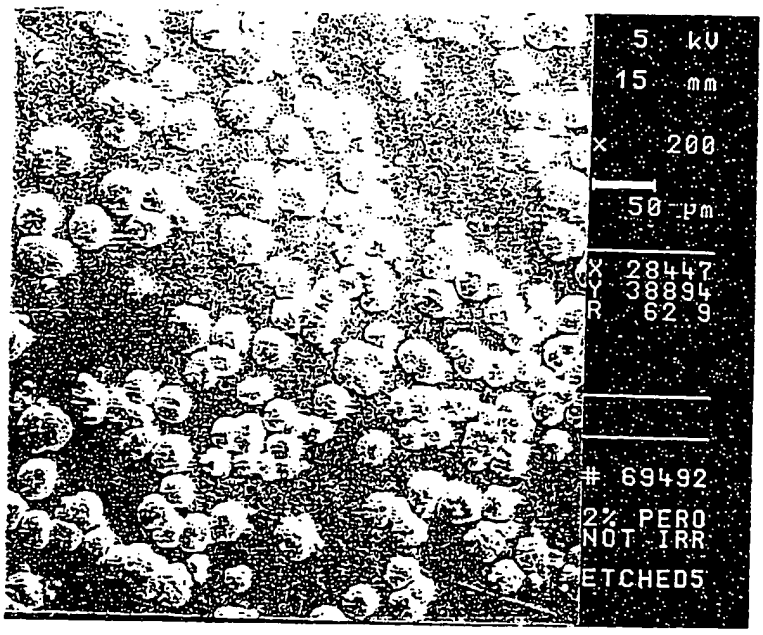

(b)

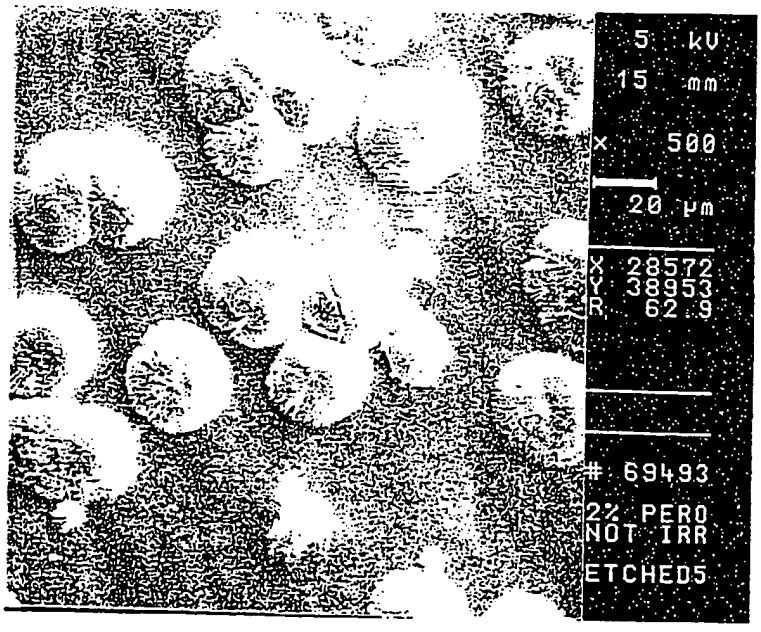

Figure 4.46. Scanning electron micrographs of etched (5 h) molded surfaces of GUR 415 (2 wt% peroxide). **Before irradiation.** (a) x 200 (b) x 500.

(a)

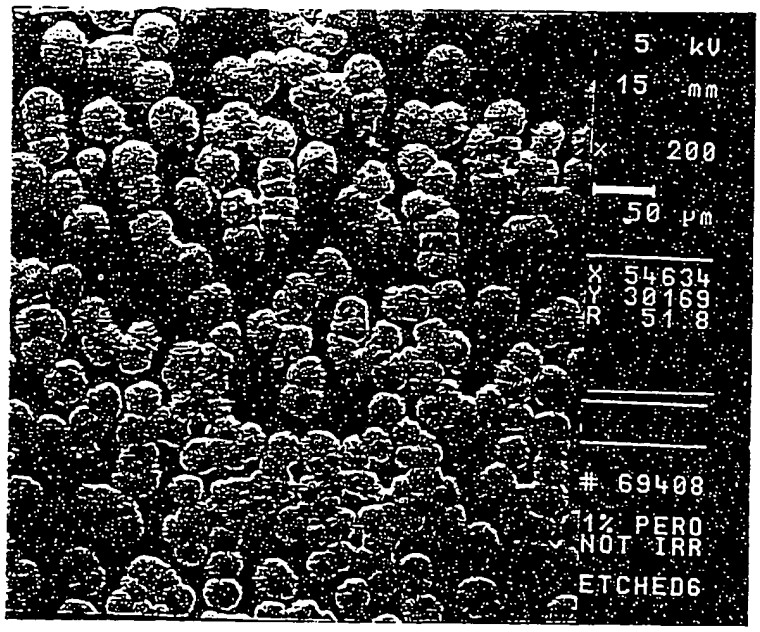

(b)

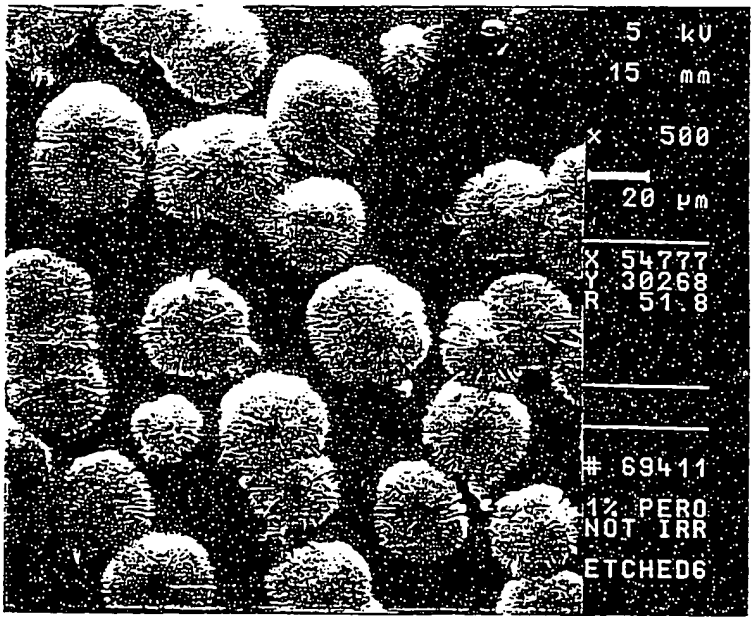

Figure 4.47. Scanning electron micrographs of etched (6 h) molded surfaces of GUR 415 (1 wt% peroxide). Before irradiation. (a) x 200 (b) x 500.

A scanning electron micrograph of the etched molded surfaces of a quenched peroxide-free sample is shown in Figure 4.48. The etching time was 8 h. Comparing Figure 4.48 (quenched, 44.2% crystallinity) to Figure 4.41 (slowly cooled, 49.2% crystallinity), it can be seen that the spherulite size of the slowly cooled sample was larger than that of the quenched sample. It is possible that there is more amorphous material existing in quenched samples and a prolonged etching time is needed to remove amorphous regions. To examine this possibility, an etching time of 10 h was used for the quenched sample and the resulting scanning electron micrograph is shown in Figure 4.49. Even after 10 h etching, the spherulite size of the quenched sample was still smaller than that of the slowly cooled sample (Figure 4.41). It can be concluded that high supercooling (i.e., quenching) increases the nucleation rate and leads to the formation of a large number of small spherulites.

After Irradiation (dose = 34 kGy)

Scanning electron micrographs of etched molded surfaces of peroxide-free, 1 and 2 wt% peroxide samples, which were compression molded at 170 °C for 2 h and subsequently slowly cooled to room temperature and then irradiated, are shown in Figures 4.50-4.52, respectively. The etching time for peroxide-free, 1 and 2 wt% peroxide samples was 8, 5 and 5 h, respectively. Comparing Figure 4.50 to Figure 4.41 (before irradiation), it appears that after irradiation, the number and size of spherulites increase for the peroxide free sample. In addition, the spherulite surfaces suffer more damage. There are several possible explanations for these results. Firstly, after irradiation, the crystallinity increases from 49.2% to 55.8%. The reason for an increase in crystallinity is that irradiation-induced scission of tie molecules permits recrystallization of broken chains from noncrystalline regions. This can result in an increase in crystallite sizes and hence, in spherulite sizes.

Secondly, irradiation induces crosslinking and unsaturation in addition to the scission of tie molecules. Thus, irradiation leads to an increase in concentrations of tertiary carbons (crosslinking), double bonds (unsaturation), and chain ends (chain scission). These species are more susceptible to oxidation. Comparing Figure 4.51 to Figure 4.45 (before irradiation), larger spherulites and more damaged surfaces are observed. Comparing Figures 4.52 and 4.46, similar results are obtained. We believe that increased oxidation resulting from the tertiary carbons, double bonds and chain ends will remove more amorphous materials, leading to an increase in spherulite sizes and to more damaged spherulite surfaces.

Scanning electron micrographs of etched molded surfaces of quenched peroxide-free samples with etching times of 8 and 10 h are shown in Figures 4.53-4.54, respectively. Compared to Figures 4.48-4.49, it can be seen that after irradiation, spherulite sizes increase in both cases. However, for an etching time of 10 h, the number of spherulites decreases. Because irradiation introduces tertiary carbons, double bonds, and chain ends, the irradiated specimen is more susceptible to oxidation. This will lead to the removal of smaller spherulites (in quenching process) and more amorphous materials. Therefore, the number of spherulites decreases, but spherulite sizes increases, as shown in Figure 4.54.

Kinetic Studies of Permanganic Etching

A plot of cumulative weight loss vs etching time for peroxide-free, 1, and 2 wt% peroxide samples before irradiation is presented in Figure 4.55. It clearly shows that the peroxide free sample has the lowest etching rate, whereas, the 2 wt% peroxide sample has the highest etching rate. There are two possible explanations for these results. Firstly, there is more amorphous fraction in the 2 wt% peroxide sample (36.5 % crystallinity). The amorphous component can be etched faster than the crystalline one because of easier

(a)

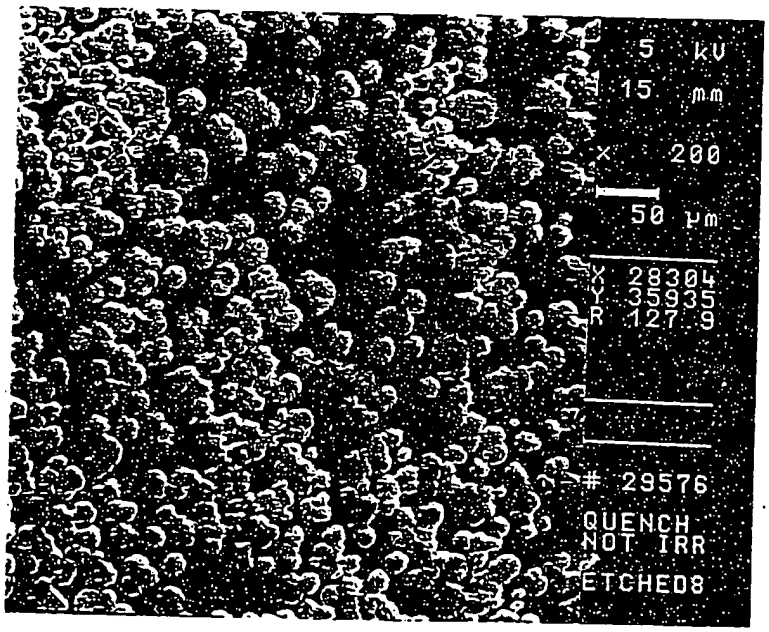

Figure 4.48. Scanning electron micrographs of etched (8 h) molded surfaces of **quenched peroxide-free** sample. **Before irradiation.** (a) x 200.

(a)

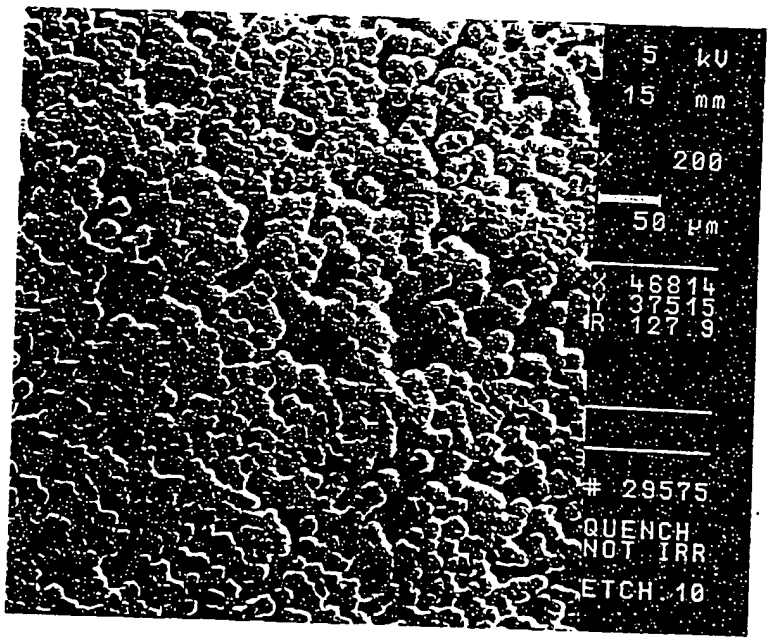

Figure 4.49. Scanning electron micrographs of etched (10 h) molded surfaces of quenched peroxide-free sample. **Before irradiation.** (a) x 200.

(a)

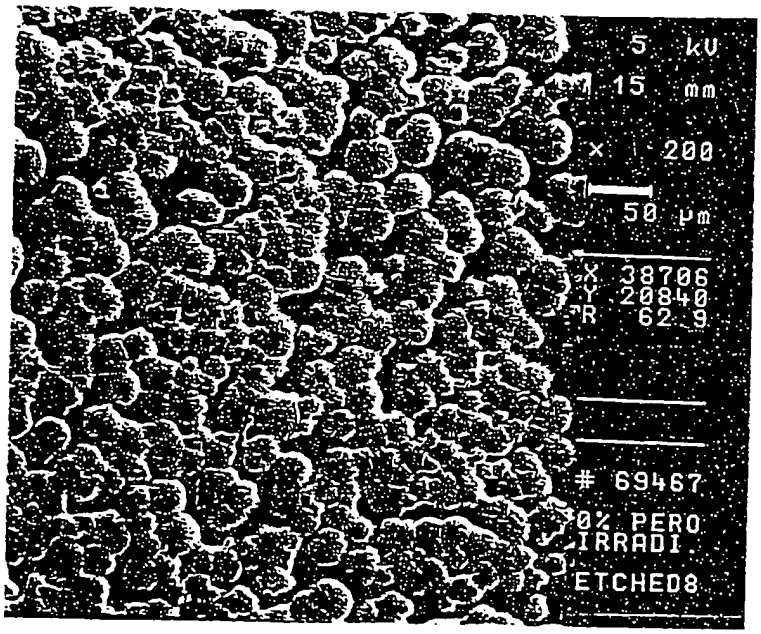

(b)

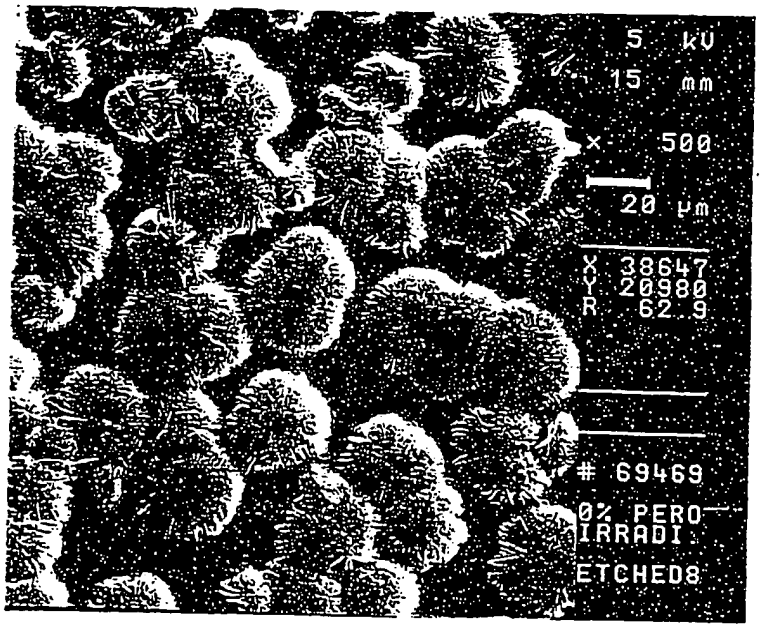

Figure 4.50. Scanning electron micrographs of etched (8 h) molded surfaces of GUR 415 (peroxide-free). After irradiation. (a) x 200 (b) x 500.

(a)

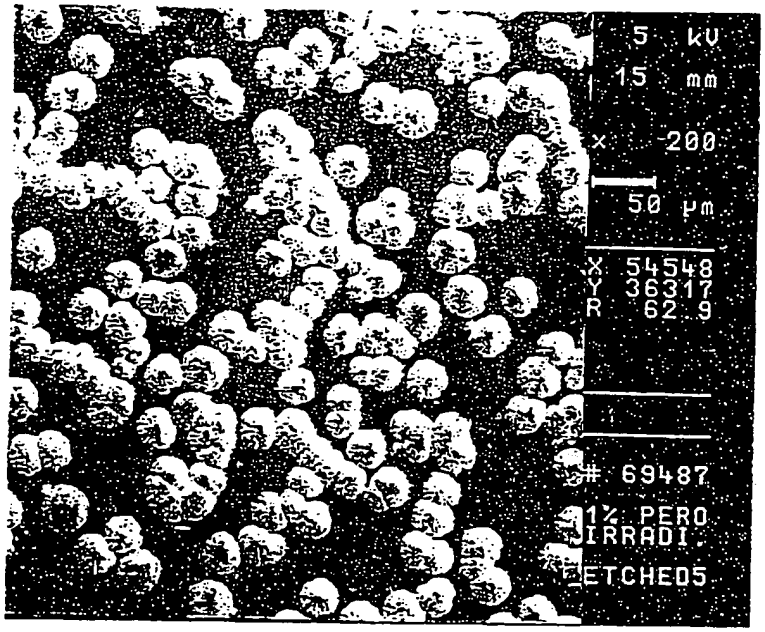

(b)

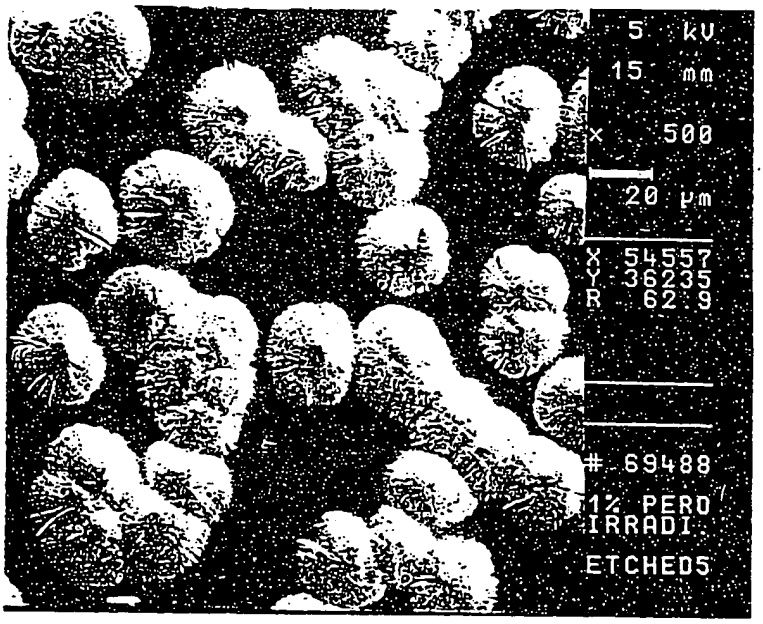

Figure 4.51. Scanning electron micrographs of etched (5 h) molded surfaces of GUR 415 (1 wt% peroxide). After irradiation. (a) x 200 (b) x 500.

(a)

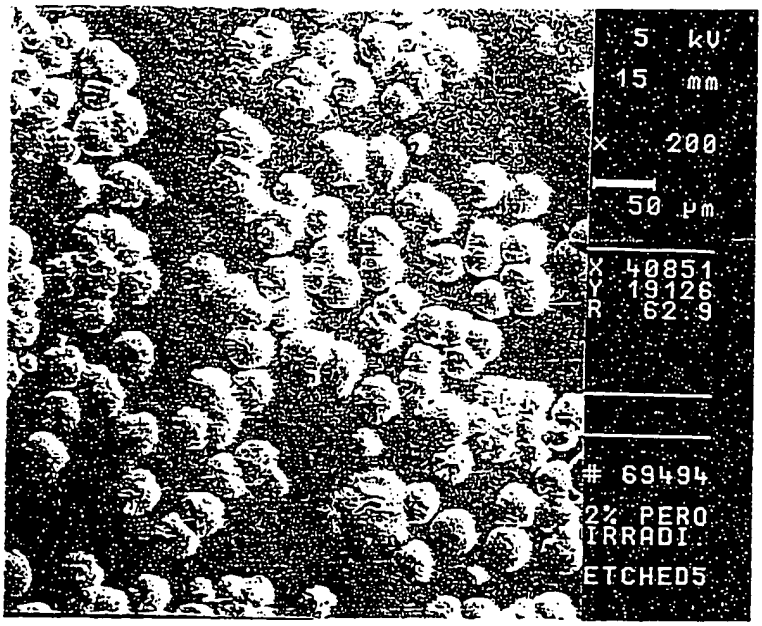

(b)

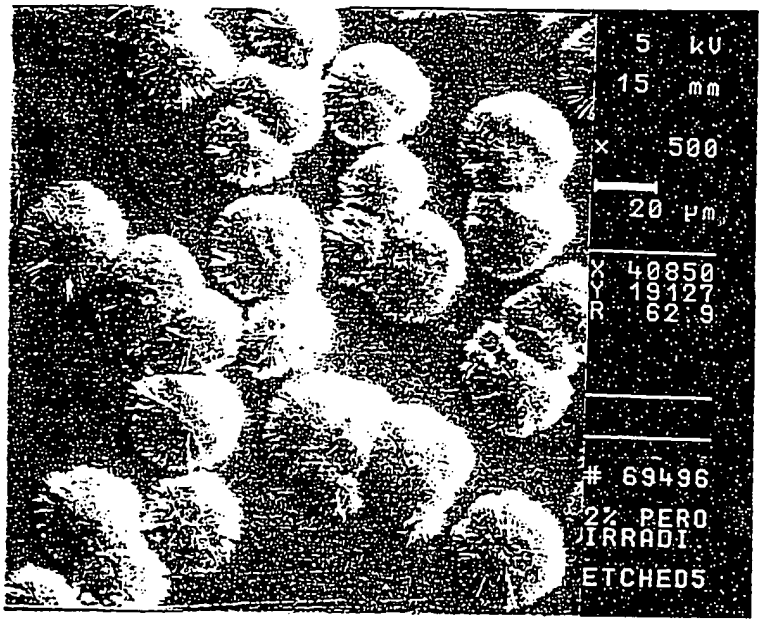

Figure 4.52. Scanning electron micrographs of etched (5 h) molded surfaces of GUR 415 (2 wt% peroxide). After irradiation. (a) x 200 (b) x 500.

(a)

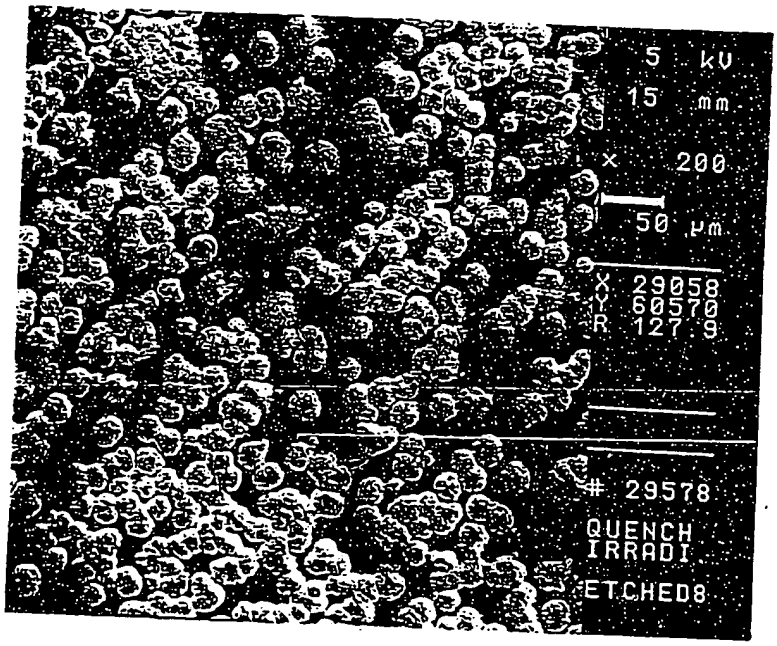

Figure 4.53. Scanning electron micrographs of etched (8 h) molded surfaces of quenched peroxide-free sample. After irradiation. (a) x 200.

(a)

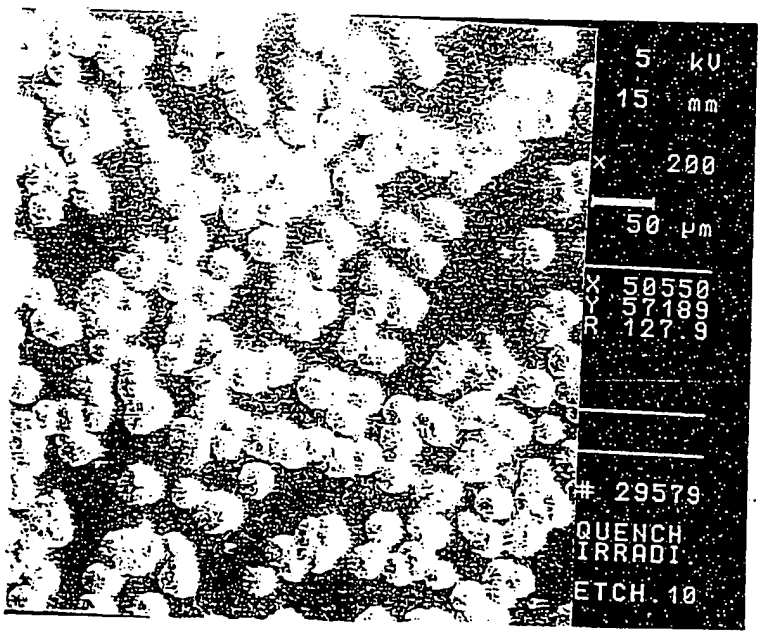

Figure 4.54. Scanning electron micrographs of etched (**10 h**) molded surfaces of **quenched peroxide-free** sample. **After irradiation.** (a) x 200.

penetration by the etchant [1]. Secondly, peroxide crosslinking introduces tertiary carbons in the polymer, which are more susceptible to etchant attack (oxidation), resulting in an increased etching rate. These also confirmed previous observation of spherulite morphology of etched surface before irradiation, which showed that optimum etching time to reveal the appearance of spherulite is 8 h for peroxide-free sample and 5 h for peroxide crosslinked samples (1 and 2 wt% peroxide). In addition, at identical etching time (5 or 6 h), the spherulite surfaces for the 2 wt% peroxide sample suffer more oxidation (damaged appearance) due to higher concentration of tertiary carbons.

After irradiation, a plot of cumulative weight loss vs etching time is presented in Figure 4.56. A slight increase in etching rate was observed for all three samples, compared to Figure 4.55 (before irradiation). This is because irradiation induces crosslinking and unsaturation in addition to the scission of tie molecules, leading to an increase in concentration of tertiary carbons (crosslinking), double bonds (unsaturation), and chain ends (chain scission). Apparently, these species are more susceptible to oxidation. These confirmed previous observation of spherulite morphology of etched surface after irradiation, which showed that spherulite surfaces suffered more damage after irradiation. The kinetic studies of etching also confirmed the FTIR measurements (as discussed in chapter 2), which shows that the concentration of carbonyl groups in peroxide crosslinked samples (after irradiation) is much higher than that of the peroxide free sample (after irradiation). Again, this is because tertiary carbons are more susceptible to etchant attack (oxidation).

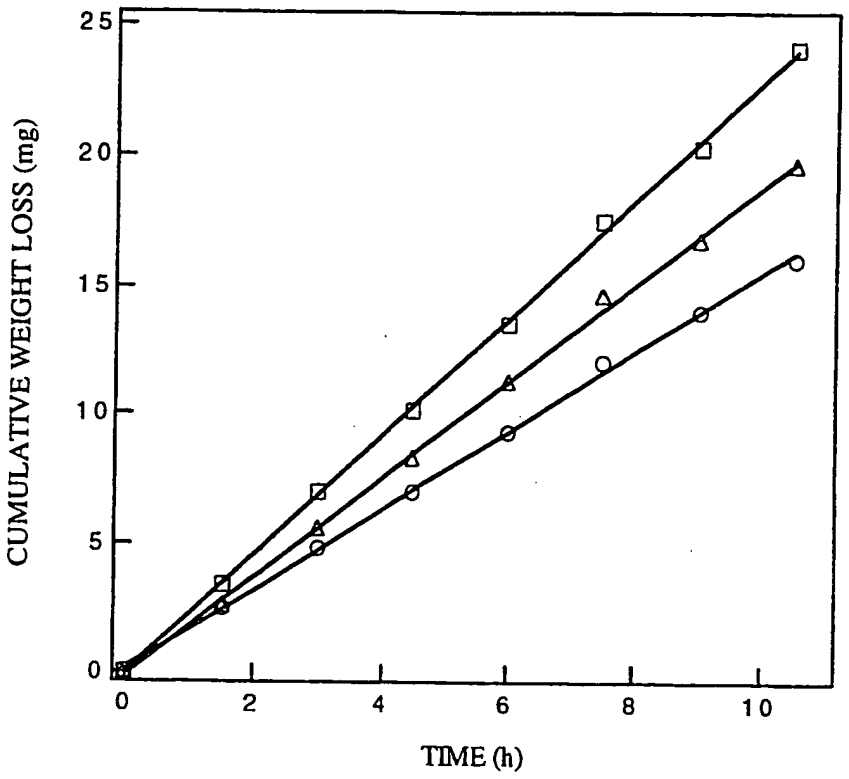

Figure 4.55. A plot of cumulative weight loss vs etching time. (○), peroxide free; (Δ) 1 wt% peroxide; (□) 2 wt% peroxide. **Before irradiation.**

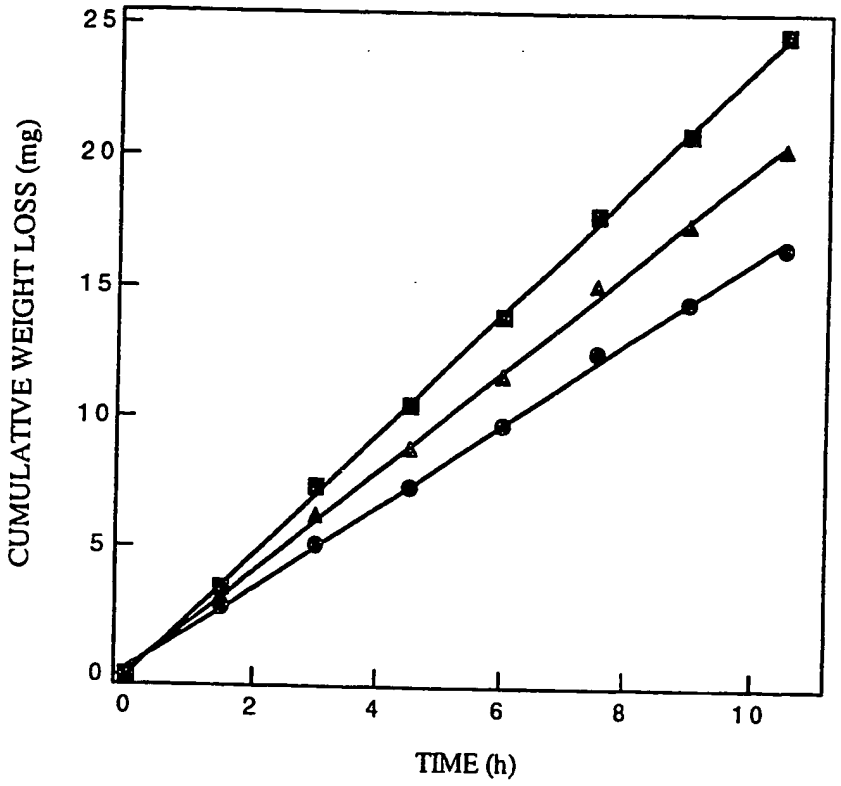

Figure 4.56. A plot of cumulative weight loss vs etching time. (●), peroxide free; (▲) 1 wt% peroxide; (■) 2 wt% peroxide. **After irradiation.**

4.4 Conclusions

Based on the present studies, the following conclusions are drawn.

(1) Nascent UHMWPE powder consists of fine particles of varying size. Surfaces of particles are highly convoluted and their shape is irregular. The particles are composed of smooth, minute (submicron) spheres.

(2) After compression molding at 170 °C for 2 h, GUR 412, GUR 413 and GUR 415 show an incomplete fusion of the original powder. Irregular fracture boundaries are seen in brittle fracture surfaces with sizes comparable to those of UHMWPE powders. In addition, fracture surfaces exhibit an oriented nodular structure.

(3) After compression molding at 220 °C for 2 h, GUR 412 shows a higher degree of melt flow than the other samples because of low molecular weight ($\overline{M_w} \cong 2.5-3\times10^6$). Fracture surfaces of the three UHMWPE samples exhibit an oriented nodular structure.

(4) After compression molding at 300 °C for 2 h, all three UHMWPE samples exhibit a complete fusion of the original particles. A "carpet-like" fracture surface is obtained and oriented nodular structures become randomized. In addition, particulate memory disappears. Particulate memory is a result of slow relaxation of an extremely viscous melt resulting from ultra-high molecular weight and of a high concentration of entanglements. Therefore, on cooling a melt (below 220 °C), particles will recoil and interparticle penetration cannot be obtained.

(5) Peroxide-free UHMWPE shows brittle fracture because of higher crystallinity, whereas, crosslinked samples (1 and 2 wt% peroxide) show ductile fracture due to lower crystallinity.

(6) The quenched peroxide-free UHMWPE shows a less brittle fracture as compared to that of the slowly cooled peroxide-free one. This is because the quenched peroxide-free sample

has lower crystallinity (44.2%) compared to 49.2% of the slowly cooled peroxide-free sample.

(7) Quenched peroxide-crosslinked sample (1 wt% peroxide) shows a similar fracture behavior as that of the slowly cooled sample (1 wt% peroxide).

(8) Quenched peroxide-crosslinked sample (2 wt% peroxide) shows a uniform "ridge-like" network in fracture surfaces. This is because the quenching process produces a more homogeneous network at high peroxide concentration. This is because UHMWPE contains a high concentration of entanglements and peroxide crosslinking inhibits molecular chain motion, a quenching process will "freeze" the entanglements and prevent chains from disentangling so that crystalline regions are very small. In addition, thermal analyses showed that melting temperatures of first and second melting during the DSC scan were equal (refer to chapter 2).

(9) After irradiation, a slowly cooled peroxide-free sample exhibits a sharper and cleaner fracture boundary. This is because irradiation-induced scission of tie molecules permits recrystallization of broken chains from the noncrystalline regions and results in an increased crystallinity.

(10) Irradiation has less effect on fracture for a slowly cooled peroxide-crosslinked sample (2 wt%) because peroxide crosslinking stabilizes the scissioned chains and suppresses recrystallization of broken chains.

(11) After irradiation, all quenched samples (peroxide-free, 1 and 2 wt% peroxide) show a more or less brittle fracture, as compared to those before irradiation.

(12) For fracture surfaces, the optimum etching time is 5 h.

(13) The spherulite surfaces of an etched fracture surface of a slowly cooled peroxide-free sample suffer more damage compared to the peroxide crosslinked sample (1 wt% peroxide). The peroxide free sample has higher crystallinity and exhibits a more brittle fracture. It is believed that peroxide free sample suffers higher forces and less deformation

during fracturing process, leading to smaller strains and more chain scission. The scissioned chains (chain ends) are more susceptible to etchant attack (i.e., oxidation), leading to a coarser spherulite surface.

(14) As peroxide concentration increases (i.e., 2 wt% peroxide), the spherulite surfaces suffer more oxidation (coarser appearance), as compared to that of 1 wt% peroxide sample. This is because peroxide crosslinking introduces tertiary carbons in the polymer, which are more susceptible to oxidation.

(15) Kinetic studies of permanganic etching shows that before irradiation, the peroxide free sample has the lowest etching rate, whereas, the 2 wt% peroxide sample has the highest etching rate. This is because the 2 wt% peroxide sample has higher amorphous components (36.5 % crystallinity) and higher concentration of tertiary carbons introduced by peroxide crosslinking, which are more susceptible to etchant attack (oxidation). Therefore, the optimum etching time to reveal the appearance of spherulite is 8 h for the molded surfaces of peroxide-free sample and 5 h for the molded surfaces of peroxide crosslinked samples (1 and 2 wt% peroxide).

(16) The etching rate and spherulite size are time-dependent.

(17) After irradiation, spherulite surfaces suffer more oxidation and some spherulites become larger. This is because irradiation of UHMWPE leads to scission of tie molecules in addition to irradiation-induced crosslinking and unsaturation, resulting in an increase in concentrations of tertiary carbons, double bonds and broken chains (i.e., chain ends). These species are more susceptible to oxidation and hence, more amorphous materials are removed during etching. In addition, irradiation-induced scission of tie molecules permits recrystallization of broken chains from noncrystalline regions and results in an increased crystallinity, which may increase the crystallite sizes and hence, the spherulite sizes.

(18) Samples compression molded at 300 °C for 2 h show larger spherulite size. This is because high crystallization temperatures provide more opportunities for molecular chain

motion in order to develop the three-dimensional order required for crystallite formation, leading to an increased spherulite size.

(19) The spherulite size of a quenched peroxide-free sample is smaller than that of slowly cooled peroxide-free sample. This is because high supercooling (i.e., quenching) increases the nucleation rate and leads to the formation of a larger number of small spherulites.

(20) After irradiation, a slight increase in etching rate was observed for all three samples. This is because irradiation induces crosslinking and unsaturation in addition to the scission of tie molecules, leading to an increase in concentration of tertiary carbons (crosslinking), double bonds (unsaturation), and chain ends (chain scission). These species are more susceptible to oxidation. This is consistent with FTIR measurements which show that the concentration of carbonyl groups in peroxide crosslinked samples (after irradiation) is much higher than that of the peroxide free sample (after irradiation).

4.5 References

[1] R. H. Olley, A. M. Hodge, and D. C. Bassett, *J. Polym. Sci., Polym. Phys. Ed.*, **17**, 627(1979).

[2] B. Wunderlich, *"Macromolecular Physics"*, **Vol. 1**, Academic Press, New York, 1973.

[3] G. N. Patel, in *"Methods of Experimental Physics"*, L. Marton and C. Marton, Eds., **Vol. 16**, Part B, Academic Press, New York, 1980.

[4] R. P. Palmer and A. J. Cobbold, *Makromol. Chem.*, **74**, 174(1964).

[5] D. J. Priest, *J. Polym. Sci.*, Part A2, **9**, 1777(1971).

[6] A. Keller and Y. Udagawa, *J. Polym. Sci.*, Part A2, **9**, 1793(1971).

[7] D. C. Bassett and A. M. Hodge, *Proc. Roy. Soc. London Ser. A*, **359**, 121(1978).

[8] D. C. Bassett and A. M. Hodge, *Proc. Roy. Soc. London Ser. A*, **377**, 25(1981).

[9] D. C. Bassett, A. M. Hodge, and R. H. Olley, *Proc. Roy. Soc. London Ser. A*, **377**, 39(1981).

[10] D. C. Bassett and A. M. Hodge, *Proc. Roy. Soc. London Ser. A*, **377**, 61(1981).

[11] R. H. Olley and D. C. Bassett, *Polymer*, **23**, 1707(1982).

[12] D. C. Bassett, in *"Comprehensive Polymer Science"*, **Vol. 1**, p841(1989).

[13] B. Franke, *J. Prakt. Chem.*, **36**, 31(1887).

[14] A. Carrington and M. C. R. Symons, *Chem. Rev.*, **63**, 443(1973).

[15] K. L. Naylor and P. J. Phillips, *J. Polym. Sci., Polym. Phys. Ed.*, **21**, 2011 (1983).

[16] A. M. Freedman, D. C. Bassett, A. S. Vaughan, and R. H. Olley, Polymer, **27**, 1163(1986).

[17] A. M. Freedman, D. C. Bassett, and R. H. Olley, *J. Macromol. Sci. Phys.*, **B27**, 319(1988).

[18] R. H. Marchessault, B. Fisa, and H. D. Chanzy, *CRC Crit. Rev. in Macromol. Sci.*, **1**, 315(1972).

[19] G. W. Halldin and I. L. Kamel, *Polym. Eng. Sci.*, **17**, 21(1977).

[20] A. Munoz-Escalona and A. Parada, *J. Cryst. Growth*, **48**, 250(1980).

[21] M. Yasuniwa and C. Nakafuku, *Polymer J.*, **19**, 805(1987).

[22] K. Nakayama, A. Furumiya, T. Okamoto, K. Yagi, A. Kaito, C. R. Choe, L. Wu, G. Zhang, L. Xiu, D. Liu, T. Masuda, and A. Nakajima, *Pure Appl. Chem.*, **63**, 1793(1991).

[23] R. W. Truss, K. S. Han, J. F. Wallace, and P. H. Geil, *Polym. Eng. Sci.*, **20**, 747(1980).

[24] B. Wunderlich, *"Macromolecular Physics"*, **Vol. 2**, Academic Press, New York, 1976.

[25] R. H. Marchessault and H. D. Chanzy, *J. Polym. Sci.*, Part C, **30**, 311(1970).

[26] H. D. Chanzy, J. F. Revol, R. H. Marchessault, and A. Lamanda, *Kolloid-Z. Z. Polym.*, **251**, 563(1973).

[27] H. D. Chanzy, E. Bonjour, and R. H. Marchessault, *Colloid Polym. Sci.*, **252**, 8(1974).

[28] R. L. Graff, G. Kortleve, and C. G. Von, *J. Polym. Sci.*, Part B, **15**, 889(1971).

[29] A. Keller and F. M. Willmouth, *Makromol. Chem.*, **121**, 42(1969).

[30] H. D. Chanzy and R. H. Marchessault, *Macromolecules*, **2**, 108(1969).

[31] B. Wunderlich, E. Hellmuth, M. Jaffe, F. Liberti, and J. Rankin, *Kolloid-Z. Z. Polym.*, **204**, 125(1965).

[32] B. Wunderlich and L. Melillo, *Makromol. Chem.*, **118**, 250(1968).

[33] A. E. Zachariades and J. A. Logan, *J. Polym. Sci., Polym. Phys. Ed.*, **21**, 821 (1983).

[34] X. Y. Wang and R. Salovey, *J. Appl. Polym. Sci.*, **34**, 593(1987).

[35] G. Broza, U. Rick, A. Kawaguchi, and J. Petermann, *J. Polym. Sci., Polym. Phys. Ed.*, **23**, 2623(1985).

[36] D. Hofmann, E. Schulz, D. Fanter, H. Fuhrmann, and D. Bilda, *J. Appl. Polym. Sci.*, **42**, 863(1991).

[37] P. Smith, H. D. Chanzy, and B. P. Rotzinger, *J. Mater. Sci.*, **22**, 523(1987).

[38] Y. M. T. Tervoort-Engelen and P. J. Lemstra, *Polym. Commun.*, **32**, 343(1991).

[39] D. J. Dijkstra, W. Hoogsteen, and A. J. Pennings, *Polymer*, **30**, 866(1989).

[40] M. Kresteva, E. Nedkov, and A. Radilova, *Colloid Polym. Sci.*, **263**, 273(1985).

[41] L. Minkova, *Colloid Polym. Sci.*, **266**, 6(1988).

[42] A. E. Zachariades, *Polym. Eng. Sci.*, **25**, 747(1985).

[43] A. E. Zachariades and T. Kanamoto, *Polym. Eng. Sci.*, **26**, 658(1986).

[44] P. Gao, M. R. Mackley, and T. M. Nicholson, *Polymer*, **31**, 237(1990).

[45] J. de Boer and A. J. Pennings, *Polymer*, **23**, 1944(1982).

[46] R. J. Young and P. A. Lovell, *"Introduction to Polymers"*, 2nd Ed., Chapman & Hall, New York, 1991.

[47] E. H. Andrews, *"Fracture in Polymers"*, American Elsevier, New York, 1968.

[48] I. M. Ward and D. W. Hadley, *"Mechanical Properties of Solid Polymers"*, John Wiley & Sons, New York, 1993.

[49] D. C. Bassett, *"Principles of Polymer Morphology"*, Cambridge, New York, 1981.

[50] R. J. Roe, E. S. Grood, R. Shastri, C. A. Gosselin, and F. R. Noyes, *J. Biomed. Mater. Res.*, **15**, 209(1981).

[51] S. K. Bhateja, *J. Macromol. Sci. Phys.*, **B22**, 159(1983).

[52] S. K. Bhateja, E. H. Andrews, and R. J. Young, *J. Polym. Sci., Polym. Phys. Ed.*, **21**, 523(1983).

[53] I. Kamel and L. Finegold, *J. Polym. Sci., Polym. Phys. Ed.*, **23**, 2407(1985).

[54] A. Shinde and R. Salovey, *J. Polym. Sci., Polym. Phys. Ed.*, **23**, 1681(1985).

[55] S. K. Bhateja and E. H. Andrews, *J. Mater. Sci.*, **20**, 2839(1985).

[56] M. Narkis, I. Raiter, S. Shkolnik, A. Siegmann, and P. Eyerer, *J. Macromol. Sci. Phys.*, **B26**, 37(1987).

[57] L. Minkova, *Colloid Polym. Sci.*, **266**, 6(1988).

[58] D. J. Dijkstra, W. Hoogsteen, and A. J. Pennings, *Polymer*, **30**, 866(1989).

[59] L. Minkova and M. Mihailov, *Colloid Polym. Sci.*, **268**, 1018(1990).

[60] Y. Zhao, Y. Luo, and B. Jiang, *J. Appl. Polym. Sci.*, **50**, 1797(1993).

CHAPTER 5

MECHANICAL PROPERTIES OF CROSSLINKED ULTRA-HIGH MOLECULAR WEIGHT POLYETHYLENE

5.1 Introduction

Ultra-high molecular weight polyethylene (UHMWPE) exhibits excellent toughness, impact resistance [1-3] and fatigue behavior [4], as well as, high wear and abrasion resistance [5-8], making it a good candidate for high tenacity fibers and a suitable substitute for thigh and knee bones [9]. Applications in orthopedic prostheses are enhanced by good sliding properties, cyclical fatigue resistance, abrasion resistance, as well as human body compatibility [10]. Because of extremely high molecular weight, UHMWPE exhibits a high concentration of entanglements and a high melt viscosity. Therefore, it is difficult to process by conventional injection and extrusion molding. Generally, UHMWPE is processed by high-pressure ram extrusion or compression molding at temperatures about 200 °C [10]. However, because of extremely high melt viscosity, complete consolidation is not possible at 200 °C and fusion defects appear [11]. Complete fusion of the crystalline phase occurred only at temperatures above 220 °C, where sufficient disentanglement and chain translation may occur [12-14]. Molten UHMWPE in the temperature range of 145-210 °C exhibits significant elasticity, which is manifested by the tendency of the powder particles to recoil upon removal of a compression load [12]. This strong elasticity is

attributed to slow relaxation of the melt because of the high melt viscosity in the temperature range of 145-210 °C which hinders formation of a molecular network between powder particles, and to the high degree of physical entanglements which hinder molecular chain motion during compression molding [12]. Specimens compression molded at 320 °C showed a higher slope of load to extension (modulus) and a higher fracture strength in comparison to specimens compression molded at 180 °C [13-14]. This indicates that a higher degree of interparticle penetration occurs at higher temperatures.

UHMWPE can be crosslinked either by high energy irradiation (gamma-rays or electron beams) or by chemical reactions (peroxide or silane crosslinking). Subjected to high-energy irradiation with gamma-rays or electron beams, UHMWPE exhibits an increase in degree of crystallinity and peak melting temperature [15-27]. It was suggested that irradiation-induced scission of taut tie molecules permits recrystallization of broken chains from noncrystalline regions, which results in an increase in the degree of crystallinity and an increased perfection of existing folded chain crystallites [15-27]. This effect is rather small in conventional high density polyethylene (HDPE), but quite pronounced in UHMWPE [18,21-23]. This was attributed to a high concentration of tie molecules in UHMWPE, which are more susceptible to scission by high-energy irradiation. Taut tie molecules are parts of polyethylene chains under tension that connect two crystals and result from the separate crystallization of parts of long polyethylene chains. In contrast to energetic irradiation, peroxide crosslinking does not involve molecular chain scission [28]. Peroxide crosslinking reactions result from the decomposition of peroxide to form free radicals and the abstraction of hydrogen atoms from polyethylene to yield alkyl radicals, with the resulting combination of alkyl radicals to produce carbon-carbon crosslinks [23,28-41]. The efficiency of peroxide crosslinking is determined by the ability to produce gel at a given peroxide concentration in polyethylene. Generally, the degree of crosslinking and gel content increase with increased peroxide concentration [23,28-41]. Because peroxide

crosslinking occurs above the melting temperature of polyethylene (i.e., in the molten state), the crystallinity and peak melting temperature of the cooled polymer decrease when the peroxide concentration increases. It was suggested that crystallization from a crosslinked melt produces an imperfect crystal as crosslinks suppress the growth of crystals, leading to a depression of melting temperature and a decreased crystallinity [23,28-41]. Since radiation-induced crosslinks are formed essentially in the amorphous regions in UHMWPE, irradiation crosslinking in the solid state produces a highly inhomogeneous network [23,24]. It had been suggested that, in order to obtain a homogeneous network, crosslinking of UHMWPE should be performed in the melt state at temperatures above 150 °C to avoid irregularities due to the presence of remnants of the initial solid state of polyethylene [28,39-40].

de Boer et al.[42-43] studied the influence of gamma-radiation at room temperature under vacuum on the mechanical properties of UHMWPE fibers in a dose range of 7-91 kGy, and reported that the tensile strength at break decreased upon irradiation. They found that the decrease of tensile strength at break depended on initial fiber strength and could be attributed to radiation-induced main-chain scission. Stronger fibers suffered a larger decrease in tensile strength at break and were more sensitive to irradiation than relatively weaker fibers [42]. It was suggested that highly stressed chains which occur in larger numbers in stronger fibers were more susceptible to high energy irradiation and broke preferentially upon irradiation [42]. Dijkstra et al. [44] studied the crosslinking of UHMWPE fibers by electron beam irradiation in a nitrogen atmosphere at various temperatures (25 °C-150 °C) and found that if the fibers were not previously annealed, the tensile strength at break decreased upon irradiation. They suggested that a reduction in tensile strength was due to chain scission of load-carrying taut tie molecules. Annealing the fibers at high temperatures allowed the overstressed taut tie molecules to relax, converting them into lax tie molecules. When lax tie molecules are fractured by irradiation,

recombination of free radicals becomes possible, especially at higher temperatures (higher molecular mobility) [44]. Therefore, no reduction in tensile strength upon irradiation was observed for annealed fibers. It also was reported that taut tie molecules were preferentially scissioned by electron beam irradiation, at low dose (2 Mrad), leading to separation of the different lamellae [45]. However, at higher irradiation doses (above 40 Mrad), the lamellae were likely to be connected again by crosslinks between folds in contacting (or successive) lamellae [45]. It also was reported that gel-spun UHMWPE fibers irradiated by electron beams (up to 10 Mrad) in a nitrogen atmosphere exhibited an increase in creep rate with increasing irradiation dose [46-47]. The increase in creep rate was ascribed to chain scission of taut tie molecules by irradiation at low doses.

From studies of the effect of electron beam radiation (up to 128 Mrad) on the tensile creep behavior of UHMWPE, Bhateja et al. [48] found that Young's modulus and yield stress increased, whereas, tensile creep decreased with increasing radiation dose. The increase in Young's modulus was attributed to an increased crystallinity resulting from radiation-induced chain scission of taut tie molecules, which allowed recrystallization of broken chains from noncrystalline regions [48]. The improvement in creep resistance was attributed to radiation-induced crosslinking in the amorphous regions in addition to increased crystallinity. Similar results were reported by Bhateja et al. [18] in a study of radiation-induced crystallinity changes in UHMWPE. Bhateja et al. [49] also studied the effect of electron beam radiation (up to 128 Mrad) on the stress-relaxation of UHMWPE and reported that stress retention improved progressively with increasing radiation dose. This effect was attributed to the increase in crystallinity after irradiation and irradiation-induced crosslinking in the amorphous regions [49]. Birkinshaw et al. [50-51] reported that tensile modulus and yield stress increased with increasing radiation dose (dose range 0-7.5 Mrad), whereas, elongation at break decreased with increasing radiation dose. It was suggested that a reduction in elongation with increasing dose was ascribed to the formation

of a more tightly bound polymer network with increasing radiation induced crosslinking, leading to a reduced ability to undergo plastic deformation and flow [50-51]. In addition, creep-resistance increased with increasing radiation dose [51]. This behavior was ascribed to the increase in crystallinity resulting from radiation-induced chain scission of taut tie molecules and to radiation-induced crosslinking in the amorphous regions [51]. An increase in Young's modulus with increasing radiation dose (0-40 Mrad) also was reported by Zhao et al. [26]. In addition, they reported that the maximum draw ratio of UHMWPE films decreased with increasing radiation dose. This was ascribed to the fact that radiation-induced crosslinking in amorphous regions limited molecular chain stretching during the drawing process [26].

de Boer et al. [39] studied the effect of peroxide crosslinking in the molten state on mechanical properties of UHMWPE and reported that yield stress, tensile strength at break, and Young's modulus decreased with increasing peroxide concentration, whereas, elongation at yield point increased with increasing peroxide concentration. The decrease in tensile strength at break, yield stress, and Young's modulus and an increased elongation at yield point were attributed to the decrease in crystallinity with increasing peroxide concentration, because these properties were mainly determined by crystallinity [39]. de Boer et al. [40] used dicumylperoxide to crosslink UHMWPE fibers and found that crystallinity, maximum draw ratio, and tensile strength at break decreased with increasing peroxide concentration. The decrease in drawability is ascribed to the fact that crosslinking increases the connectivity of polyethylene molecules in the filaments and hinders chain movements during hot-drawing. The decrease in tensile strength at break is due to reduced draw ratio (due to peroxide crosslinking), which is essential for producing high strength fibers [40]. Narkis et al. [23] studied the tensile properties of peroxide crosslinked UHMWPE and reported that tensile stress at yield and tensile strength at break decreased with increasing peroxide concentration. The decrease in tensile stress at yield is attributed to

the degree of crystallinity, the higher the tensile strength at break. In addition, higher drawability leads to higher tensile strength at break. This result was correlated with elongation at break (Figure 5.3), which shows that elongation at break also decreased with increasing peroxide concentration. Young's modulus vs peroxide concentration is illustrated in Figure 5.5. A systematic decrease in Young's modulus with increasing peroxide concentration was observed, in agreement with literature [39,52-53]. This was attributed to the decrease in crystallinity by peroxide crosslinking (as discussed in chapter 2). A photograph of fractured specimens is shown in Figure 5.6. Immediately after fracture, the peroxide-free specimen underwent considerable twisting and kinking. This behavior results from non-homogeneous deformation and recovery [50,54]. However, this behavior became less noticeable with increasing peroxide concentration. For instance, no twisting and kinking were observed for the 1.5 and 2.0 wt% peroxide specimens. This indicates that much more homogeneous deformation and recovery occur for the highly crosslinked network.

In chapter 2, we reported that peroxide crosslinking during compression molding at elevated temperature (170 °C) followed by crystallization on cooling reduced the degree of crystallinity and the melting temperature of UHMWPE because crosslinks inhibit recrystallization from the molten state. In addition, the degree of swelling decreases with increasing peroxide concentration, whereas, the crosslink density of network increases with increasing peroxide concentration. We believe that the decrease in crystallinity and an increased crosslink density play an important role in determining the mechanical properties of crosslinked UHMWPE.

Because polyethylene is a semicrystalline material, it displays brittle-ductile transition behavior between T_g and T_m, and undergoes cold-drawing before ultimate failure [55]. Polymer single-crystal fibers exhibit brittle fracture at very high stresses, leading to very small strain and higher tensile modulus. Yield point is defined as the first point on the

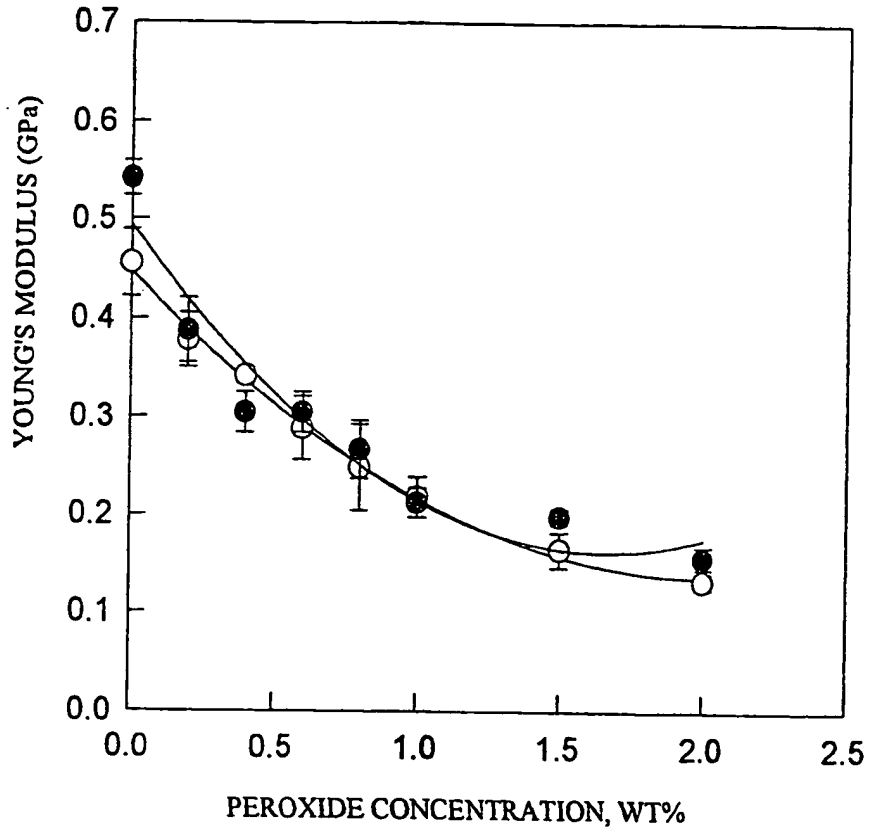

Figure 5.5. Young's modulus as a function of peroxide concentration before (○) and after (●) irradiation.

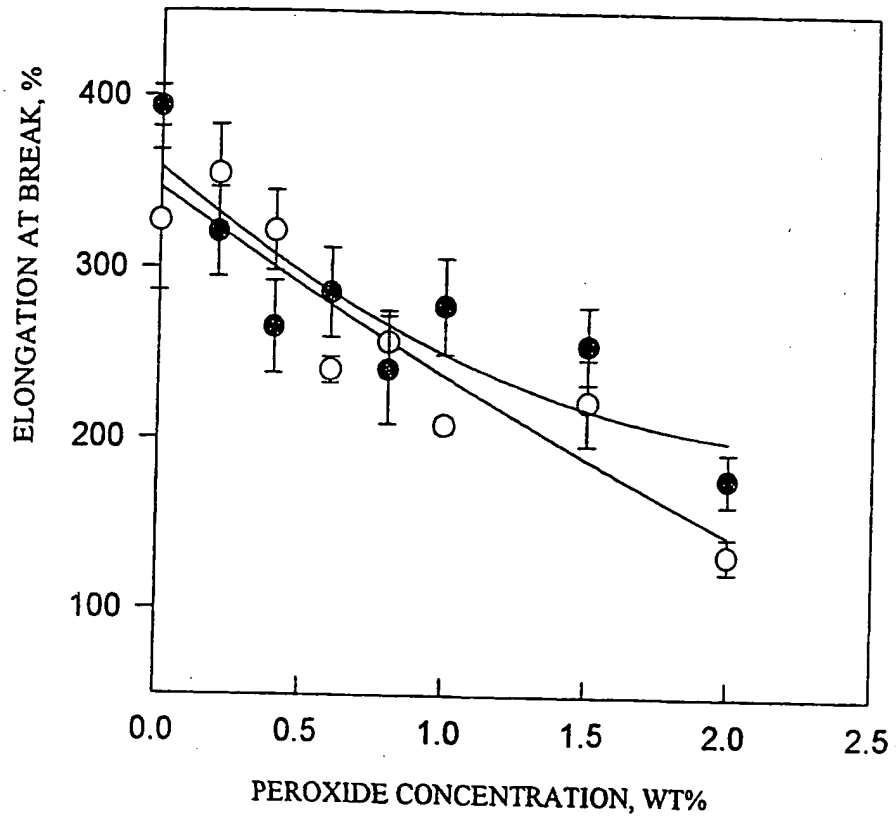

Figure 5.3. Elongation at break as a function of peroxide concentration before (○) and ater (●) irradiation.

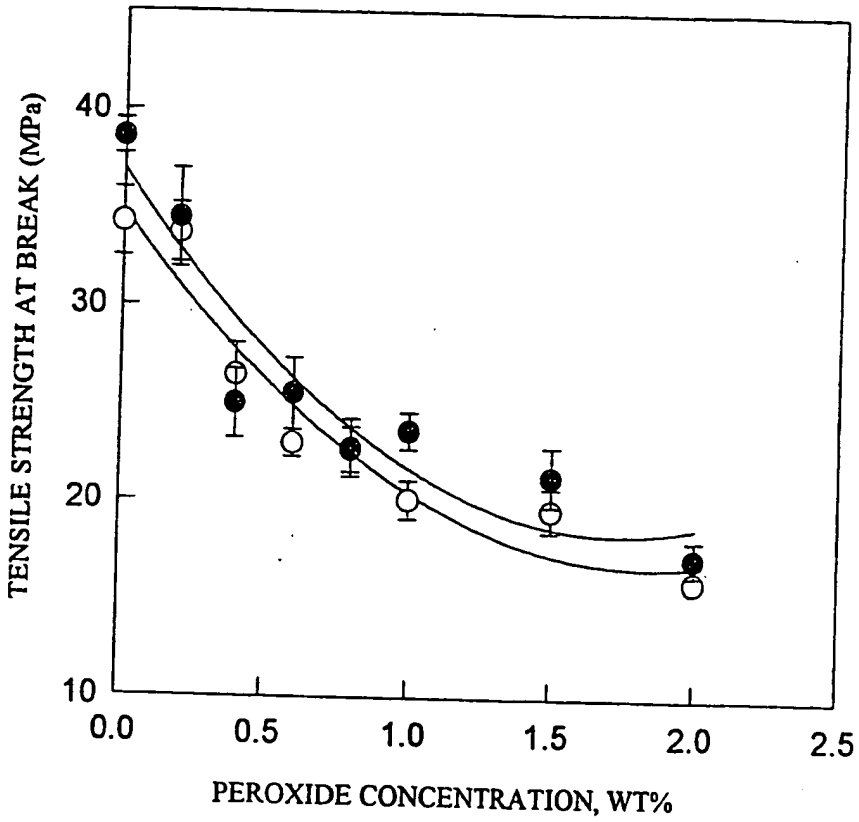

Figure 5.4. Tensile strength at break as a function of peroxide concentration before (○) and after (●) irradiation.

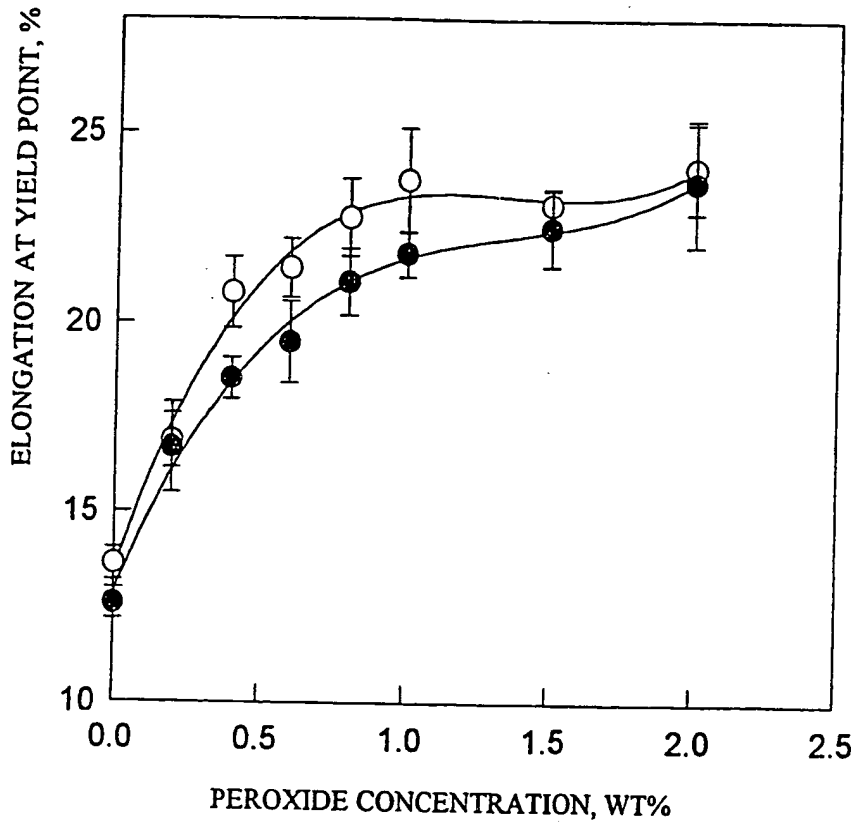

Figure 5.1. Elongation at yield point as a function of peroxide concentration before (○) and after (●) irradiation.

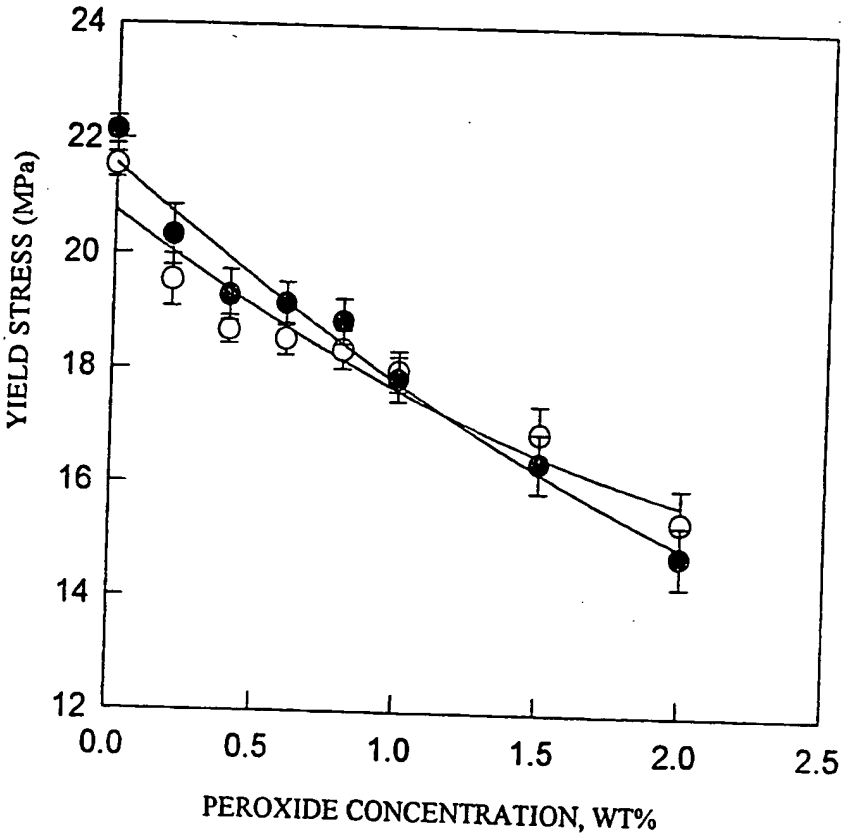

Figure 5.2. Yield stress as a function of peroxide concentration before (○) and after (●) irradiation.

a decreased crystallinity, whereas, the decrease in tensile strength at break is ascribed to reduced drawability after peroxide crosslinking because drawability prior to failure strongly affects the tensile strength at break [23].

In this chapter, we attempt to examine mechanical properties of crosslinked UHMWPE before and after irradiation, using an MTS test machine. Mechanical properties such as elongation at yield point, yield stress, elongation at break, tensile strength at break, and Young's modulus will be compared before and after irradiation.

5.2 Experimental Details

Mixing of the UHMWPE and the peroxide was described in chapter 2. Networks were synthesized by compression molding the mixed powder into 3.2 mm thick sheets in a Dake press. Specimens were compressed in 3.2 mm thick square mold between two stainless-steel plates at 170 °C and ram pressure 7.5 x 10^3 kPa for 2 h. After 2 h, pressure was increased to 15 x 10^3 kPa to avoid cavities inside the polymer and sink marks on the surface and specimens were slowly cooled in the press to room temperature. Compression molded sheets were irradiated with gamma-rays at room temperature in air by SteriGenics International (Tustin, CA). Cobalt-60 was used as the source of gamma irradiation and radiation doses were delivered at a dose rate of 5 kGy/h. Specimens received doses up to 32 kGy (3.2 Mrad).

Uniaxial tensile tests of crosslinked UHMWPE before and after irradiation were performed according to ASTM Standard D-638, using an MTS test machine. Test conditions were at 23±2 °C and 50±5% relative humidity. Specimens were type IV and test speed was 50 mm/min. The gage length was 25 mm. Specimens were die cut from unirradiated and irradiated sheets. For each specimen, five measurements were made. Tensile strength at yield or break was calculated by dividing the maximum load in newtons

by the original minimum cross-sectional area of specimen in square meters (expressed in MPa). Percent elongation was calculated by dividing the extension in gage length by the original gage length and multiplied by 100. Young's modulus (expressed in GPa) was calculated by extending the initial linear part of the load-extension curve and dividing the difference in stress by the corresponding difference in strain. Young's modulus was calculated using the average initial cross-sectional area of the test specimens.

5.3 Results and Discussion

Before Irradiation

Elongation at yield point vs peroxide concentration is illustrated in Figure 5.1. Elongation at yield point increases with increasing peroxide concentration, in agreement with literature [39]. This could be due to a decreased crystallinity following peroxide crosslinking in the melt, making the materials more ductile (softer). Yield stress vs peroxide concentration is illustrated in Figure 5.2. A decreased yield stress with increasing peroxide concentration is observed, in agreement with literature [23,39,52]. The decrease in yield stress is also attributed to a decreased crystallinity. Elongation at break vs peroxide concentration is illustrated in Figure 5.3. As shown in Figure 5.3, elongation at break decreases with increasing peroxide concentration, in agreement with literature [30,40]. The reason for this behavior is that peroxide crosslinking increases the connectivity between polyethylene chains and inhibits chain motion during tensile drawing, leading to a decrease in drawability. Tensile strength at break vs peroxide concentration is shown in Figure 5.4. A decreased tensile strength with increasing peroxide concentration was observed, in agreement with literature [23,30, 39-40]. This was ascribed to the fact that tensile strength at break was depressed by the reduced degree of crystallinity and drawability. The higher

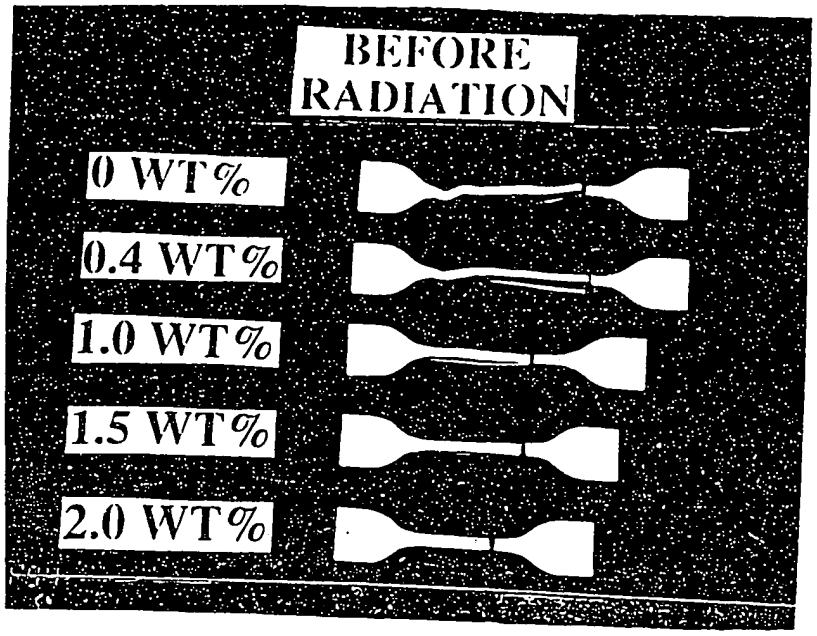

Figure 5.6. Photograph of fractured specimens. **Before irradiation.**

stress-strain curve for a polymer at which an increased strain occurs without an increase in stress. The yield process in a polymer was considered to be a softening due to a local rise in temperature and was referred to as a localized melting [56]. Yield stress can be regarded as the minimum stress at which permanent strain is produced when the stress is subsequently removed, and is defined as the load at yield point divided by the cross-sectional area of specimen [56]. Generally, the higher the degree of crystallinity, the higher the yield stress. Thus, higher crystallinity (stiffer) polymers are more difficult to deform (higher yield stress and small yield strain). On the other hand, crosslinking in amorphous regions increases chain connectivity and inhibits chain slippage during drawing, leading to a higher yield stress [57-59]. Our experimental results show that yield stress decreases with increasing peroxide concentration, whereas, elongation at the yield point increases with increasing peroxide concentration. However, the degree of crystallinity decreases (from 49.2% for a peroxide free sample to 36.5% for a 2 wt% peroxide sample), whereas, the crosslink density of the network increases with increasing peroxide concentration. Therefore, we believe that the decrease in crystallinity is the predominant factor in determining yield stress and elongation at yield point. Lower crystallinity polymers are softer and more ductile, and suffer larger deformation.

Because crosslinking in amorphous regions increases chain connectivity and inhibits chain slippage during drawing, a decrease in elongation at break is expected. Our results show that elongation at break decreases with increasing peroxide concentration, consistent with this explanation. Tensile strength at break is mainly determined by the degree of crystallinity and drawability of specimens [23,30,40]. The higher the degree of crystallinity, the higher the tensile strength at break. Similarly, lower drawability will result in a lower tensile strength at break. Our experimental results, which show that tensile strength at break decreases with increasing peroxide concentration, are consistent with

these explanations of lower crystallinity and drawability. Lower drawability also explains the decrease in elongation at break when peroxide concentration increases (Figure 5.3).

Young's modulus is the ratio of stress to corresponding strain below the proportional limit (elastic deformation) of a polymer, and is a measure of stiffness or rigidity of a polymer. Young's modulus is largely determined by specimen crystallinity. Generally, high crystallinity (stiffer) polymers exhibit higher Young's modulus. Our experimental results show that Young's modulus decreases with increasing peroxide concentration corresponding to the decrease in crystallinity when peroxide concentration increases.

After Irradiation (32 kGy)

It is interesting to compare the effect of irradiation on the mechanical properties of UHMWPE. It is known that on exposure to high energy irradiation, UHMWPE exhibits an increase in the degree of crystallinity and peak melting temperature [15-27]. This is because radiation-induced scission of taut tie molecules permits recrystallization of broken chains from noncrystalline regions, and results in an increase in the degree of crystallinity and an increased perfection of existing folded chain crystallites [15-27]. In addition, radiation-induced crosslinking also occurs in the amorphous regions. Therefore, after irradiation, UHMWPE exhibits an increase in Young's modulus and yield stress [18,23,26,48,50,60], and a reduced drawability [26,50] with increasing radiation dose. However, the radiation-induced crystallinity increase only occurs below a dose range of 12-16 Mrad [18,23]. Therefore, the increase in Young's modulus and yield stress is attributed to a radiation-induced crystallinity increase at low doses. At higher doses, radiation-induced crosslinking predominates. Because crosslinking increases chain connectivity and inhibits chain slippage during uniaxial extension, the Young's modulus and yield stress continue to increase. It is worth noting that radiation in the solid state produces a very different molecular structure,

compared to peroxide crosslinked UHMWPE. Radiation at low doses leads to an increased crystallinity plus minor crosslinking, whereas, at higher doses, the original crystallinity of UHMWPE can be preserved and many crosslinks are introduced. Moreover, solid UHMWPE contains crystalline and amorphous regions which differ in susceptibility to irradiation, leading to an inhomogeneous network.

Comparison of elongation at the yield point before and after irradiation is illustrated in Figure 5.1. It was shown that after irradiation, elongation at the yield point decreased. This was attributed to the increase in crystallinity produced by radiation-induced chain scission of taut tie molecules which allowed broken chains to recrystallize from the amorphous regions. At higher peroxide concentrations (above 1.5 wt% peroxide), the effect of irradiation became less noticeable. This is because at high peroxide concentration, crosslinks stabilize chain fragments resulting from the scission of taut tie molecules and suppress recrystallization of broken chains, leading to a reduced effect of radiation on crosslinked UHMWPE (as discussed in chapter 2). Comparison of yield stress before and after irradiation is shown in Figure 5.2. Below 1 wt% peroxide, yield stress increases after irradiation, again, due to a radiation-induced increase in crystallinity. Above 1.5 wt% peroxide, yield stress decreases after irradiation. Here, the degree of crystallinity almost remained constant after irradiation (as discussed in chapter 2). However, extensive chain scission occurred at 32 kGy, which destroyed chain connectivity and resulted in a reduced yield stress at higher peroxide concentration.

Comparison of elongation at break before and after irradiation is illustrated in Figure 5.3. After irradiation, an increase in elongation at break was observed, especially, at higher peroxide concentrations. We believe that extensive chain scission at 32 kGy destroys chain connectivity resulting from peroxide crosslinking so that chain slippage occurs during uniaxial extension. Thus, elongation at break may increase after irradiation above 1 wt% peroxide. Comparison of tensile strength at break before and after irradiation is illustrated

in Figure 5.4. After irradiation, an increase in tensile strength at break was observed. As discussed before, tensile strength at break depends on crystallinity and drawability. Irradiation-induced chain scission results in an increased crystallinity (below 1 wt% peroxide) and drawability (as shown in Figure 5.3). Therefore, an increase in tensile strength at break is expected. Comparison of Young's modulus before and after irradiation is shown in Figure 5.5. After irradiation, the peroxide-free sample exhibits an increased Young's modulus, in agreement with literature [18,23,26,48,50,60]. This is due to a crystallinity increase from 49.2 % before irradiation to 55.8 % after irradiation. For peroxide crosslinked samples, the changes in Young's modulus became less noticeable. A photograph of fractured irradiated specimens is shown in Figure 5.7. After irradiation, elongation at break increased (compared to Figure 5.6). In addition, even more considerable twisting and kinking were observed for the peroxide-free sample. The 1.5 wt% peroxide sample also showed slight twisting and kinking. This is a result of chain scission on irradiation.

Uniaxial tensile stress-strain behavior before and after irradiation for 0, 1, and 2 wt% peroxide samples is illustrated in Figures 5.8 and 5.9, respectively. As shown in Figure 5.8, the peroxide-free sample has the highest yield strength and tensile strength at break, whereas, the 2 wt% peroxide sample has the lowest yield strength and tensile strength at break. In the post-yield region, peroxide-free UHMWPE exhibits strain-hardening behavior [54], whereas, peroxide crosslinked (above 1 wt% peroxide) UHMWPE undergoes plastic deformation with cold drawing, implying peroxide crosslinked samples are more ductile (lower crystallinity). In addition, no localized macroscopic necking was observed for all three samples. The strain hardening has two possible sources [56]: (i) molecular alignment caused by drawing, so that the drawing stress (i.e., the flow stress) is increased; (ii) strain-induced crystallization, similar to the crystallization observed in rubbers at high degree of stretching. For peroxide crosslinked samples, since crosslinks

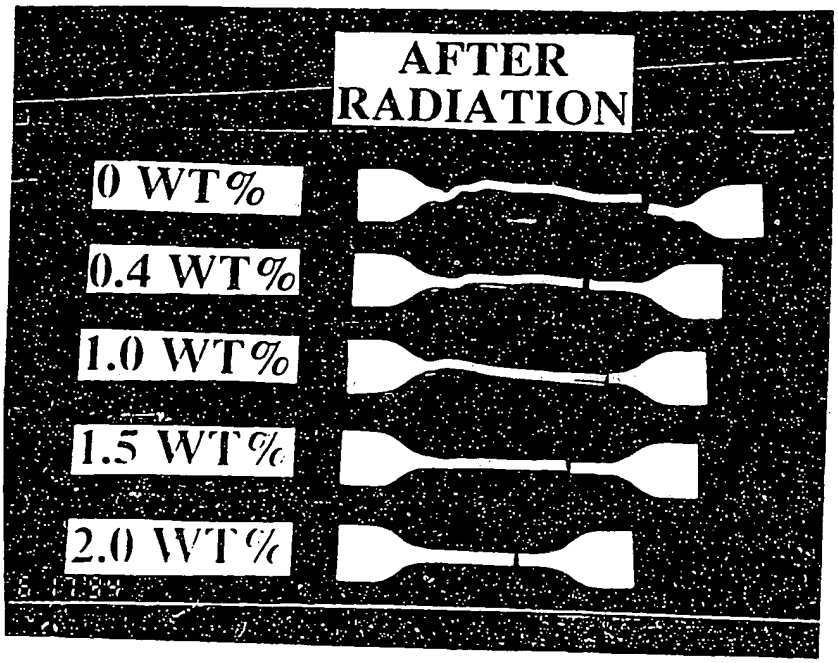

Figure 5.7. Photograph of fractured specimens. After irradiation.

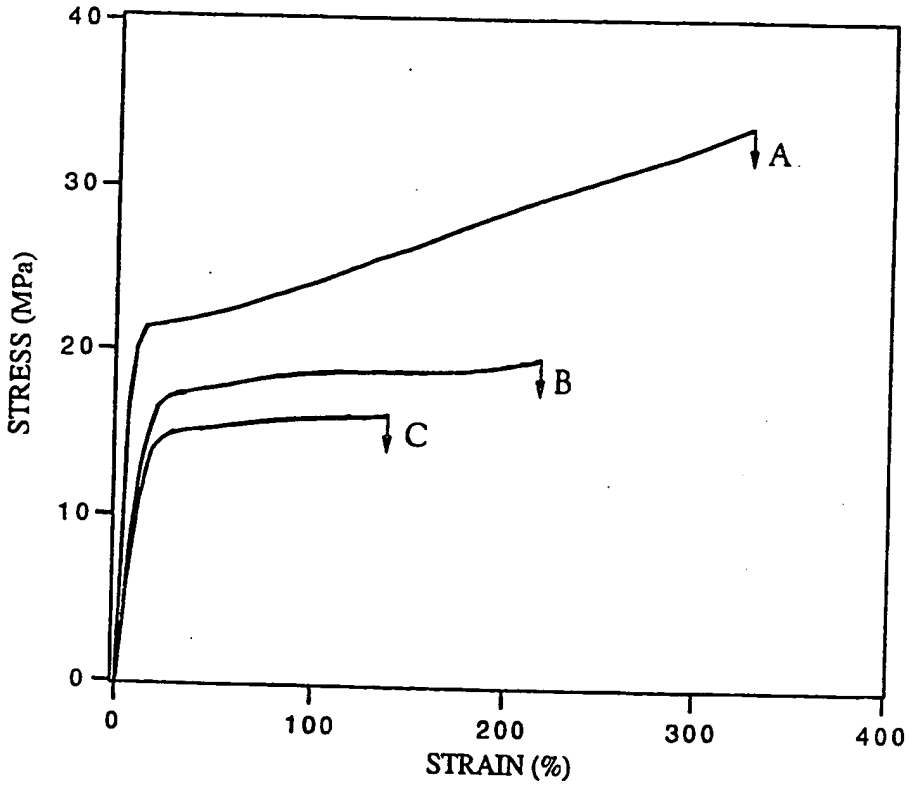

Figure 5.8. Uniaxial tensile stress-strain curves. Curve A, peroxide free; B, 1 wt% peroxide; C, 2 wt% peroxide. **Before irradiation.**

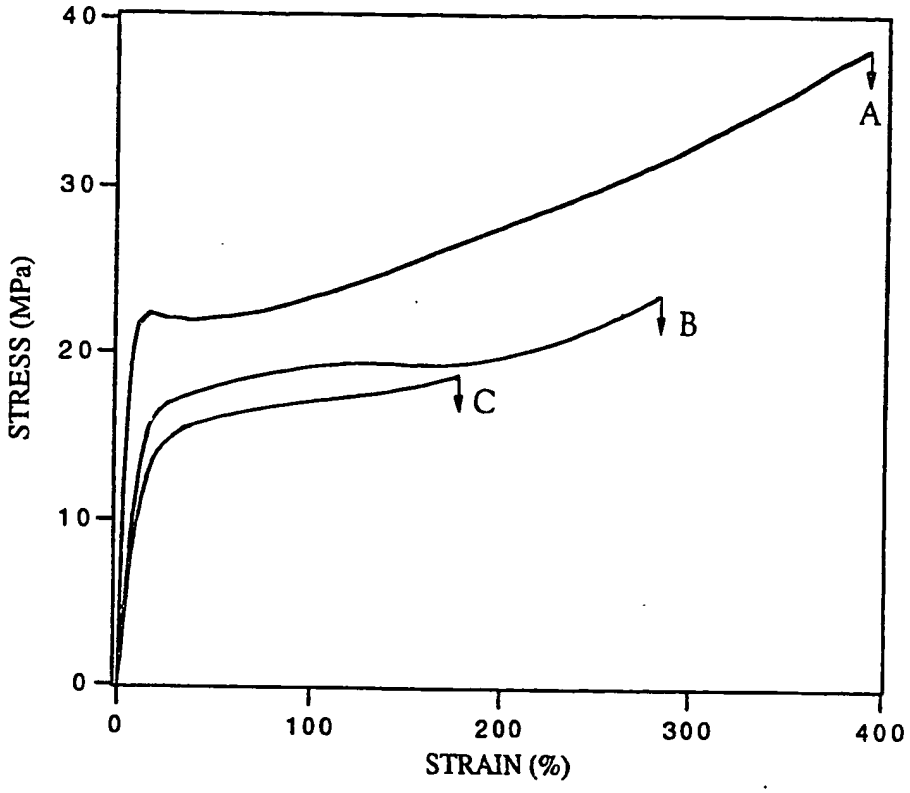

Figure 5.9. Uniaxial tensile stress-strain curves. Curve A, peroxide free; B, 1 wt% peroxide; C, 2 wt% peroxide. **After irradiation.**

introduced by peroxide increase chain connectivity and inhibit chain slippage during drawing, molecular alignment during drawing and strain-induced crystallization are more difficult. Combined with low crystallinity, therefore, no strain hardening is observed for peroxide crosslinked samples (above 1 wt% peroxide).

As illustrated in Figure 5.9 (after irradiation), for the peroxide-free sample, the initial slope of the stress-strain curve increases, implying an increased Young's modulus after irradiation. The yield strength and ultimate strength increase because of irradiation-induced crystallinity increase. For peroxide crosslinked samples, ultimate strength and elongation at break increase because of irradiation-induced chain scission. In addition, slight strain hardening was observed after irradiation for peroxide crosslinked samples. This is because irradiation-induced chain scission makes chain slippage (or alignment) easier during drawing.

5.4 Conclusions

Before Irradiation

(1) Elongation at yield point increases with increasing peroxide concentration. This is because peroxide induced crosslinking in the molten state inhibits the growth of crystals on cooling and leads to a decreased crystallinity, making the materials more ductile (softer).
(2) Yield stress decreases with increasing peroxide concentration. This is also due to the crystallinity decrease resulting from peroxide crosslinking.
(3) Elongation at break decreases with increasing peroxide concentration. This is because peroxide crosslinking increases the connectivity between polyethylene chains and inhibits chain slippage during uniaxial extension, leading to a decrease in drawability at high extensions in spite of the reduced crystallinity.

(4) Tensile strength at break decreases with increasing peroxide concentration. Tensile strength at break depends on the degree of crystallinity and drawability, a decrease in crystallinity and drawability with increasing peroxide concentration leads to a reduced tensile strength at break.

(5) Young's modulus decreases with increasing peroxide concentration due to the decrease in crystallinity by peroxide crosslinking.

(6) Fractured peroxide-free specimens exhibit considerable twisting and kinking. This is because of non-homogeneous deformation and recovery. This behavior becomes less noticeable with increasing peroxide concentration, since the uniformly crosslinked network deforms more uniformly.

(7)Uniaxial tensile stress-strain curves show that in the post-yield region, the peroxide-free UHMWPE exhibits strain-hardening behavior, whereas, the peroxide crosslinked (above 1 wt% peroxide) UHMWPE undergoes plastic deformation with cold drawing, implying peroxide crosslinked samples are more ductile (lower crystallinity). The strain hardening results from molecular alignment caused by drawing and strain-induced crystallization.

After Irradiation (32 kGy)

(1) Elongation at the yield point decreases because of the increase in crystallinity produced by irradiation-induced chain scission of taut tie molecules, which allows broken chains to recrystallize from the amorphous regions. At higher peroxide concentration (above 1.5 wt% peroxide), this becomes less noticeable. At high peroxide concentration, crosslinks introduced by peroxide crosslinking stabilize chain fragments resulting from the scission of taut tie molecules and suppress recrystallization of broken chains, leading to a reduced effect of radiation on crosslinked UHMWPE.

(2) Yield stress increases after irradiation due to irradiation-induced increase in crystallinity. However, above 1.5 wt% peroxide, yield stress decreases after irradiation. This is because extensive chain scission at low radiation dose (32 kGy) destroys chain connectivity and results in a reduced yield stress at higher peroxide concentrations. Moreover, at high peroxide concentration, the crystallinity does not increase.

(3) Elongation at break increases after irradiation because extensive chain scission destroys chain connectivity and enhances chain slippage during uniaxial extension.

(4) Tensile strength at break increases after irradiation because irradiation-induced chain scission results in an increased crystallinity (below 1 wt% peroxide) and drawability.

(5) For the peroxide-free samples, Young's modulus increases after irradiation. This is due to a radiation-induced crystallinity increase from 49.2 % before irradiation to 55.8 % after irradiation. For peroxide crosslinked samples, changes in Young's modulus become less noticeable.

(6) Even more considerable twisting and kinking are observed for the peroxide-free sample, whereas, the 1.5 wt% peroxide sample shows slight twisting and kinking due to chain scission on irradiation.

(7) For peroxide crosslinked samples (above 1 wt% peroxide), slight strain hardening was observed after irradiation. This is because irradiation-induced chain scission makes chain slippage (or alignment) easier during drawing.

5.5 References

[1] S. K. Bhateja, J. K. Rieke, and E. H. Andrews, *J. Mater. Sci.*, **14**, 2103 (1979).

[2] S. K. Bhateja, J. K. Rieke, and E. H. Andrews, *Ind. Eng. Chem. Prod. Res. Dev.*, **19**, 607 (1980).

[3] W. N. Findley and J. F. Tracy, *Polym. Eng. Sci.*, **14**, 577 (1974).

[4] J. A. Sauer, E. Foden, and D. R. Morrow, *Polym. Eng. Sci.*, **17**, 246 (1977).

[5] J. H. Dumbleton and C. Shen, *Wear*, **37**, 279 (1976).

[6] J. R. Atkinson, K. J. Brown, and D. Dowson, *J. Lub. Technol.*, **100**, 208 (1978).

[7] S. K. Bhateja, *Polymer*, **22**, 23 (1981).

[8] J. H. Dumbleton, C. Shen, and E. H. Miller, *Wear*, **29**, 163 (1974).

[9] A. M. Grugnola, E. L. Radin, R. M. Rose, J. L. Paul, S. R. Simon, and M. B. Berry, *J. Appl. Polym. Sci.*, **20**, 809 (1976).

[10] P. Eyerer, R. Ellwanger, H. A. Federolf, M. Kurth, and H. Madler, in *"Concise Encyclopedia of Medical & Dental Materials"*, D. Williams, Ed., Pergamon Press, 1990.

[11] R. M. Rose and E. L. Radin, *Biomaterials*, **11**, 63 (1990).

[12] A. E. Zachariades and J. A. Logan, *J. Polym. Sci., Polym. Phys. Ed.*, **21**, 821 (1983).

[13] A. E. Zachariades, *Polym. Eng. Sci.*, **25**, 747 (1985).

[14] A. E. Zachariades and T. Kanamoto, *Polym. Eng. Sci.*, **26**, 658 (1986).

[15] S. K. Bhateja, *Polymer*, **23**, 654 (1982).

[16] R. J. Roe, E. S. Grood, R. Shastri, C. A. Gosselin, and F. R. Noyes, *J. Biomed. Mater. Res.*, **15**, 209 (1981).

[17] S. K. Bhateja, *J. Macromol. Sci. Phys.*, **B22**, 159 (1983).

[18] S. K. Bhateja, E. H. Andrews, and R. J. Young, *J. Polym. Sci., Polym. Phys. Ed.*, **21**, 523 (1983).

[19] I. Kamel and L. Finegold, *J. Polym. Sci., Polym. Phys. Ed.*, **23**, 2407 (1985).

[20] A. Shinde and R. Salovey, *J. Polym. Sci., Polym. Phys. Ed.*, **23**, 1681 (1985).

[21] S. K. Bhateja and E. H. Andrews, *J. Mater. Sci.*, **20**, 2839 (1985).

[22] L. Minkova, *Colloid Polym. Sci.*, **266**, 6 (1988).

[23] M. Narkis, I. Raiter, S. Shkolnik, A. Siegmann , and P. Eyerer, *J. Macromol. Sci. Phys.*, **B26**, 37 (1987).

[24] D. J. Dijkstra, W. Hoogsteen, and A. J. Pennings, *Polymer*, **30**, 866 (1989).

[25] L. Minkova and M. Mihailov, *Colloid Polym. Sci.*, **268**, 1018 (1990).

[26] Y. Zhao, Y. Luo, and B. Jiang, *J. Appl. Polym. Sci.*, **50**, 1797 (1993).

[27] R. S. Boggan, H. H. Trieu, K. C. Richelsoph, R. D. Paxson, and M. C. Carroll, *The 19th Annual Meeting of the Society for Biomaterials*, Birmingham, AL, 1993.

[28] A. Posthuma de Boer and A. J. Pennings, *J. Polym. Sci., Polym. Phys. Ed.*, **14**, 187 (1976).

[29] M. Narkis and J. Miltz, *J. Appl. Polym. Sci.*, **13**, 713 (1969).

[30] T. R. Manley and M. M. Qayyum, *Polymer*, **12**, 176 (1971).

[31] G. E. Hulse, R. J. Kersting, and D. R. Warfel, *J. Polym. Sci., Polym. Chem. Ed.*, **19**, 655 (1981).

[32] Y. H. Kao and P. J. Phillips, *Polymer*, **27**, 1669 (1986).

[33] A. J. Peacock, *Polym. Commun.*, **28**, 259 (1987).

[34] A. K. Mukherjee, P. K. Tyagi, and B. D. Gupta, *Angew. Makromol. Chemie*, **173**, 205 (1989).

[35] T. Bremner, A. Rudin, and S. Haridoss, *Polym. Eng. Sci.*, **32**,939 (1992).

[36] K. W. Lem and C. D. Han, *J. Appl. Polym. Sci.*, **27**, 1367 (1982).

[37] E. M. Kampouris and A. G. Andreopoulos, *J. Appl. Polym. Sci.*, **34**, 1209 (1987).

[38] T. Bremner and A. Rudin, *J. Appl. Polym. Sci.*, **49**, 785 (1993).

[39] J. de Boer and A. J. Pennings, *Polymer*, **23**, 1944 (1982).

[40] J. de Boer, H. J. van den Berg, and A. J. Pennings, *Polymer*, **25**, 513 (1984).

[41] P. J. Hendra, A. J. Peacock, and H. A. Willis, *Polymer*, **28**, 705 (1987).

[42] J. de Boer and A. J. Pennings, *Polym. Bull.*, **5**, 317 (1981).

[43] J. de Boer and A. J. Pennings, *Polym. Bull.*, **7**, 309 (1982).

[44] D. J. Dijkstra and A. J. Pennings, *Polym. Bull.*, **17**, 507 (1987).

[45] D. J. Dijkstra and A. J. Pennings, *Polym. Bull.*, **20**, 557 (1988).

[46] D. J. Dijkstra and A. J. Pennings, *Polym. Bull.*, **19**, 73 (1988).

[47] P. G. Klein, D. W. Woods, and I. M. Ward, *J. Polym. Sci., Polym. Phys. Ed.*, **25**, 1359 (1987).

[48] S. K. Bhateja and E. H. Andrews, *Polymer*, **24**, 160 (1983).

[49] S. K. Bhateja and E. H. Andrews, *J. Appl. Polym. Sci.*, **34**, 2809 (1987).

[50] C. Birkinshaw, M. Buggy, and J. J. White, *Mater. Chem. Phys.*, **14**, 549 (1986).

[51] C. Birkinshaw, M. Buggy, and S. Daly, *J. Appl. Polym. Sci.*, **38**, 1967 (1989).

[52] K. A. Kunert, *J. Polym. Sci., Polym. Lett. Ed.*, **19**, 479 (1981).

[53] A. G. Andreopoulos and E. M. Kampouris, *J. Appl. Polym. Sci.*, 31, 1061 (1986).

[54] S. K. Bhateja, *Polymer*, 22, 23 (1981).

[55] R. J. Young and P. A. Lovell, *"Introduction to Polymers"* 2nd Ed., Chapman & Hall, 1991.

[56] I. M. Ward and D. W. Hadley, *"Mechanical Properties of Solid Polymers"*, John Wiley & Sons, 1993.

[57] G. Capaccio, I. M. Ward, and M. A. Wilding, *J. Polym. Sci., Polym. Phys. Ed.*, 16, 2083 (1978).

[58] E. H. Andrews, *Pure Appl. Chem.*, 31, 91 (1972).

[59] L. G. Shadrake and F. Guiu, *J. Mater. Sci.*, 17, 145 (1982).

[60] S. K. Bhateja and E. H. Andrews, *J. Mater. Sci.*, 20, 2839 (1985).

CHAPTER 6

CONCLUSIONS

Chemically crosslinked ultra-high molecular weight polyethylene (UHMWPE) networks were synthesized by compression molding of polyethylene in the presence of peroxide at 170 °C for 2 h. Crosslinked networks were irradiated with gamma-rays in the atmosphere up to 34 kGy (3.4 Mrad) and the effect of irradiation on thermal properties, swelling properties, crystal perfection, surface morphology, and mechanical properties of peroxide crosslinked UHMWPE was extensively studied.

Peroxide crosslinking leads to a decrease in the degree of crystallinity, peak melting temperatures, and recrystallization temperatures for both slowly cooled and quench crystallized samples. This is because peroxide crosslinking inhibits the growth of crystals on cooling a crosslinked melt, leading to crystal imperfections and a decreased crystallite size. In addition, the degree of swelling decreases with increasing peroxide concentration because of increased crosslinking. Because of extremely long polymer chains in UHMWPE, only a few crosslinks (i.e., very low peroxide concentration) were needed for gelation. For peroxide free UHMWPE, irradiation leads to an increase in the degree of crystallinity and peak melting temperature. This is because irradiation-induced scission of taut tie molecules allows recrystallization of broken chains from the noncrystalline regions, and results in an increased crystallinity and perfection of existing folded chain crystallites. For peroxide crosslinked UHMWPE, irradiation produces further crosslinking in amorphous regions plus extensive chain scission of taut tie molecules which leads to increased crystallinity and crystal perfection, reduces gel content, and increases the degree

of swelling of the crosslinked network. However, peroxide crosslinking reduces the effect of irradiation on the crosslinked network because crosslinks introduced by peroxide crosslinking can stabilize the chain fragments resulting from the scission of taut tie molecules and suppress recrystallization of broken chains. FTIR measurements show that a significant increase in carbonyl concentration is observed for all three irradiated samples (peroxide free, 1, and 2 wt% peroxide samples). This is because the free radicals produced by irradiation react with oxygen dissolved and/or diffused in the polymer. In addition, carbonyl concentration in the irradiated peroxide-crosslinked samples is higher, compared to the peroxide free sample (after irradiation). Since peroxide crosslinking produces tertiary carbons which are more susceptible to oxidation during irradiation, the carbonyl concentration in irradiated peroxide-crosslinked samples increases with increasing peroxide concentration.

Wide-angle x-ray scattering shows that peroxide crosslinking during compression molding leads to a reduction in the intensities of crystalline reflections, a decrease in the relative area of the crystalline reflections, and to an increase in FWHM (full width at half maximum). This indicates that the crystal size and perfection and the crystallinity are reduced. Quenching further reduces crystal sizes, amount of crystals and perfection, leading to decreased intensities of crystalline reflections and x-ray crystallinity, and to increased FWHM, compared to those of slowly cooled samples. For slowly cooled samples, interplanar spacings d_{110} and d_{200} essentially remain constant with peroxide concentration, while for quench crystallized samples, the interplanar spacings remain constant at low peroxide concentration but may increase slightly at high peroxide concentration. It is possible that increased defects introduced by higher levels of peroxide crosslinking introduce changes in interplanar spacings in quenched samples. Compared to x-ray scattering from all samples, the measurements of the heat of fusion from DSC show a systematically higher value of crystallinity. This may be because DSC can measure changes

in the thermodynamic heat of fusion from small crystals and is sensitive to the formation of small crystals after peroxide crosslinking and quenching, whereas, x-ray diffraction may require a larger crystallite size and longer range order and may not measure very small crystals. Irradiation to 3.4 Mrad (34 kGy) with gamma-rays from cobalt-60 leads to increased intensities and relative area of crystalline reflections, and decreased FWHM, implying increased size and perfection of crystals and increased crystallinity. The interplanar spacings d_{110} and d_{200} are not affected after irradiation for both slowly cooled and quench crystallized samples. Compared to DSC crystallinity, x-ray crystallinity shows a smaller increase after irradiation. This is because irradiation-induced scission of taut tie molecules could generate small crystals which may be insensitive to x-ray diffraction.

Nascent UHMWPE powder consists of fine particles of varying size. Surfaces of particles are highly convoluted and their shape is irregular. The particles are composed of smooth, minute (submicron) spheres. Examination of the morphology of fracture surfaces by scanning electron microscopy (SEM) shows that after compression molding at 170 °C for 2 h, GUR 412, GUR 413 and GUR 415 exhibit an incomplete fusion of the original powder. Irregular fracture boundaries are seen in brittle fracture surfaces with sizes comparable to those of UHMWPE powders. In addition, fracture surfaces exhibit an oriented nodular structure. After compression molding at 300 °C for 2 h, all three UHMWPE samples exhibit a complete fusion of the original particles. A "carpet-like" fracture surface is obtained and oriented nodular structures become randomized. In addition, particulate memory disappears. Particulate memory is a result of slow relaxation of an extremely viscous melt resulting from ultra-high molecular weight and of high concentration of entanglements. Examination of the morphology of fracture surfaces by SEM shows that peroxide-free UHMWPE exhibits brittle fracture because of higher crystallinity, whereas, crosslinked samples (1 and 2 wt% peroxide) show ductile fracture due to lower crystallinity. After irradiation, a slowly cooled peroxide-free sample exhibits a

sharper and cleaner fracture boundary. This is because irradiation-induced scission of tie molecules permits recrystallization of broken chains from the noncrystalline regions and results in an increased crystallinity. Irradiation has less effect on fracture for a slowly cooled peroxide-crosslinked sample (2 wt%) because peroxide crosslinking stabilizes the chain fragments resulting from the scission of taut tie molecules and suppresses recrystallization of broken chains.

Kinetic studies of permanganic etching shows that before irradiation, the peroxide free sample has the lowest etching rate, whereas, the 2 wt% peroxide sample has the highest etching rate. This is because the 2 wt% peroxide sample has higher amorphous components (36.5 % crystallinity) and higher concentration of tertiary carbons introduced by peroxide crosslinking, which are more susceptible to etchant attack (oxidation). Therefore, the optimum etching time to reveal the appearance of spherulite is 8 h for the molded surfaces of peroxide-free sample and 5 h for the molded surfaces of peroxide crosslinked samples (1 and 2 wt% peroxide). The spherulite surfaces of the etched fracture surface of a slowly cooled peroxide-free sample suffer more damage compared to peroxide crosslinked sample (1 wt% peroxide). Since the peroxide free sample has higher crystallinity and exhibits a more brittle fracture, it is believed that peroxide free sample suffers higher forces and less deformation during fracturing process, leading to smaller strains and more chain scission. The scissioned chains (chain ends) are more susceptible to etchant attack (i.e., oxidation), leading to a coarser spherulite surface. Examination of the morphology of etched molded surfaces by SEM shows that as peroxide concentration increases (i.e., 2 wt% peroxide), the spherulite surfaces suffer more oxidation (coarser appearance), as compared to that of a 1 wt% peroxide sample. This is because peroxide crosslinking introduces tertiary carbons in the polymer, which are more susceptible to oxidation. Samples compression molded at 300 °C for 2 h show larger spherulite size. This is because high crystallization temperatures provide more opportunities for molecular chain motion to develop the three-dimensional

order required for crystallite formation, leading to an increased spherulite size. The spherulite size of a quenched peroxide-free sample is smaller than that of slowly cooled peroxide-free sample. This is because high supercooling (i.e., quenching) increases the nucleation rate and leads to the formation of a larger number of small spherulites. In addition, the spherulite size is time-dependent. The longer the etching time, the larger the spherulite size. After irradiation, a slight increase in etching rate is observed for all three samples (peroxide free, 1, and 2 wt% peroxide samples), and the spherulite surfaces suffer more oxidation and some spherulites become larger. This is because irradiation on UHMWPE leads to scission of tie molecules in addition to irradiation-induced crosslinking and unsaturation, resulting in an increase in concentrations of tertiary carbons, double bonds and broken chains (i.e., chain ends). These species are more susceptible to oxidation and hence, more amorphous materials are removed during etching. This is also consistent with the FTIR measurements which show that the concentration of carbonyl groups in peroxide crosslinked samples (after irradiation) is much higher than that of the peroxide free sample (after irradiation). In addition, irradiation-induced scission of tie molecules permits recrystallization of broken chains from noncrystalline regions and results in an increased crystallinity, which may increase the crystallite sizes and hence, the spherulite sizes.

Tensile tests shows that elongation at yield point increases with increasing peroxide concentration. This is because peroxide induced crosslinking in the molten state inhibits the growth of crystals on cooling and leads to a decreased crystallinity, making the materials more ductile (softer). Yield stress decreases with increasing peroxide concentration. This is also due to the crystallinity decrease resulting from peroxide crosslinking. Elongation at break decreases with increasing peroxide concentration. This is because peroxide crosslinking increases the connectivity between polyethylene chains and inhibits chain slippage during uniaxial extension, leading to a decrease in drawability at high extensions

in spite of the reduced crystallinity. Tensile strength at break decreases with increasing peroxide concentration. Tensile strength at break depends on the degree of crystallinity and drawability, a decrease in crystallinity and drawability with increasing peroxide concentration leads to a reduced tensile strength at break. Young's modulus decreases with increasing peroxide concentration due to the decrease in crystallinity by peroxide crosslinking. Fractured peroxide-free specimens exhibit considerable twisting and kinking. This is because of non-homogeneous deformation and recovery. This behavior becomes less noticeable with increasing peroxide concentration, since the uniformly crosslinked network deforms more uniformly. Uniaxial tensile stress-strain curves show that in the post-yield region, the peroxide-free UHMWPE exhibits strain-hardening behavior, whereas, the peroxide crosslinked (above 1 wt% peroxide) UHMWPE undergoes plastic deformation with cold drawing, implying peroxide crosslinked samples are more ductile (lower crystaliinity). The strain hardening results from molecular alignment caused by drawing and strain-induced crystallization.

After irradiation, elongation at the yield point decreases because of the increase in crystallinity produced by irradiation-induced chain scission of taut tie molecules, which allows broken chains to recrystallize from the amorphous regions. At higher peroxide concentration (above 1.5 wt% peroxide), this becomes less noticeable. At high peroxide concentration, crosslinks introduced by peroxide crosslinking stabilize chain fragments resulting from the scission of taut tie molecules and suppress recrystallization of broken chains, leading to a reduced effect of radiation on crosslinked UHMWPE. Yield stress increases after irradiation due to irradiation-induced increase in crystallinity. Above 1.5 wt% peroxide, yield stress decreases after irradiation. This is because extensive chain scission at low radiation dose (32 kGy) destroys chain connectivity and results in a reduced yield stress at higher peroxide concentrations. Moreover, at high peroxide concentration, the crystallinity does not increase. Elongation at break increases after irradiation because

extensive chain scission destroys chain connectivity and enhances chain slippage during uniaxial extension. Tensile strength at break increases after irradiation because irradiation-induced chain scission results in an increased crystallinity (below 1 wt% peroxide) and drawability. For the peroxide-free samples, Young's modulus increases after irradiation. The radiation-induced crystallinity increases from 49.2 % before irradiation to 55.8 % after irradiation. For peroxide crosslinked samples, changes in Young's modulus become less noticeable. Even more considerable twisting and kinking are observed for the peroxide-free sample, whereas, the 1.5 wt% peroxide sample shows slight twisting and kinking due to chain scission on irradiation. For peroxide crosslinked samples (above 1 wt% peroxide), slight strain hardening was observed after irradiation. This is because irradiation-induced chain scission makes chain slippage (or alignment) easier during drawing.